

2017

# Design, Synthesis, and Evaluation of Innovative BODIPY-Peptidic Conjugates for Biological Application

Tyrslai Menyae Williams

Louisiana State University and Agricultural and Mechanical College, twil161@lsu.edu

Follow this and additional works at: [https://digitalcommons.lsu.edu/gradschool\\_dissertations](https://digitalcommons.lsu.edu/gradschool_dissertations)



Part of the [Chemistry Commons](#)

---

## Recommended Citation

Williams, Tyrslai Menyae, "Design, Synthesis, and Evaluation of Innovative BODIPY-Peptidic Conjugates for Biological Application" (2017). *LSU Doctoral Dissertations*. 4327.

[https://digitalcommons.lsu.edu/gradschool\\_dissertations/4327](https://digitalcommons.lsu.edu/gradschool_dissertations/4327)

This Dissertation is brought to you for free and open access by the Graduate School at LSU Digital Commons. It has been accepted for inclusion in LSU Doctoral Dissertations by an authorized graduate school editor of LSU Digital Commons. For more information, please contact [gradetd@lsu.edu](mailto:gradetd@lsu.edu).

DESIGN, SYNTHESIS, AND EVALUATION OF INNOVATIVE  
BODIPY-PEPTIDIC CONJUGATES FOR BIOLOGICAL APPLICATION

A Dissertation

Submitted to the Graduate Faculty of the  
Louisiana State University and  
Agricultural and Mechanical College  
in partial fulfillment of the  
requirements for the degree of  
Doctor of Philosophy

in

The Department of Chemistry

by

Tyrslai Menyaeé Williams

B.S., Southern University A&M College Baton Rouge, LA, 2011

August 2017

To my guardian angels Jency Williams, Libby Thompson, and Ann Glover we did it! To my heartbeats' Marleigh Wright and Daviah Glover your unconditional love motivates me daily.

## ACKNOWLEDGEMENTS

The impeccable journey of achieving my Doctorate of Philosophy in organic chemistry has been one of continuous learning and growth as a scientist and more importantly a woman. I would first like to thank God for being my light and salvation in everything that I do. I know that I am nothing without you, and pray you always get the glory in all I do. I am very thankful for the opportunity he has given me to encounter a great mentor and advisor, the sweetest person I've ever met, Professor M. Graça H. Vicente. Dr. Vicente not only took me into her group and allowed me to develop my foundation as a scientist. But she has been a true mentor to me over the years. The critical and independent thinking skills I have developed under her leadership are etched in my mind, and I will definitely apply them to my next chapter in life. She has been a pillar of encouragement uplifting me through all areas of my life, especially when I doubted myself. Words cannot express the level of adoration I have for her, thank you Professor M. Graça H. Vicente. I would also like to thank my dissertation committee members, Professor Kevin M. Smith, Professor Isiah Warner, and Professor Marcia Newcomer for their continued support and advice during this journey. A special thank you to my committee member Dr. Warner, over the years you have encouraged me in many ways said and unsaid, and it has been an honor to have you serve as one of my mentors. Your contribution to the world of science is ever-growing, however it never seems to shield the devotion you have for the minority students here at LSU. We are forever indebted to you. I would also like to thank Ms. Connie David for her advice and guidance in using MALDI-TOF-TOF analyses; Dr. Thomas Weldegiorghis in the LSU NMR Facility for training me on various NMR techniques; Dr. Seetharama Jois at the University of Louisiana at Monroe for his guidance in developing peptide sequences; and Dr. Martha Sibrian-Vazquez none of this work would be possible without you. You are truly talented and very much appreciated.

Thank you to the past and present members of the Vicente and Smith research groups: Dr. Krystal Fontenot Dr. Alecia M. McCall, Dr. Jaime Gibbs, Dr. Dinesh Bhupathiraju, Dr. Moses Ihachi, Dr. Benson Ongorora, Dr. Haijun Wang, Dr. Timsy Uppal, Dr. Waruna Jindasa, Dr. Ning

Zhao, Dr. Sunting Xuan, Dr. Alex Ngyuen, Elizabeth Okoth, Qianli Meng, Daniel LaMaster, Maodie Wang, Guangyu Zhang, Dr. Liqiang Luan, and Nichole E Kaufman. A special thank you to Zehua Zhou for all of her expertise in cell studies; Dr. Mathis for his patience and time with mice studies; and Dr. Caitlin Ayala, for being a devoted friend and support system regardless of the miles between us.

Words cannot express how grateful I am to my exceptional family. To my mother, thank you for your many sacrifices, hard-work, and dedication to my siblings and I. Words can never express how much I appreciate your devotion to being a good mother, provider, and person over the years. The unwavering love and support you have offered over me has always lifted me up during this process. To my grandmother, your constant prayers, livelihood, and dedication throughout this process. Your love has kept me grounded and humble. Thank you will never indicate just how much you mean to me. To my brilliant brother and marvelous sister, I hope that this journey sparks a light in you to pursue your wildest dreams. You two are capable of anything and I will forever support you as you have supported me. Finally to my fiancé, Keyala S. Carter, thank you for always being my biggest cheerleader, my rock, my partner, and most importantly my purifier through it all, I truly appreciate your commitment to this process and me. You manage to always guide me to the light at the end of the tunnel no matter what the situation looks like. Enduring these difficult times has not been easy, but there is no one else I would rather share these tender moments with than you. I am truly thankful for your commitment and love during these years, and allowing me to be vulnerable with you. Because of you I now know what it means to be whole. Thank you all for every seed you have sown in me. My only wish is that I affect change in others the way you all have done so for me.

## TABLE OF CONTENTS

|   |     |
|---|-----|
| ABBREVIATIONS .....   | vii |
| ABSTRACT .....  | ix  |
| CHAPTER 1. Introduction to methods of targeting Colorectal Cancer for In Vivo <i>Imaging</i> .....                                | 1   |
| 1.1 Colorectal Cancer (CRC) .....   | 1   |
| 1.2 Methods for Detecting Colorectal Cancer .....   | 5   |
| 1.3 Photodynamic Therapy as a method of treatment for CRC .....   | 9   |
| 1.4 Epidermal Growth Factor Receptor .....  | 11  |
| 1.5 BODIPY Dyes and Applications to <i>In Vivo</i> Imaging .....  | 14  |
| 1.6 Research Focus .....  | 21  |
| 1.7 References .....  | 22  |
| CHAPTER 2. Design and Synthetic Strategies for Peptides that Target EGFR .....  | 34  |
| 2.1 Introduction to EGFR-L1 and EGFR-L2 .....   | 34  |
| 2.2 Results and Discussion .....  | 35  |
| 2.3 Derivatives of EGFR-L1 and EGFR-L2 .....  | 42  |
| 2.4 Characterization of Peptides .....  | 51  |
| 2.5 Conclusions .....   | 56  |
| 2.6 Experimental .....  | 57  |
| 2.7 References .....  | 62  |
| CHAPTER 3. Design and Synthetic Strategies for BODIPY-Peptidic Conjugates for Diagnosis of CRC via Peptide Linkages .....         | 67  |
| 3.1 Introduction .....  | 67  |
| 3.2 Results and Discussion .....  | 69  |
| 3.3 Characterization of BODIPY-Peptide Conjugates .....   | 88  |
| 3.3 Conclusion .....  | 101 |
| 3.4 Experimental .....  | 102 |
| 3.5 References .....  | 109 |
| CHAPTER 4. Design and Synthetic Strategies for BODIPY-Peptidic Conjugates for Diagnosis of CRC via Isothiocyanate Chemistry ..... | 67  |
| 4.1 Introduction .....  | 113 |
| 4.2 Results and Discussion .....  | 114 |
| 4.3 Characterization of BODIPY-Peptide Conjugates .....   | 120 |
| 4.4 Conclusion .....  | 133 |
| 4.5 Experimental .....  | 134 |
| 4.6 Reference .....   | 139 |
| CHAPTER 5. Design and Synthetic Strategies for BODIPY-Peptidic Conjugates for Diagnosis of CRC via Click Chemistry .....          | 145 |
| 5.1 Introduction .....  | 145 |
| 5.2 Results and Discussion .....  | 147 |
| 5.3 Conclusion and Future Work .....  | 158 |
| 5.4 Experimental .....  | 159 |
| 5.5 References .....  | 162 |
| APPENDIX A: Characterization of Chapter 2 Compounds .....   | 166 |
| APPENDIX B: Characterization of Chapter 3 Compounds .....   | 207 |
| APPENDIX C: Characterization of Chapter 4 Compounds .....   | 231 |

|  |     |
|--|-----|
| APPENDIX D: Characterization of Chapter 5 Compounds..... | 241 |
| APPENDIX E: Letters of Permission.....                   | 250 |
| VITA .....   | 251 |

## ABBREVIATIONS

|                           |  |
|---------------------------|--|
| $\alpha$                  | Alpha  |
| $\beta$                   | Beta   |
| $^{11}\text{B-NMR}$       | Boron-11 NMR   |
| $^{13}\text{C-NMR}$       | Carbon- 13 NMR   |
| $^1\text{H-NMR}$          | Proton NMR   |
| 3-PEG                     | Triethylene glycol                                       |
| ACN                       | Acetonitrile   |
| ACS                       | American Cancer Society                                  |
| $\text{BF}_3\text{OEt}_2$ | Boron trifluoride etherate                               |
| BODIPY                    | Boron dipyrromethene                                     |
| BT-SPPS                   | Benchtop Solid Phase Peptide Synthesis                   |
| CHCA                      | $\alpha$ -cyano-4-hydroxycinnamic acid                   |
| CLE                       | Confocal Laser endomicroscopy                            |
| CRC                       | Colorectal Cancer  |
| CTB                       | Cell Titer Blue  |
| CTC                       | Chlorotriyl chloride                                     |
| DCC                       | Dicyclohexylcarbodiimide                                 |
| DDQ                       | 2,3-Dichloro-5,6-dicyano-1,4-benzoquinone                |
| DEPBT                     | 3-(diethoxyphosphoryloxy)-1,2,3-benzotriazin-4(3H)-one   |
| DIPEA                     | Diisopropylethylamine                                    |
| DMF                       | Dimethyl formamide                                       |
| DMSO                      | Dimethylsulfoxide  |
| DNA                       | Deoxyribonucleic acid                                    |
| EDC                       | N-ethyl N-(dimethylaminopropyl)                          |
| EDTA                      | Ethylenediaminetetraacetic acid                          |
| EGF                       | Epidermal Growth Factor                                  |
| EGFR                      | Epidermal Growth Factor Receptor                         |
| EPR                       | Enhanced Permeability and Retention                      |
| ER                        | Endoplasmic reticulum                                    |
| EtOAc                     | Ethyl acetate  |
| FBS                       | Fetal bovine serum                                       |
| FDA                       | Food and drug administration                             |
| FIT                       | Immunochemical Fecal Occult Blood Test                   |
| Fmoc                      | 9-fluorenylmethoxycarbonyl                               |
| FOBT                      | High-Sensitivity Fecal Occult Blood Test                 |
| gFOBT                     | Guaiac Fecal Occult Blood Test                           |
| Gly                       | Glycine  |
| HEPES                     | 2-[4-(2-hydroxyethyl)piperazin-1-yl]ethane sulfonic acid |
| HOAc                      | Acetic acid  |
| HOBT                      | Hydroxybenzotriazole                                     |
| HPLC                      | High performance liquid chromatography                   |
| IFOBT                     | Immunochemical Fecal Occult Blood Test                   |
| Lys                       | Lysine   |



|              |   |
|--------------|---|
| MeOH         | Methanol  |
| MO           | Molecular orbital   |
| MW           | Molecular Weight  |
| MW-SPPS      | Microwave Solid Phase Peptide Synthesis   |
| NaHCO        | Sodium Bicarbonate  |
| NHS          | N-hydroxysuccinimide  |
| NHS          | N-hydroxysuccinimide  |
| PBS          | Phosphate buffered saline   |
| Pc           | Phthalocyanines   |
| PDT          | Photodynamic therapy  |
| PEG          | Polyethylene glycol   |
| pH           | Potential of Hydrogen   |
| ROS          | Reactive oxygen species   |
| RP-HPLC      | Reverse Phase HPLC  |
| SPR          | Surface plasmon resonance   |
| SPPS         | Solid Phase Peptide Synthesis   |
| TEA          | Triethylamine   |
| TFA          | Trifluoroacetic acid  |
| TGF $\alpha$ | Transforming growth factor $\alpha$   |
| THF          | Tetrahydrofuran   |
| TLC          | Thin layer chromatography   |
| TM           | Transmembrane   |
| Tris         | Triisopropylsilane  |
| TBTU         | <i>O</i> -(Benzotriazol-1-yl)- <i>N,N,N',N'</i> -tetramethyluronium tetrafluoroborate       |
| TSTU         | <i>O</i> -( <i>N</i> -Succinimidyl)- <i>N,N,N',N'</i> -tetramethyluronium tetrafluoroborate |
| USPSTF       | U.S. Preventive Services Task Force   |
| UV-VIS       | Ultraviolet Visible Spectroscopy  |

## ABSTRACT

Chapter 1 provides a brief introduction to colorectal cancer (CRC), methods of detection, photodynamic therapy (PDT), and EGFR as an attractive targeting strategy for imaging CRC.

Chapter 2 details the synthesis of ten peptide sequences for targeting EGFR receptors at the site of CRC, as a collaborative work with Dr. Seetharama Jois. This chapter also investigates the efficacy of these peptides for EGFR.

Chapter 3 offers the first synthetic strategy for developing BODIPY-peptide conjugates via amide linkages. All conjugates were optimized for the best reaction conditions and good yields were observed. Each conjugate was subjected to photophysical, SPR, and characterization studies. Cell studies obtained by Mrs. Zehua Zhou suggesting the conjugate bearing the hydrophobic peptide sequence had a greater cellular uptake then compared to conjugates containing a charged peptide sequence.

Chapter 4 details the conjugation strategy via NCS- chemistry. NCS-BODIPY dyes were conjugated to two pegylated peptides. These conjugates were synthesized in 30 minutes with excellent yields. Tests administered by Mrs. Zehua Zhou determined the conjugates to have low dark and phototoxicity to human carcinoma HEp2 cells over-expressing EGFR, and to be taken up in to cells efficiently.

Chapter 5 discusses the conjugation of BODIPY dyes and peptides via click chemistry to build peptide-BODIPY conjugates with cyclic or linear peptide sequences. The conjugates were synthesized efficiently in 24 hours with great yields and minimal side products were observed. Preliminary cell studies suggest conjugates bearing mono-styryl group were

## **CHAPTER 1. Introduction to methods of targeting Colorectal Cancer for In Vivo *Imaging***

### **1.1 Colorectal Cancer (CRC)**

Cancer remains one of the most challenging ailments to cure in the world due to its genetic variability, effects, and symptoms. Colorectal cancer (CRC), also known as colon cancer, rectal cancer, or bowel cancer, is the third most common cancer diagnosed in both men and women when reviewed separately in the United States.<sup>1</sup> In 2017, The American Cancer Society (ACS) estimated that there would be 95,520 new cases of colon cancer, and 39,910 new cases of rectal cancer. CRC is expected to cause nearly 50,260 deaths in the year 2017. Commonly, the lifetime risk of developing CRC is about 1 in 22.<sup>1</sup> However, the ratio of obtaining CRC is marginally lower in women than in men. Recent studies have suggested that CRC age specificity is now rising as previously seen with patients who were born around the 1890s.<sup>2</sup> These studies suggest a probability of births occurring in 1990 doubling the amount of patients who will be affected by colon cancer and quadrupling those affected by rectal cancer.<sup>2</sup>

Over time, many simple life factors have been associated with colorectal cancer. Research ties diet, weight, and exercise together to compare against colorectal cancer risk. The results show that the correlations are strongly matched when compared to other cancers.<sup>3</sup> Generally, if you are a person who is heavily overweight or obese the risk factors for developing CRC are greater, with the odds leading in men over women. People, who are lethargic throughout the day, prefer a meal with considerable amounts of red meat, and prefer meat cooked at high temperatures have a greater chance in developing CRC.<sup>4</sup> ACS suggests the more active you are, having a diet high in vegetables, fruit and whole grains, the better your chances are at prevention of CRC.<sup>5</sup>

The mortality rate from CRC has continually decreased in both men and women for over 20 years. There is a sum of likely reasons for this such as an increase in dieting, exercising, and changed lifestyle may be the cause, however, the most important reason is due to screening.<sup>5</sup> As seen with dieting, people who use tobacco products and indulge in frequent alcoholic beverages are at an increased risk for colorectal

cancer.<sup>5</sup> All these factors are adaptable and can be altered to reduce the risks of obtaining CRC, however certain factors are inescapable and affect people every day.

Factors such as old age amplifies your chances of obtaining CRC, however certain diseases and syndromes have been known to lead to CRC. Diseases such as Crohn's disease or inherited syndromes such as Lynch syndrome have shown increased connection to CRC.<sup>6</sup> In fact, inherited syndromes have shown to make up 5 to 10 percent of the population living with CRC.<sup>5</sup> Like any other cancer or disease having a family history of adenomatous polyps, or CRC, puts you at a higher risk of development, however early screening can aid in treatment and longevity.

Patients that are partaking in early screening are aiding in the fight against CRC. Polyps are being found by screening, and removed before they can develop into cancers.<sup>7</sup> Early screening is also permitting more CRCs to be discovered earlier when the disease is easier to cure and free from metastatic behavior. In addition, treatment for CRC has enhanced over the last several years. As a result, there are now more than 1 million survivors of CRC in the United States.<sup>1</sup>

Generally, CRC occurs when cells that line the colon or rectum become abnormal and grow in extreme measures (Figure 1). The colon, is a connection that extends six feet long that connects the small intestine directly to the rectum. The colon is a highly functional portion of the body in which waste is managed and water removal occurs to store the stool in a dry form. The stool is then removed from the colon once or twice a day and passed down to the rectum to be excreted from the body. The rectum is much smaller in size averaging around eight inches, and is also a connection similar to the colon extending from the colon to the anus. The rectum has a unique job of primarily collecting dried stool from the colon, notifying the body that there is waste that is ready to be removed, and to act as a holding area of collected stool until removal. The colon and rectum collectively makeup the large intestine, and cancer formation in either is termed "colorectal cancer" or CRC.

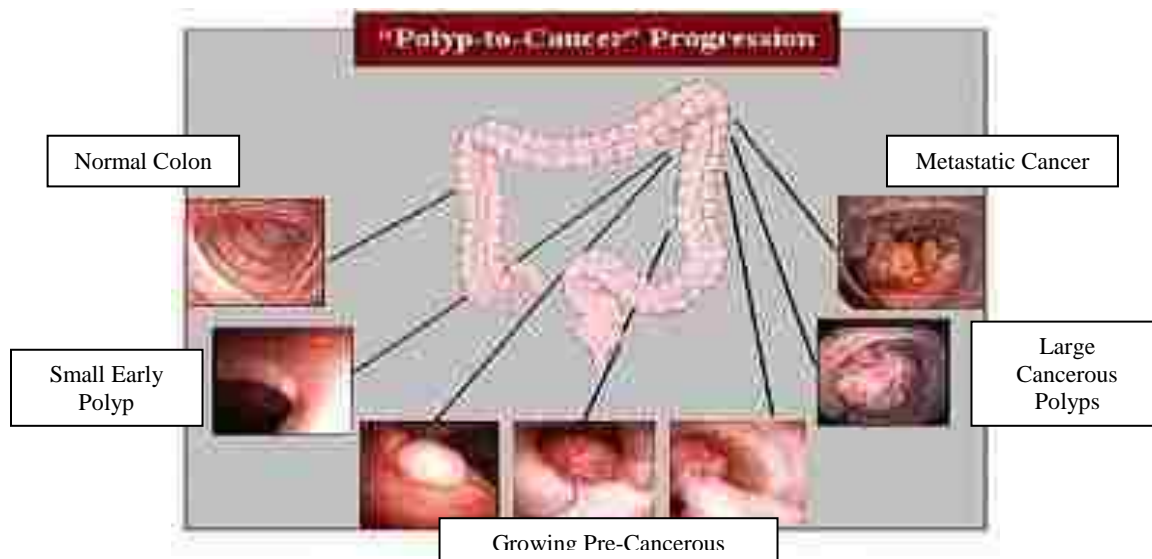


Figure 1. Progression of polyp to cancer in CRC.<sup>8</sup>

The evolution of uncontrolled cell growth in the colon or rectum, can be either benign or malignant.<sup>7</sup> Benign CRC contains cancer cells that are not invasive to surrounding environments. The surrounding normal tissue and cells are not poisoned by the tumors, and will not spread to other parts of the body.<sup>9</sup> Malignant CRC is a more severe case, as the tumor is transportable, and will spread to bordering tissues and may move around the body causing more tumor sites to occur and ultimately becoming more deadly.

Interestingly in CRC the majority of cancers ascend in the colon where the fluid separation takes place, however development of cancer in the rectum may still appear. Furthermore, CRC has been known to be a quiet tumor and not producing any noticeable indications until the cancer is large in size.<sup>10</sup>

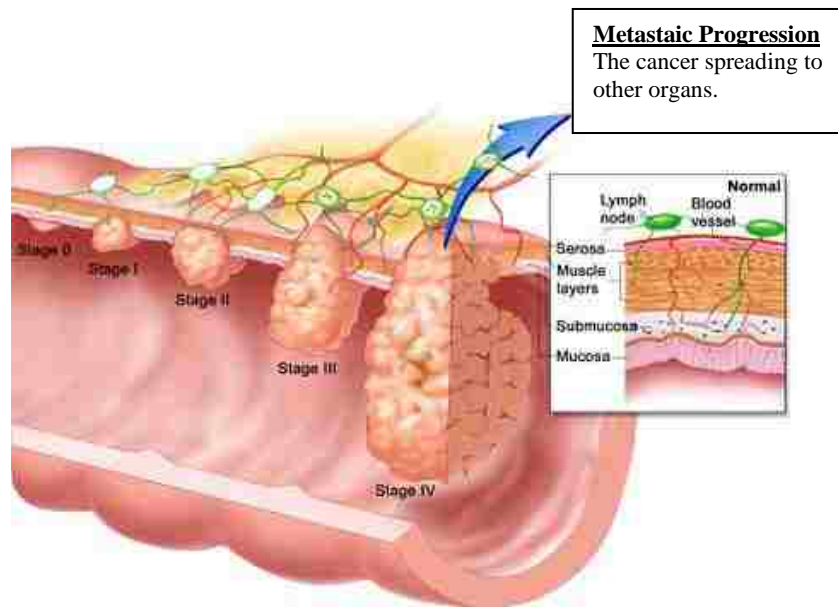
The characteristic polyps of CRC usually develop to include a stalk that allows for protrusion from the surface of the inner colon.<sup>11</sup> These polyps begin as a non-cancerous or benign growth but may later ripen into malignant cancer. CRC polyps progress into two main categories of hyperplastic polyps and adenomas or adenocarcinomas. Hyperplastic polyps are of less risk as they are typically benign, however if located on the right side of the body and of large size should be removed completely.<sup>12</sup> Typically most CRCs are adenocarcinomas, which tend to begin in cells that make and release mucus and other fluids.<sup>13</sup>

Adenocarcinomas are of higher risk, as they will develop more often in size, quantity, and tend to be pre-cancerous in comparison to hyperplastic polyps.

Cancer is typically diagnosed in stages that are dependent solely on the degree or amount of cancer found throughout the body. In particular, CRC stages of cancer are diagnosed based on the depth of the cancer in the interior lining, if the surrounding tissue is infected, and if the cancer has reached nearby lymph nodes.<sup>14</sup> CRC can be diagnosed from two phases clinical and pathological. In the clinical phase, stage determination is based on findings from physical exams, biopsies, and imaging tests. In the pathological phase, the results from clinical findings are combined with necessary surgery to determine the stage of cancer.<sup>15</sup>

In colorectal cancer, there are five stages (Figure 2). Stage 0 indicated that the cancer is in its earliest state. Stage 0 is also known as carcinoma *in situ* and has not yet grown beyond the inner layer of the intestine.<sup>15</sup> The next stage is stage I, where the cancer has protruded through the mucosa or inner layer but has not passed the submucosa. Stage II is broken down into three portions A, B, and C. In stage IIA, the cancer has cultivated through the lining both mucosa and submucosa, but has not grown out of the outermost lining. In stage IIB, the cancer has grown through the outermost lining, but has not traveled to nearby organs. Stage IIC is indicative that the cancer has attached to nearby organs but has not travelled to nearby lymph nodes. Like stage II, stage III is broken down into three portions A, B, C. The stages are similar to stage II cancer, however IIIA includes spreading from 1 to 3 nearby lymph nodes or the fat surrounding the nodes, but not toward distant sites. In IIIB spreading is advanced from 3 to 6 nodes and no distant sites. Finally, stage IIIC indicates the cancer has advanced to 7 or more sites and no distant sites. Stage IV is broken down into only two portions A and B, and interestingly enough, may or may not protrude through the wall of the colon or rectum as well as to other lymph nodes.<sup>15</sup> In stage IVA, there is a present distinction of spreading to one distant organ, normally lung or liver, or a distant set of lymph nodes. In stage IVB, the progression will have advanced as seen in IVA however there may also slight spreading to the abdominal cavity.<sup>15</sup>

Among these five stages, stage IV is the most dangerous due to the metastatic cells spreading through the lymphatic system to other parts of the body. A dangerous mechanism due to the extent of the organs the lymphatic system can reach. Finding a method to detect these polyps at earlier stages such as stage 0 or stage I is of extreme importance in aiding in the fight for survivors against CRC.



## 1.2 Methods for Detecting Colorectal Cancer

Although CRC is considered a “silent cancer” by providing minimal symptoms of issues, physical exams and past family medical history serves as a great foundation for screening as well as various other tools. Presently, several assessments have been advanced to notice CRC sooner, so that it is more operable. There are a limited amount of tests that can be rendered as a method to prevent the progress of polyps and adenomas.<sup>1</sup> The United States has directed a group of experts, U.S. Preventive Services Task Force (USPSTF), to coordinate and suggest the best methods of screening for cancers such as CRC.<sup>5</sup> USPSTF advocates high-sensitivity fecal occult blood tests (FOBT), stool DNA test (FIT-DNA), sigmoidoscopy, virtual colonoscopy, and optical or standard colonoscopy as the most effective methods for detecting CRC.<sup>5</sup>

### **1.2.1 High-Sensitivity Fecal Occult Blood Test (FOBT)**

High-Sensitivity Fecal Occult Blood Test (FOBT) is a non-invasive screening technique that is performed annually. A typical FOBT consists of collection of stool samples that are then analyzed and inspected for blood particles.<sup>16</sup> Polyps and CRC may lead to evidence of patients bearing blood in their stool, thus the patient will then collect their stool and bring the sample in to a primary care physician to determine the result. There are two types of FOBTs that can be performed: Guaiac FOBT (gFOBT) and fecal immunochemical test (FIT or IFOBT).<sup>7, 16</sup>

Blood samples are analyzed by gFOBT and determined by the detection of heme in the collected sample. The chemical used during investigation of samples can also detect heme from other sources such as digested foods, requiring patients to maintain a certain diet before analysis in order to prevent test interference.<sup>12, 17</sup> Though gFOBT is the government-approved method, and the most widely used FOBT method in the US, FIT provides a method that is more specific to patients.

Unlike gFOBT, FIT maintains specificity by utilizing antibodies as the measure to detect human hemoglobin protein. Patients who are able to acquire FIT testing are not required to maintain diets restricting the consumption of certain foods.<sup>15, 18</sup> Subsequently gFOBT has become extremely convenient for patients by allowing simple at-home tests as well as being cost efficient for patients who are considered “at risk age” for developing CRC.<sup>19</sup> The problem with gFOBT testing is that the specificity of the test for CRC is not as sensitive as seen with IFOBT. Other issues such as hemorrhoids can lead to fecal bleeding and may be detected in gFOBT samples. FOBT has become a vital point of detection of CRC for patients over the age of 50 who maintain 1 or 2 screening tests per year; however, if positive identification is obtained, patients will still need to undergo a colonoscopy to determine the stage of the cancer.

### **1.2.2 Stool DNA Test**

This test is very similar to the FIT as it is an immunochemical test that detects any blood that may be in the stool. This time, however, nine other DNA biomarkers are also detected.<sup>20</sup> These biomarkers provide information in regard to three genes that are associated with precancerous adenomas. Patients collect samples and have them mailed off to a laboratory that uses a computer to perform diagnosis. The



computerized testing confers either a positive or negative result. Although this test is more sensitive than IFOBT due to the three genes, the specificity comes at a price, yielding more false positive results than seen with IFOBT.<sup>19</sup>

### **1.2.3 Sigmoidoscopy**

Sigmoidoscopy requires the use of a sigmoidoscope, a lighted flexible tube that bears a lens that allows physicians to view inside of the rectum and sigmoid colon as well as a tool for biopsing tissue. In order to perform the test, doctors insert the tube through the anus into the rectum after the colon has been pumped with air to expand it. This expansion is important for viewing abnormal growths. The colon, in particular the lower colon, is cleared of stool before the test is performed. To prepare for sigmoidoscopy, patients are not sedated making this test less extensive than others.

Sigmoidoscopy has its disadvantages, where abnormalities growing in the upper part of the colon are normally missed during testing.<sup>21</sup> This is due to the lower part of the colon being the highest view of range. The test also requires patients to need their lower bowel cleansed prior to testing. As seen with FOBT, if any abnormal results are detected, further measures, such as colonoscopy, and are still necessary. Sigmoidoscopy could also result in patients incurring small tears in the lining of the colon during testing leading to post screening bleeding as an unwanted side effect.

### **1.2.4 Standard Colonoscopy**

In a standard or normal colonoscopy, the entire colon and rectum are investigated using a colonoscope, which is quite similar to a sigmoidoscope. The colonoscope is a small flexible tube that is also lighted with a lens and equipped with a tool for removing any necessary tissue. The process of colonoscopy also parallels sigmoidoscopy where the colonoscope is inserted through the anus into the rectum and the colon that is filled with air for viewing more clearly. Colonoscopy screening is extremely beneficial as any abnormalities found throughout the entire colon and rectum can be removed right away, unlike with sigmoidoscopy. However, with this method, the entire colon and rectum must be cleansed before requiring patients to undergo sedation.<sup>22</sup> This process tends to be painful for patients, but it is well suited for diagnosing and removal of adenomas.

### **1.2.5 Virtual Colonoscopy**

Virtual colonoscopy is a form of computed tomography that requires a special X-ray scanner that produces several pictures of the colon and rectum from the exterior of the body. A computer is used in order to assemble all of the pictures into a detailed image of the colon and rectum. Virtual colonoscopy has several benefits: 1) The detailed images show polyps and abnormalities; 2) Does not require sedation; 3) Procedure is less invasive compared to normal colonoscopy.<sup>23-24</sup> As seen with normal colonoscopy, the entire colon and rectum must be cleansed and pumped with air for viewing. Ideally, the specificity and sensitivity are parallel to those seen in normal colonoscopy, and the risk of tearing or complications are much lower with virtual colonoscopy. However, the biggest downfall is that unlike with normal colonoscopy, if abnormalities are found in the screening, they cannot be removed *in situ*.<sup>25</sup> A standard method of colonoscopy must be performed to remove them.

### **1.2.6 Confocal Laser Endomicroscopy (CLE)**

Confocal Laser Endomicroscopy (CLE) has become a renewed area of interest in colonoscopy. CLE is a technique for acquiring high-resolution optical images with depth selectivity during an ongoing endoscopy, upgrading detection from colonoscopy procedures.<sup>26</sup> Investigation of the *in vivo* microarchitecture is desirable in targeting distinct areas for biopsies, allowing for an in depth, real-time look at the biological environment of the patient.<sup>27</sup>

Probe-based CLE, a specialization of CLE, has brought much attention to the benefits of endomicroscopy, where it allows real-time *in vivo* scanning of mucosal surfaces during standard endoscopy.<sup>28</sup> Fluorescence cystoscopy (i.e. photodynamic diagnosis) and narrow band imaging are additional endoscope-based optical imaging modalities that can be combined with CLE to achieve multimodal and multidirectional imaging of various cancer types.<sup>29</sup>

Compared to other methods of colonoscopy, CLE provides a method of achieving better spatial resolution. The laser light is emitted on colorectal tissue at the mucosal surface deeper levels of the tissue,

and multiple images are compiled to reveal detailed information regarding the tissue imaged. Clinical trials have suggested CLE to also be an effective method of imaging cancer tissue such as CRC. One study obtained results of CLE that expressed a change in a particular polyp with 97.4% sensitivity, 99.4% specificity, and 99.2% accuracy.<sup>30</sup> Other imaging agents, such as cresyl violet blue, acriflavine, and fluorescein tend to stain cells in a nonselective manner permitting normal and cancerous cells to appear colored (Figure 3).<sup>31</sup> These dyes also exhibit poor water solubility, lower quantum yields, and emit at lower wavelengths that are not close to the NIR-range, providing an intense amount of interference and feedback.

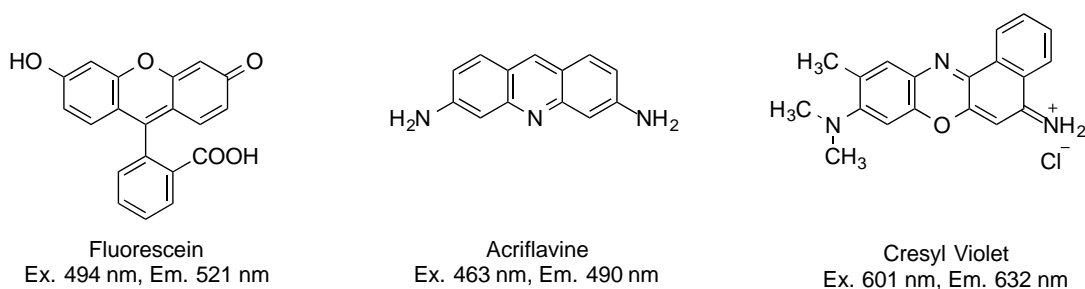


**Figure 3.** Common imaging agents used in CLE.

### 1.3 Photodynamic Therapy as a method of treatment for CRC

Photodynamic Therapy (PDT) is identified as a method of administering photosensitizers, followed by activation with a specific wavelength of light to produce reactive oxygen species (ROS).<sup>32-33</sup> ROS then goes on to cause oxidative damage to proliferating cancer cells that results in cell death through apoptosis or necrosis.<sup>34-36</sup> PDT is a very selective process due to its reactivity being based solely on the irradiation of the photosensitizer and biochemistry of tumor cells. Thus, providing cell death only in the affected area where the photosensitizer is localized.

In order to enhance cancer treatment in the 1950s, a fluorescent marker, porfimer sodium (Photofrin<sup>®</sup>) was designed to enhance the amount of dye accumulated in tumor cells.<sup>37</sup> Over time, porfimer sodium became the first drug to receive approval for treatment during PDT by the FDA. Porfimer sodium is a hematoporphyrin derivative, and has been used to treat patients for over two decades. Porfimer sodium

is the most commonly used PS for PDT; however, some patients tend to suffer from side effects in particular sunlight that may cause severe sunburn.<sup>38</sup> Porphimer sodium is considered a “first generation” photosensitizer that has been used in the treatment of cancerous and precancerous lesions due to its safe and effective treatment. Although it is approved, porphimer sodium still lacks attributes necessary for ultimate treatment: such as isolation of one compound, limited tissue penetration, and poor distribution ratios.<sup>39</sup>

In the past twenty years PDT has been an area of increased interest for since the advance studies into porphimer sodium versus its counterparts (such as surgery, chemotherapy, and radiotherapy). However, the setbacks of porphimer sodium turned scientists’ attention to creating photosensitizers that conquered issues surrounding chemical distinction, enhanced photophysical properties, and enriched tumor selectivity. To aid in photophysical tuning, researchers worked on inducing a bathochromic shift in photosensitizers in the near-IR region of the electromagnetic spectrum. This region allows PDT to have decreased background interference during treatment and sharpens the accuracy of therapy. These compounds became known as the “second generation” photosensitizers. These photosensitizers consisted of new macrocycles, such as phthalocyanines, porphyrins, chlorins, and naphthalocyanines (Figure 4). These compounds could be isolated and purified versus the previous hematoporphyrin.

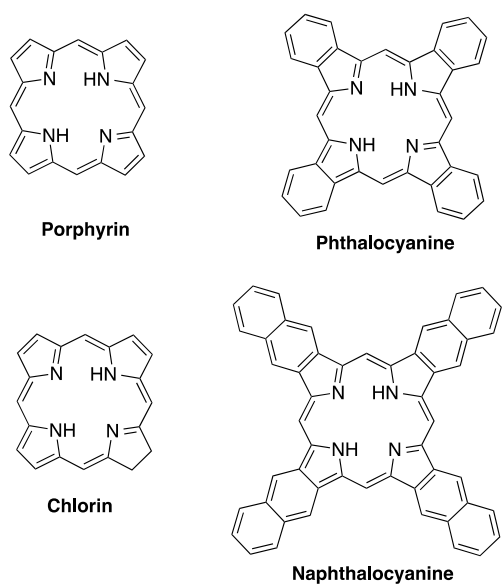


Figure 4. Macrocycles commonly used as photosensitizers.

Although second generation photosensitizers refreshed the face of PDT, issues regarding tumor selectivity were still a remarkable challenge. Avoiding destruction of surrounding healthy tissue was inevitable due to its low enhanced permeability and retention (EPR) effect.<sup>40-41</sup> To tackle tumor selectivity and cellular uptake issues, investigators focused on the design of photosensitizers. The center of most investigations relied heavily on the option to focus on the light delivery and the amount of photosensitizer absorbed by the tumor cells. Photosensitizers are capable of localizing in tumor cells more than they would in normal cells, however the possibility remains of healthy cell uptake. To enhance tumor selectivity, data suggested using devices that were able to improve tumor accrual, biomolecules with selectivity precedence for tumor sites,<sup>42</sup> or overexpression on the surface of tumor tissue. These photosensitizers were denoted as “third generation photosensitizers.”

Photosensitizers conjugated to various biomolecules create promising selectivity for PDT. Approaches to increase specific accumulation of photosensitizers at the target site recently involve the use of various designs some of which including polymer conjugated photosensitizers, encapsulated photosensitizers in different carriers.<sup>43</sup> Although these methods provide an increased selectivity, they were not effective enough to allow restricted selectivity and neglect neighboring healthy tissue. Through covalent linkage, several biomolecules were chosen for selectivity enhancement. Several studies have investigated the ability of photosensitizer conjugations to biomolecules such as antibodies,<sup>44</sup> sugars,<sup>45</sup> oligonucleotides,<sup>46</sup> proteins,<sup>47</sup> hormones,<sup>48</sup> and metabolites.<sup>49</sup>

#### **1.4 Epidermal Growth Factor Receptor**

Epidermal growth factor receptors (EGFRs) are ligand-stimulated cell-surface receptors that play a crucial role in the regulation of cellular functions, comprising cell proliferation and survival.<sup>50-53</sup> The receptor EGFR is a single polypeptide backbone chain that is considered a transmembrane glycoprotein consisting of 1186 amino acid residues, and it has proven to be an integral piece in ruling an effective treatment for cancers including CRC. The receptor tyrosine kinase group that EGFR belongs to is known as the ErbB family. The ErbB family consists of four members: EGFR, ErbB2/HER2, ErbB3/HER3, and

ErbB4/HER4.<sup>54</sup> At maturity, each ErbB receptor includes: an extracellular ligand-binding region, a single transmembrane (TM) domain, and an intracellular tyrosine kinase domain that is bordered by regulatory regions.<sup>55</sup> Each member of the ErbB family plays a critical role as proteins involved in carcinogenesis as the membrane protein expression is upregulated.<sup>56</sup>

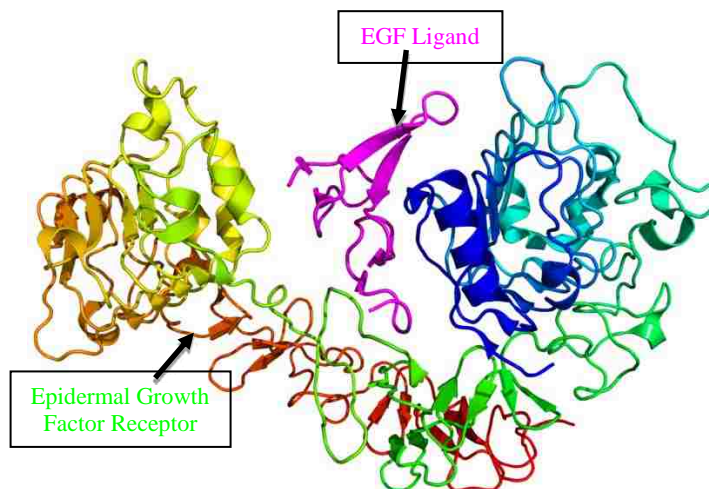


Figure 5. Crystal Structure of EGF localized in the binding pocket of EGFR.<sup>57</sup>

Receptor activation of ErbB occurs during the binding of the receptor and its specific ligand (Figure 5). ErbB has over 12 different growth factors including epidermal growth factor and transforming growth factor  $\alpha$  (TGF $\alpha$ ). The growth factor EGF consists of 53 amino acid residues that stimulates cell growth, proliferation, and differentiation by binding to EGFR with high affinity.<sup>58</sup> Strong mitogenic and neo-angiogenic activity that causes this overexpression of EGFR is all due to the EGF ligand.<sup>59-61</sup> This excessive expression of the EGFR greatly improves receptor targeting and is a growing area in cancer studies.

Activated first by binding of growth factor ligands in eukaryotic cells, EGFR undergoes dimerization, then stimulates its inherent protein-tyrosine kinase activity, thereby catalyzing the phosphorylation of tyrosine residues.<sup>62-63</sup> Growth factor binding induces homo- and/or heterodimerization of the receptor, leading to trans-autophosphorylation and subsequent activation of SH<sub>2</sub> domain-dependent downstream signaling pathways as seen in Figure 6.<sup>55</sup>

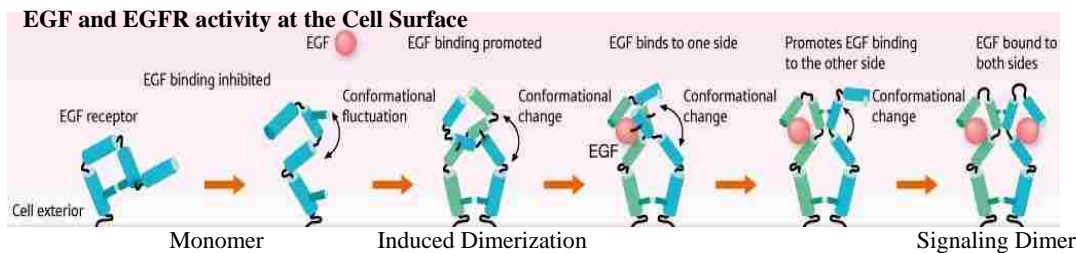


Figure 6. Binding of EGF to EGFR.<sup>64</sup>

98% of colon cancers have had an identification of EGFR, and are amply over-expressed on small cancers including non-small cell lung cancer (NSCLC), breast, head and neck (SCCHN), gastric colorectal, esophageal, prostate, bladder, renal, pancreatic, and ovarian cancers.<sup>59, 62</sup> This overexpression of EGFR is considered a mutation that may cause uninhibited cell proliferation and has therefore been associated with cancer.<sup>63</sup> The cause of this overexpression is a result of mutations occurring during the binding of EGFR to one of its endogenous ligands, EGF, as represented in Figure 5. Over the past two decades, as a result of mirroring the native ligand EGF,<sup>65</sup> several different practices have been advanced for targeting EGFR,<sup>51</sup> containing FDA-approved anti-EGFR antibody cetuximab,<sup>66-68</sup> single-chain anti-EGFR ScFvEGFR,<sup>69</sup> anti-EGFR affibody,<sup>70-71</sup> accessible small peptides,<sup>59, 62, 72-77</sup> and non-peptidic tyrosine kinase inhibitors.<sup>78</sup>

The discovery of EGFR's importance to CRC and other cancers has led to the discovery of peptide ligands, with high specificity for the receptor. Among these ligands, those containing short sequences are particularly attractive for EGFR-targeting due to a variety of reasons, mainly their low cost, readily availability, low immunogenicity, moderately fast diffusion rates, ease of alteration, as well as their easiness of conjugation to various molecules. Computer-based design and screen phage display libraries were used to identify two peptides (Figure 7), LARLLT (designated "D4" or EGFR-L1) and YHWYGYTPQNVI (designated "GE11" or EGFR-L2). These peptides have established particularly efficient binding to the extracellular domain of EGFR over-expressed on cancers cells. This binding has been established *in vivo* in cell lines such as SKBR-3 and BT-474 cells, and *in vitro* in nude mice with A431 tumors.<sup>59, 62, 73-77, 79-80</sup>

Moreover, determination of successful binding of these peptides to EGFR through the extracellular domain has been detected via computational studies.<sup>59, 62, 76</sup> Two prominent binding sites were identified: EGFR-L1 binds to EGFR away from the binding pocket, while EGFR-L2 binds to the EGF binding pocket.

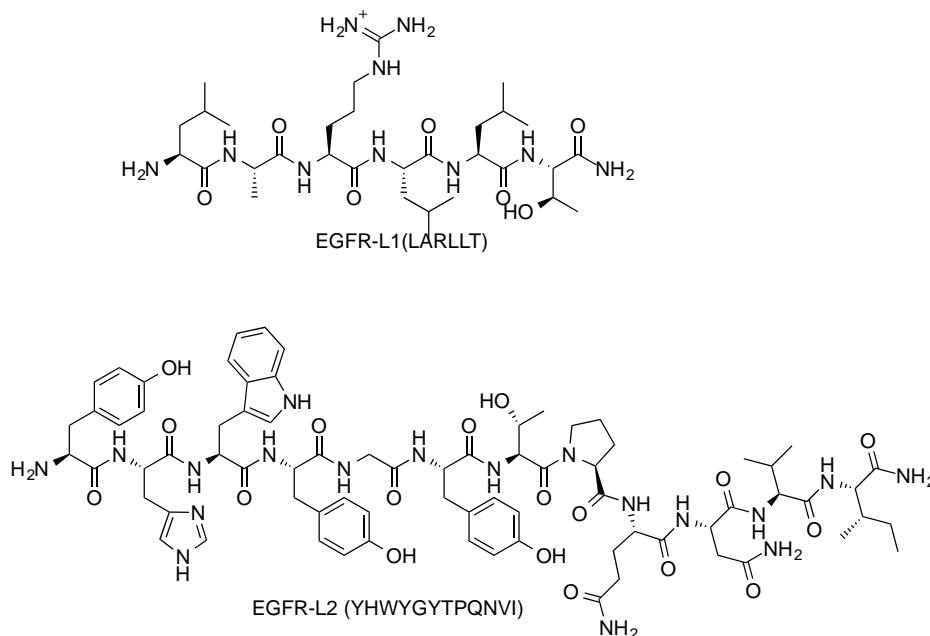


Figure 7. Structures of EGFR-L1 and EGFR-L2

## 1.5 BODIPY Dyes and Applications to *In Vivo* Imaging

### 1.5.1 Introduction to BODIPY Dyes

4,4-Difluoro-4-bora-3a,4a-diaza-s-indacenes, commonly known as BODIPYs are a group of small fluorescent dyes. BODIPY dyes were first synthesized by Treibs and Kreuzer in 1968 for use in their angiographic studies.<sup>81</sup> Conversely, BODIPY dyes did not gain extensive appreciation until the 1980s.<sup>81</sup> Today, BODIPY dyes have been extremely useful to scientists due to their versatility and stability as a fluorophore, as they inherently present exceptional photophysical properties.<sup>82</sup>

Structurally, BODIPY dyes possess a conjugated framework of  $\Pi$ -electrons, and are numbered using the indacene system (Figure 8). This framework is named dipyrromethene, and it is complexed with a boron difluoride salt.<sup>83</sup> The complexation of the boron difluoride salt and dipyrromethene is restricting in



structure causing minimal flexibility of the compound. This limited flexibility leads the dye to exhibit high fluorescence quantum yields.<sup>84</sup>

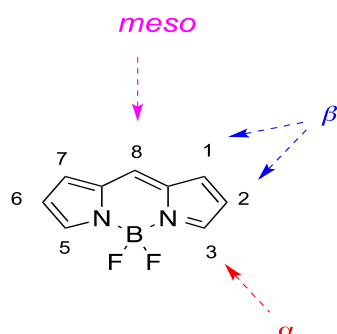


Figure 8. BODIPY core structure following the indacene numbering system.

The BODIPY core C-8 is termed the “*meso*-position,” while positions -1, -2, -6, and -7 are termed the “ $\beta$ -positions.” The “ $\alpha$ -“ positions are at C-3 and C-5.<sup>84</sup> BODIPY dyes are not only small cyclic UV-Vis absorbing molecules (507 nm), they emit in the Vis (520 nm), possess high quantum yields, and have reduced aggregation in aqueous media. BODIPYs are stable in physiological conditions, various pH, solvent, and polarity values. The BODIPY core can be functionalized to induce bathochromic (red) shifts in the optical spectrum, useful for bioimaging.<sup>84-85</sup> This alteration of the BODIPY core permits the opportunity for fluorescence tuning and introduction of water-soluble moieties, therefore these small molecules are useful in labeling proteins and DNA.<sup>82, 86</sup>

Normal absorption spectra of a BODIPY dye showcases a narrow and intense band due to S<sub>0</sub>-S<sub>1</sub> ( $\pi$ - $\pi^*$ ) transitions with a  $\lambda$  max between 500-525 nm, a shoulder peak is observed at high energy centered around  $480 \pm 5$  nm assigned to the 0-1 vibrational transition, and finally a very broad absorption band around  $375 \pm 5$  nm is attributed to the S<sub>0</sub>-S<sub>2</sub> ( $\pi$ - $\pi^*$ ) transition as a quite weak peak. Ideally, phosphorescence is a rare occurrence in BODIPY-based dyes due to negligible triplet energy state and a slow rate of intersystem crossing (except for one report due to heavy-atom effect of diiodoBODIPY).<sup>87</sup> To aid in increasing bathochromic shifts of the absorption bands into the NIR region, simplistic derivatives of the BODIPY core are desired. The photophysical characteristics of altered BODIPYs vary with respect to

the number, nature, as well as the position of the attached substituents.<sup>88</sup> Additionally, the emission behavior of BODIPY fluorophores are vastly dependent on the steric interactions between their components and intramolecular rotations of the BODIPY scaffold.<sup>89</sup> Ever-growing success of BODIPY dyes has inspired a large amount of investigations into the design, synthetic modifications, and spectroscopic/photophysical characterization of these bright small molecule fluorophores.

Current developments in various fields of science, have powered the creation of new fluorophores that can be excited to emit within the red or near-infrared (NIR) region of the spectrum.<sup>88</sup> This is in part attributed to the “biological window” (700-900 nm) of the spectrum involving minimal obstruction from endogenous chromophores, optimum penetration of tissue, and minimal damage to cells.<sup>90-93</sup> Current fluorophores can no longer work as mono-functional entities, whereas fluorophores are now called to be more flexible in the scope in which they are used. There are several classes of nonradioactive fluorophores that are used to date. For instance, the FDA approved fluorescein and rhodamine platforms, however BODIPY dyes have acquired much attention due to its platform versatility in synthesis and its smaller framework.<sup>82</sup>

### **1.5.2 The Early Years of BODIPY Dyes**

Treibs and Kreuzer were the first to synthesize a BODIPY dye, and ironically, the synthesis happened by accident. The group reacted 2,4-dimethylpyrrole with acetic anhydride in the presence of  $\text{BF}_3 \cdot \text{OEt}_2$  to create a green fluorescent BODIPY dye. The received dye was kindly denoted as “porphyrins little sister” and utilized as a tunable laser dye.<sup>83</sup> This iconic reaction afforded a mixture of mono- and di-acetylated BODIPY fluorophores. However in 1968, Treibs and Kreuzer’s worked pioneered the field of BODIPY dyes and revealed that the 2,6-positions on BODIPY chromophore are highly electron deficient, i.e. susceptible to electrophilic substitution reactions.<sup>81</sup> Throughout the mid- ‘90s studies have continually surfaced on the future applications of BODIPY dyes and the wondrous optical properties that can be easily tuned to meet a cascade of desired products. Methodology studies have suggested the synthesis of BODIPY dyes that entail bathochromic shifts and the use of BODIPYs as light-emitting devices,<sup>94</sup> drug delivery

devices,<sup>95</sup> fluorescent switches,<sup>96</sup> and pH switches,<sup>97</sup> solar cells,<sup>98</sup> and for labeling biomolecules for imaging.<sup>99</sup>

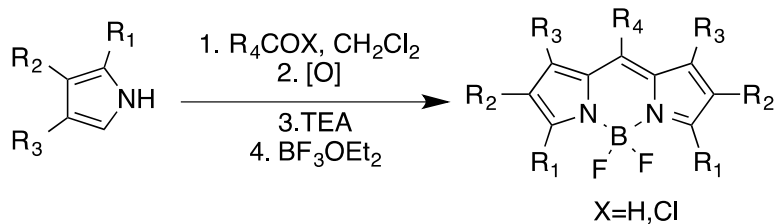
Founders of Life Technologies Inc., previously known as Molecular Probes, Haugland and Kang were heavy contributors to the world of BODIPY dyes in 1993.<sup>100-102</sup> Haugland and Kang were able to design various derivatives of BODIPYs ready for biomolecule conjugation or conjugated ready for testing. These findings helped the scientists to create over 80 United States patents and become the largest commercial supplier of BODIPY dyes and bioconjugates.<sup>100-102</sup>

### 1.5.3 BODIPY Synthetic Strategies

Typical methodology for BODIPY dyes is devised from pyrrole moieties that interact with electrophilic carbonyl compounds to create the desired dipyrromethene. This dipyrromethene is then complexed with a BF<sub>2</sub> source by deprotonating with a non-nucleophilic base such as a bulky secondary or tertiary amine to afford the BODIPY dye. The yields for these reactions are typically modest however reproducible.

#### 1.5.3.1 Symmetric BODIPY Synthesis

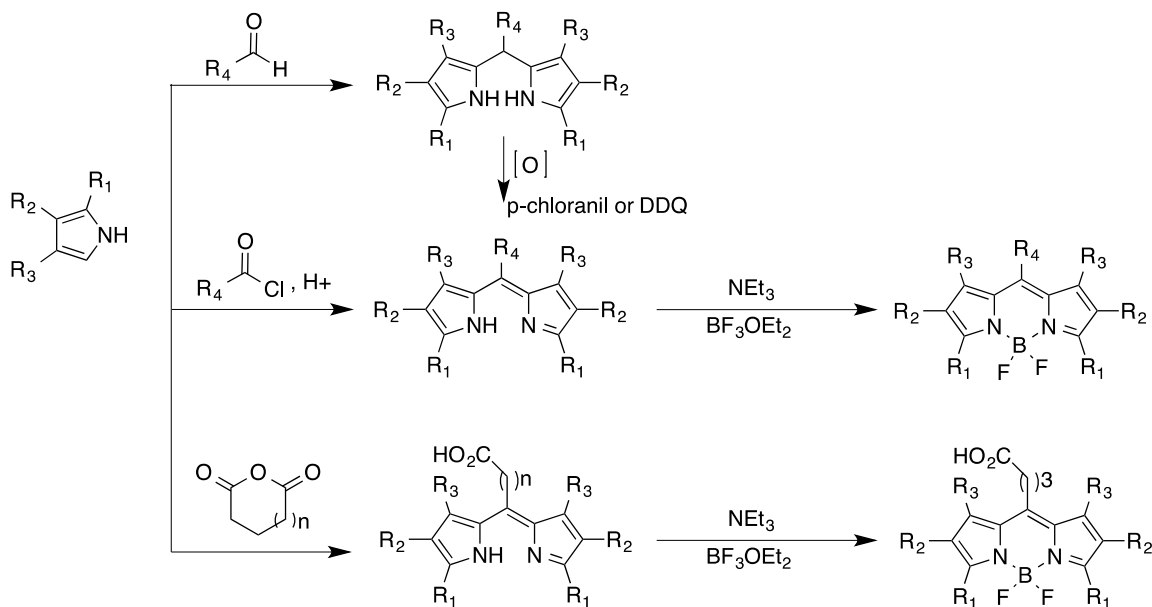
Synthesis of symmetric BODIPY dyes can allow for substitution at either position, however the most visited synthesis happens where the *meso*- or 8-position of the core is substituted. The symmetric synthesis is commonly prepared by acid-catalyzed condensation of pyrroles with acid chlorides, anhydrides or aldehydes to install the dipyrromethene (or dipyrromethanes from aldehydes which are subsequently oxidized). The corresponding dipyrromethene is then complexed using boron trifluoro-diethyl etherate in the presence of a bulky base that is non-nucleophilic, normally a tertiary amine base (Scheme 1). In order to prevent any polymerization of pyrrolic units, the pyrroles have to be protected by implications of substitution at the C-2 position.<sup>103</sup>



Scheme 1. General scheme of symmetric BODIPY synthesis.

This platform allows for the installation of various BODIPY dyes that can be further functionalized to meet several application measures. The apparent diversity of meso- substitution has developed a platform for building fluorophores that are capable of multiple purposes, such as labeling with biomolecules. BODIPY dyes with substituents at the meso-position may possess improved stability when compared to their meso-unsubstituted counterparts.

One common route for synthesis of symmetric BODIPY dyes is through the condensation of an aryl aldehyde that is combined with an excess (2 equiv.) of an  $\alpha$ -free pyrrole. Like the previous method, the corresponding dipyrromethane that is created must be oxidized to the dipyrromethene followed by complexation. Oxidation normally occurs when using an agent such as DDQ (2,3,-dichloro-5,6, dicyano-p-benzoquinone) or p-chloranil. The downfall of using oxidizing agents is the amount of side products that can be formed during dipyrromethene formation. These side products tend to be very difficult to remove through chromatography. However, the resulting complexed BODIPY provides an aryl moiety at the 8-position (Scheme 2).



Scheme 2. Methodology for the synthesis of symmetrical BODIPY via condensation of pyrroles with an activated carbonyl source.

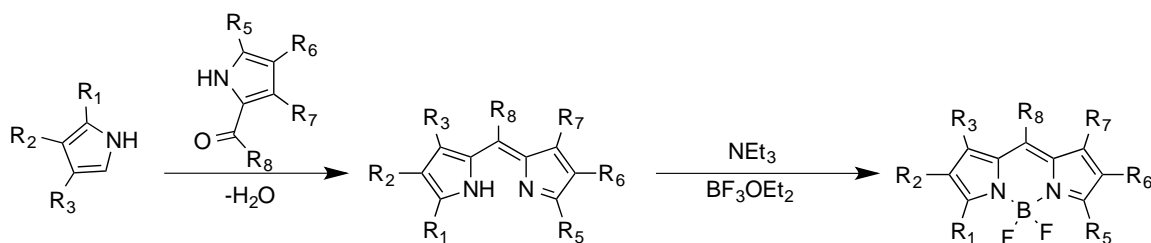
Another method of installing *meso*-substituted symmetrical BODIPY dyes is the condensation of acid chloride with free pyrroles. The condensation of acid chloride is quite different than that of aryl aldehyde as the synthesis goes straight to a dipyrromethene by passing the need for oxidizing agents. Elimination of the oxidizing agent aids in freeing the reaction of the byproducts associated with the oxidation yielding more of the desired compound (Scheme 2).

Symmetric BODIPY dyes unsubstituted at the *meso*-position are obtainable, and can be created by self-condensation of a desired pyrrole bearing a carbonyl and an  $\alpha$ -free pyrrole. However the use of an acid catalyst is necessary such as *p*-toluenesulfonic acid, Montmorillonite clay, and more recently phosphorous oxychloride.<sup>104-106</sup> This acidic environment aids in creating the carbonyl cation that is needed to condense with the second equivalent of  $\alpha$ -free pyrrole. The combination of these two portions creates the desired dipyrromethene that is later complexed.

### 1.5.3.2 Unsymmetrical BODIPY Synthesis

To synthesize the asymmetric BODIPY, the MacDonald coupling approach usually attains dyes, substituted or unsubstituted at the *meso*-position. The condensation of two different pyrroles as seen in

Woods and coworkers; where pyrrole-2-carbaldehyde and an  $\alpha$ -free pyrrole were condensed under an acidic catalyzed environment leading to the desired BODIPY dye.<sup>107</sup> The use of electron-deficient pyrroles tends to lead to the undesired product of a symmetric BODIPY, however, the use of electron rich pyrroles leads to the high yielding unsymmetrical product. After the acid condensation is complete, the anticipated dipyrromethene is generally isolated in its salt form subsequent complexation with  $\text{BF}_3 \cdot \text{OEt}_2$  affords the required BODIPY dye (Scheme 3). Unsymmetrical BODIPY dyes have a great advantage as the possibility to attach different functional moieties on the BODIPY scaffold for further derivatizing or bio-conjugation is endless.



Scheme 3. Generic synthesis of unsymmetrical BODIPY dyes

#### 1.5.4 BODIPY Dyes and Biolabeling

Fluorophores that are equipped to visualize and investigate the functions of biological materials such as proteins, enzymes, and living cells are highly desired. The necessity of a fluorescent molecule that is easily tuned to the desired labeled fluorescent probe has delivered BODIPY dyes to the foreground of fluorescent markers. The smaller size of the BODIPY core when compared to other fluorescent entities such as porphyrins is significant in allowing the dye to form bioconjugates without alteration of the components of the targeting molecule. Several reports have observed synthesis of bioconjugation between BODIPY dyes and targeting components such as amino acids and proteins.<sup>108</sup> To prepare conjugates, motifs are established via BODIPY dyes to connect the two. A more frequently used component is carboxylic acids, sulphonic acids, PEG moieties, polysaccharides, and oligonucleotides.<sup>81, 83</sup>

In recent years, BODIPY dyes have been shown to attach to extracellular proteins and DNA to create probes that are able to engage in living cells as labeling moieties. Some reports to date have observed

promising results in both single and two photon microscopy of living tissue.<sup>109</sup> Groups such as Wolfbeis and coworkers<sup>110</sup> suggested that biomolecules were conjugated to items such as sugars, amino acids, and nucleotides via a copper-free and copper-mediated cycloaddition. These BODIPY fluorophores bearing clickable alkynyl groups were created for labeling azide modified surface glycans of Chinese hamster ovary (CHO) cells. In the same manner, Vicente et al.<sup>111</sup> also suggested the conjugation of clickable BODIPY dyes to azide bearing carbohydrates and PEG linkers. These conjugates bearing either one or two styryl groups were tested in HEp2 cells, to determine their affinity.<sup>111</sup> Zhang and coworkers also aid in development of BODIPY bioconjugates by developing a C-C linkage between a tryptophan amino acid and the BODIPY dye spacer-free. The fluorescent antimicrobial peptides remain intact while incorporating a fluorogenic amino acid that has no effect on the specificity of the peptide sequence. The peptide sequence is still able to provide real-time imaging of fungal infection and enhance the fluorescence in hydrophobic microenvironments.

Although conjugation measures have proceeded, drawbacks still remain for bioconjugation of BODIPY dyes.<sup>112</sup> Of these drawbacks, in particular, relatively low wavelength absorption and emission maxima (around 500 nm),<sup>113</sup> small Stokes shifts, poor aqueous solubility, and lack of functional groups for conjugation to biological materials are of urgent concern.<sup>114</sup> These apparent drawbacks limit the scope of BODIPY fluorophores for various biomedical and bioanalytical applications, and require additional steps to achieve the desired fluorophore. Many of these problems are under attack in various research groups. The BODIPY core itself is essentially electron-rich and can be conveniently amended at various positions to analogues that span the entire visible spectrum and beyond.

## 1.6 Research Focus

Despite the varied developments released in BODIPY methodology, there is definitely more work to be done. The synthesis of BODIPY derivatives that exhibit bathochromic shifts in the NIR region and beneficial conjugation to various target biomolecules, represent an established challenge in the BODIPY

biomarker world. For instance, BODIPY bioconjugates that not only emit in the NIR but also possess a water-solubilizing moiety in the presence of targeting modules that are suitable for in vivo imaging are very few reports in literature. Current methods for CRC diagnosis, including different types of colonoscopy and radiography, have relatively low sensitivity for detection of small adenomas (< 5 mm) in the early stages of CRC, when it usually causes no outward symptoms in patients.<sup>115</sup> Therefore, the molecular targeting of EGFR over-expressed in CRC cells, especially during the early stages of cancer, is a valuable tool in CRC diagnosis and treatment.<sup>116</sup> Conscious of these issues, endeavors in the synthesis, characterization and in vitro evaluations of novel BODIPY bioconjugates will be discussed in the next chapters.

## 1.7 References

1. Sovich, J. L.; Sartor, Z.; Misra, S., Developments in Screening Tests and Strategies for Colorectal Cancer. *BioMed Research International* **2015**, *2015*, 326728.
2. Siegel, R. L.; Fedewa, S. A.; Anderson, W. F.; Miller, K. D.; Ma, J.; Rosenberg, P. S.; Jemal, A., Colorectal Cancer Incidence Patterns in the United States, 1974–2013. *JNCI: Journal of the National Cancer Institute* **2017**, *109* (8), djw322-djw322.
3. McTiernan, A., *Cancer prevention and management through exercise and weight control*. CRC Press: 2016.
4. Ryan-Harshman, M.; Aldoori, W., Diet and colorectal cancer Review of the evidence. *Canadian Family Physician* **2007**, *53* (11), 1913-1920.
5. Force, U. S. P. S. T., Screening for colorectal cancer: Us preventive services task force recommendation statement. *JAMA* **2016**, *315* (23), 2564-2575.
6. Vasen, H., Clinical diagnosis and management of hereditary colorectal cancer syndromes. *Journal of clinical oncology* **2000**, *18* (suppl 1), 81s-92s.
7. Hol, L.; Van Leerdam, M. E.; Van Ballegooijen, M.; Van Vuuren, A. J.; Van Dekken, H.; Reijerink, J. C.; Van der Togt, A. C.; Habbema, J.; Kuipers, E. J., Screening for colorectal cancer: randomised trial comparing guaiac-based and immunochemical faecal occult blood testing and flexible sigmoidoscopy. *Gut* **2010**, *59* (01), 62-68.



8. Patient Education Library. [http://www.prevention.md/sgdpc\\_patient\\_library\\_old.htm](http://www.prevention.md/sgdpc_patient_library_old.htm) (accessed April 17, 2017).
9. Benign Tumors. <http://www.webmd.com/a-to-z-guides/benign-tumors-causes-treatments#1> (accessed April 19,).
10. Odike, M. A. C.; Dongo, A. E.; Alufohai, E. F.; Odike, A. I., Colonic cancer in adolescents. A report of three cases. *Rare Tumors* **2009**, *1* (2), e34.
11. Bujanda, L.; Cosme, A.; Gil, I.; Arenas-Mirave, J. I., Malignant colorectal polyps. *World Journal of Gastroenterology : WJG* **2010**, *16* (25), 3103-3111.
12. Tests to Detect Colorectal Cancer and Polyps. <https://www.cancer.gov/types/colorectal/screening-fact-sheet> (accessed April 18).
13. Hoffman, A.; Goetz, M.; Vieth, M.; Galle, P. R.; Neurath, M. F.; Kiesslich, R., Confocal laser endomicroscopy: technical status and current indications. *Endoscopy* **2006**, *38* (12), 1275-1283.
14. Vachani, C. D., Gloria; Giantonio, Bruce J. Understanding Your Pathology Report: Colon Cancer. <http://www.oncolink.org/cancers/gastrointestinal/colon-cancer/treatments/understanding-your-pathology-report-colon-cancer> (accessed April 19,).
15. Burch, J. A.; Soares-Weiser, K.; John, D. J. B. S.; Duffy, S.; Smith, S.; Kleijnen, J.; Westwood, M., Diagnostic accuracy of faecal occult blood tests used in screening for colorectal cancer: a systematic review. *Journal of Medical Screening* **2007**, *14* (3), 132-137.
16. Levin, B.; Brooks, D.; Smith, R. A.; Stone, A., Emerging technologies in screening for colorectal cancer: CT colonography, immunochemical fecal occult blood tests, and stool screening using molecular markers. *CA: a cancer journal for clinicians* **2003**, *53* (1), 44-55.
17. Van Dam, J.; Bond, J. H.; Sivak, M. V., Fecal occult blood screening for colorectal cancer. *Archives of internal medicine* **1995**, *155* (22), 2389-2402.
18. Ouyang, D. L.; Chen, J. J.; Getzenberg, R. H.; Schoen, R. E., Noninvasive Testing for Colorectal Cancer: A Review. *Am J Gastroenterol* **2005**, *100* (6), 1393-1403.

19. van Ballegooijen, M.; Habbema, J. D. F.; Boer, R.; Zauber, A. G.; Brown, M. L., AHRQ Technology Assessments. In *A Comparison of the Cost-Effectiveness of Fecal Occult Blood Tests with Different Test Characteristics in the Context of Annual Screening in the Medicare Population*, Agency for Healthcare Research and Quality (US): Rockville (MD), 2003.
20. Phalguni, A.; Seaman, H.; Routh, K.; Halloran, S.; Simpson, S., Tests detecting biomarkers for screening of colorectal cancer: What is on the horizon? *GMS Health Technology Assessment* **2015**, *11*, Doc01.
21. Cappell, M. S., Reducing the incidence and mortality of colon cancer: mass screening and colonoscopic polypectomy. *Gastroenterology Clinics of North America* **2008**, *37* (1), 129-160.
22. Rex, D. K.; Bond, J. H.; Winawer, S.; Levin, T. R.; Burt, R. W.; Johnson, D. A.; Kirk, L. M.; Litlin, S.; Lieberman, D. A.; Wayne, J. D., Quality in the technical performance of colonoscopy and the continuous quality improvement process for colonoscopy: recommendations of the US Multi-Society Task Force on Colorectal Cancer. *The American journal of gastroenterology* **2002**, *97* (6), 1296.
23. Sonnenberg, A.; Delcò, F.; Bauerfeind, P., Is virtual colonoscopy a cost-effective option to screen for colorectal cancer? *The American journal of gastroenterology* **1999**, *94* (8), 2268-2274.
24. Ferrucci, J. T., Colon cancer screening with virtual colonoscopy: promise, polyps, politics. *American Journal of Roentgenology* **2001**, *177* (5), 975-988.
25. Svensson, M. H.; Svensson, E.; Lasso, A.; Hellström, M., Patient Acceptance of CT Colonography and Conventional Colonoscopy: Prospective Comparative Study in Patients with or Suspected of Having Colorectal Disease 1. *Radiology* **2002**, *222* (2), 337-345.
26. Hoffman, A.; Goetz, M.; Vieth, M.; Galle, P.; Neurath, M.; Kiesslich, R., Confocal laser endomicroscopy: technical status and current indications. *Endoscopy* **2006**, *38* (12), 1275-1283.
27. Chang, T. C.; Liu, J.-J.; Liao, J. C., Probe-based confocal laser endomicroscopy of the urinary tract: the technique. *JoVE (Journal of Visualized Experiments)* **2013**, (71), e4409-e4409.
28. Liu, J.-J.; Droller, M. J.; Liao, J. C., New optical imaging technologies for bladder cancer: considerations and perspectives. *The Journal of urology* **2012**, *188* (2), 361-368.

29. Herbst, R. S., Review of epidermal growth factor receptor biology. *International Journal of Radiation Oncology\* Biology\* Physics* **2004**, 59 (2), S21-S26.
30. Kiesslich, R.; Burg, J.; Vieth, M.; Gnaendiger, J.; Enders, M.; Delaney, P.; Polglase, A.; McLaren, W.; Janell, D.; Thomas, S., Confocal laser endoscopy for diagnosing intraepithelial neoplasias and colorectal cancer in vivo. *Gastroenterology* **2004**, 127 (3), 706-713.
31. Dolmans, D. E.; Fukumura, D.; Jain, R. K., Photodynamic therapy for cancer. *Nature reviews cancer* **2003**, 3 (5), 380-387.
32. Celli, J. P.; Spring, B. Q.; Rizvi, I.; Evans, C. L.; Samkoe, K. S.; Verma, S.; Pogue, B. W.; Hasan, T., Imaging and Photodynamic Therapy: Mechanisms, Monitoring and Optimization. *Chemical reviews* **2010**, 110 (5), 2795-2838.
33. Dougherty, T. J.; Gomer, C. J.; Henderson, B. W.; Jori, G.; Kessel, D.; Korblik, M.; Moan, J.; Peng, Q., Photodynamic Therapy. *Journal of the National Cancer Institute* **1998**, 90 (12), 889-905.
34. MACDONALD, I. J.; DOUGHERTY, T. J., Basic principles of photodynamic therapy. *Journal of Porphyrins and Phthalocyanines* **2001**, 05 (02), 105-129.
35. Castano, A. P.; Mroz, P.; Hamblin, M. R., Photodynamic therapy and anti-tumour immunity. *Nature reviews. Cancer* **2006**, 6 (7), 535-545.
36. Brown, S. B.; Brown, E. A.; Walker, I., The present and future role of photodynamic therapy in cancer treatment. *The Lancet Oncology* **2004**, 5 (8), 497-508.
37. Lipson, R. L.; Baldes, E. J.; Olsen, A. M., The use of a derivative of hematoporphyrin in tumor detection. *Journal of the National Cancer Institute* **1961**, 26, 1-11.
38. Razum, N.; Balchum, O. J.; Profio, A. E.; Carstens, F., SKIN PHOTSENSITIVITY: DURATION and INTENSITY FOLLOWING INTRAVENOUS HEMATOPORPHYRIN DERIVATES, HpD and DHE. *Photochemistry and Photobiology* **1987**, 46 (5), 925-928.
39. Gilson, D.; Ash, D.; Driver, I.; Feather, J. W.; Brown, S., Therapeutic ratio of photodynamic therapy in the treatment of superficial tumours of skin and subcutaneous tissues in man. *British Journal of Cancer* **1988**, 58 (5), 665-667.

40. Barth, R. F.; Coderre, J. A.; Vicente, M. G. H.; Blue, T. E., Boron Neutron Capture Therapy of Cancer: Current Status and Future Prospects. *Clinical Cancer Research* **2005**, *11* (11), 3987-4002.
41. Josefsen, L. B.; Boyle, R. W., Photodynamic therapy: novel third-generation photosensitizers one step closer? *British Journal of Pharmacology* **2008**, *154* (1), 1-3.
42. Chatterjee, D. K.; Fong, L. S.; Zhang, Y., Nanoparticles in photodynamic therapy: An emerging paradigm. *Advanced Drug Delivery Reviews* **2008**, *60* (15), 1627-1637.
43. Konan, Y. N.; Gurny, R.; Allémann, E., State of the art in the delivery of photosensitizers for photodynamic therapy. *Journal of Photochemistry and Photobiology B: Biology* **2002**, *66* (2), 89-106.
44. Hamblin, M. R.; O'donnell, D. A.; Murthy, N.; Rajagopalan, K.; Michaud, N.; Sherwood, M. E.; Hasan, T., Polycationic photosensitizer conjugates: effects of chain length and Gram classification on the photodynamic inactivation of bacteria. *Journal of Antimicrobial Chemotherapy* **2002**, *49* (6), 941-951.
45. Zheng, G.; Graham, A.; Shibata, M.; Missert, J. R.; Oseroff, A. R.; Dougherty, T. J.; Pandey, R. K., Synthesis of  $\beta$ -galactose-conjugated chlorins derived by enyne metathesis as galectin-specific photosensitizers for photodynamic therapy. *The Journal of organic chemistry* **2001**, *66* (26), 8709-8716.
46. Ullman, E. F.; Singh, R.; De Keczer, S.; Davalian, D., Amplified signal in binding assays. Google Patents: 2009.
47. Li, G.; Pandey, S. K.; Graham, A.; Dobhal, M. P.; Mehta, R.; Chen, Y.; Gryshuk, A.; Rittenhouse-Olson, K.; Oseroff, A.; Pandey, R. K., Functionalization of OEP-Based Benzochlorins To Develop Carbohydrate-Conjugated Photosensitizers. Attempt To Target  $\beta$ -Galactoside-Recognized Proteins $\pm$ . *The Journal of organic chemistry* **2004**, *69* (1), 158-172.
48. Rahimipour, S.; Ben-Aroya, N.; Ziv, K.; Chen, A.; Fridkin, M.; Koch, Y., Receptor-mediated targeting of a photosensitizer by its conjugation to gonadotropin-releasing hormone analogues. *Journal of medicinal chemistry* **2003**, *46* (19), 3965-3974.
49. Tirand, L.; Thomas, N.; Dodeller, M.; Dumas, D.; Frochot, C.; Maunit, B.; Guillemin, F.; Barberi-Heyob, M., Metabolic profile of a peptide-conjugated chlorin-type photosensitizer targeting neuropilin-1: an in vivo and in vitro study. *Drug metabolism and disposition* **2007**, *35* (5), 806-813.

50. Tomas, A.; Futter, C. E.; Eden, E. R., EGF receptor trafficking: consequences for signaling and cancer. *Trends Cell Biol.* **2014**, *24* (1), 26-34.
51. Yewale, C.; Baradia, D.; Vhora, I.; Patil, S.; Misra, A., Epidermal growth factor receptor targeting in cancer: A review of trends and strategies. *Biomaterials* **2013**, *34* (34), 8690-8707.
52. Hynes, N. E.; Lane, H. A., ERBB receptors and cancer: the complexity of targeted inhibitors. *Nat. Rev. Cancer* **2005**, *5* (5), 341-354.
53. Burgess, A. W.; Cho, H.-S.; Eigenbrot, C.; Ferguson, K. M.; Garrett, T. P. J.; Leahy, D. J.; Lemmon, M. A.; Sliwkowski, M. X.; Ward, C. W.; Yokoyama, S., An Open-and-Shut Case? Recent Insights into the Activation of EGF/ErbB Receptors. *Mol. Cell* **2003**, *12* (3), 541-552.
54. Yarden, Y.; Sliwkowski, M. X., Untangling the ErbB signalling network. *Nature reviews Molecular cell biology* **2001**, *2* (2), 127-137.
55. Dawson, J. P.; Berger, M. B.; Lin, C.-C.; Schlessinger, J.; Lemmon, M. A.; Ferguson, K. M., Epidermal Growth Factor Receptor Dimerization and Activation Require Ligand-Induced Conformational Changes in the Dimer Interface. *Molecular and Cellular Biology* **2005**, *25* (17), 7734-7742.
56. Kondapaka, S. B.; Fridman, R.; Reddy, K. B., Epidermal growth factor and amphiregulin up-regulate matrix metalloproteinase-9 (MMP-9) in human breast cancer cells. *International journal of cancer* **1997**, *70* (6), 722-726.
57. Epidermal Growth Factor.  
[https://en.wikipedia.org/wiki/Epidermal\\_growth\\_factor\\_receptor](https://en.wikipedia.org/wiki/Epidermal_growth_factor_receptor) (accessed April 19,).
58. Harris, R. C.; Chung, E.; Coffey, R. J., EGF receptor ligands. *The EGF receptor family biologic mechanisms and role in cancer. Elsevier, California* **2004**, 3-14.
59. Li, Z.; Zhao, R.; Wu, X.; Sun, Y.; Yao, M.; Li, J.; Xu, Y.; Gu, J., Identification and characterization of a novel peptide ligand of epidermal growth factor receptor for targeted delivery of therapeutics. *The FASEB Journal* **2005**, *19* (14), 1978-1985.
60. Woodburn, J., The epidermal growth factor receptor and its inhibition in cancer therapy. *Pharmacology & therapeutics* **1999**, *82* (2), 241-250.

61. Michael, S.; Hong, J.; Curiel, D.; Engler, J., Addition of a short peptide ligand to the adenovirus fiber protein. *Gene therapy* **1995**, *2* (9), 660-668.
62. Song, S.; Liu, D.; Peng, J.; Deng, H.; Guo, Y.; Xu, L. X.; Miller, A. D.; Xu, Y., Novel peptide ligand directs liposomes toward EGF-R high-expressing cancer cells in vitro and in vivo. *The FASEB Journal* **2009**, *23* (5), 1396-1404.
63. Oda, K.; Matsuoka, Y.; Funahashi, A.; Kitano, H., A comprehensive pathway map of epidermal growth factor receptor signaling. *Molecular systems biology* **2005**, *1* (1).
64. Sako, Y.; Minoghchi, S.; Yanagida, T., Single-molecule imaging of EGFR signalling on the surface of living cells. *Nature cell biology* **2000**, *2* (3), 168-172.
65. Bhirde, A. A.; Patel, V.; Gavard, J.; Zhang, G.; Sousa, A. A.; Masedunskas, A.; Leapman, R. D.; Weigert, R.; Gutkind, J. S.; Rusling, J. F., Targeted Killing of Cancer Cells in Vivo and in Vitro with EGF-Directed Carbon Nanotube-Based Drug Delivery. *ACS Nano* **2009**, *3* (2), 307-316.
66. Patra, C. R.; Bhattacharya, R.; Wang, E.; Katarya, A.; Lau, J. S.; Dutta, S.; Muders, M.; Wang, S.; Buhrow, S. A.; Safgren, S. L.; Yaszemski, M. J.; Reid, J. M.; Ames, M. M.; Mukherjee, P.; Mukhopadhyay, D., Targeted Delivery of Gemcitabine to Pancreatic Adenocarcinoma Using Cetuximab as a Targeting Agent. *Cancer Res.* **2008**, *68* (6), 1970-1978.
67. Saki, M.; Toulany, M.; Sihver, W.; Zenker, M.; Heldt, J.-M.; Mosch, B.; Pietzsch, H.-J.; Baumann, M.; Steinbach, J.; Rodemann, H. P., Cellular and molecular properties of 90Y-labeled cetuximab in combination with radiotherapy on human tumor cells in vitro. *Strahlentherapie und Onkologie* **2012**, *188* (9), 823-832.
68. Leonidova, A.; Foerster, C.; Zarschler, K.; Schubert, M.; Pietzsch, H.-J.; Steinbach, J.; Bergmann, R.; Metzler-Nolte, N.; Stephan, H.; Gasser, G., In vivo demonstration of an active tumor pretargeting approach with peptide nucleic acid bioconjugates as complementary system. *Chemical Science* **2015**, *6* (10), 5601-5616.
69. Yang, L.; Mao, H.; Wang, Y. A.; Cao, Z.; Peng, X.; Wang, X.; Duan, H.; Ni, C.; Yuan, Q.; Adams, G.; Smith, M. Q.; Wood, W. C.; Gao, X.; Nie, S., Single Chain Epidermal Growth Factor Receptor Antibody Conjugated Nanoparticles for in vivo Tumor Targeting and Imaging. *Small* **2009**, *5* (2), 235-243.

70. Sexton, K.; Tichauer, K.; Samkoe, K. S.; Gunn, J.; Hoopes, P. J.; Pogue, B. W., Fluorescent Affibody Peptide Penetration in Glioma Margin Is Superior to Full Antibody. *PLoS ONE* **2013**, *8* (4), e60390.
71. Nordberg, E.; Friedman, M.; Göstring, L.; Adams, G. P.; Brismar, H.; Nilsson, F. Y.; Ståhl, S.; Glimelius, B.; Carlsson, J., Cellular studies of binding, internalization and retention of a radiolabeled EGFR-binding affibody molecule. *Nuclear Medicine and Biology* **2007**, *34* (6), 609-618.
72. Bell, A.; Wang, Z. J.; Arbabi-Ghahroudi, M.; Chang, T. A.; Durocher, Y.; Trojahn, U.; Baardsnes, J.; Jaramillo, M. L.; Li, S.; Baral, T. N.; O'Connor-McCourt, M.; MacKenzie, R.; Zhang, J., Differential tumor-targeting abilities of three single-domain antibody formats. *Cancer Lett.* **2010**, *289* (1), 81-90.
73. Mickler, F. M.; Möckl, L.; Ruthardt, N.; Ogris, M.; Wagner, E.; Bräuchle, C., Tuning Nanoparticle Uptake: Live-Cell Imaging Reveals Two Distinct Endocytosis Mechanisms Mediated by Natural and Artificial EGFR Targeting Ligand. *Nano Lett.* **2012**, *12* (7), 3417-3423.
74. Chariou, P. L.; Lee, K. L.; Wen, A. M.; Gulati, N. M.; Stewart, P. L.; Steinmetz, N. F., Detection and Imaging of Aggressive Cancer Cells Using an Epidermal Growth Factor Receptor (EGFR)-Targeted Filamentous Plant Virus-Based Nanoparticle. *Bioconjugate Chem.* **2015**, *26* (2), 262-269.
75. Zarschler, K.; Prapainop, K.; Mahon, E.; Rocks, L.; Bramini, M.; Kelly, P. M.; Stephan, H.; Dawson, K. A., Diagnostic nanoparticle targeting of the EGF-receptor in complex biological conditions using single-domain antibodies. *Nanoscale* **2014**, *6* (11), 6046-6056.
76. Ongarora, B. G.; Fontenot, K. R.; Hu, X.; Sehgal, I.; Satyanarayana-Jois, S. D.; Vicente, M. G. H., Phthalocyanine–Peptide Conjugates for Epidermal Growth Factor Receptor Targeting. *J. Med. Chem.* **2012**, *55* (8), 3725-3738.
77. Song, S.; Liu, D.; Peng, J.; Sun, Y.; Li, Z.; Gu, J.-R.; Xu, Y., Peptide ligand-mediated liposome distribution and targeting to EGFR expressing tumor in vivo. *Int. J. Pharm.* **2008**, *363* (1–2), 155-161.
78. Bröring, M.; Köhler, S.; Kleeberg, C., Norcorrole: Observation of the Smallest Porphyrin Variant with a N4 Core. *Angew. Chem. Int. Ed.* **2008**, *47* (30), 5658-5660.
79. Viehweger, K.; Barbaro, L.; García, K. P.; Joshi, T.; Geipel, G.; Steinbach, J.; Stephan, H.; Spiccia, L.; Graham, B., EGF Receptor-Targeting Peptide Conjugate Incorporating a Near-IR

Fluorescent Dye and a Novel 1,4,7-Triazacyclononane-Based  $^{64}\text{Cu}(\text{II})$  Chelator Assembled via Click Chemistry. *Bioconjugate Chem.* **2014**, *25* (5), 1011-1022.

80. Banappagari, S.; McCall, A.; Fontenot, K.; Vicente, M. G. H.; Gujar, A.; Satyanarayanajois, S., Design, synthesis and characterization of peptidomimetic conjugate of BODIPY targeting HER2 protein extracellular domain. *European Journal of Medicinal Chemistry* **2013**, *65*, 60-69.
81. Loudet, A.; Burgess, K., BODIPY dyes and their derivatives: syntheses and spectroscopic properties. *Chemical reviews* **2007**, *107* (11), 4891-4932.
82. Ulrich, G.; Ziessel, R.; Harriman, A., The chemistry of fluorescent bodipy dyes: versatility unsurpassed. *Angewandte Chemie International Edition* **2008**, *47* (7), 1184-1201.
83. Ziessel, R.; Ulrich, G.; Harriman, A., The chemistry of Bodipy: a new El Dorado for fluorescence tools. *New Journal of Chemistry* **2007**, *31* (4), 496-501.
84. Zheng, Q.; Xu, G.; Prasad, P. N., Conformationally restricted dipyrromethene boron difluoride (BODIPY) dyes: highly fluorescent, multicolored probes for cellular imaging. *Chemistry-a European Journal* **2008**, *14* (19), 5812-5819.
85. Ziessel, R.; Ulrich, G.; Harriman, A.; Alamiry, M. A.; Stewart, B.; Retailleau, P., Solid - State Gas Sensors Developed from Functional Difluoroboradiazaindacene Dyes. *Chemistry-A European Journal* **2009**, *15* (6), 1359-1369.
86. Karolin, J.; Johansson, L.; Strandberg, L.; Ny, T., Fluorescence and absorption spectroscopic properties of dipyrrometheneboron difluoride (BODIPY) derivatives in liquids, lipid-membranes, and proteins. *Journal of the American Chemical Society* **1994**, *116* (17), 7801-7806.
87. Yogo, T.; Urano, Y.; Ishitsuka, Y.; Maniwa, F.; Nagano, T., Highly efficient and photostable photosensitizer based on BODIPY chromophore. *Journal of the American Chemical Society* **2005**, *127* (35), 12162-12163.
88. Boens, N.; Leen, V.; Dehaen, W., Fluorescent indicators based on BODIPY. *Chemical Society Reviews* **2012**, *41* (3), 1130-1172.
89. Kowada, T.; Yamaguchi, S.; Ohe, K., Highly fluorescent BODIPY dyes modulated with spirofluorene moieties. *Organic letters* **2009**, *12* (2), 296-299.



90. Escobedo, J. O.; Rusin, O.; Lim, S.; Strongin, R. M., NIR dyes for bioimaging applications. *Current opinion in chemical biology* **2010**, *14* (1), 64-70.
91. Ntziachristos, V.; Bremer, C.; Weissleder, R., Fluorescence imaging with near-infrared light: new technological advances that enable in vivo molecular imaging. *European radiology* **2003**, *13* (1), 195-208.
92. Amiot, C. L.; Xu, S.; Liang, S.; Pan, L.; Zhao, J. X., Near-infrared fluorescent materials for sensing of biological targets. *Sensors* **2008**, *8* (5), 3082-3105.
93. Niu, S. L.; Massif, C.; Ulrich, G.; Ziessel, R.; Renard, P.-Y.; Romieu, A., Water-solubilisation and bio-conjugation of a red-emitting BODIPY marker. *Organic & biomolecular chemistry* **2011**, *9* (1), 66-69.
94. Liras, M.; Iglesias, M.; Sánchez, F., Conjugated microporous polymers incorporating BODIPY moieties as light-emitting materials and recyclable visible-light photocatalysts. *Macromolecules* **2016**, *49* (5), 1666-1673.
95. Quan, L.; Liu, S.; Sun, T.; Guan, X.; Lin, W.; Xie, Z.; Huang, Y.; Wang, Y.; Jing, X., Near-infrared emitting fluorescent BODIPY nanovesicles for in vivo molecular imaging and drug delivery. *ACS applied materials & interfaces* **2014**, *6* (18), 16166-16173.
96. Yin, S.; Leen, V.; Van Snick, S.; Boens, N.; Dehaen, W., A highly sensitive, selective, colorimetric and near-infrared fluorescent turn-on chemosensor for Cu<sup>2+</sup> based on BODIPY. *Chemical Communications* **2010**, *46* (34), 6329-6331.
97. Baruah, M.; Qin, W.; Basarić, N.; De Borggraeve, W. M.; Boens, N., BODIPY-based hydroxyaryl derivatives as fluorescent pH probes. *The Journal of organic chemistry* **2005**, *70* (10), 4152-4157.
98. Erten-Ela, S.; Yilmaz, M. D.; Icli, B.; Dede, Y.; Icli, S.; Akkaya, E. U., A panchromatic boradiazaindacene (BODIPY) sensitizer for dye-sensitized solar cells. *Organic letters* **2008**, *10* (15), 3299-3302.
99. Kowada, T.; Maeda, H.; Kikuchi, K., BODIPY-based probes for the fluorescence imaging of biomolecules in living cells. *Chemical Society Reviews* **2015**, *44* (14), 4953-4972.
100. Haugland, R. P.; Kang, H. C., Long wavelength heteroaryl-substituted dipyrrometheneboron difluoride dyes. Google Patents: 1993.

101. Kang, H. C.; Haugland, R. P., Ethenyl-substituted dipyrrometheneboron difluoride dyes and their synthesis. Google Patents: 1993.
102. Kang, H. C.; Haugland, R. P., Long wavelength chemically reactive dipyrrometheneboron difluoride dyes and conjugates. Google Patents: 1993.
103. Goud, T. V.; Tutar, A.; Biellmann, J.-F., Synthesis of 8-heteroatom-substituted 4, 4-difluoro-4-bora-3a, 4a-diaza-s-indacene dyes (BODIPY). *Tetrahedron* **2006**, *62* (21), 5084-5091.
104. Jackson, A. H.; Pandey, R. K.; Rao, K. N.; Roberts, E., Reactions on solid supports part II: a convenient method for synthesis of pyrromethanes using a montmorillonite clay as catalyst. *Tetrahedron letters* **1985**, *26* (6), 793-796.
105. Bari, S. E.; Iturraspe, J.; Frydman, B., Synthesis of biliverdins with stable extended conformations. Part II. *Tetrahedron* **1995**, *51* (8), 2255-2266.
106. Wu, L.; Burgess, K., A new synthesis of symmetric boraindacene (BODIPY) dyes. *Chemical Communications* **2008**, (40), 4933-4935.
107. Wood, T. E.; Thompson, A., Advances in the chemistry of dipyrins and their complexes. *Chemical reviews* **2007**, *107* (5), 1831-1861.
108. Hermanson, G. T., *Bioconjugate techniques*. Academic press: 2013.
109. Zhang, D.; Wang, Y.; Xiao, Y.; Qian, S.; Qian, X., Long-wavelength boradiazaindacene derivatives with two-photon absorption activity and strong emission: versatile candidates for biological imaging applications. *Tetrahedron* **2009**, *65* (39), 8099-8103.
110. Kele, P.; Li, X.; Link, M.; Nagy, K.; Herner, A.; Lőrincz, K.; Béni, S.; Wolfbeis, O. S., Clickable fluorophores for biological labeling—with or without copper. *Organic & biomolecular chemistry* **2009**, *7* (17), 3486-3490.
111. Uppal, T.; Bhupathiraju, N. D. K.; Vicente, M. G. H., Synthesis and cellular properties of Near-IR BODIPY-PEG and carbohydrate conjugates. *Tetrahedron* **2013**, *69* (23), 4687-4693.
112. Hein, C. D.; Liu, X.-M.; Wang, D., Click chemistry, a powerful tool for pharmaceutical sciences. *Pharmaceutical research* **2008**, *25* (10), 2216-2230.

113. Umezawa, K.; Matsui, A.; Nakamura, Y.; Citterio, D.; Suzuki, K., Bright, color - tunable fluorescent dyes in the Vis/NIR region: establishment of new “tailor - made” multicolor fluorophores based on borondipyrromethene. *Chemistry–A European Journal* **2009**, *15* (5), 1096-1106.
114. Li, L.; Han, J.; Nguyen, B.; Burgess, K., Syntheses and spectral properties of functionalized, water-soluble BODIPY derivatives. *The Journal of organic chemistry* **2008**, *73* (5), 1963-1970.
115. Kiesslich, R.; Goetz, M.; Vieth, M.; Galle, P. R.; Neurath, M. F., Technology Insight: confocal laser endoscopy for in vivo diagnosis of colorectal cancer. *Nat. Clin. Prac. Oncol.* **2007**, *4* (8), 480-490.
116. Hudson, R.; Boyle, R. W., Strategies for selective delivery of photodynamic sensitizers to biological targets. *J. Porphyrins Phthalocyanines* **2004**, *08* (07), 954-975.

## CHAPTER 2. Design and Synthetic Strategies for Peptides that Target EGFR

### 2.1 Introduction to EGFR-L1 and EGFR-L2

Several studies have suggested various replacements for EGFR's endogenous ligands. Replacements such as antibodies, proteins, and peptides are often considered when searching for targeting tools of EGFR. Of the aforementioned list of possibilities, peptides have shown prominent interest among the community because they are readily diffusible, have low immunogenicity, and are easy to incorporate into imaging devices.<sup>1</sup>

To improve current detection methods for CRC two peptides were developed by Li and Song to target EGFR with high binding affinity.<sup>2,3</sup> Li and Song investigation included two expenditures towards prominent EGFR selectivity. One method employed was the use of computer-aided designs that were screened against an X-ray crystal structure of EGFR *in silico* and tested through *in vitro* and *in vivo* studies.<sup>3</sup> As a result EGFR-L1 (LARLLT) a six-member amino acid sequence was selected (Figure 1). Screening phage display libraries discovered a second peptide. The resulting enriched phage clone gave an encoding of amino acids YHWYGYTPQNVI, also known as EGFR-L2 (Figure 2).<sup>2</sup>

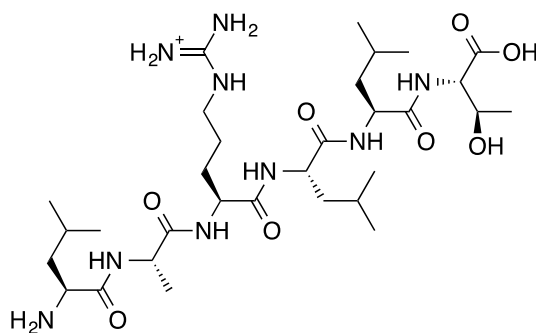


Figure 1. Peptide ligand structure EGFR-L1 (LARLLT).

Peptides are compounds comprised of several amino acids that are connected through amide bonds. Peptides in particular are an extremely striking source due to their relative small size, low immunogenicity, ease of conjugation, comparative ease of synthesis, ready availability, and more importantly high binding affinity.<sup>4</sup>

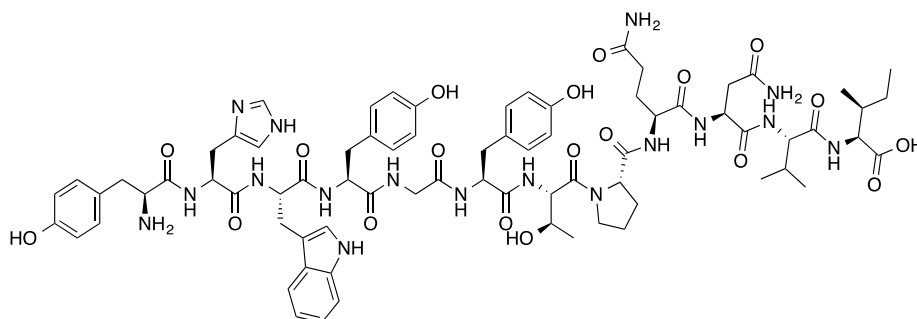


Figure 2. Peptide ligand structure EGFR-L2 (YHWYGYTPQNVI).

The efficient cell penetration of peptides, selective binding ability, and low toxic behavior makes peptides a focal point in areas such as *in vivo* imaging and photosensitizer-biomolecule conjugation for PDT. Peptides are easily modified to use for imaging.<sup>5</sup>

Peptides found through screening of phage display peptide libraries, or virtual peptide libraries as seen in Li and Song's work behave as an antagonist for the targeted receptor.<sup>2-3</sup> Peptide targeting is an extreme benefit for *in vivo* studies especially in certain tumor cases such as glioblastomas. Peptide application is a growing area with endless possibilities. Select peptides have been developed to act as ligands for different receptors or cell lines. This essential application is advantageous as it provides a way to selectively target specific receptor sites. Developing imaging probes based upon peptides as the targeting molecule will ensure the final receptor destination is met.

## 2.2 Results and Discussion

Peptide chemistry is a valuable asset of organic chemistry that employs the conjugation of multiple amino acids via an amide linkage or peptide bond. Peptides are synthesized by the union of a free carboxyl group of one amino acid to the amino group of another amino acid molecule. Peptides are normally translated from left to right. The beginning of a peptide sequence is normally the N-terminus or where the amino acid has a free or protected amino group. The C-terminus is where the carboxyl group is normally located (Figure 3). To develop the functionality of the C-terminus specific resin supports are chosen in solid phase peptide synthesis (SPPS), and initial amino acids are chosen for solution phase peptide synthesis. Due to the opportunity of side reactions, protecting groups are usually necessary.<sup>6</sup> While peptides are read

from N-terminus to C-terminus, synthesizing peptide sequences tend to begin at the C-terminus or carboxyl end of the peptide, and proceeds toward the N-terminus.

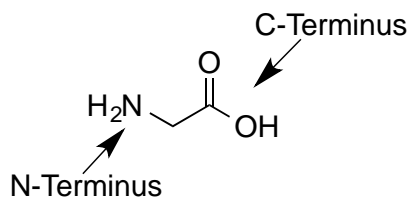


Figure 3. Glycine Amino Acid termini.

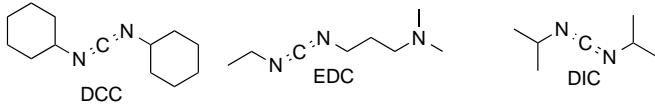
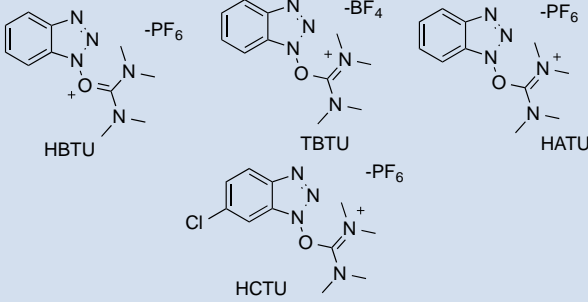
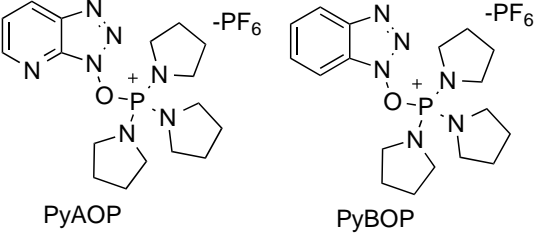
In peptide chemistry the use of coupling agents and coupling additives are the most efficient routes. To date the most commonly used coupling agents vary, however they all fall under three types: carbodiimides, phosphonium, and aminiums (Table 1).<sup>7-10</sup> Over time carbodiimides have been used as activators in SPPS, and have remained relevant. However in current years coupling agents phosphonium and aminium reagents have attracted more interest (Table 1). Each class of coupling agents has distinct methods of creating the amide bond, however in the presence of additives they work together to minimize the amount of racemization that may occur. An example of a suitable coupling additive used to date is hydroxybenzotriazole (HOBT) and its chlorinated counterpart (Cl-HOBT) which together fall under the class of OBt active esters.

SPPS has become a favorite method for producing peptide sequences particularly sequences that consist of 4 or more amino acids. The method first discovered by Merrifield<sup>11</sup>, provides ease of removal of side products by rinsing after coupling, and the simplicity of addition of amino acids.<sup>11</sup> Normally, when synthesizing peptides by SPPS Fmoc protecting methods are usually applied.<sup>11</sup> Fmoc chemistry allows for successful conjugation of amino acids through the C-terminus to N-terminus. A Fmoc-Pal-PEG resin is used to yield an amide at the C-terminus when synthesizing peptides EGFR-L1 and EGFR-L2. To complete the desired sequences, the amino acids were selected purchased from AAPTEC. These amino acids were chosen with certain side chain protecting groups to prevent alternative reactions from occurring.

### 2.2.1 BT-SPPS of EGFR-L1 and EGFR-L2

EGFR-L1 and EGFR-L2 were synthesized using two techniques of SPPS, Microwave SPPS (MW-SPPS) and Bench-top or Normal phase SPPS (BT-SPPS). In both methods a Fmoc-Pal-PEG resin was then allowed to swell in dimethylformamide (DMF). Resin expansion is particularly important, as it will allow for maximum coverage of resin beads for amino acids to follow.

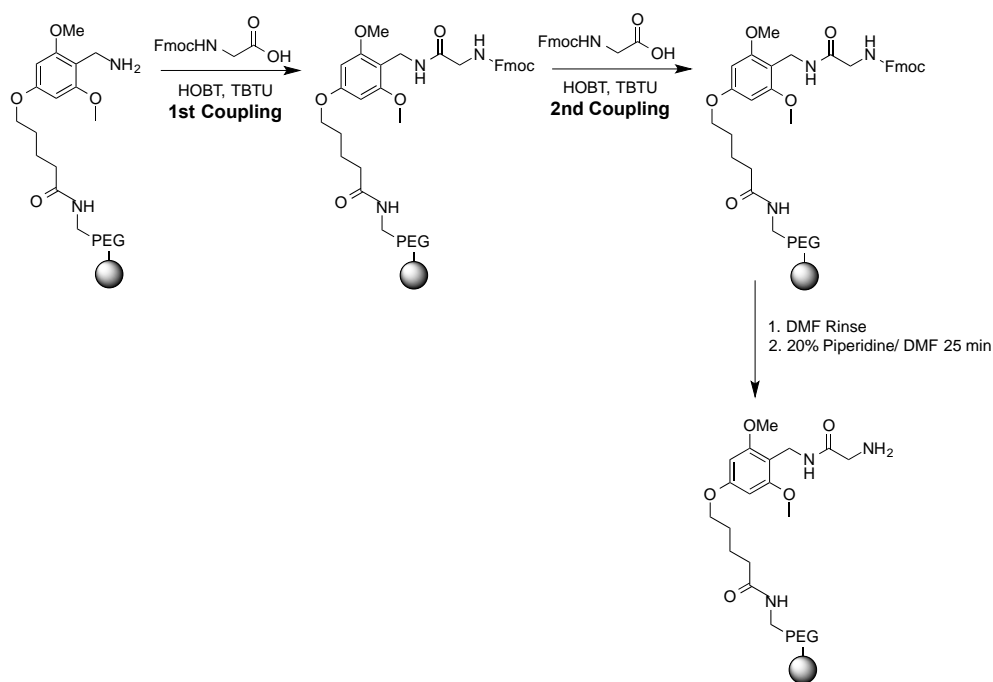
**Table 1: Solid Phase Peptide Synthesis (SPPS) Common Coupling Agents**

| Coupling Class | Structures   |
|----------------|--|
| Carbodiimide   |    |
| Aminium        |   |
| Phosphonium    |  |

After expanding the resin beads, a wash cycle with DMF, the first amino acid is allowed to double couple. Double coupling is a procedure where the first amino acid of each sequence is introduced to the resin beads in the presence of coupling agents TBTU and additive HOBT in a DIEA/DMF solution. After this addition is complete and drained, the same amino acid under identical conditions is added to the resin beads and repeated coupling occurs.

After completion of double coupling the first amino acid is then deprotected of the Fmoc protection

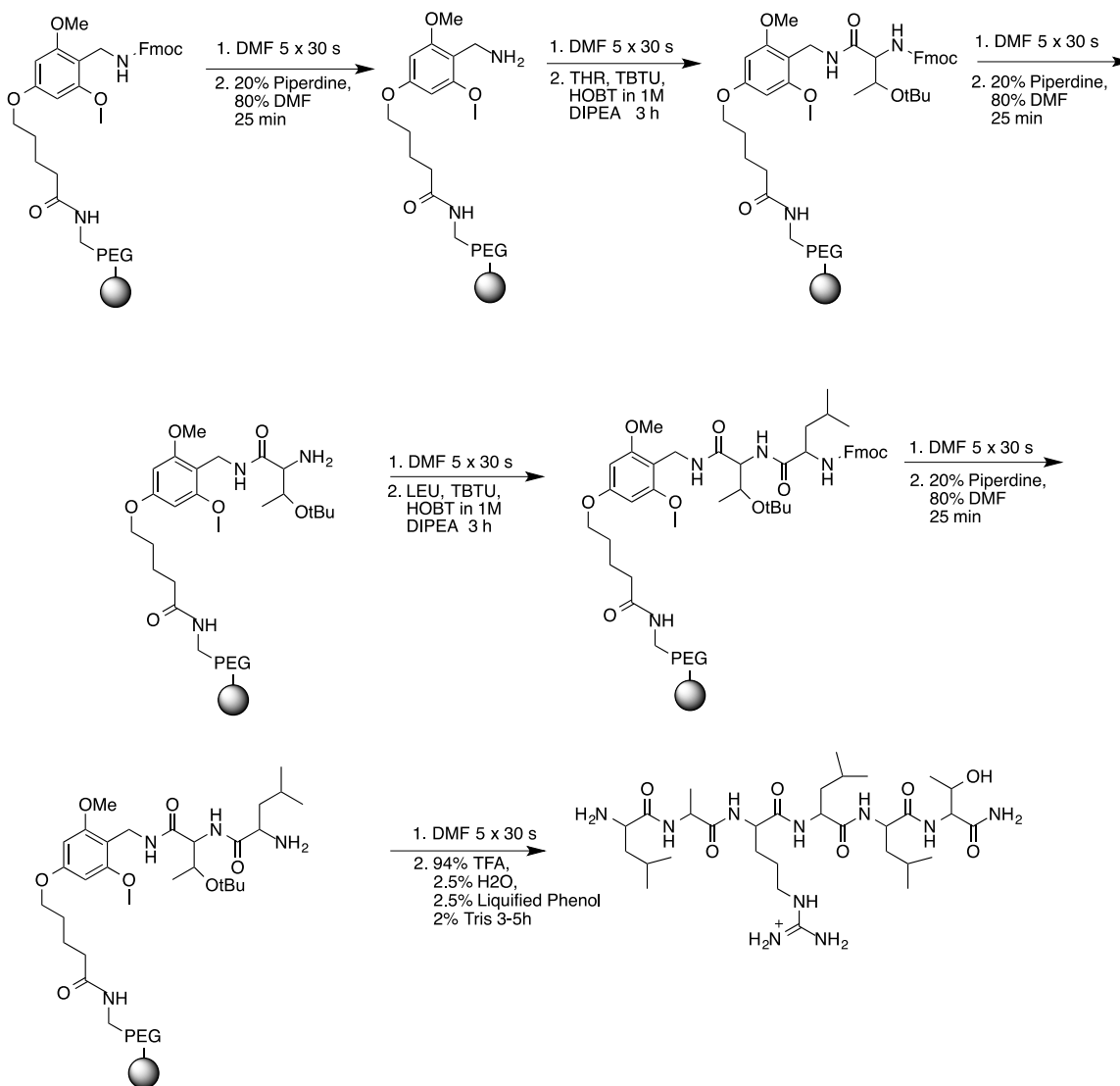
group using a piperidine/DMF solution. The resulting free amine is then coupled to the next amino acid of each sequence under the same coupling conditions. This cycle is continued until all desired amino acids are coupled to the resin <sup>12-14</sup> (Scheme 1).



Scheme 1. Generic double coupling procedure.

For BT-SPPS methods deprotecting the Fmoc group took 15 min, and the coupling of each amino acid took around three hours (Scheme 2).





Scheme 2. BT-SPPS of EGFR-L1. The same steps occur for synthesis of EGFR-L2.

### 2.2.2 MW-SPPS Synthesis of EGFR-L1 and EGFR-L2

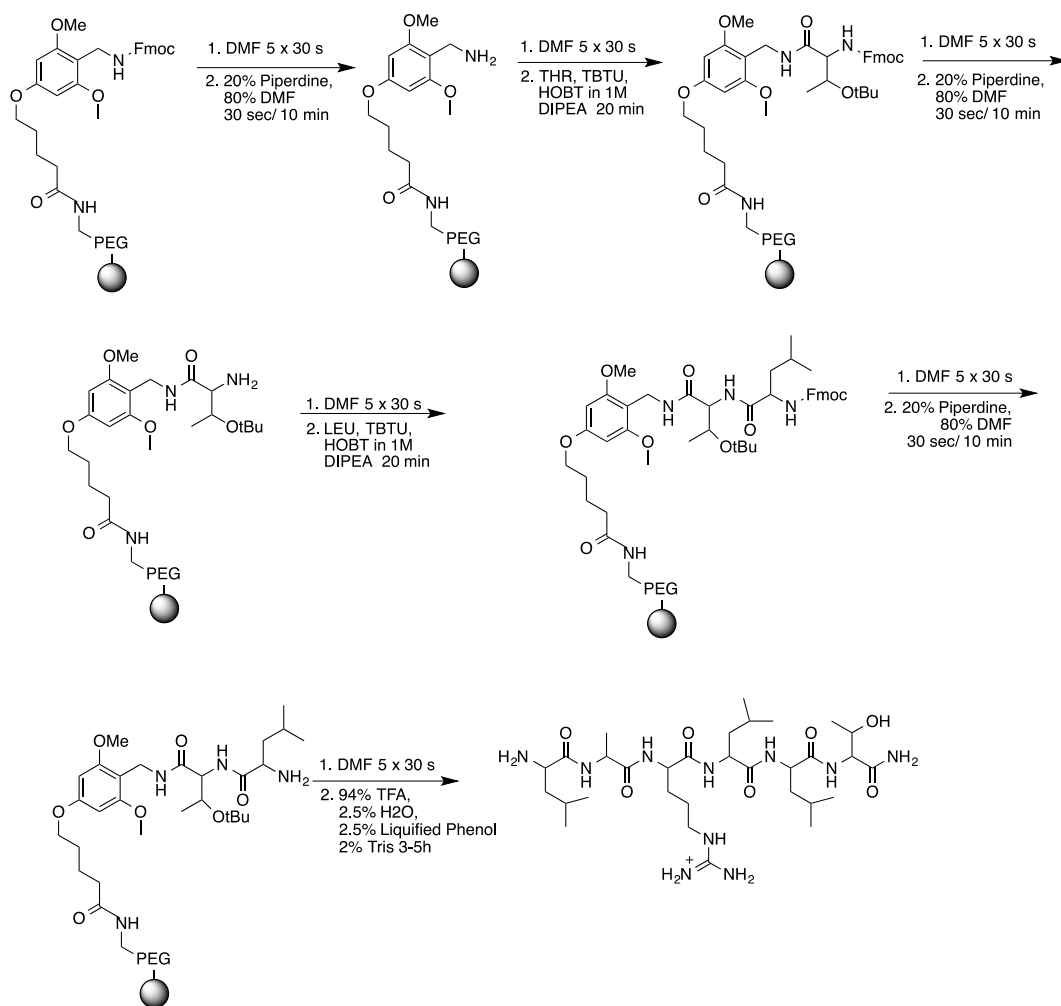
In solid phase peptide synthesis (SPPS), there are many polar and ionic species present that can be rapidly heated by use of microwave energy. Ideal conditions for microwave coupling include polar solvents, the peptide framework or resin, the terminal amine group (if coupling through C-terminus), bases for deprotection, and polar/ionic activators such as TBTU.<sup>15</sup> The increase in temperature is beneficial to SPPS as well, as this can aid the reaction by disruption of chain aggregation due to intra- and interchain association and allow for easier access to the growing end of the chain.<sup>15</sup>

In MW-SPPS, we used microwave-assisted chemistry to achieve deprotection of Fmoc groups, as well as for coupling each amino acid in the sequence used in BT-SPPS. To deprotect the Fmoc group, the solid support is suspended in piperidine/DMF solution for 30 seconds, followed by removal of the solution. The resin was then covered in piperidine/DMF solution for only five minutes, and then allowed to cool to room temperature for five minutes. To couple amino acids to the resin, the same mixture was created as for the BT-SPPS method, but the reaction was run for 20 minutes and then continued until completion of sequences (Scheme 3). Completed peptide sequences can then be cleaved from the resin to perform solution phase conjugation to the fluorophore, or left on the resin to perform solid support conjugation.

Both methods' products were deprotected at the last amino acid. Rinsed with DMF and DCM to ensure all free by products and reaction conditions are removed. The dry resin beads are then introduced into cleavage conditions using a trifluoroacetic acid (TFA) cocktail. The TFA cocktail contains a mixture of TFA, H<sub>2</sub>O, phenol, and Tris (94/2.5/2.5/1). Each method product was then precipitated out of solution using cold anhydrous diethyl ether. The precipitate in diethyl ether is centrifuged and the supernatant was decanted and new diethyl ether is added.

This procedure was repeated three times. The final time the residual peptides were dissolved in a water/acetonitrile (ACN) mixture 90:10 ratio. The solution was then frozen by liquid nitrogen and lyophilized where the frozen solution is brought to a solid form. The free peptides were then purified using reverse phase HPLC.

MW-SPPS at first glance is the most efficient method due to its rapid production time. EGFR-L1 and EGFR-L2 can be completed in a fraction of the time using MW-SPPS. However when looking closely at the percent yields of each method, MW-SPPS does not provide a substantial difference in yields, however the reactions are extremely faster. The yields were comparable to each other regardless of the methods. From this comparison, however, MW-SPPS showcases a method that is faster, easier, and comparable to the traditional method of synthesizing peptides as seen in Table 2.



Scheme 3. MW-SPPS synthesis of EGFR-L1. The same steps occur for synthesis of EGFR-L2.

Table 2: Comparison of BT-SPPS and MW-SPPS of EGFR-L1 and EGFR-L2

| Name    | Abbreviation | Synthesis Method          | Molecular Weight | % Yield |
|---------|--------------|---------------------------|------------------|---------|
| EGFR-L1 | 2-1          | Synthesizer <sup>16</sup> | 685.39 g/mol     | 48      |
| EGFR-L1 | 2-1          | Bench-top                 | 685.39 g/mol     | 35      |
| EGFR-L1 | 2-1          | Microwave                 | 685.39 g/mol     | 43      |

Table cont'd

| Name        | Abbreviation | Synthesis Method          | Molecular Weight | % Yield |
|-------------|--------------|---------------------------|------------------|---------|
| EGFR-L2     | 2-2          | Synthesizer <sup>16</sup> | 1538.73 g/mol    | 37      |
| EGFR-L2     | 2-2          | Bench-top                 | 1538.73 g/mol    | 39      |
| EGFR-L2-Gly | 2-3          | Bench-top                 | 1595.75 g/mol    | 44      |

### 2.3 Derivatives of EGFR-L1 and EGFR-L2

The EGFR-L2 (**2-2**) sequence was initially modified to EGFR-L2-Glycine (**2-3**) to account for the steric hindrance at the N-Terminus foreseen for future conjugations with fluorophores. The tyrosine of the last amino acid has a bulky side chain that could possibly cause extreme issues when conjugating with BODIPY dyes for completion of probe structure (Figure 4).

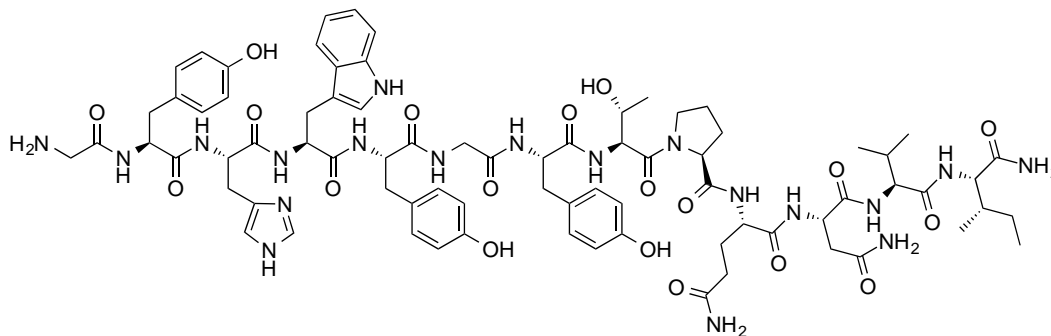


Figure 4. Peptide ligand structure 2-3. (GYHWYGYTPQNVI).

The yields in Table 2 obtained for the addition of glycine via BT-SPPS for synthesis of peptide **2-3**, revealed an increase in percent yield compared to the yield obtained for peptide **2-2**. Due to the error in coupling, the additional amino acid was completed using BT-SPPS under normal Fmoc conditions. The completed sequence was purified as seen previously with peptides **2-1** and **2-2**.

Current studies suggest that peptides as targeting agents conjugated to fluorophores require linkers or spacers to ensure the affinity for binding is remained. Choosing a linker there are various points to consider, finding linkers that can aid the entire probe in solubility while still providing space between each portion is an essential benefit. Polyethylene glycol (PEG) is often sought after due to its capabilities of performing as a linker. PEG groups offer improved water solubility to molecules, as well as a decrease aggregation due to extension of the molecules conformation.<sup>17-19</sup> PEG groups come in various chain lengths, and are easily tunable for attaching to different compounds. Ideally a PEG group that is transformed to mimic an amino acid is desirable. Terminating the PEG group with an amino group at one end and carboxylic acid at the other are beneficial aspects. To complete the linker Fmoc-NH-PEG3-propionic acid (PEG3) was chosen from AAPTEC, as it possessed each component necessary, and protects the amino group using the same Fmoc chemistry applied during peptide synthesis (**Figure 5**).

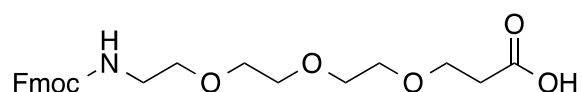


Figure 5. Structure of Fmoc- NH-PEG3-Propionic acid (PEG3).

BT-SPPS was used to couple peptides EGFR-L1 and EGFR-L2 to PEG3. PEG3 was introduced to the resin beads containing peptides in the presence of coupling agents TBTU and additive HOBT in a DIEA/DMF solution as previously described. Although PEG3 resembles an amino acid because of terminus, a double coupling was performed to ensure maximum attachment of PEG3 (Scheme 4).

The Fmoc groups were removed from PEG3-EGFR-L1 and PEG3-EGFR-L2 as described previously, and the sequences cleaved from resin beads to reveal the white fluffy crude peptides **2-4** and **2-5**. Each pegylated peptide was purified using RP-HPLC in good yields (Table 3).

Although peptides have sustained properties as targeting molecules various drawbacks exist to date. One persistent boundary is the inherent low chemical stability peptides exhibit.<sup>20-21</sup>

**Table 3: Results of BT-SPPS of Pegylated peptides 2-4 and 2-5**

| Name         | Abbreviation | Molecular Weight | % Yield |
|--------------|--------------|------------------|---------|
| PEG3-EGFR-L1 | 2-4          | 888.59 g/mol     | 38      |
| PEG3-EGFR-L2 | 2-5          | 1798.867 g/mol   | 39      |

Peptides tend to be extremely susceptible to enzymatic cleavage, which allows the molecules to break down into smaller portions upon cleavage *in vivo*. The free termini of peptides allow possibilities of degradation as well.<sup>22-23</sup> This nagging attribute limits the scope of peptides unless stability modulations are performed. To counter act these issues several efforts are possible such as termini modifications, cyclization of peptides, and substituting L-amino acids for D-amino acids (Figure 6).<sup>24-27</sup>

Altering the peptide sequence to enhance stability is essential, however the most viable point is to not alter the receptor-binding affinity of the peptide after enhancement, hence, and some studies have suggested using a linker to avoid these issues.

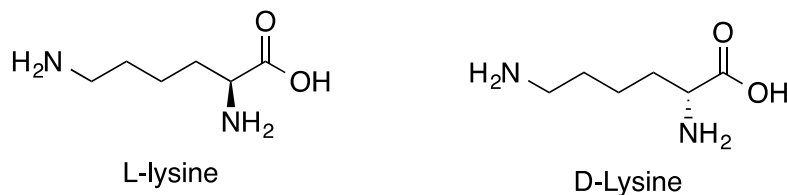
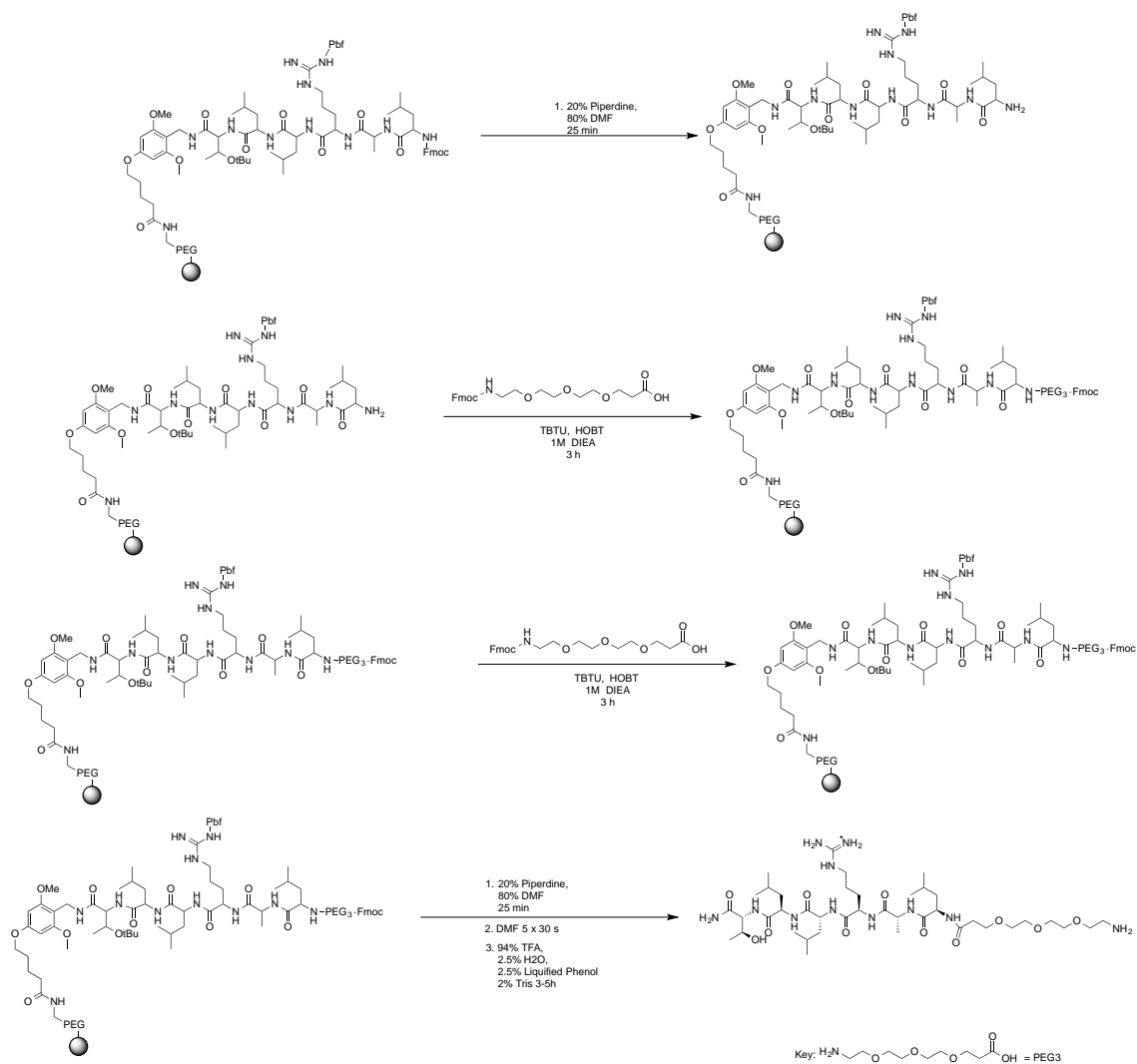


Figure 6. L-amino acid configuration and D-amino acid confirmation of Lysine.

A top of stability, maintaining binding affinity, the ease of access should also be considered when developing alternative sequences. Determining which sequence to tackle was based on previous studies that suggest that EGFR-L1 would be a better suite.<sup>4</sup> Peptides **2-1** and **2-3** were both conjugated to Phthalocyanines (Pc) via a small PEG linker (Figure 7). The Pc-EGFR-L1 conjugate was found to have enhanced water solubility and higher targeting for EGFR versus Pc-EGFR-L2-Gly, which showed lower solubility due to the more hydrophobic peptide sequence.



Scheme 4. BT-SPPS of peptide 2-4. (The same steps occur for synthesis of peptide 2-5).

The EGFR-L1 conjugate exhibited a 17-fold higher accumulation in EGFR overexpressing cells over EGFR-L2 conjugate. The Pc-EGFR-L1 conjugates increased cellular uptake was thought to be due to the arginine charge side chain providing an enhanced solubility for the entire conjugate. Due to the multiple highlights of EGFR-L1 such as the ease of synthesis, the smaller backbone structure, and enhanced solubility this sequence was chosen for modification.

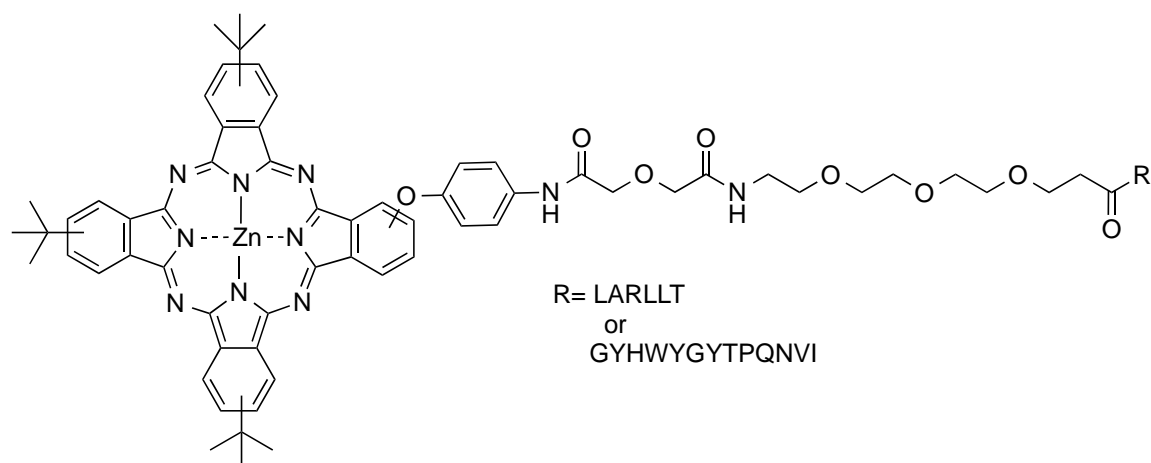


Figure 7. Pc-Peptide Conjugates previously investigated.<sup>4</sup>

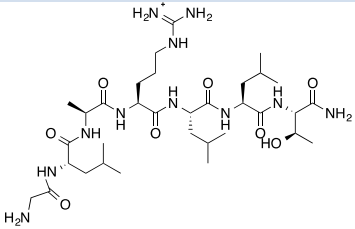
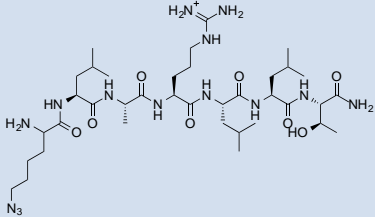
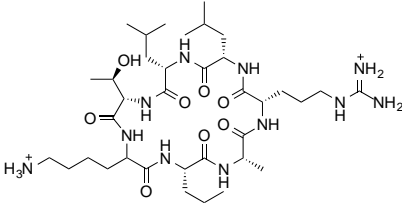
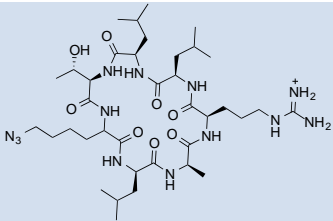
Several modifications were considered to enhance the stability of EGFR-L1 sequence (Table 4), and examined for effectiveness. EGFR-L1 N-terminus was first investigated to determine if altering would increase the stability.

**Table 4: Derivatives of EGFR-L1 obtained by BT-SPPS**

| Peptide sequence                     | Abbrev. | Structure | Molecular Weight | % Yield |
|--------------------------------------|---------|-----------|------------------|---------|
| <b>tlrral-CONH<sub>2</sub></b>       | 2-6     |           | 685.47<br>g/mol  | 40      |
| <b>KLARLLT-<br/>CONH<sub>2</sub></b> | 2-7     |           | 813.57<br>g/mol  | 39      |



Table cont'd

| Peptide sequence                               | Abbrev.   | Structure  | Molecular Weight | % Yield |
|--|-----------|--|------------------|---------|
| GLARLLT-<br>CONH <sub>2</sub>                  | 2-8       |    | 742.49<br>g/mol  | 37      |
| K(N <sub>3</sub> )LARLLT-<br>CONH <sub>2</sub> | 2-9       |    | 839.56<br>g/mol  | 59      |
| cyclo[KLARLLT]                                 | cycloL1.1 |   | 796.61<br>g/mol  | -       |
| Cyclo[K(N <sub>3</sub> )larllt]                | cycloL1.2 |  | 822.62<br>g/mol  | -       |

Peptide **2-1** is synthesized with a Leucine amino acid as the final addition to the sequence. However adding an additional amino acid could possibly change the activity of the peptide sequence, as well as provide increase stability for conjugation. Increasing the distance of attachment for fluorophores could act as a small linker or extend the confirmation as seen with PEG linkers. Two amino acids were considered in this approach Lysine (Lys) (Figure 6) and Glycine (Gly) (Figure 3). Each sequence was synthesized by BT-

SPPS and purified by RP-HPLC. The yields of each sequence were comparable to those achieved with EGFR-L1 (Table 4).

The second endeavor to aid stability was synthesizing EGFR-L1 with D-amino acids. D-amino acids have been shown to withhold their integrity under enzymatic cleavage allowing peptide sequences to reach their target goal. D-amino acids are observed in multiple peptides that are naturally synthesized in animal cells.<sup>28-30</sup> These D-amino acids are formed when a posttranslational alteration occurs from L-amino acids into D-amino acids. Studies have also shown that peptides that are partially made up of D-amino acids exhibit a higher degree of stability to enzymatic cleavage over sequences that are fully designed with L-amino acids.<sup>25, 31-32</sup>

To synthesize EGFR-L1 with D-amino acid a retroinverso of EGFR-L1 must be considered. Retroinverso peptides are synthesized by taking the normal LARLLT sequence of EGFR-L1 replacing them with D-amino acids respectively, however a reverse order of D-amino acids addition to the resin must be performed (Figure 9). Using a retroinverso-EGFR-L1 (tlarl) may result in retention of the biological activity of the EGFR-L1 sequence, but allows for an enhanced biological stability.

Synthesis of **2-6** was performed on PAL-PEG-PS resin beads under BT-SPPS Fmoc chemistry as described previously. The resulting peptide were purified by RP-HPLC and confirmed by MALDI-TOF.

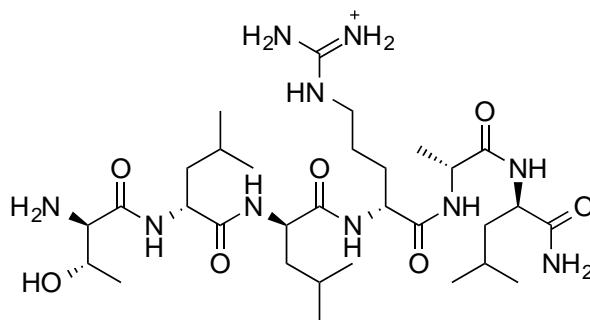
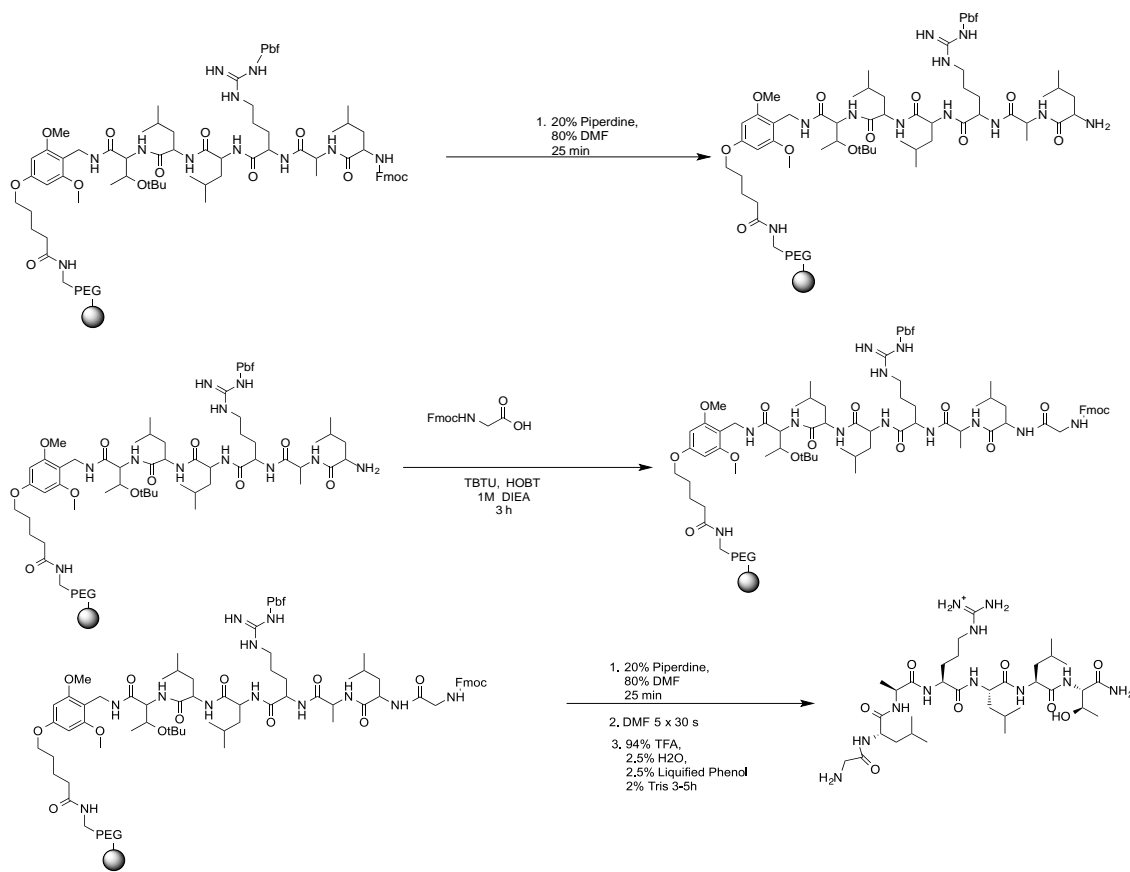


Figure 9. Structure of retroinverso peptide sequence (tlarl).



Scheme 5. Synthesis of peptide 2-8. The same steps occur for synthesis of peptide 2-7.

The final modification considered to enhance the metabolic state of peptide **2-1** was to cyclize the backbone of the EGFR-L1 sequence. A current study in Dr. Seetharama Jois, our collaborator, suggests that the linear peptides may exhibit random or flexible structure in solution. However, in the presence of our peptide **2-1** the definition of the structure may obtain a folded firm structure. Docking studies of the sequence with EGFR were performed and several low energy docked structures were analyzed and determined to indeed acquire a folded structure in the presence of the receptor. With this information, and to increase the peptide stability, a cyclized derivative of **2-1** was considered.

The preferred method to cyclize was head to tail cyclization due to the counter method involving an acid sensitive disulfide bridge. Although a more difficult feat, head to tail cyclization provides a more stable peptide backbone structure. However, head to tail cyclization of **2-1** would result in a cyclic structure without an N or C-termini. EGFR-L1 sequence does not include a free amine on the side chain thus

removing all necessary components for conjugation. Therefore a lysine residue was introduced in the peptide sequence at the N-terminus. The side chain of Lys can be used for subsequent conjugation to a fluorophore via amide bond formation. The cyclization was performed under the direction of collaborators in the Agriculture building headed by Dr. Gauthier and coworkers. The cyclic sequence was synthesized using standard Fmoc peptide chemistry protocol using chlorotriyl chloride (CTC) as the resin.<sup>33</sup>

The degree of loading was determined by coupling of the first amino acid (Leu) to the resin for one hour in the presence of HCTU as the coupling agent. After coupling was complete the Fmoc group was removed via 20% piperidine in DMF. The resin bearing Leu was then “capped” using DCM/MeOH/DIPEA (80:15:5). Followed by washing of the resin using DMF and DCM, and drying under vacuo overnight. The substitution level of the resin was determined by a quantitative Fmoc test wear UV analysis were acquired at 466nm. After acquisition of the substitution level the synthesis of the linear sequence of **Cyclo.L1.1** [KLARLLT] was performed in the same manner. To ensure the head to tail cyclization proceeded the side chains remained protected therefore a different cocktail was necessary for cleavage. The side chain protected peptides were cleaved from the resin with 5 mL of 1% TFA in DCM for 5 min. The cleavage conditions were repeated on the resin 10 times. The cleavage solutions were combined and concentrated in vacuo. The residue was dissolved in a 1:1 ratio of water and acetonitrile mixture containing 0.05% TFA frozen and lyophilized to yield white solids. To cyclize the white solid was taken up in DMF in a 2 mM solution. To this solution HATU and DIPEA were added. The mixture was allowed to stir for 3 hours after which time the peptides were concentrated to remove as much DMF overnight. Protecting groups were then removed by dissolving the oil in a second cleavage cocktail consisting of TFA/water/TIPS (96:2:2) for two and a half hours. The resulting mixture was then subjected to cold diethyl ether and centrifuged to precipitate out the crude cyclized peptide. The pellet was then removed from the old diethyl ether and resuspended in fresh cold diethyl ether and centrifuged. This process was repeated five times. After the final ether wash, the peptide pellet was dissolved in a minimal amount of water containing 0.1% TFA, frozen and lyophilized.

In considering potential conjugation measures of the peptide sequences for future conjugation to BODIPY fluorophores, an azido group at the lysine side chain was also considered for the cyclic sequence and linear sequence of EGFR-L1. This small measure would allow the peptides to be suitable for conjugation via “click” chemistry without any further modifications performed. To complete the modification lysine amino acids bearing azide moieties, Fmoc-Lys(N<sub>3</sub>)-OH, at the side chain was chosen from Anaspec, as it possessed the desired functionalities, and protects the amino group using the same Fmoc chemistry applied during peptide synthesis (Figure 10).

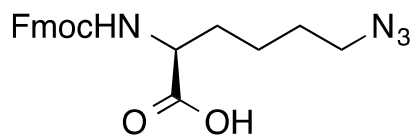


Figure 10. Structure of Fmoc-Lys(N<sub>3</sub>)-OH.

Dr. Gautier performed the cyclic peptide bearing the azide as the side chain for the lysine amino acid, however the sequence was not able to cyclize as the sequence K(N<sub>3</sub>)LARLLT and required the incorporation of d amino acids for all AA included except the azido bearing lysine. The final sequence confirmed was **cycloL1.2** [K(N<sub>3</sub>)larllt]. This was a very interesting observation by far as the initial cyclic peptide **cycloL1.1** was cyclized with no issues, however the azide moiety may have provided a steric interaction with the side chains of the other amino acids in the L-configuration requiring an alleviation of stress, and the D-configuration possibly aided in this manner. The linear sequence K(N<sub>3</sub>)LARLLT (**2-9**) was performed as achieved previously via BT-SPPS and was purified via HPLC analysis of the crude fluffy peptide received. The pure peptide was then characterized with MS, 1H-NMR, and HSQC NMR.

## 2.4 Characterization of Peptides

### 2.4.1 Determination of Peptide Sequencing

To ensure all sequences are as expected various characterization techniques exist. One important technique is the use of MALDI-TOF MSMS. MALDI-MSMS provides a method that is robust in nature but easy to use to determine the sequencing of peptides. Fragmentations are developed in three ion types for sequences a, b, and y. These ions are selectively used to determine the sequence. The first ions a and b

are generated from the N-terminus of a peptide and the y ion is generated from the C-terminus. A suitable amount of fragments from either terminus should be observed, however preferably b and y ions are expected for peptide sequences.<sup>34</sup> Parent peptides EGFR-L1 and EGFR-L2 sequences were first investigated to ensure the methods of synthesis were accurate and the expected fragmentations were recognized. EGFR-L1 showed more fragmentations associated with b ions followed by only a few ions associated with the y ions (Figure 11). This shows that the fragmentation appears to extend from the amino terminus to the c-terminus.

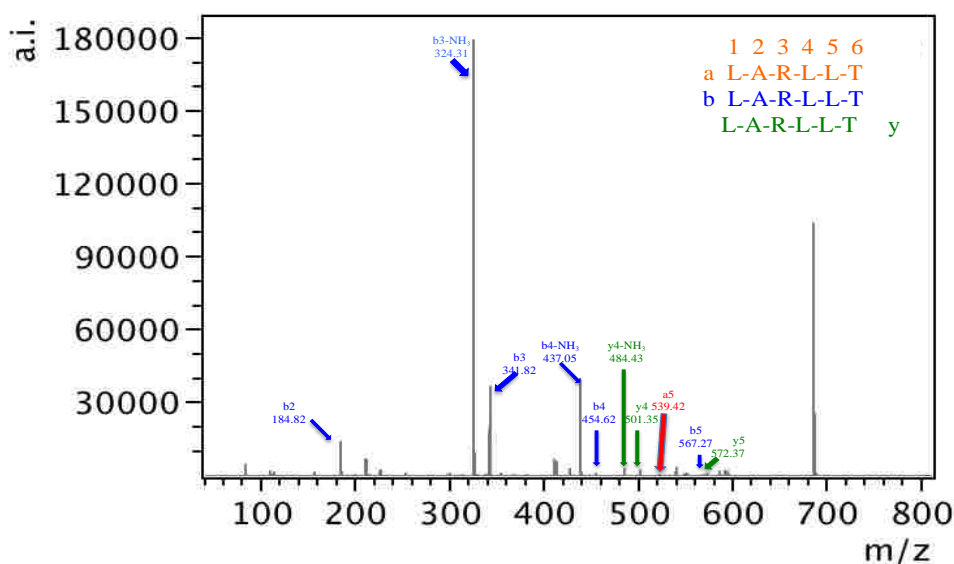


Figure 11. MALDI-TOF-TOF (MSMS) spectrum of 2-1.

Peptide **2-1** MALDI-TOF MSMS spectra is indicative of the fragmentation pattern favoring the loss of amino acids from the N-terminus. The ions associated with this spectra reveal the preference of b ions with only one a ion present and three y ions. The overall amount of b and y ions were good indicators of the desired peptide **2-1** sequence was formed.

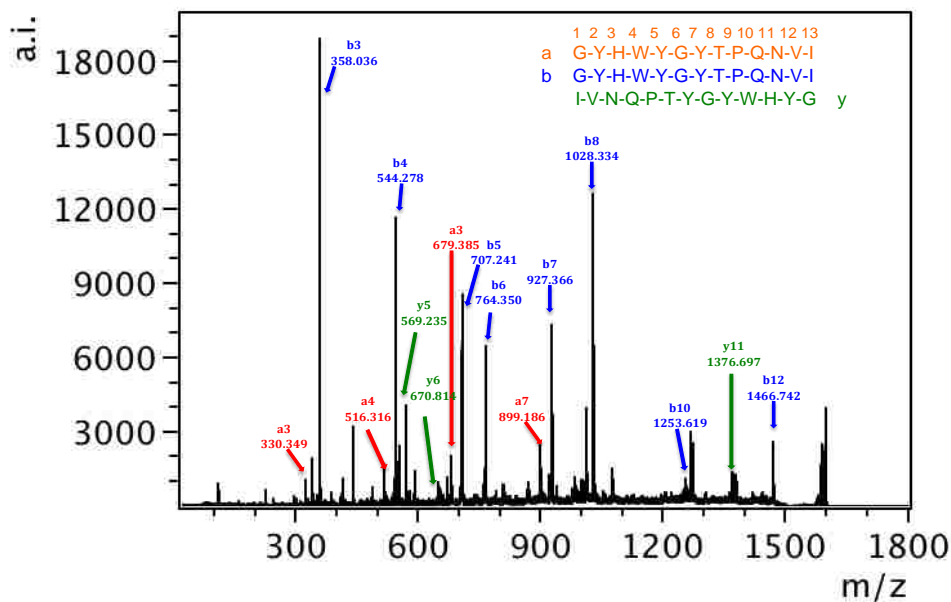


Figure 12. MALDI-TOF-TOF (MSMS) spectrum of 2-3.

Peptide **2-3** MALDI-TOF MSMS spectra indicates the same fragmentation noted in peptide **2-1** more fragmentations associated with b ions followed by y ions as preferred. However with peptide **2-3** more a ions were present than those noted with peptide **2-1** (Figure 12). Both peptides prefer fragmentation from the amino or N-terminus than the C-terminus. Each parent peptide and derivative of peptide **2-1** was then explored for binding efficacy.

#### 2.4.2 Spatial Plasmon Resonance (SPR) of Peptides

Another insightful tool for determining the efficacy of peptide sequences is Surface Plasmon Resonance (SPR). SPR is an intricate tool that can be used to characterize the affinity of two ligands for one another.<sup>35-36</sup> SPR is essential for this manner as it can aid in finding binding constants. The target receptor extracellular domain of EGFR was immobilized on a CM5 sensor chip and used as the bait ligand. Through a microfluidic system of 10 uL/min, each peptide was used as the prey ligand and passed through the chip to determine the protein peptide interaction. The association and dissociation rates are measured in response units at a function of time.<sup>37</sup>

SPR of all peptides were performed in a concentration manner of varying concentrations from 0  $\mu\text{M}$  to 200  $\mu\text{M}$  and sensograms were attained at each concentration. Parent peptides **2-1** (Figure 13) and **2-3** (Figure 14) showed similar results as seen before.

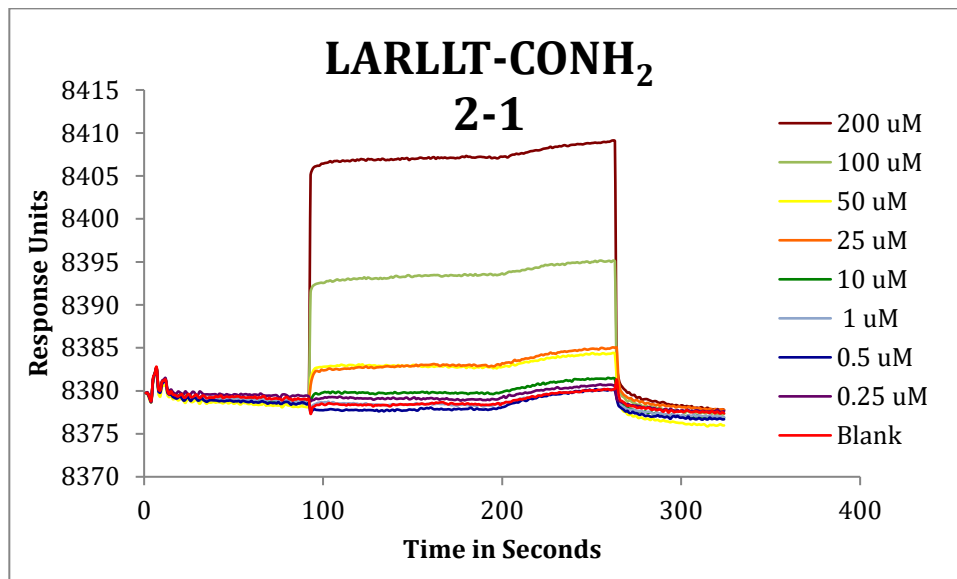


Figure 13. SPR sensogram of EGFR-L1.

As previously reported<sup>2, 38</sup> peptide **2-1** showed an affinity for EGFR. A linear increase in binding via response units from .25  $\mu\text{M}$  to 200  $\mu\text{M}$ . There was no evidence of non-specific binding at any concentration indicating the benefit of using EGFR-L1 for its specificity. The  $K_d$  value determined for **2-1** was in the nanmolar range (Table 5).

Peptide **2-3** also possessed a linear increase in the association and disassociation of the peptide to EGFR in a concentration manner. This concentration difference was investigated from .25  $\mu\text{M}$  to 200  $\mu\text{M}$ . However the binding constant value determined for **2-3** was in the micromolar range proving that the charged sequence EGFR-L1 acquires a better affinity for EGFR. All peptides binding efficacy was studied via SPR and the results can be found in Table 5.



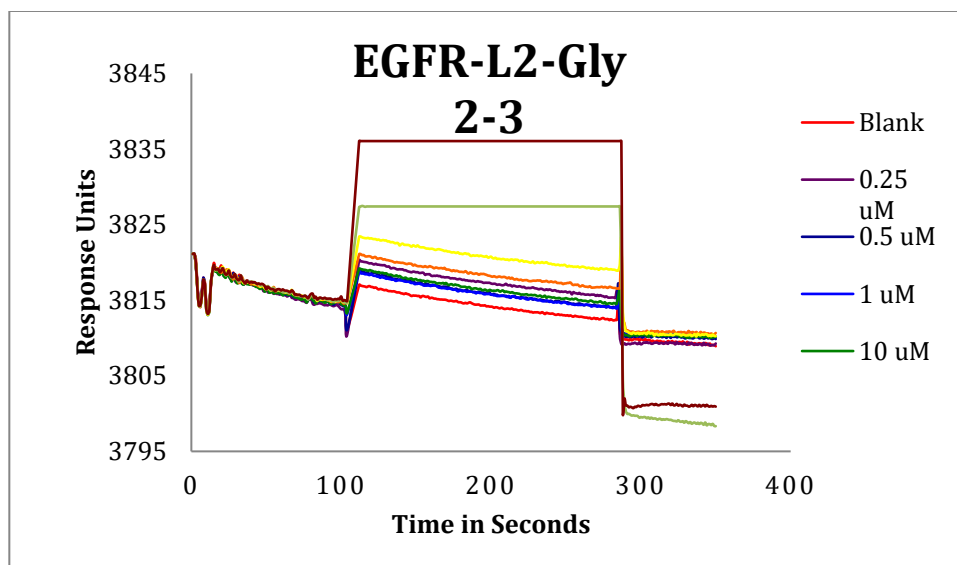


Figure 14. SPR sensogram of EGFR-L2-Gly.

All peptide derivative **2-4 to 2-9** and cyclic peptides **cycloL1.1** and **cycloL1.2** were also investigated. Surprisingly retroinverso peptide **2-6** showed no binding although previous studies suggested possible increased binding affinity.<sup>39</sup> Of the other peptides pegylated peptides **2-4** and **2-5** showed an increased binding affinity for EGFR over their parent peptides with a greater binding constant. While Peptide **2-6** showed a decrease in affinity. Of the peptide derivatives **2-7** shows the strongest binding affinity for EGFR this may be due to the additional positive charge exhibited by inserting the Lys amino acid in the sequence. Comparing the results of Peptide **2-7** and **2-9** the azido group added in peptide **2-9** showed to have a negative effect on binding to EGFR.

This notion was also confirmed with cyclic peptides **cycloL1.1** and **cycloL1.2**. Peptide **cycloL1.1** showed to have a better affinity over its azido counterpart. Previous computational studies have shown that EGFR-L1 binds to EGFR in an open or closed conformation.<sup>40</sup> The immobilized EGFR did not have the endogenous ligand EGF bound to the receptor thus the receptor is thought to maintain mostly a closed conformation.

**Table 5: K<sub>D</sub> Values of All Peptides**

| Compound         | Molecular Weight | K <sub>D</sub> Value<br>(nM) |
|------------------|------------------|------------------------------|
| <b>2-1</b>       | 685.39 g/mol     | 6.55                         |
| <b>2-3</b>       | 1595.75 g/mol    |                              |
| <b>2-4</b>       | 888.59 g/mol     | 3.29                         |
| <b>2-5</b>       | 1798.867 g/mol   | 3.61                         |
| <b>2-6</b>       | 685.47 g/mol     | 29.1                         |
| <b>2-7</b>       | 813.57 g/mol     | 2.41                         |
| <b>2-8</b>       | 742.49 g/mol     | 18.2                         |
| <b>2-9</b>       | 839.56 g/mol     | 120.7                        |
| <b>cycloL1.1</b> | 796.61 g/mol     | 1.75                         |
| <b>cycloL1.2</b> | 822.62 g/mol     | 64,870                       |

## 2.5 Conclusions

Peptides have proven to be essential targeting molecules for imaging agents, and seven potential EGFR ligands were developed and tested. EGFR-L1 and EGFR-L2 were synthesized by SPPS in two fashions, bench-top and microwave. Each method utilized Fmoc chemistry as the standard and provided comparable yields. MW-SPPS provided a faster method that maintained similar, and efficiency to BT-SPPS. EGFR-L2 sequence was initially modified to EGFR-L2-Gly due to the possible steric hindrance at the N-Terminus and potential increase in stability. Both peptide sequences EGFR-L1 and EGFR-L2 were conjugated to 3-PEG linkers to aid in solubility and to potentially provide probe development spacing between peptide ligands and fluorophore. EGFR-L1 was modified to aid in stabilizing the sequence to minimize the amount of enzymatic cleavage seen in *in vivo* studies. Peptide derivatives 2-1 to 2-9 were synthesized in good yields and tested for binding affinities by SPR. Peptide **2-6** showed no binding affinity for the EGFR receptor while **2-8** and **2-9** displayed good affinity for the receptor. **CycloL1.1** showed great

binding affinity for EGFR while **cycloL1.2** showed a decrease affinity for EGFR similar to the efficacy observed with peptide **2-9**. Of all EGFR-L1 derivatives synthesized and characterized by SPR **2-7** provided the best binding affinity. All peptides have been characterized and their sequences confirmed using MALDI-TOF.

## **2.6 Experimental**

### ***2.6.1 General Information***

All solvents and reagents used in the synthesis of peptides were performed with reagents purchased from Sigma Aldrich peptide synthesis grade. Required amino acids and resin were purchased from either Anaspec, AAPPTec or Applied Biosystems.

### ***2.6.2 General Procedure for Synthesis for Linear Peptide Sequences***

Peptide sequences were prepared on a 0.2 mmol scale following standard Fmoc Chemistry. A 4-fold excess of the L-Fmoc protected amino acids or D-Fmoc protected amino acids were coupled using TBTU/HOBT as the activating agent and coupling additive. The peptide sequences prepared using this methodology are found in Table 4. After the final amino acid is added a final Fmoc deprotection was performed using 20% piperidine in DMF for 10 minutes and released from the resin beads followed by a second addition for 15 minutes. This was trailed by washing the resin beads with DMF five times and then with DCM five times. The resin beads were then allowed to dry overnight under high vacuum. Cleavage from resin: Following drying of resin beads a cleavage cocktail consisting of TFA (94%), Water (2.5%), Liquid Phenol (2.5%), and Triisopropylsilane (1%) is added to the resin for 3 hours. The cocktail was then released into cold anhydrous ethyl ether, and centrifuged. The supernatant was decanted away, and repeated three times. The pellet is then dissolved in water and acetonitrile (90/10). The solution is then frozen and lyophilized. Reverse-phase HPLC analysis was performed with a Waters 2545 Quaternary Gradient Module (Waters, USA), Waters Sample Injector, and 2489 UV/Visible Detector, which are controlled by Waters Empower 2 software (Waters, USA). Separations were completed on an X-Bridge BEH300 Prep C18 (5  $\mu\text{m}$ , 10 x 250 mm) with a X-Bridge BEH300 Prep Guard cartridge 300  $\text{\AA}$  (5  $\mu\text{m}$  10 x 10 mm) at a 4 mL/min

flow rate with UV detection for peptides 220 nm using a stepwise gradient. The solvent system for peptide purification consisted of milpure water and HPLC grade acetonitrile with 0.1% TFA. Mass Spectra were acquired using Bruker Ultraflex Extreme MALDI Tandem TOF Mass Spectrometer with  $\alpha$ -cyano-4-hydroxycinnamic acid (CHCA) was used for the matrix. Fractions of HPLC purity (> 95%) with the anticipated mass were combined and lyophilized.

### **2.6.3 General Procedure for Synthesis for Cyclic Peptide Sequences**

Cyclic peptides were prepared using 1.2mmol/g of CTC resin was placed in a polypropylene reaction vessel including a polypropylene frit. The resin was swollen with dry DCM (10 mL/gram of resin) for 30 minutes after which the solvent was drained. Fmoc-Leu-OH (297 mg, 0.84 mmol, 0.7 equivalents) was dissolved in dry DCM and DIEA (3.5 equiv) was added. The amino acid solution was added to the resin and shaken for 1 hour. After this time, the resin was drained and washed with DMF. Unreacted sites on the resin were capped with DCM/MeOH/DIEA (80:15:5) twice for 15 minutes. The resin was washed again with DMF (5 x 30 sec) followed by DCM. After drying the resin under vacuum overnight, the substitution level of the resin was determined by a quantitative Fmoc test or UV test. After the substitution level was determined (usually about 0.5 mmol/g), the Fmoc-Leu-CTC resin was deprotected using 20% piperidine in DMF and washed with DMF followed by DCM. The H-Leu-CTC resin was dried under vacuum and then stored at 4°C. The **Cyclo.L1.1** and **Cyclo.L1.2** were prepared on a Tribute peptide synthesizer (Protein Technologies, Tucson, AZ) utilizing a standard Fmoc peptide chemistry protocol on a .1 mmol scale using the previously loaded H-Leu-CTC and H-(d)Leu-CTC resins, respectively. Side-chain functionalities were protected with tert-butyl (Thr), N<sup>G</sup>-2,2,4,6,7-pentamethyldihydrobenzofuran-5-sulfonyl (Arg) and tert-butyloxycarbonyl (Lys). In the case of peptide **Cyclo.L1.2**, Fmoc-Lys(N<sub>3</sub>)-OH was used. Five fold excess of Fmoc-amino acids and HCTU, in the presence of 10 equivalents of DIEA were used for each of the coupling steps (10 min) with DMF as the solvent. After the synthesis of each sequence was complete, the final Fmoc groups are removed using 20% piperidine in DMF for 15 minutes. The resin from each synthesis was washed with DMF and DCM. The side chain protected peptides were cleaved from the resin with 5 mL of 1% TFA in DCM for 5 min. The cleavage reactions were repeated for a total of 10

times. The cleavage solutions for each respective peptide were combined and concentrated under vacuum. The residues were dissolved in water:acetonitrile containing 0.05% TFA (1:1, 20 mL), frozen and lyophilized to yield white solids. The peptides were dissolved in DMF to yield 2 mM solutions after which HATU (2.5 equivalents) and DIEA (5 equivalents) were added. The cyclization reactions were stirred for 3 hours, and then the peptides were placed under high vacuum to remove the DMF (usually overnight) to yield an oil. Protecting groups were removed from the peptides using TFA/water/TIPS (3 mL, 96:2:2) for 2.5 hours. Cold diethyl ether was then added to the peptide solutions to precipitate the crude cyclized peptides. The peptides were centrifuged for 10 minutes (10,000 rpm) and the ether layers decanted. Fresh cold diethyl ether was added, and the pelleted peptides were resuspended. The peptides were centrifuged again, and the procedure was repeated 5 times for each peptide. After the final ether wash, the peptide pellets were dissolved in a minimal amount of water containing 0.1% TFA, frozen and lyophilized. HPLC analysis was performed with a Waters 616 pump, Waters 2707 Autosampler, and 996 Photodiode Assay Detector which are controlled by Waters Empower 2 software. The separation was performed on an Agilent Zorbax 300 SB-C18 (5  $\mu$ m, 4.6 x 250 mm) with an Agilent guard column Zorbax 300 SB-C18 (5  $\mu$ m, 4.6 x 12.5 mm). Elution was done with a linear 5% to 55% gradient of solvent B (0.1% TFA in acetonitrile) into A (0.1% TFA in water) over 50 min at a 1 mL/min flow rate with UV detection at 215 nm. Preparative HPLC runs were performed with a Waters prep LC Controller, Waters Sample Injector, and 2489 UV/Visible Detector that are controlled by Waters Empower 2 software. The separation was performed on a Agilent Zorbax 300SB-C18 PrepHT column (7  $\mu$ m, 21.2 x 250 mm) with Zorbax 300SB-C18 PrepHT guard column (7  $\mu$ m 21.2 x 10 mm) using a linear 5% to 55% gradient of solvent B (0.1% TFA in acetonitrile) into A (0.1% TFA in water) over 50 min at a 20 mL/min flow rate with UV detection at 215 nm. Fractions of high (>95%) HPLC purity with the expected mass were combined and lyophilized followed by high resolution mass spectra of each peptide.

**2-1: Peptide Sequence: LARLLT-CONH<sub>2</sub>** <sup>1</sup>H NMR (500 MHz, DMSO-d<sub>6</sub>, 308K):  $\delta$  8.65 (d,  $J$  = 7.40 Hz, 2H), 8.10 (d,  $J$  = 7.9 Hz, 4H), 7.91 (d,  $J$  = 8.1 Hz, 2H), 7.52 (t,  $J$  = 5.8 Hz, 1H), 7.44 (d,  $J$  = 8.5 Hz, 2H), 7.09 (d,  $J$  = 9.0 Hz, 3H), 4.41 (t,  $J$  = 7.2 Hz, 2H), 4.33 (t,  $J$  = 7.8 Hz, 3H), 4.27 (d,  $J$  = 7.1 Hz, 1H), 4.07

(dd,  $J = 8.4$  Hz, 2H), 4.02 (s, 1H), 3.80 (s, 1H), 1.74 (m, 9H), 1.51 (m, 8H), 1.24 (d,  $J = 6.7$  Hz, 5H), 1.00 (d,  $J = 6.3$  Hz, 3H), 0.87 (m, 18H). MS(MALDI-TOF):  $m/z$  685.390 . Calc'd. for  $C_{31}H_{61}N_{10}O_7^+$  685.891.

**2-3: Peptide Sequence: GYHWYGYTPQNVI-CONH<sub>2</sub>.** <sup>1</sup>H NMR (500 MHz, DMSO-*d*<sub>6</sub>)  $\delta$  9.13 (d,  $J = 20.0$  Hz, 5H), 8.45 (m, 3H), 8.20 (t,  $J = 9.6$  Hz, 2H), 8.04 (m, 4H), 7.90 (t,  $J = 10.5$  Hz, 3H), 7.66 (d,  $J = 9.0$  Hz, 2H), 7.55 (d,  $J = 7.9$  Hz, 3H), 7.38 (d,  $J = 10.7$  Hz, 1H), 7.29 (d,  $J = 8.2$  Hz, 1H), 7.16 (d,  $J = 23.0$  Hz, 3H), 7.08 (s, 1H), 6.98 (m, 9H), 6.74 (s, 2H), 6.62 (m, 6H), 4.55 (m, 5H), 4.39 (m, 4H), 4.12 (m, 5H), 3.89 (m, 1H), 2.12 (t,  $J = 7.6$  Hz, 2H), 2.02 (m, 4H), 1.88 (m, 4H), 1.75 (d,  $J = 18.1$  Hz, 5H), 1.43 (m, 3H), 1.24 (s, 4H), 1.10 (s, 5H), 0.81 (m, 18H). MS(MALDI-TOF):  $m/z$  calcd for  $C_{77}H_{101}N_{19}O_{19}$  [M+H]<sup>+</sup> 1595.752; found 1596.697.

**2-4: Peptide Sequence:3PEG-LARLLT-CONH<sub>2</sub>.** <sup>1</sup>H NMR (500 MHz, DMSO)  $\delta$  8.13 (d,  $J = 7.4$  Hz, 2H), 8.00 (dd,  $J = 19.6, 7.7$  Hz, 2H), 7.93 (d,  $J = 8.1$  Hz, 1H), 7.78 (s, 2H), 7.57 (t,  $J = 5.4$  Hz, 1H), 7.38 (d,  $J = 8.5$  Hz, 1H), 7.05 (d,  $J = 20.9$  Hz, 3H), 4.28(m, 5H), 4.05 (m, 3H), 3.57 (m, 16H), 3.10 (m, 2H), 2.98 (dd,  $J = 10.5, 5.2$  Hz, 2H), 1.64 (m, 4H), 1.49 (m, 10H), 1.20 (d,  $J = 7.0$  Hz, 4H), 1.00 (d,  $J = 6.2$  Hz, 3H), 0.87 (m, 18H). MS(MALDI-TOF):  $m/z$  calcd for  $C_{40}H_{78}N_{11}O_{11}$  [M]<sup>+</sup> 888.588; found 888.542.

**2-5: Peptide Sequence:3PEG-GYHWYGYTPQNVI-CONH<sub>2</sub>.** <sup>1</sup>H NMR (500 MHz, DMSO)  $\delta$  13.96 (s, 1H), 10.72 (s, 1H), 9.12 (s, 3H), 8.89 (s, 1H), 8.07 (m, 6H), 7.68 (m, 4H), 7.40 (s, 1H), 7.30 (d,  $J = 7.9$  Hz, 1H), 7.20 (m, 3H), 7.01 (m, 9H), 6.75 (s, 1H), 6.61 (m, 5H), 4.73 (m, 8H), 4.42 (m, 5H), 4.16 (m, 3H), 4.08 (m, 2H), 3.91 (m, 3H), 3.70 (m, 4H), 3.58 (m, 16H), 2.91 (m, 5H), 2.65 (m, 3H), 2.37 (m, 2H), 2.06 (m, 7H), 1.90 (d,  $J = 15.3$  Hz, 3H), 1.74 (m, 2H), 1.43 (m, 2H), 1.25 (s, 3H), 1.10 (m, 4H), 0.84 (m, 10H). MS(MALDI-TOF):  $m/z$  calcd for  $C_{86}H_{119}N_{20}O_{23}$  [M+H]<sup>+</sup> 1799.876; found  $m/z$  1799.972.

**2-6: Peptide Sequence: tllarl-CONH<sub>2</sub>.** <sup>1</sup>H NMR (500 MHz, DMSO-*d*<sub>6</sub>, 308K)  $\delta$  8.53 (d,  $J = 8.0$  Hz, 1H), 8.19 (d,  $J = 7.9$  Hz, 1H), 8.09 (s, 3H), 7.93 (dd,  $J = 10.8$  Hz, 2H), 7.78 (d,  $J = 8.3$  Hz, 1H), 7.54 (t,  $J = 5.7$  Hz, 1H), 7.26 (s, 2H), 6.96 (s, 2H), 4.40 (m, 1H), 4.24 (m, 4H), 3.78 (t,  $J = 6.8$  Hz, 1H), 3.58 (s, 1H), 3.09 (q,  $J = 6.5$  Hz, 3H), 1.63 (m, 5H), 1.47 (m, 9H), 1.21 (d,  $J = 7.1$  Hz, 4H), 1.14 (d,  $J = 6.3$  Hz, 3H), .88 (m, 18H). MS(MALDI-TOF):  $m/z$  685.361. Calc'd for  $C_{31}H_{61}N_{10}O_7^+$  685.891.

**2-7: Peptide Sequence: GLARLLT-CONH<sub>2</sub>.** <sup>1</sup>H NMR (500 MHz, DMSO-d<sub>6</sub>, 308K): δ 8.44 (d, *J* = 8.3 Hz, 1H), 8.30 (d, *J* = 7.2 Hz, 1H), 8.13 (d, *J* = 8.0 Hz, 2H), 7.93 (m, 4H), 7.43 (d, *J* = 8.5 Hz, 2H), 7.08 (d, *J* = 13.4 Hz, 3H), 4.43 (m, 1H), 4.28 (m, 4H), 4.04 (m, 3H), 3.84 (d, *J* = 5.6 Hz, 1H), 3.08 (q, *J* = 6.5 Hz, 2H), 1.60 (m, 5H), 1.47 (m, 10H), 1.20 (d, *J* = 7.1 Hz, 3H), 0.99 (d, *J* = 6.3 Hz, 4H), 0.86 (m, 18H). MS(MALDI-TOF): m/z 742.991. Calc'd. for C<sub>33</sub>H<sub>64</sub>N<sub>11</sub>O<sub>8</sub><sup>+</sup> 742.493.

**2-8: Peptide Sequence: KLARLLT-CONH<sub>2</sub>.** <sup>1</sup>H NMR (500 MHz, DMSO-d<sub>6</sub>, 308K) δ 8.49 (s, 1H), 8.25 (d, *J* = 7.3 Hz, 1H), 8.14 (d, *J* = 7.8 Hz, 4H), 7.92 (m, 3H), 7.52 (d, *J* = 5.5 Hz, 1H), 7.44 (d, *J* = 8.6 Hz, 2H), 7.08 (d, *J* = 9.8 Hz, 2H), 4.39 (q, *J* = 7.1 Hz, 2H), 4.29 (m, 5H), 4.07 (m, 2H), 3.78 (s, 1H), 3.08 (d, *J* = 7.2 Hz, 4H), 2.75 (t, *J* = 7.8 Hz, 2H), 1.64 (m, 6H), 1.48 (m, 10H), 1.22 (m, 6H), 0.99 (d, *J* = 6.3 Hz, 4H), 0.86 (m, 18H). MS (MALDI-TOF): m/z [M+H] 814.0550. Calc'd. for C<sub>37</sub>H<sub>73</sub>N<sub>12</sub>O<sub>8</sub><sup>+</sup> 813.567.

**2-9: Peptide Sequence:K(N<sub>3</sub>)LARLLT-CONH<sub>2</sub>.** <sup>1</sup>H NMR (500 MHz, DMSO-d<sub>6</sub> 308K) δ 8.45 (d, *J* = 8.2 Hz, 1H), 8.17 (d, *J* = 7.2 Hz, 1H), 8.06 (s, 4H), 7.91 (dd, *J* = 14.7 Hz, 3H), 7.43 (d, *J* = 11.0 Hz, 2H), 7.08 (d, *J* = 12.7 Hz, 2H), 4.88 (t, *J* = 5.3 Hz, 1H), 4.34 (m, 6H), 4.06 (m, 3H), 3.79 (s, 1H), 3.09 (q, *J* = 6.5 Hz, 2H), 1.66 (m, 6H), 1.49 (m, 11H), 1.37 (t, *J* = 7.5 Hz, 2H), 1.20 (d, *J* = 7.1 Hz, 4H), 1.00 (d, *J* = 6.3 Hz, 4H), 0.87 (m, 18H). MS (MALDI-TOF): m/z 839.4219. Calc'd. for C<sub>37</sub>H<sub>71</sub>N<sub>14</sub>O<sub>8</sub><sup>+</sup> 839.558.

**Cyclo.L1.1 Peptide sequence: Cyclo(KLARLLT).** <sup>1</sup>H NMR (500 MHz, DMSO-d<sub>6</sub>) δ 8.51 (d, *J* = 8.9 Hz, 1H), 8.43 (d, *J* = 5.6 Hz, 1H), 8.30 (d, *J* = 7.4 Hz, 1H), 8.10 (s, 1H), 7.78 (t, *J* = 9.6 Hz, 2H), 4.32 (m, 2H), 4.22 (m, 6H), 4.03 (q, *J* = 7.3 Hz, 1H), 3.91 (m, 1H), 2.93 (d, *J* = 50.6 Hz, 6H), 2.77 (t, *J* = 8.4 Hz, 1H), 1.78 (m, 5H), 1.58 (m, 12H), 1.29 (d, *J* = 7.2 Hz, 4H), 1.09 (d, *J* = 6.3 Hz, 1H), 1.03 (d, *J* = 6.4 Hz, 4H), 0.97 (d, *J* = 6.6 Hz, 4H), 0.90 (m, 18H). MS (MALDI-TOF): m/z 796.609. Calc'd. for C<sub>37</sub>H<sub>70</sub>N<sub>11</sub>O<sub>8</sub><sup>+</sup> 796.540.

**Cyclo.L1.2. Peptide sequence: Cyclo (K(N<sub>3</sub>)larllt).** <sup>1</sup>H NMR (500 MHz, DMSO-d<sub>6</sub>) δ 8.23 (dd, *J* = 21.2, 7.5 Hz, 1H), 8.07 (d, *J* = 37.3 Hz, 1H), 7.91 (d, *J* = 9.3 Hz, 2H), 7.53 (t, *J* = 5.4 Hz, 1H), 4.35 (m, 4H), 4.16 (q, *J* = 7.3 Hz, 2H), 4.09 (dd, *J* = 9.8, 5.4 Hz, 3H), 4.01 (m, 4H), 3.94 (d, *J* = 7.9 Hz, 1H), 1.77 (m, 7H), 1.53 (m, 6H), 1.56 – 1.50 (m, 11H), 1.35 (d, *J* = 7.3 Hz, 4H), 1.07 (d, *J* = 5.9 Hz, 4H), 0.87 (m, 18H). ). MS (MALDI-TOF): m/z 822.616. Calc'd. for C<sub>37</sub>H<sub>68</sub>N<sub>13</sub>O<sub>8</sub><sup>+</sup> 822.530.

#### 2.6.4 SPR Methods

Surface Plasmon Resonance was performed using Biacore X100 from GE Health Sciences. Pure recombinant protein EGFR was obtained from Leinco Technologies (St. Louis, MO). HBS-EP+ buffer and 100 mM glycine at pH 4, 4.5, 5, 5.5 were purchased from GE Health Science. The extracellular domain of EGFR protein was immobilized on a CM5 sensor chip (GE Healthcare Biosciences) at a rate of 10  $\mu\text{L}/\text{min}$  using a normal amine coupling procedure. The carboxyl groups on the CM5 chip were activated using a solution containing 0.2 M N-ethyl N-(dimethylaminopropyl) carbodiimide (EDC) and 0.05 M N-hydroxysuccinimide (NHS) (35  $\mu\text{L}$  solution, with a flow rate of 5  $\mu\text{L}/\text{min}$ ). The running buffer for peptides was HBS-EP+ buffer was diluted 10 times to contain 0.01 M HEPES, 0.15 M NaCl, 3mM EDTA, and 0.005% surfactant P20 at pH 7.5. Peptides were dissolved in buffer were used as analyte. The running buffer for conjugates and BODIPY was HBS-EP+ buffer was diluted 10 times to contain 0.01 M HEPES, 0.15 M NaCl, 3mM EDTA, 0.005% surfactant P20 at pH 7.5, but brought to a 4% DMSO concentration. SPR sensograms were obtained and the association and dissociation rates were obtained from 0 to 200  $\mu\text{M}$  concentrations.

#### 2.7 References

1. Faustino, M. A. F.; Neves, M. G. P. M. S.; Cavaleiro, J. A. S.; Neumann, M.; Brauer, H.-D.; Jori, G., Part 2. meso-Tetraphenylporphyrin Dimer Derivatives as Potential Photosensitizers in Photodynamic Therapy. *Photochemistry and Photobiology* **2000**, 72 (2), 217-225.
2. Li, Z.; Zhao, R.; Wu, X.; Sun, Y.; Yao, M.; Li, J.; Xu, Y.; Gu, J., Identification and characterization of a novel peptide ligand of epidermal growth factor receptor for targeted delivery of therapeutics. *The FASEB Journal* **2005**, 19 (14), 1978-1985.
3. Song, S.; Liu, D.; Peng, J.; Deng, H.; Guo, Y.; Xu, L. X.; Miller, A. D.; Xu, Y., Novel peptide ligand directs liposomes toward EGF-R high-expressing cancer cells in vitro and in vivo. *The FASEB Journal* **2009**, 23 (5), 1396-1404.
4. Ongarora, B. G.; Fontenot, K. R.; Hu, X.; Sehgal, I.; Satyanarayana-Jois, S. D.; Vicente, M. G.  $\beta$ . H., Phthalocyanine,  $\Delta$ Peptide Conjugates for Epidermal Growth Factor Receptor Targeting. *Journal of Medicinal Chemistry* **2012**, 55 (8), 3725-3738.



5. Lee, S.; Xie, J.; Chen, X., Peptides and Peptide Hormones for Molecular Imaging and Disease Diagnosis. *Chemical Reviews* **2010**, *110* (5), 3087-3111.
6. Erickson, B. W.; Merrifield, R. B., Acid stability of several benzylic protecting groups used in solid-phase peptide synthesis. Rearrangement of O-benzyltyrosine to 3-benzyltyrosine. *Journal of the American Chemical Society* **1973**, *95* (11), 3750-3756.
7. Bodanszky, M., *Peptide chemistry*. Springer: 1988.
8. Jones, J., *Amino Acid and Peptide Synthesis*. Second ed.; Oxford University Press: New York, 2002.
9. Gutte, B., *Peptides: synthesis, structures, and applications*. Academic Press: 1995.
10. Marder, O.; Albericio, F., Industrial application of coupling reagents in peptides. *Chimica oggi* **2003**, *21* (6), 35-40.
11. Merrifield, R. B., Solid Phase Peptide Synthesis. I. The Synthesis of a Tetrapeptide. *Journal of the American Chemical Society* **1963**, *85* (14), 2149-2154.
12. Chan, W. C.; White, P. D., *Fmoc Solid Phase Peptide Synthesis: A Practical Approach*. Oxford University Press: Oxford, UK, 2004.
13. Grant, G. A., *Synthetic peptides: a user's guide*. Oxford University Press on Demand: 2002.
14. Benoiton, N. L., *Chemistry of peptide synthesis*. CRC Press: 2006.
15. Lew, A.; Krutzik, P. O.; Hart, M. E.; Chamberlin, A. R., Increasing Rates of Reaction: Microwave-Assisted Organic Synthesis for Combinatorial Chemistry. *Journal of Combinatorial Chemistry* **2002**, *4* (2), 95-105.
16. Fontenot, K. Design, Synthesis, Characterization, and Application of peptides in Medicine. Louisiana State University, Dissertation, 2012.
17. Sibrian-Vazquez, M.; Jensen, T. J.; Hammer, R. P.; Vicente, M. G. H., Peptide-Mediated Cell Transport of Water Soluble Porphyrin Conjugates. *Journal of Medicinal Chemistry* **2006**, *49* (4), 1364-1372.

18. Chatterjee, J.; Ovadia, O.; Zahn, G.; Marinelli, L.; Hoffman, A.; Gilon, C.; Kessler, H., Multiple N-Methylation by a Designed Approach Enhances Receptor Selectivity. *Journal of Medicinal Chemistry* **2007**, *50* (24), 5878-5881.
19. Sibrian-Vazquez, M.; Jensen, T. J.; Fronczek, F. R.; Hammer, R. P.; Vicente, M. G. H., Synthesis and Characterization of Positively Charged Porphyrin–Peptide Conjugates. *Bioconjugate Chemistry* **2005**, *16* (4), 852-863.
20. Sato, A. K.; Viswanathan, M.; Kent, R. B.; Wood, C. R., Therapeutic peptides: technological advances driving peptides into development. *Current Opinion in Biotechnology* **2006**, *17* (6), 638-642.
21. Góngora-Benítez, M.; Tulla-Puche, J.; Albericio, F., Multifaceted Roles of Disulfide Bonds. Peptides as Therapeutics. *Chemical Reviews* **2014**, *114* (2), 901-926.
22. Vlieghe, P.; Lisowski, V.; Martinez, J.; Khrestchatisky, M., Synthetic therapeutic peptides: science and market. *Drug discovery today* **2010**, *15* (1), 40-56.
23. Jenssen, H.; Aspino, S. I., Serum stability of peptides. *Peptide-based drug design* **2008**, 177-186.
24. Hess, S.; Ovadia, O.; Shalev, D. E.; Senderovich, H.; Qadri, B.; Yehezkel, T.; Salitra, Y.; Sheynis, T.; Jelinek, R.; Gilon, C., Effect of structural and conformation modifications, including backbone cyclization, of hydrophilic hexapeptides on their intestinal permeability and enzymatic stability. *Journal of medicinal chemistry* **2007**, *50* (24), 6201-6211.
25. Tugyi, R.; Uray, K.; Iván, D.; Fellingner, E.; Perkins, A.; Hudecz, F., Partial D-amino acid substitution: Improved enzymatic stability and preserved Ab recognition of a MUC2 epitope peptide. *Proceedings of the National Academy of Sciences of the United States of America* **2005**, *102* (2), 413-418.
26. Horswill, A. R.; Benkovic, S. J., Cyclic peptides, a chemical genetics tool for biologists. *Cell Cycle* **2005**, *4* (4), 552-555.
27. Cudic, M.; Wade, J. D.; Otvos Jr, L., Convenient synthesis of a head-to-tail cyclic peptide containing an expanded ring. *Tetrahedron Letters* **2000**, *41* (23), 4527-4531.

28. Huo, L.; van der Donk, W. A., Discovery and Characterization of Bicerucin, an Unusual d-Amino Acid-Containing Mixed Two-Component Lantibiotic. *Journal of the American Chemical Society* **2016**, *138* (16), 5254-5257.
29. Bai, L.; Romanova, E. V.; Sweedler, J. V., Distinguishing endogenous D-amino acid-containing neuropeptides in individual neurons using tandem mass spectrometry. *Analytical chemistry* **2011**, *83* (7), 2794-2800.
30. Kreil, G., D-amino acids in animal peptides. *Annual review of biochemistry* **1997**, *66* (1), 337-345.
31. Adessi, C.; Soto, C., Converting a Peptide into a Drug: Strategies to Improve Stability and Bioavailability. *Current Medicinal Chemistry* **2002**, *9* (9), 963-978.
32. Dedkova, L. M.; Fahmi, N. E.; Golovine, S. Y.; Hecht, S. M., Enhanced D-amino acid incorporation into protein by modified ribosomes. *Journal of the American Chemical Society* **2003**, *125* (22), 6616-6617.
33. Ieronymaki, M.; Androutsou, M. E.; Pantelia, A.; Friligou, I.; Crisp, M.; High, K.; Penkman, K.; Gatos, D.; Tselios, T., Use of the 2-chlorotriyl chloride resin for microwave-assisted solid phase peptide synthesis. *Peptide Science* **2015**, *104* (5), 506-514.
34. Omenn, G. S.; States, D. J.; Adamski, M.; Blackwell, T. W.; Menon, R.; Hermjakob, H.; Apweiler, R.; Haab, B. B.; Simpson, R. J.; Eddes, J. S., Overview of the HUPO Plasma Proteome Project: Results from the pilot phase with 35 collaborating laboratories and multiple analytical groups, generating a core dataset of 3020 proteins and a publicly - available database. *Proteomics* **2005**, *5* (13), 3226-3245.
35. Mozsolits, H.; Aguilar, M.-I., Surface plasmon resonance spectroscopy: An emerging tool for the study of peptide-membrane interactions. *Peptide Science* **2002**, *66* (1), 3-18.
36. Karlsson, R.; Stahlberg, R., Surface Plasmon Resonance Detection and Multispot Sensing for Direct Monitoring of Interactions Involving Low-Molecular-Weight Analytes and for Determination of Low Affinities. *Analytical Biochemistry* **1995**, *228* (2), 274-280.
37. Patching, S. G., Surface plasmon resonance spectroscopy for characterisation of membrane protein-ligand interactions and its potential for drug discovery. *Biochimica et Biophysica Acta (BBA) - Biomembranes* **2014**, *1838* (1, Part A), 43-55.

38. Fontenot, K. R.; Ongarora, B. G.; LeBlanc, L. E.; Zhou, Z.; Jois, S. D.; Vicente, M. G. H., Targeting of the epidermal growth factor receptor with mesoporphyrin IX-peptide conjugates. *Journal of porphyrins and phthalocyanines* **2016**, *20* (01n04), 352-366.
39. Lee, Y. S.; Agnes, R. S.; Davis, P.; Ma, S.-w.; Badghisi, H.; Lai, J.; Porreca, F.; Hruby, V. J., Partial Retro–Inverso, Retro, and Inverso Modifications of Hydrazide Linked Bifunctional Peptides for Opioid and Cholecystokinin (CCK) Receptors. *Journal of medicinal chemistry* **2007**, *50* (1), 165-168.
40. Xu, Y.; Song, S.; Liu, D., Peptide Ligand Directed Drug Delivery. Google Patents: 2008.

## **CHAPTER 3. Design and Synthetic Strategies for BODIPY-Peptidic Conjugates for Diagnosis of CRC via Peptide Linkages**

### **3.1 Introduction**

Visualizing the integrity of cells, especially cancerous cells, has become a technique of interest. Integration of labeling entities such as peptides, proteins, or DNA with non-radioactive fluorescent labels is a widely applicable area for understanding the cellular mechanisms.<sup>1</sup> In this instance BODIPY dyes are attractive and promising for labeling with fluorescence and have progressed as highly sought after entities for biomarker labeling.<sup>2</sup>

Recent advantages in the synthesis of BODIPY fluorophores have yielded a multitude of BODIPY conjugates readily available commercially. Companies such as Invitrogen, in particular, have designed various BODIPY fluorophores that cover the full visible spectrum, and have functionalization for conjugation to various sources such as proteins, lipids, polysaccharides, and peptides, which are available and ready to partake in labeling experiments.<sup>3-5</sup> However, disadvantages to these commercially available probes are apparent due to their small Stokes shifts; moreover, the readily available conjugates are exceptionally expensive and unsuitable for standard bioconjugation procedures on small or large scales. As a result, conquering the most important challenge of BODIPY probe development includes developing a fluorophore equipped with functional groups ready to covalently link BODIPY dyes to biomolecules.<sup>6-7</sup>

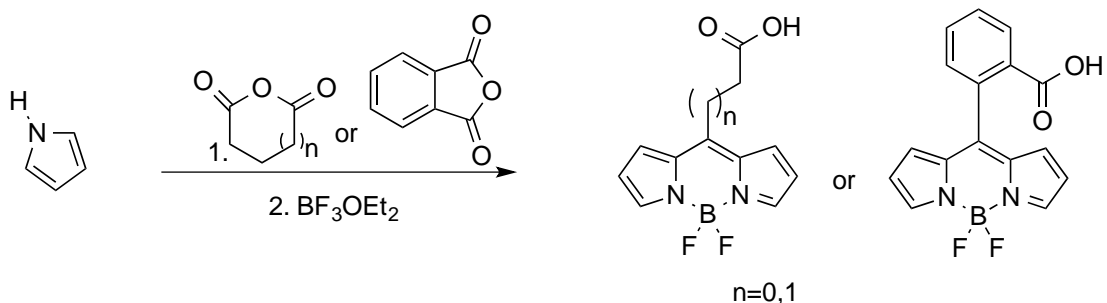
Developing an efficient method for attaching BODIPY dyes and peptides together insists that a clear position for attachment be present. In peptide synthesis, the most evident attachment point is revealed during the last deprotection of the Fmoc group yielding a free amino group at the N-terminus of the sequence. This reactive amino group can undergo a variety of transformations, however, the most common method is amidation. The free amino group of the peptide sequence can react in the presence of coupling agents and base with a carboxylic BODIPY dye to return the desired amide derived conjugate.

The simplicity of amino group formation for peptide sequence is important, as carboxylic BODIPY dyes are not as easily developed. There are various methods that exist to create carboxylic BODIPY dyes at either the *meso*, 2,6-, or 3.5- position. Among these methods, introduction of the carboxyl moiety is most often seen via 2,6-<sup>8-9</sup> or 3.5- positions<sup>10-11</sup>, on the BODIPY core through asymmetrical dye formation. The synthesis of asymmetrical dyes is usually created from the condensation of two different pyrroles with one pyrrole bearing a carboxyl group. The condensation of mixed pyrroles is more challenging as removal of side products tends to be lengthy.<sup>12-13</sup> This difficulty in purification can lead to percent yields being extremely low, and tedious for future bioconjugation steps.<sup>14-15</sup>

Past synthetic approaches to achieve carboxylic BODIPY dyes involved protection/deprotection steps that caused potential issues for the BODIPY core.<sup>16</sup> Protecting the carboxylic acid as an ester normally requires the use of basic conditions to remove the ester and reveal the necessary carboxylic acid. However, the core of the BODIPY dye is particularly unstable under basic conditions.<sup>6, 17-19</sup> Although favoring methods to remove esters under aqueous acidic conditions exist, to date yields for the corresponding BODIPY dye have the potential of yielding low yields due to removal of the BF<sub>2</sub> chelation unit. Consequently, carboxylic BODIPYs with easier and more convenient syntheses are significant for their practical applications. Due to the photophysical attractiveness of BODIPYs, synthesizing the necessary carboxylic BODIPY that is formed in minimal steps and high yielding is desirable for creating a fluorescent probe that is capable of *in vivo* imaging of CRC.

In 2009, a method for carboxylic BODIPY formation that bypassed the need for mixed pyrrole was revealed. Peng and coworkers developed a cascade of syntheses that eliminated the formation of protected carboxyl groups, asymmetrical dyes, and released the necessary acid in a two-step one pot reaction.<sup>20</sup> The synthetic strategy investigated the condensation of pyrrole entities with various anhydrides to determine the efficacy for carboxyl BODIPY formation. In these

reactions, the first step involves reacting a pyrrolic moiety with an anhydride to create the dipyrromethene structure, followed by complexation of the molecule with boron trifluoro diethyletherate to form the full BODIPY structure with a free carboxyl chain in 21-25% yields (Scheme 1).<sup>20</sup>



Scheme 1. Peng and coworkers' one pot two-step synthesis of carboxylic BODIPYs.<sup>20</sup>

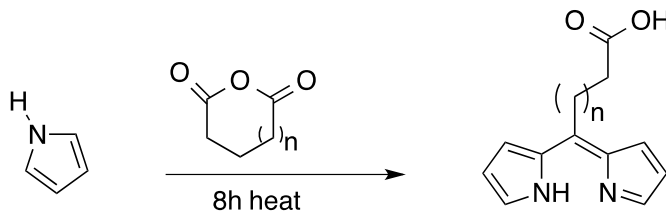
Peng's efforts revealed a method to achieve the desired BODIPY core bearing a free carboxylic acid, and the dismissal of the normal harsh conditions, long reaction times, and varied steps were reduced to a one-pot, two-step reaction under reflux. In order to prepare a carboxylic BODIPY core under moderate conditions to pair with the peptides designed in Chapter 2, the methods mentioned above were further explored. The performance of the new probes is studied for determination of the photophysical and *in vitro* properties.

## 3.2 Results and Discussion

### 3.2.1 Carboxylic BODIPY Dyes

Peng *et al.* investigation's contained synthesis of carboxylic BODIPYs by way of condensation of pyrroles and carboxylic anhydrides to form the necessary carboxyl dipyrromethene. Following the dipyrromethene formation, the BODIPY core is developed by coordination with  $\text{BF}_3\text{OEt}_2$ . The key step in this reaction was reported as the formation of the carboxyl dipyrromethene, or step one (Scheme 2). The conditions during the condensation were noted to be of great success under anhydrous conditions, thus molecular sieves are applied to rid

the reaction of the water produced during the dipyrromethene construction. Dehydration of the ensuing water produced allows the reaction to bypass dipyrromethane, an unstable intermediate, and form the dipyrromethene *in situ*.

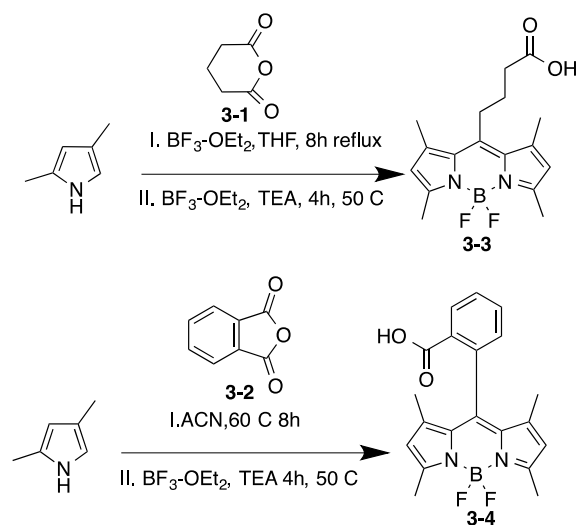


Scheme 2. Peng and coworkers' pivotal step in the synthesis of carboxylic BODIPYs.<sup>20</sup>

To replicate Peng's reactions, glutaric anhydride (**3-1**) and phthalic anhydride (**3-2**) were used for the dicarboxylic anhydrides. Compounds **3-1** and **3-2** were condensed with 2,4-dimethylpyrrole under inert conditions to yield the corresponding dipyrromethene. This condensation is done in the presence of an acid catalyst  $\text{BF}_3 \cdot \text{OEt}_2$  in tetrahydrofuran (THF) over the course of eight hours to promote the formation of the dipyrromethene by coordinating to the anhydride inserting a partial positive charge and ensuring the pyrroles nucleophilic behavior. The resulting dipyrromethene was then deprotonated under basic conditions using triethylamine (TEA) the following dipyrromethene is then complexed with boron trifluoride etherate ( $\text{BF}_3 \cdot \text{OEt}_2$ ) to form carboxylic BODIPY compounds **3-3** and **3-4** in four hours (Scheme 3).

Purifications of these BODIPY dyes were performed on these compounds using two different systems deemed by Peng *et al.* BODIPY **3-3** and **3-4** was purified by silica gel column chromatography using a hexane, ethyl acetate (EtOAc), acetic acid (HOAc) mixture 80:40:1; and hexane, ethyl acetate, methanol (MeOH) mixture 100:30:3 respectively. Purification of these compounds proved to be quite strenuous as thin layer chromatography (TLC) showed several impurities and column chromatography was equally inefficient, and a pure product was only achieved in trace amounts as shown by mass spectrometry. Separation of the crude mixture proved difficult due to numerous impurities near impossible to remove.





Scheme 3. Synthesis of carboxylic BODIPYs 3-3 and 3-4 using conventional heating methods.<sup>30</sup>

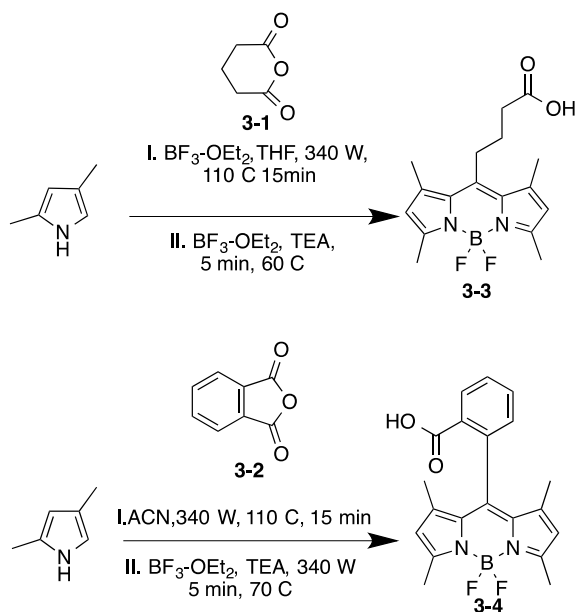
In an attempt to improve the carboxylic BODIPY yields, microwave-assistance (MW) was applied as seen in SPPS. Previously MW provided cleaner reaction efforts at a fraction of the time seen in conventional bench-top synthesis of peptides in Chapter 2. In BODIPY synthesis, we speculated that the homogeneous and speedy heating would result in substantial accelerations in the key step (i.e. dipyrromethene development.) The enhanced heating of the reaction mixture would allow for ideal conditions that are often neglected in normal heating measures such as reflux.

21

Irradiating the reaction mixture under microwave conditions produces an efficient thorough internal heating over the entire solution based on dielectric properties. The extent of the energy transferred is dependent on the dielectric properties of the molecules in the mixture. Compounds or solvents with high dielectric constants tend to absorb microwave energy, whereas less polar substances absorb poorly.<sup>22</sup> Therefore, reactions performed in MW can manufacture high yields while diminishing the quantity of side-products.<sup>21</sup>

The same constituents used before, 2,4-dimethylpyrrole, compounds **3-1** and **3-2** were subjected to condensation, however this time, using MW conditions to form the dipyrromethene

core, and then cooled to room temperature before subjecting each reaction to complexation in the microwave to form BODIPYs **3-3** and **3-4** (Scheme 4).



Scheme 4. Synthesis of carboxylic BODIPYs **3-3** and **3-4** using microwave-assistance.

As assumed, TLC analysis of each compound showed fewer impurities, and column purification was indeed successful. Carboxylic BODIPY **3-3** initially was not produced in reasonable yield, which we believed was partially due to the solvent used, tetrahydrofuran (THF). THF is not a good microwave solvent as it does not absorb the microwave radiation as well as other solvents, and this is due to its low dielectric constant, 7.58 as seen in Table 1. The polar atmosphere necessary to push reactions to completion is not applicable in THF, however attempts to aid in this effort with the incorporation of solvents with higher dielectric constants were applied. Acetonitrile (ACN), is a prime solvent for MW synthesis as it holds a dielectric constant of 37.5, which is 5-fold higher than that seen with THF. Conversely, the adaptation of ACN as the solvent during MW synthesis of BODIPY **3-3** still did not produce an increase in BODIPY formation as no product was found. This could be partially due to solubility issues of anhydride **3-1** in ACN.

Several efforts to increase the yields of BODIPY **3-3** and **3-4** were attempted, such as changing solvent and temperature conditions, however neither alteration was able to yield BODIPY

**3-4**, or cause a true increase in yield of BODIPY **3-3** were found (Table 1).

Table 1: Synthesis of Carboxylic BODIPYs from 2,4-dimethylpyrrole

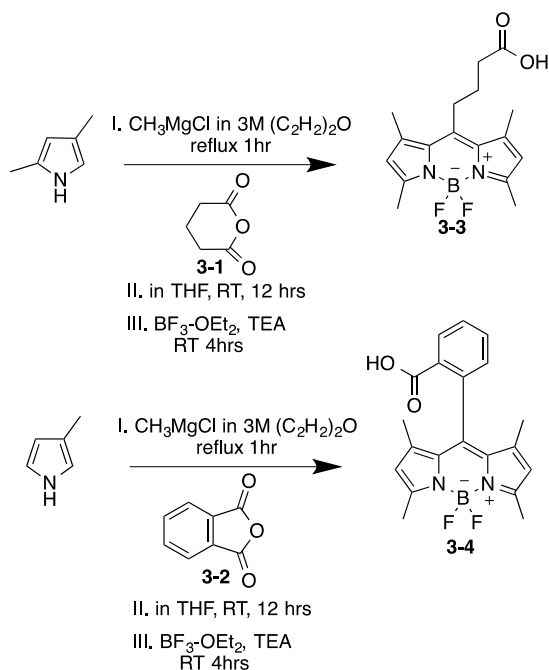
| BODIPY     | METHOD | TEMP (°C) | SOLVENT | % YIELD |
|------------|--------|-----------|---------|---------|
| <b>3-3</b> | BT     | 77        | THF     | 3.3     |
| <b>3-3</b> | MW     | 110       | THF     | 1.7     |
| <b>3-3</b> | MW     | 110       | ACN     | -       |
| <b>3-4</b> | BT     | 60        | ACN     | 2.4     |
| <b>3-4</b> | MW     | 100       | ACN     | 4.8     |

### 3.2.2 Optimization of BODIPY Synthesis

Several attempts to rectify downfalls associated with carboxylic BODIPY dye synthesis led to an evaluation of anhydrides **3-1** and **3-2**, and the premise for BODIPY formation. Condensation of anhydride **3-1** with 2,4-dimethylpyrrole releases a very short alkyl chain between the core of the BODIPY dye and the point of attachment at the meso-position. This short alkyl chain is beneficial for allowing each entity to extend in a preferred conformation, away from the core (Figure 1). Anhydride **3-2** condensation with 2,4-dimethylpyrrole source would yield a more sterically hindered carboxylic BODIPY however the possibility of a more fluorescent probe due to the restriction of rotation of the phenyl substituent at the meso position containing the carboxylic acid allowing for an increased quantum yield.<sup>23</sup>

Ultimately, the disadvantage of using either anhydride is the reactivity of the anhydride toward the addition of 2,4-dimethylpyrrole during the formation of the dipyrromethene. To counter this issue, increased nucleophilicity of the pyrrole, in the reaction is strongly desired. To achieve this goal, a Grignard of the desired 2, 4-dimethylpyrrole was considered to increase the reactivity and push the reaction toward BODIPY formation.

To form the desired Grignard pyrrole, 2,4-Dimethylpyrrole was allowed to react with methyl magnesium chloride in 3M diethyl ether and refluxed for one hour. The resulting Grignard pyrrole was then condensed with anhydride **3-1** and **3-2** in THF at room temperature for 12 hours. The more nucleophilic pyrrole was still engaged with boron trifluoride source to coordinate with anhydrides in solution to provide the optimal conditions for condensation of the two entities. The consequential dipyrromethene was then coordinated as seen before using TEA and  $\text{BF}_3\text{OEt}_2$  to yield BODIPY **3-3** and **3-4** in improved yields (Scheme 5).



Scheme 5. Synthesis of carboxylic BODIPYs **3-3** and **3-4** Grignard pyrroles.

The one pot two step carboxylic BODIPY dye concept was expelled and used as a one pot reaction, but now requiring three steps producing yields that showed a considerable increase over 10-fold as shown in Table 2. The development of BODIPY dyes with a carboxylic acid as a point of attachment identified several disadvantages such as poor yields, multiple impurities, and various complications. However, instituting a more reactive pyrrole has resulted in the increase the yields of product formation considerably, and also assist with limiting the amount of side products formed.

The reactions were purified in the same manner as Peng's method, and were readied for conjugation.

Table 2: Synthesis of Carboxylic BODIPYs from 2,4-dimethylpyrrole under Grignard Conditions

| BODIPY | Equiv of Grignard | % YIELD |
|--------|-------------------|---------|
| 3-3    | None              | 3.3%    |
| 3-3    | 1.1               | 50%     |
| 3-4    | None              | 2.4%    |
| 3-4    | 1.1               | 70%     |

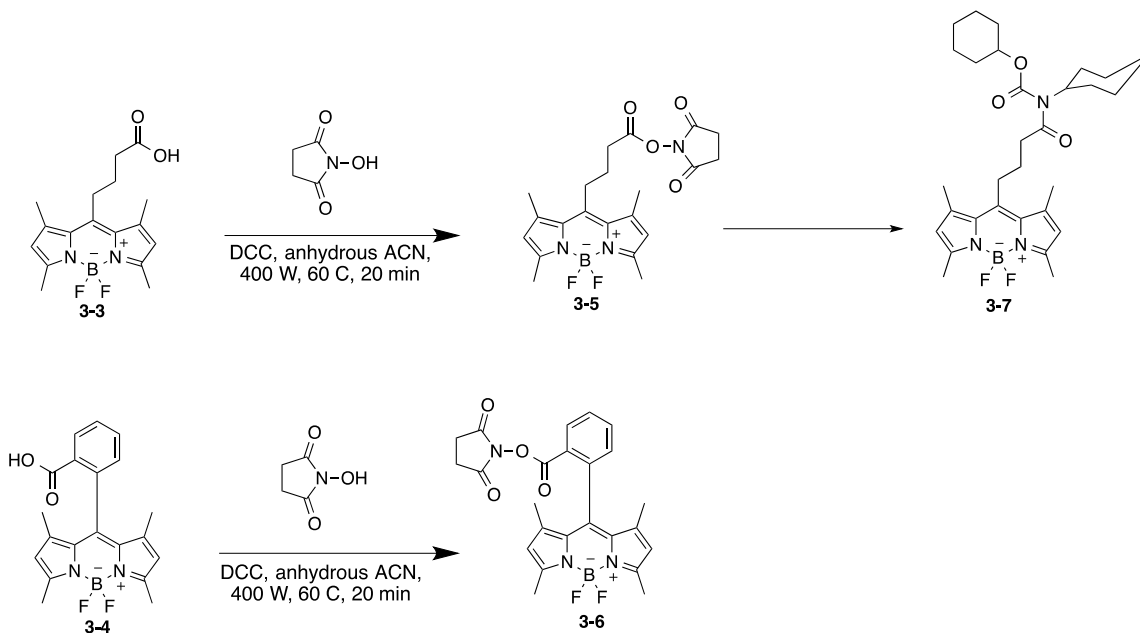
### 3.2.3 Activation of BODIPY dye

Conjugation of fluorescent dyes and peptide/amino acids is most frequently performed using peptide chemistry via SPPS or solution phase. Of these techniques, SPPS provides a cleaner reaction and is considered most convenient for peptide synthesis, however, there are several factors of SPPS that deems this method unfavorable for some fluorophore conjugation procedures. Normal SPPS solvents used, such as DMF, are not favored due to possible solubility issues for fluorophores. Another prominent issue is the adsorption of the fluorophore to the resin beads, making it almost impossible to retrieve conjugates after cleavage.<sup>24</sup> Lastly, the conditions of cleavage of product from the resin may be harsh for certain fluorophores, especially BODIPY dyes.<sup>19</sup> The TFA cocktail used can potentially degrade the core of the BODIPY dye. For these reasons conjugation methods tend to lean toward solution phase protocols for amide bond formation.

Solution phase protocols to connect dyes to biomolecules have shown to be mostly low yielding; thus, activating dyes prior to interaction with biomolecules have been employed to combat these issues. Activation of BODIPY dyes with N-hydroxysuccinimide (NHS) or another coupling agent that is most prominent in peptide building are routes to create a highly active BODIPY dye

that is more reactive than its carboxylic counterpart to interact with free amino group on desired peptides **2-1** and **2-2**.<sup>20, 25-26</sup>

Activation of BODIPYs **3-3** and **3-4** were first completed using dicyclohexylcarbodiimide (DCC) to create an electrophile that is then attacked by N-hydroxyl succinimide (NHS) in anhydrous acetonitrile (ACN). These reactions should yield stable active NHS-BODIPY ester intermediates BODIPY **3-5** and **3-6**. However the desired product was an intermediate to the actual product isolated BODIPY **3-7** using microwave-assistance (Scheme 6).



Scheme 6. Activation of carboxylic BODIPYs **3-3** and **3-4** using N-hydroxysuccinimide using MW.

A side product with comparable molecular weight was formed, and was determined through X-ray crystallography to be an undesired product **3-7** (Figure 1). Activation of BODIPY **3-4** was more promising and product **3-6** was formed in 84% yield (Table 3), however including a method to improve the yield of reaction is also preferred.

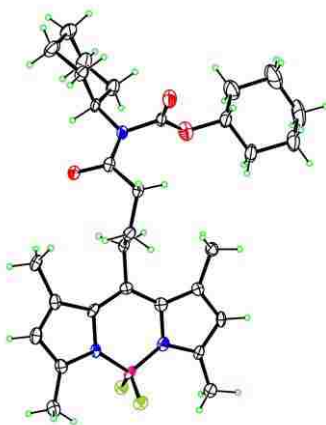
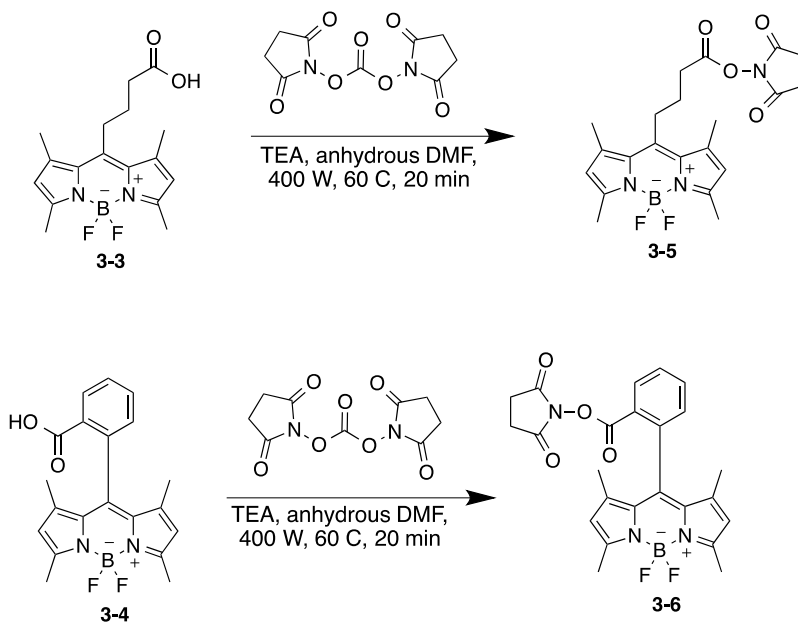


Figure 1. Crystal Structure of undesired BODIPY 3-7 of activated Glutaric BODIPY.

To counter the formation of BODIPY **3-7** and bids to increase the yield of BODIPY **3-5**, a second method for producing NHS-activated BODIPY dye was investigated. BODIPY **3** and **4** were reacted with triethylamine to activate the carboxylic acid in the presence of *N,N'*-disuccinimidyl carbonate in anhydrous DMF (Scheme 7).



Scheme 7. Activation of carboxylic BODIPYs 3-3 and 3-4 using *N,N'*-disuccinimidyl carbonate.

Activated BODIPY 3-3 and 3-4 varied depending on the method used to activate them as shown in Table 3, as well as the product created. BODIPY 3-5 was synthesized from method 2 in higher yield where N,N'-disuccinimidyl carbonate was the source to create the ester. BODIPY 3-6 was produced from method 1 in higher yield using NHS. BODIPY 3-6 preference of NHS may be due to a steric interaction involving N,N'-disuccinimidyl carbonate and the methyl groups located at C1 and C7 positions of the BODIPY core. BODIPY 3-5 and 3-6 were purified on silica gel using dichloromethane (DCM) and ethyl acetate (EtOAc) in a 12:1 ratio .

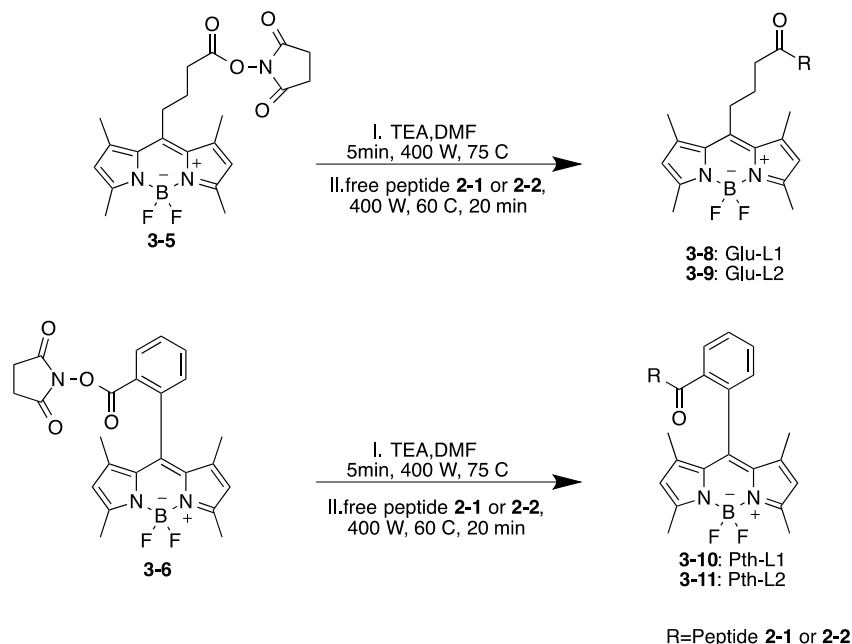
Table 3: Activation of Carboxylic BODIPY dyes 3-3 and 3-4

| Method | Product | SUCCINIMIDE                      | TEMP<br>(°C) | SOLVENT | %YIELD |
|--------|---------|----------------------------------|--------------|---------|--------|
| 1      | 3-5     | NHS                              | 110          | ACN     | trace  |
| 1      | 3-6     | NHS                              | 100          | ACN     | 84.1   |
| 2      | 3-5     | N,N'-DISUCCINIMIDYL<br>CARBONATE | 77           | DMF     | 76.3   |
| 2      | 3-6     | N,N'-DISUCCINIMIDYL<br>CARBONATE | 60           | DMF     | 25.3   |

### 3.2.4 Conjugation of BODIPY dyes to Peptide Ligands

Compounds 3-5 and 3-6 were first introduced to peptides 2-1 and 2-2 using microwave-assistance to form the desired conjugates. Compounds 3-5 and 3-6 were activated using TEA and coupled to each peptide in DMF. The resulting compounds were then removed from the resin using the aforementioned TFA cocktail, and lyophilized, which should have produced conjugates 3-8, -9, -10, and -11 (Scheme 8).





Scheme 8. Coupling of activated BODIPYs 3-5 and 3-6 to peptide.

Of the four conjugates, conjugate **3-11** was the only compound not to show any molecular ion through MALDI mass spectrometry (Table 4). Conjugate **3-10** did show product, however, the product was produced only in trace amounts. These two compounds are believed to have larger steric interaction preventing full conjugation of the peptide to the BODIPY dye. Conjugates **3-8** and **3-9** were synthesized, but after purification, conjugate **3-8** no longer fluoresced which was confirmed by mass spectrometry to be missing the  $\text{BF}_2$  chelation. In an attempt to restore the  $\text{BF}_2$  complex the dipyrromethene product of conjugate **3-8** was subjected to complexation with boron trifluoroetherate and TEA, which was unsuccessful. Conjugate **3-9** synthesis did not yield enough compound for further studies, and as seen with conjugate **8** the  $\text{BF}_2$  complex was also removed after a while.

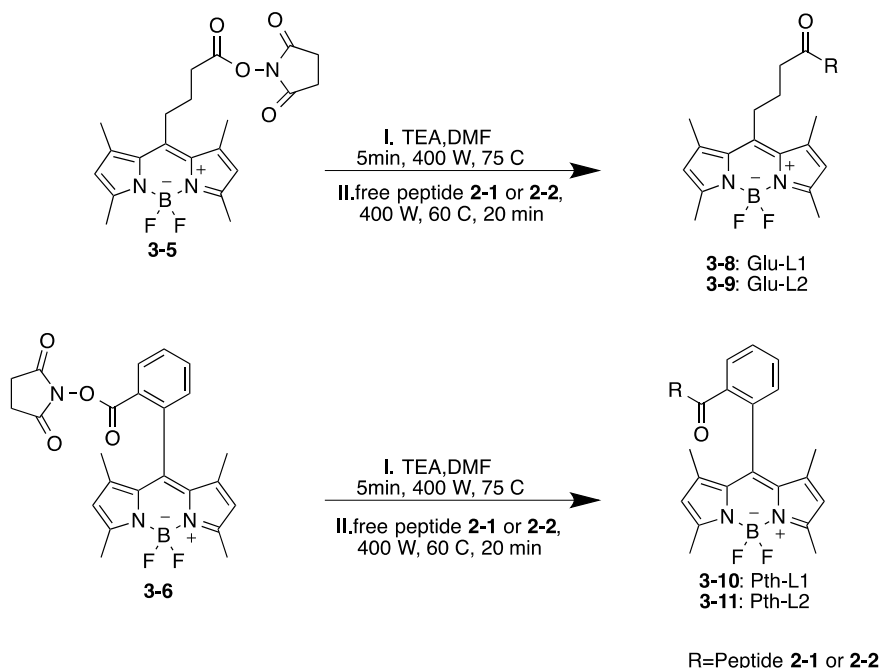
Table 4: Results of Solution Phase Conjugation of BODIPY-peptide Conjugates

| Compound    | Molecular Weight | % Yield |
|-------------|------------------|---------|
| <b>3-8</b>  | 1001.62          | 5.8     |
| <b>3-9</b>  | 1855.88          | .6      |
| <b>3-10</b> | 1035.06          | .13     |
| <b>3-11</b> | 1889.89          | -       |

Each successful conjugate was purified using RP-HPLC, and identified by mass spectrometry. Overall, all conjugates were confirmed in very low yields, therefore, indicating the need for optimization of reaction conditions and purifications for conjugates in Table 4. Of the products, conjugates containing peptide EGFR-L1 proved to be more promising for the conjugation via NHS activation.

Although studies suggested SPPS is unfavorable in conjugation procedures for peptides and fluorophores, an attempt to confirm these findings were performed. SPPS chemistry was investigated with peptide **2-1** and activated BODIPYs **3-5** and **3-6**. Each activated dye was allowed to stir with TEA for one hour, followed by introduction to EGFR-L1 and allowed to react for 36 to 72 hours (Scheme 9).

After 72 hours the anticipated conjugates were cleaved from resin beads and investigated via Mass Spectrometry, however no product was determined. While minimal fluorescence was noted on resin beads, the desired conjugates **3-8**, **3-9**, **3-10**, or **3-11** were also not returned as expected. This observation confirmed the previously mentioned rigorous cleavage cocktails, possibly degrading any possible conjugates. To ensure activated BODIPY **3-5** and **3-6** were not the issues regarding the conjugation, BODIPYs **1** and **2** were further investigated.



Scheme 9. Coupling of activated BODIPYs **3-5** and **3-6** to resin bound peptides **2-1** or **2-2**.

Overall, activated BODIPY dyes **3-5** and **3-6** interaction with either peptide returned very little to no compound, and SPPS strategies showed no alleviation to conjugation issues, thus requiring the return to carboxylic BODIPY dyes **3-3** and **3-4** to strategize the next step. The determination of the more beneficial dye for synthesis of Peptide-BODIPY conjugates was vital. Carboxylic BODIPY **3-4** would have a stronger steric interaction with either peptide during conjugation, leading to a decrease in percent yields. Alternatively, BODIPY **3-3** has a short alkyl chain, distancing the core of the BODIPY dye from the point of attachment making conjugation through the *meso*-position quite easier from this scaffold. For this reason, further efforts toward BODIPY-peptide conjugation procedure with BODIPY **3-3** were sustained.

Solution phase coupling provided minimal product using activated BODIPY dyes, and prompting the need for an alternative-coupling agent that would possibly push each reaction to completion. Choosing the appropriate coupling agent depends on the chemical properties of every component. These properties consist of items such as reactivity, sterics, and stability to name a few.<sup>27</sup> Various coupling agents are available for peptide synthesis with different advantages for

synthesis, however, three coupling agents were investigated for these fluorophore-peptide conjugations TBTU, TSTU, and DEPBT (Figure 2).

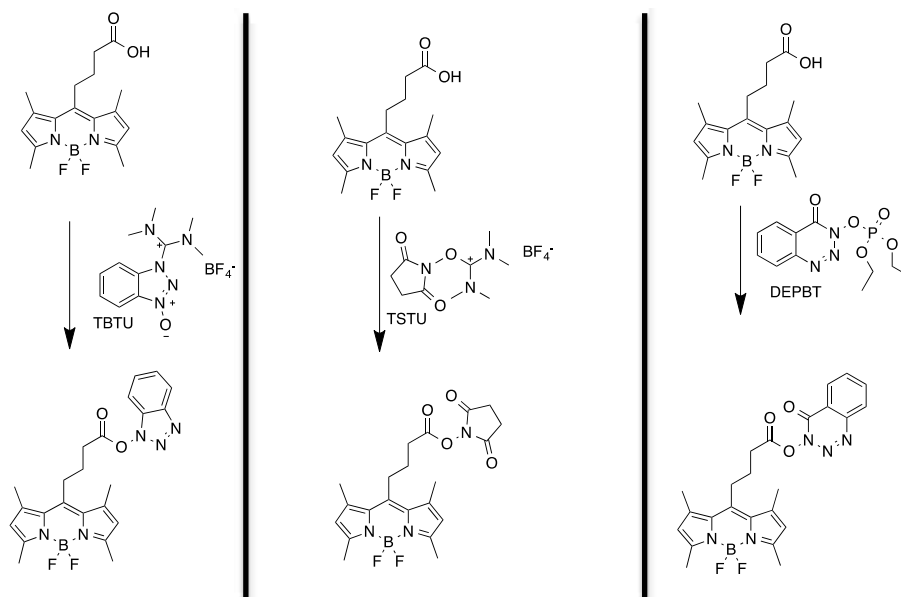
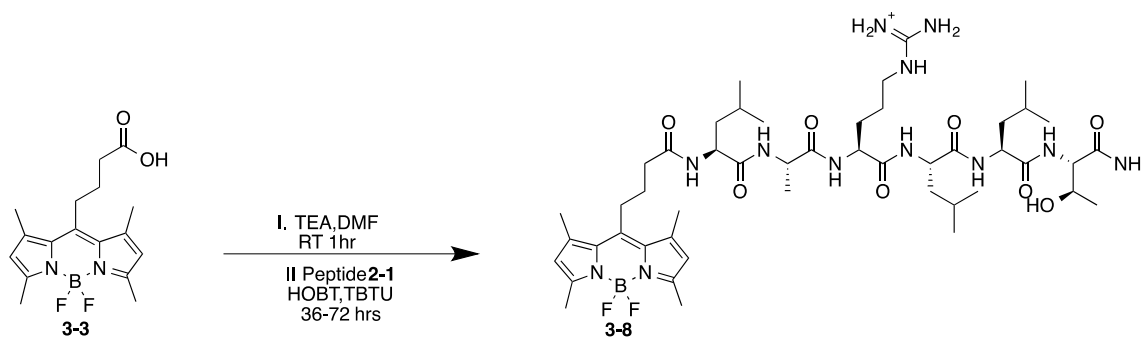


Figure 2. Coupling reagents TBTU, TSTU, and DEPBT interaction with BODIPY 3-3.

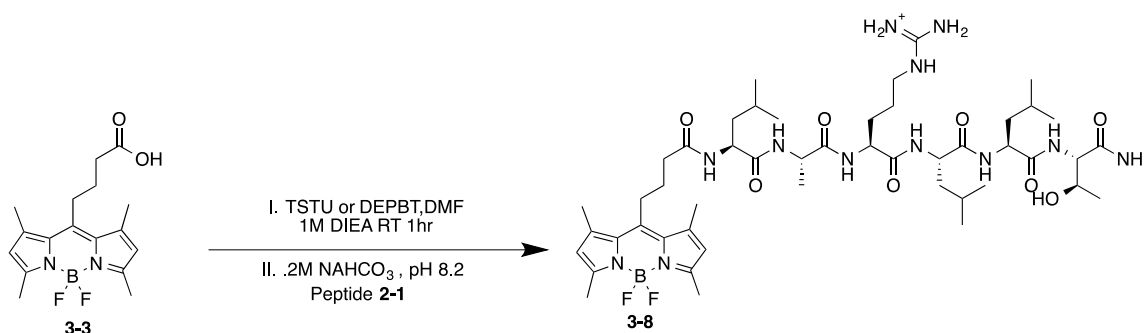
The first coupling agent considered was TBTU that was used in Chapter 2 for peptide synthesis. TBTU was introduced to the carboxylic acid of BODIPY **3-3** in a similar manner. The carboxylic acid was allowed to stir for one hour in the presence of TEA followed by the addition of a mixture of coupling agent TBTU, additive HOBT, and free peptide **2-1**. Conjugation of peptide **2-1** and BODIPY **3-3** was successfully, however in 12% yield, slightly higher than what was obtained with the NHS activated BODIPY (Scheme 10).



Scheme 10. Coupling of BODIPY 3-3 solution phase to peptide 2-1.

Coupling agents TSTU and DEPBT were then investigated under different procedures. Unlike TBTU, coupling agents TSTU and DEPBT do not require an additive to assist with coupling.<sup>28</sup> BODIPY **3-3** was allowed to activate, with either coupling agent TSTU or DEPBT, for one hour in the presence of diisopropylethylamine (DIPEA) in DMF. After each reaction showed activation by mass spectrometry, each activated BODIPY was added slowly to a solution of .2M sodium bicarbonate (NaHCO<sub>3</sub>) at pH 8.2 containing peptide **2-1** at 0°C. The solution was then allowed to stir at 8°C overnight (Scheme **11**). Each reaction showed successful conjugation by MS, which was purified by RP-HPLC.

The yield for this reaction was noted at 18% yield, with TSTU proving to be a better coupling agent. This increase in percent yield could be explained by the structure of the coupling agents (Figure 2). Comparing TSTU to DEPBT and TBTU the NHS-activated BODIPY formed is a smaller intermediate than what is formed in the other cases, furthermore possibly allowing for more of the activated intermediate to be formed. The reactivity of TSTU compared to NHS during the in situ activation maybe a driving force for conjugate formation.

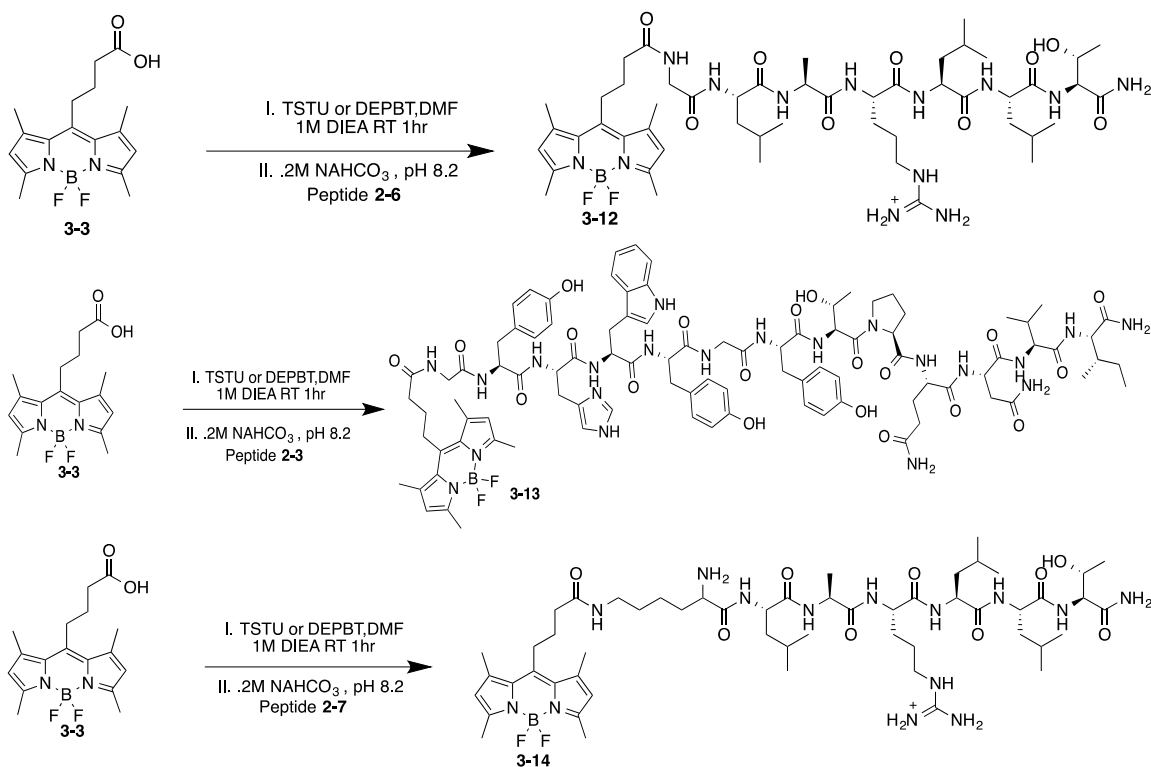


Scheme 11. Coupling of BODIPY **3-3** solution phase to peptide **2-1** using TSTU or DEPBT coupling agents.

Although 18% yield was the highest percent yield obtained, further expansion on the conjugation platform was necessary. However, an expansion on the peptides utilized was considered to assist in increasing the percent yields of the reaction. Two peptide derivatives of parent peptide **2-1** were considered, which have amino acids present that can behave as a small

linker between BODIPY **3-3** and the core sequence of the peptides. Peptides **2-6** (GLARLLT) and **2-7** (KLARLLT) from Chapter 2 were investigated for their potential as targeting molecules with BODIPY **3-3**. As a comparison peptide **2-3** (GYHWYGYTPQNVI) was also investigated.

The new peptides were first tested with coupling agents TSTU and DEPBT to identify any difference in reaction yields. Under the conditions seen with peptide **2-1**, BODIPY **3-3** was allowed to activate, with either coupling agent, for one hour in the presence of diisopropylethylamine (DIPEA) in DMF. Each activated BODIPY was added slowly to a solution of the peptide and stirred overnight (Scheme 12).



Scheme 12. Coupling of BODIPY **3-3** solution phase to peptide **2-3**, **2-6**, **2-7** using TSTU or DEPBT coupling agents.

It was determined that TSTU was the ideal coupling agent needed to continue synthesis as for all peptide derivatives produced as summarized in Table 5. For conjugates **3-12** and **3-13**, no product was obtained, which was probably due to the steric interaction at the N-terminus of each conjugate when trying to activate with coupling agent DEPBT. A longer linker/amino acid is necessary, similar to that of conjugate **3-12**. When also comparing conjugate **3-12** and conjugate

**3-8**, the small linker seems to have played a positive role in increasing the yield of desired BODIPY conjugates to up to 22% yield.

The effect of the amount of compound solubilized during activation has the potential to increase the amount of conjugate returned, and minimize the amount of side products formed.

Table 5: Results of Coupling Agent Studies for Synthesis of Peptide-BODIPY conjugates

| Compound    | Molecular Weight | 7.5 equiv of Coupling Agent | % Yield |
|-------------|------------------|-----------------------------|---------|
| <b>3-12</b> | 1058.64          | <b>TSTU</b>                 | 22      |
| <b>3-12</b> | 1058.64          | <b>DEPBT</b>                | 0       |
| <b>3-13</b> | 1911.91          | <b>TSTU</b>                 | 26      |
| <b>3-13</b> | 1911.91          | <b>DEPBT</b>                | 0       |
| <b>3-14</b> | 1129.72          | <b>TSTU</b>                 | 21      |
| <b>3-14</b> | 1129.72          | <b>DEPBT</b>                | 10      |

The stability of each reaction was tested in two well-known peptide solvents DMF and NMP. Both solvents have similar properties and belong to a class of solvents noted as dipolar aprotic solvents that will not interfere with the synthesis of conjugates, but provide good solvency of the organic BODIPY dyes. BODIPY **3-3** was dissolved in either DMF or NMP and allowed to activate using TSTU coupling agent for 1 hour in the presence of DIPEA. After one hour the activated dye was added in a drop wise manner to each peptide in .2M NaHCO<sub>3</sub> at pH 8.2.

Overall, the most efficient solvent for amide bond conjugation remained as DMF for conjugates **3-12**, **3-13**, **3-14** as shown in Table 6. The solubility of each BODIPY in either solvent was good; however, when the coupling agent was added to NMP solvation proved to be quite difficult, as extra solvent was necessary to dissolve the coupling agent. This measure possibly diluted the agent causing for a less effective synthesis of activated BODIPY **3-3** and **3-4**. To

maintain the efficiency of the reaction thus far, DMF was considered the most viable solvent, and carried forward for more optimizing. Next, the conjugates reactions were optimized by varying the temperature.

Table 6: Results of Solvent Studies for Synthesis of BODIPY-peptide Conjugates

| Compound | Solvent | % Yield |
|----------|---------|---------|
| 3-12     | DMF     | 30%     |
| 3-12     | NMP     | 12%     |
| 3-13     | DMF     | 26%     |
| 3-13     | NMP     | 18%     |
| 3-14     | DMF     | 21%     |
| 3-14     | NMP     | 13%     |

Conjugate **3-12** peptide solution was allowed to sit at 0°C longer than the other solutions due to the slow addition of activated BODIPY dyes. After purification, an increase in the amount of compound returned, and an ease of purification was noted. To determine if allowing peptide solutions in .2M NaHCO<sub>3</sub> to stir longer at 0°C will have a positive effect on all conjugates, all reactions were studied. This time before addition of activated BODIPY **3-3**, all solutions were allowed to stir at 0°C for 30 minutes.

Reaching the optimal temperature for peptides before interacting with the reactive BODIPY dyes is indeed a vital component as observed in Table 7. The lower reaction temperatures minimize the reactivity of the peptide and allow the reaction to push the desired products to complete formation, thus, an increase of each conjugate was afforded.

The final strategy was to determine the effects of the reactions pH on the percent yield. The method previously utilized had allowed the reaction to maintain a pH of 8.2. Considering the environment of our peptides that were not previously desalted to remove any residual triflate salts,

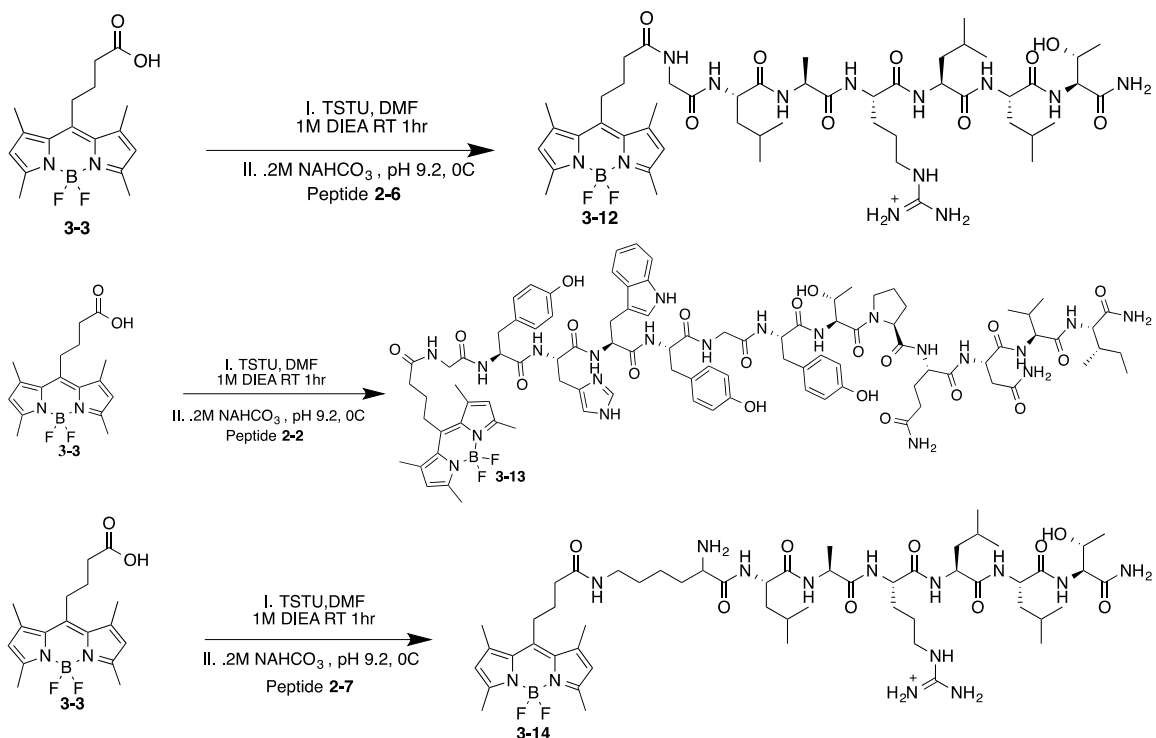


the pH of the reaction mixture could possibly be slightly more acidic than desired. To counter this issue, increasing the pH of the reaction mixture to a pH of 9.2 was performed. The activation of BODIPY **3-3** was performed as previously mentioned, and the solubilizing of each peptide in the .2M NaHCO<sub>3</sub> now at 9.2 pH was carried out (Scheme **13**).

Table 7: Results of Temperature Studies of Peptide-BODIPY Conjugates

| Compound    | Temperature | % Yield |
|-------------|-------------|---------|
| <b>3-12</b> | <b>RT</b>   | 22%     |
| <b>3-12</b> | <b>0C</b>   | 30%     |
| <b>3-13</b> | <b>RT</b>   | 26%     |
| <b>3-13</b> | <b>0C</b>   | 46%     |
| <b>3-14</b> | <b>RT</b>   | 21%     |
| <b>3-14</b> | <b>0C</b>   | 49%     |

The results for each conjugation nearly doubled allowing more anticipated yields to be attained as seen in Table 8. Controlling the reaction environment was found to be promising, allowing for ideal conjugation procedures under slightly more basic conditions. This effect showed that reactions mixtures were cleaner during purification by minimizing the quantity of side products allowing for higher percent yields. All conjugates were purified by RP-HPLC to a purity of 95% or higher and prepared for characterization.



Scheme 13. Coupling of BODIPY 3-3 solution phase to peptides 2-2, 2-6, and 2-7 using pH 9.2.

Table 8: Results of pH Studies of Peptide-BODIPY Conjugates

| Compound | Molecular Weight | pH  | % Yield |
|----------|------------------|-----|---------|
| 3-12     | 1058.64          | 8.2 | 30%     |
| 3-12     | 1058.64          | 9.2 | 71%     |
| 3-13     | 1911.91          | 8.2 | 46%     |
| 3-13     | 1911.91          | 9.2 | 65%     |
| 3-14     | 1129.72          | 8.2 | 49%     |
| 3-14     | 1129.72          | 9.2 | 73%     |

### 3.3 Characterization of BODIPY-Peptide Conjugates

#### 3.3.1 NMR Studies

Proton NMR ( $^1\text{H-NMR}$ ) and HSQC were used to characterize all conjugates.  $^1\text{H-NMR}$  was used to test BODIPY 3-3. From the  $^1\text{H-NMR}$  spectra of BODIPY 3-3 the methyl groups present at the 1,7- and 3,5- positions of the dyes scaffold yield a single peak (Appendix B). These singlets are

typically observed in each conjugate approximately around 2.5 and 2.3 ppm respectively. These significant peaks, representing the scaffold of the BODIPY's core, were essential in investigating the proton NMR due to various overlaps of the BODIPY's alkyl chain present at the meso-positions' protons, and the methyl protons at the side chains of each peptide sequence were observed around 1.5-1.8 ppm. Furthermore the backbone of the peptides sequence were also used to analyze the <sup>1</sup>H-NMR as the protons of each amide linkage are noted as one multiplet near approximately .86 ppm.

### 3.3.2 Photophysical Studies

UV-Vis spectroscopy and fluorescence were used to investigate the absorption and emission properties of BODIPY conjugates **3-12**, **3-13**, and **3-14**. All studies were recorded in dimethylsulfoxide (DMSO) at room temperature, and the conjugates were then compared to the carboxylic precursor BODIPY **3-3**. Particular emphasis on spectroscopic properties such as: the maximum absorption ( $\lambda_{\text{abs}}$ ) and emission ( $\lambda_{\text{em}}$ ) wavelengths, Stokes' shifts, and molar extinction coefficients ( $\log \epsilon$ ), were studied and the results are summarized in Table 9 and Figure 3.

Figure 3 shows the normalized absorption and emission spectra for BODIPY **3-3** and the corresponding conjugates **3-12**, **3-13**, and **3-14**. As reported in literature carboxyl BODIPY **3-3** showed characteristic strong absorption band at 500 nm with a  $\log \epsilon$  value of 3.97 with an emission at 509 nm.

All BODIPY-peptide conjugates have parallel absorption and emission spectra, due to their similar BODIPY cores which is slightly blue shifted from the parent compound BODIPY **3-3** as shown in Table 9 and Figure 3.

Table 9. Spectroscopic properties of BODIPYs in DMSO at room temperature

| Compound    | $\lambda_{\text{abs}}$ | $\lambda_{\text{em}}$ | Stokes shift | $\text{Log}\epsilon$ |
|-------------|------------------------|-----------------------|--------------|----------------------|
| <b>3-3</b>  | 500 nm                 | 509nm                 | 9 nm         | 3.97                 |
| <b>3-12</b> | 499 nm                 | 508 nm                | 9 nm         | 4.40                 |
| <b>3-13</b> | 499 nm                 | 508 nm                | 9 nm         | 4.30                 |
| <b>3-14</b> | 499 nm                 | 508 nm                | 9 nm         | 4.21                 |

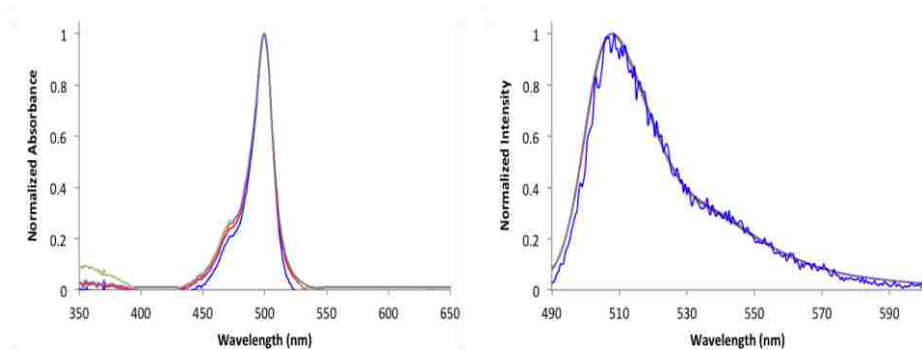


Figure 3. Normalized UV-Vis and fluorescence spectra of BODIPY 3-3 (Blue), BODIPY peptide conjugates 3-12 (Red), 3-13 (Green), and 3-14 (Purple) in DMSO at room temperature.

This instance is also noted in the emission of all conjugates as they all exhibit a band at 508 nm. The similarity in absorbance and emission may be an indication that conjugation through a short alkyl chain at the *meso* position of the BODIPYs core will result in negligible blue-shifts of the compounds spectroscopic properties. The Stokes shifts for all BODIPY dyes, precursor and conjugates, exhibit in the range of (~9 nm). Determination of Quantum Yields are still underway.

### 3.3.2 SPR of BODIPY-Peptide Conjugates

SPR of all BODIPY-Peptide conjugates and precursor were tested in a concentration manner from .25  $\mu\text{M}$  to 250  $\mu\text{M}$ . The results found are shown in Figures (3-6). BODIPY 3-3 and

conjugates **3-12**, **3-13**, and **3-14** were diluted to desired concentrations with a solution of running buffer HBS-EP+ used in Chapter 2, however this time containing 4% of DMSO. The association and disassociation rates of the compounds with EGFR are constant and were further assessed.

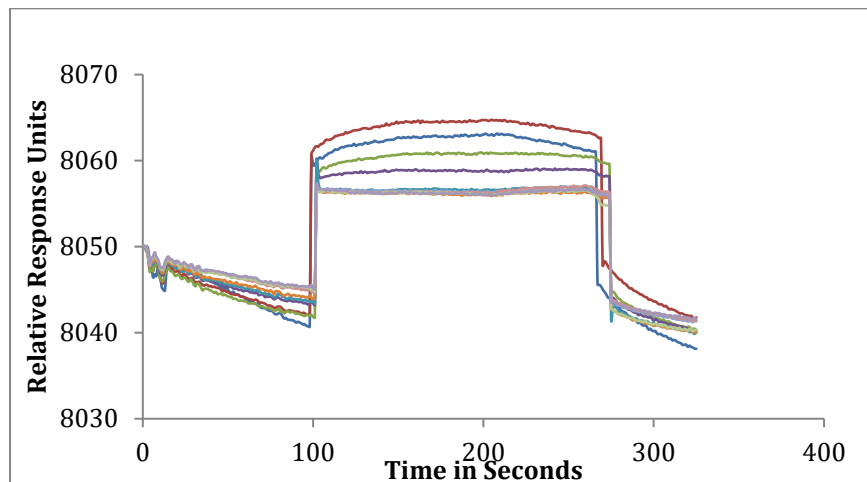


Figure 4. SPR sensogram for BODIPY 3-3 at concentrations up to 250  $\mu\text{M}$ . 250  $\mu\text{M}$  (burgundy), 200  $\mu\text{M}$  (lime), 100  $\mu\text{M}$  (yellow), 50  $\mu\text{M}$  (orange), 25  $\mu\text{M}$  (green), 10  $\mu\text{M}$  (royal blue), 1  $\mu\text{M}$  (navy blue), .5  $\mu\text{M}$  (purple), blank (mint).

BODIPY **3-3** showed a linear increase in response units or binding affinity for the EGFR receptor from concentrations 50 to 200  $\mu\text{M}$ , however at 250  $\mu\text{M}$  the response units begin to decrease indicating at concentrations above 200  $\mu\text{M}$  a non-specific binding may occur (Figure 4).

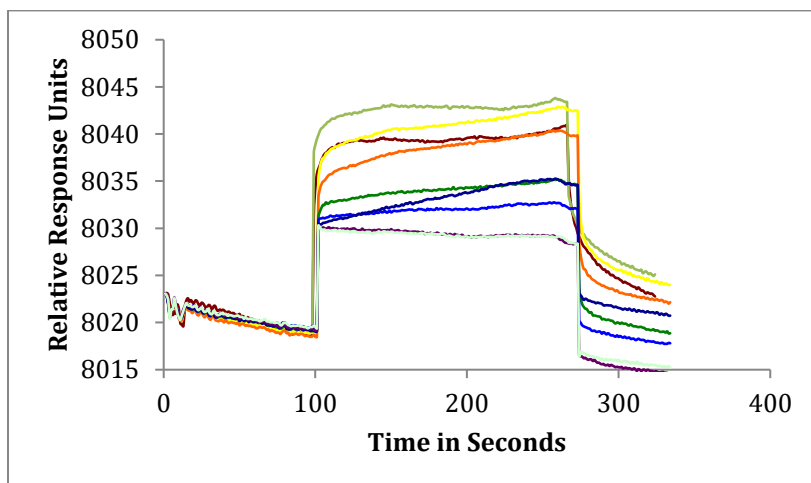


Figure 5. SPR sensogram for conjugate 3-12 at concentrations up to 250  $\mu\text{M}$ . 250  $\mu\text{M}$  (burgundy), 200  $\mu\text{M}$  (lime), 100  $\mu\text{M}$  (yellow), 50  $\mu\text{M}$  (orange), 25  $\mu\text{M}$  (green), 10  $\mu\text{M}$  (royal blue), 1  $\mu\text{M}$  (navy blue), .5  $\mu\text{M}$  (purple), blank (mint).

The SPR sensograms of all conjugates showed a higher binding affinity for EGFR than BODIPY 3-3 (Figures 4). The binding affinity of conjugates 3-12 and 3-13 behaved similar to BODIPY 3-3, however conjugate 3-13 plateaued much earlier than BODIPY 3-3 and conjugate 3-12 (Figure 5).

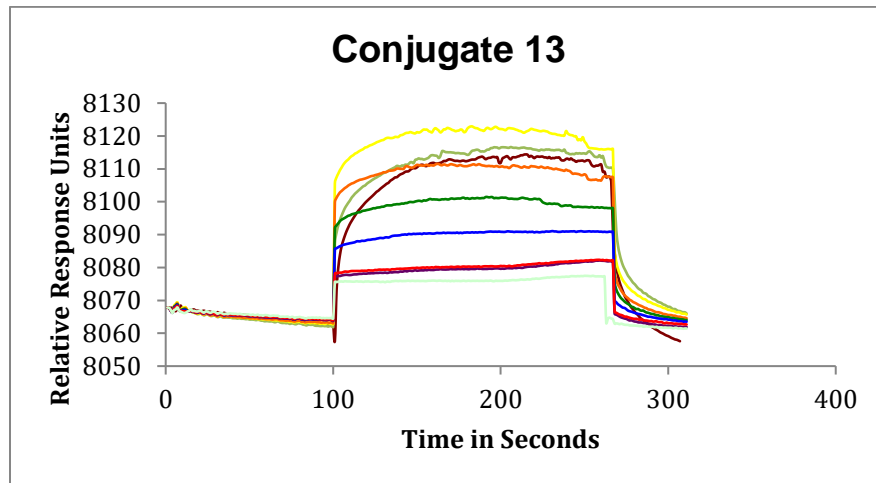


Figure 6. SPR sensogram for conjugate 3-13 at concentrations up to 250 μM. 250 μM (burgundy), 200 μM (lime), 100 μM yellow), 50 μM (orange), 25 μM (green), 10 μM (royal blue), 1 μM (navy blue), .5 μM (purple), blank (mint).

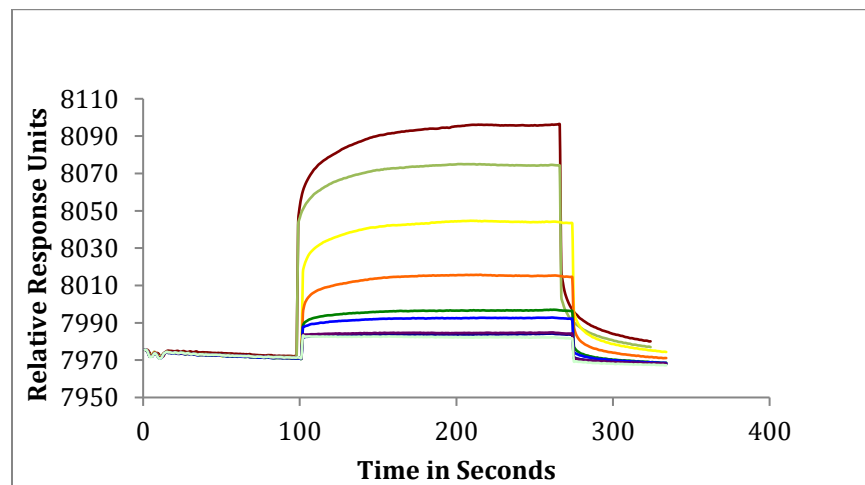


Figure 7. SPR sensogram for conjugate 3-14 at concentrations up to 250 mM. 250 μM. 250 μM (burgundy), 200 μM (lime), 100 μM yellow), 50 μM (orange), 25 μM (green), 10 μM (royal blue), 1 μM (navy blue), .5 μM (purple), blank (mint).

Conjugate **3-13** starts to exhibit non-specific binding at the 50  $\mu\text{M}$  concentration (Figure 6). Conjugate **3-14**, conversely demonstrated a continual linear increase in the binding affinity from concentration .25 to 250  $\mu\text{M}$  (Figure 7) when compared to the other conjugates demonstrating a stronger affinity for EGFR.

Table 10: Molecular Weight and  $K_D$  Values of BODIPY and BODIPY-peptide Conjugates

| Compound        | Molecular Weight | $K_D$ Value (nM) |
|-----------------|------------------|------------------|
| <b>BODIPY 3</b> | 334.16           | 35.13            |
| <b>12</b>       | 1058.64          | 6.06             |
| <b>13</b>       | 1911.91          | 19.29            |
| <b>14</b>       | 1129.72          | 2.85             |

The kinetics of binding of the conjugates to EGFR were analyzed assuming Langmuir 1:1 binding and the sensograms were fit using the Langmuir equation to provide the  $K_D$  values. Of all the conjugates, conjugate **3-14** displayed the higher dissociation conjugate as seen in Table 10 at 2.85 nM followed by conjugate **3-12** at 6.06 nM indicating a higher affinity for EGFR.

### 3.3.3 In vitro studies

*In vitro* cellular studies were conducted by Mrs. Zehua Zhou and examined against human carcinoma HEP2 cell lines including cellular uptake and cytotoxicity (phototoxicity and dark toxicity), in Cell Titer Blue (CTB) Assay a fluorescence-based assay used to measure toxicity of various substrates.

**3.3.3.1 Cytotoxicity.** The phototoxic effect of BODIPY 3-3 and conjugates 3-12, 3-13, and 3-14 were tested under a low dose of light irradiated at 1.5  $\text{J}/\text{cm}^2$ . The dose-dependent survival curves of each compound over a course of 24 hours in the dark or after light irradiation are shown in

Figures 8 and 9. The results of this test is then expressed in values of  $IC_{50}$ , the concentration of dye in units of micromolar necessary to kill 50% of the cells.

In the absence of light the cell viability using CTB was determined to possess a  $IC_{50}$  value of greater than 200  $\mu M$  proving to be non-toxic in the dark. All compounds proved non-toxic in the presence of light with  $IC_{50}$  values greater than 100  $\mu M$ . Table 11 summarizes the cell viability of conjugates 3-12, 3-13, and 3-14 and BODIPY 3-3 in HEp2 cells.

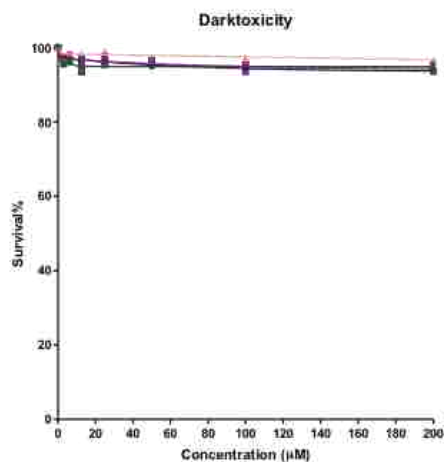


Figure 8. Dark Toxicity of BODIPY 3-3 (black), conjugate 3-13 (green), conjugate 3-14 (pink), conjugate 3-15 (purple) using a CTB assay.

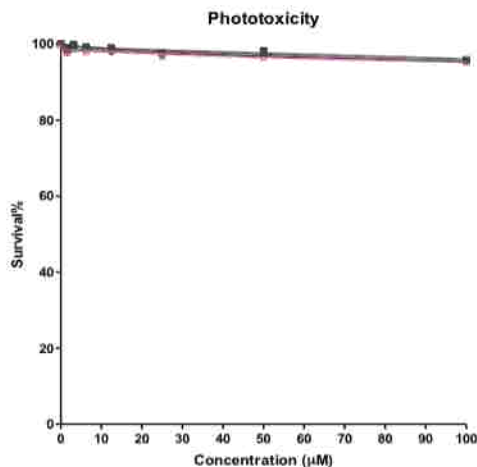


Figure 9. Phototoxicity ( $1.5 J/cm^2$ ) of BODIPY 3-3 (black), conjugate 3-13 (green), conjugate 3-14 (pink), conjugate 3-15 (purple) using a CTB assay.



| Compound     | Dark toxicity (IC <sub>50</sub> , $\mu$ M) | Phototoxicity (IC <sub>50</sub> , $\mu$ M) |
|--------------|--|--|
| BODIPY 3     | > 200                                      | >100                                       |
| Conjugate 12 | > 200                                      | >100                                       |
| Conjugate 13 | > 200                                      | >100                                       |
| Conjugate 14 | > 200                                      | >100                                       |

3.3.3.2 *Time Dependent Cellular Uptake*. Measurements of time-dependent cellular uptake for all four compounds were performed at a 10  $\mu$ M concentration in HEp2 cells, and the results are indicated in Figure 10. After 24 h, conjugates 3-13 accrued more than BODIPY 3-3 and all other conjugates in the HEp2 cell line. Additionally, BODIPY 3-3 and the other conjugates accrued in cells at similar rates. This was particularly surprising as all other reports obtained with EGFR-L1 or EGFR-L2 sequences show a reverse result with the short charged peptide sequence accruing more and at a faster rate into cells.<sup>29-30</sup> This occurrence may be due to the smaller core structure of BODIPY 3-3. The smaller size of the BODIPY dye may allow for more of the peptide to reach the binding pocket of EGFR.

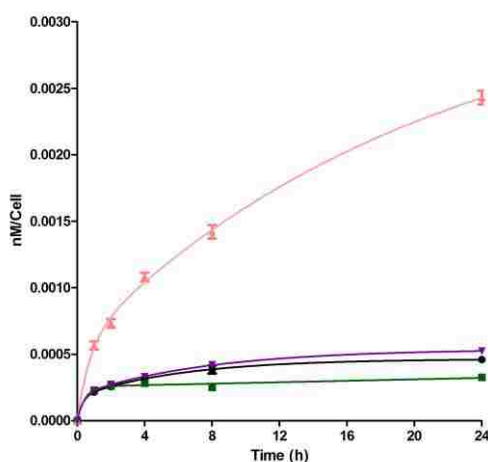


Figure 10. Cellular Uptake of BODIPY 3-3 (black), conjugate 3-13 (green), conjugate 3-14 (pink), conjugate 3-15 (purple).

*3.3.3.3. Subcellular Distribution.* To determine the intracellular localization of all compounds within cells fluorescence microscopy was used. To clearly determine the localization of conjugates various organelle specific fluorescent trackers were used such as ER (endoplasmic reticulum) Tracker Blue/white, LysoSensor Green (lysosomes), MitoTracker Green (mitochondria), and BODIPY FL C5 ceramide (Golgi). The fluorescent patterns of HEP2 cell lines containing localized BODIPY **3-3** and conjugates **3-12**, **3-13**, and **3-14** were investigated and the results are shown in Figures **10-13**. All compounds were found to preferably localize in the cell mitochondria, unlike BODIPY **3-3**, all conjugates were also found to localize in the lysosomes summarized in Table **12**. Additionally, small amounts of localization were determined in the Golgi apparatus for conjugate **3-14**, while conjugates **3-13** and BODIPY **3-3** were found to also localize in the ER.

Table 12. Subcellular localization of BODIPY 3 and Conjugates 12-14

| Compound    | Major sites of localization |
|-------------|-----------------------------|
| <b>3-3</b>  | ER, Mito                    |
| <b>3-12</b> | Mito, Lyso                  |
| <b>3-13</b> | ER, Mito, Lyso              |
| <b>3-14</b> | Golgi,Mito, Lyso            |

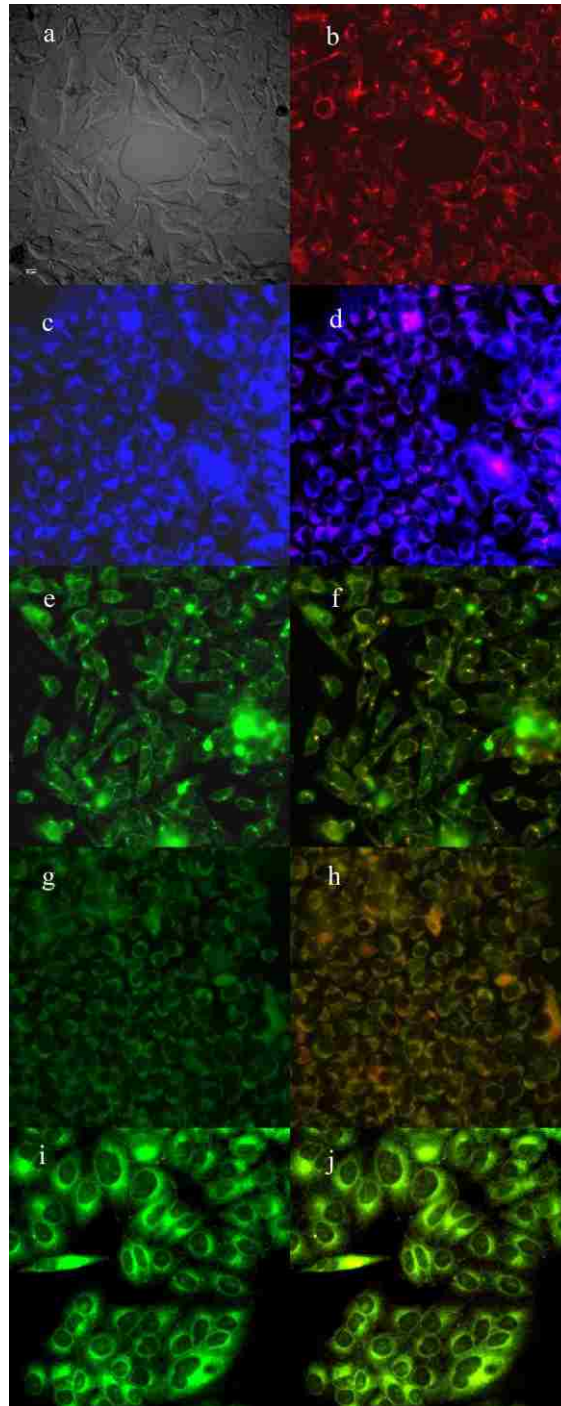


Figure 10. Subcellular fluorescence of BODIPY 3-3 in HEP2 cells at 10  $\mu$ M for 6 h. (a) Phase contrast; (b) overlay of BODIPY 3-3 fluorescence and phase contrast; (c) ER tracker Blue/White fluorescence; (d) overlay of BODIPY 3-3 fluorescence and ER Tracker; (e) BODIPY ceramide; (f) overlay of BODIPY 3-3 fluorescence and BODIPY ceramide; (g) MitoTracker Green fluorescence; (h) overlay of BODIPY 3-3 fluorescence and MitoTracker; (i) LysoSensor Green fluorescence; (j) overlay of BODIPY 3-3 fluorescence and LysoSensor. Scale bar: 10  $\mu$ m.

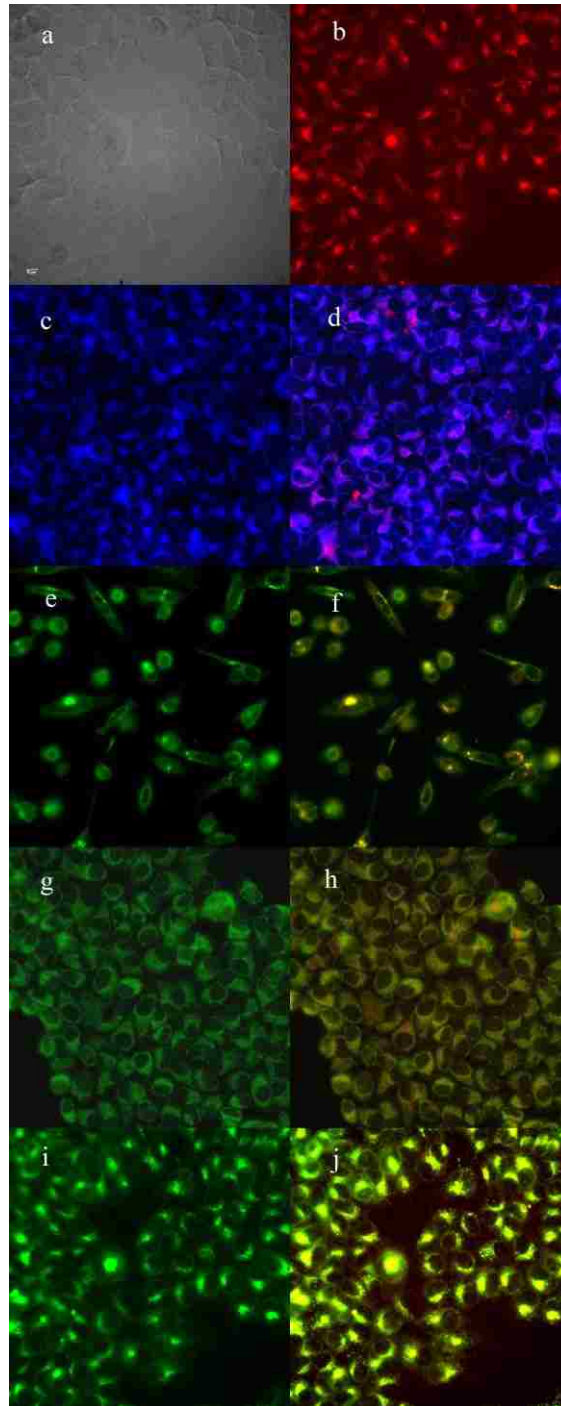


Figure 11. Subcellular fluorescence of conjugate 3-12 in HEp2 cells at 10  $\mu$ M for 6 h. (a) Phase contrast; (b) overlay of conjugate 3-12 fluorescence and phase contrast; (c) ER tracker Blue/White fluorescence; (d) overlay of conjugate 12 fluorescence and ER Tracker; (e) BODIPY ceramide; (f) overlay of conjugate 3-12 fluorescence and BODIPY ceramide; (g) MitoTracker Green fluorescence; (h) overlay of conjugate 3-12 fluorescence and MitoTracker; (i) LysoSensor Green fluorescence; (j) overlay of conjugate 3-12 fluorescence and LysoSensor. Scale bar: 10  $\mu$ m.

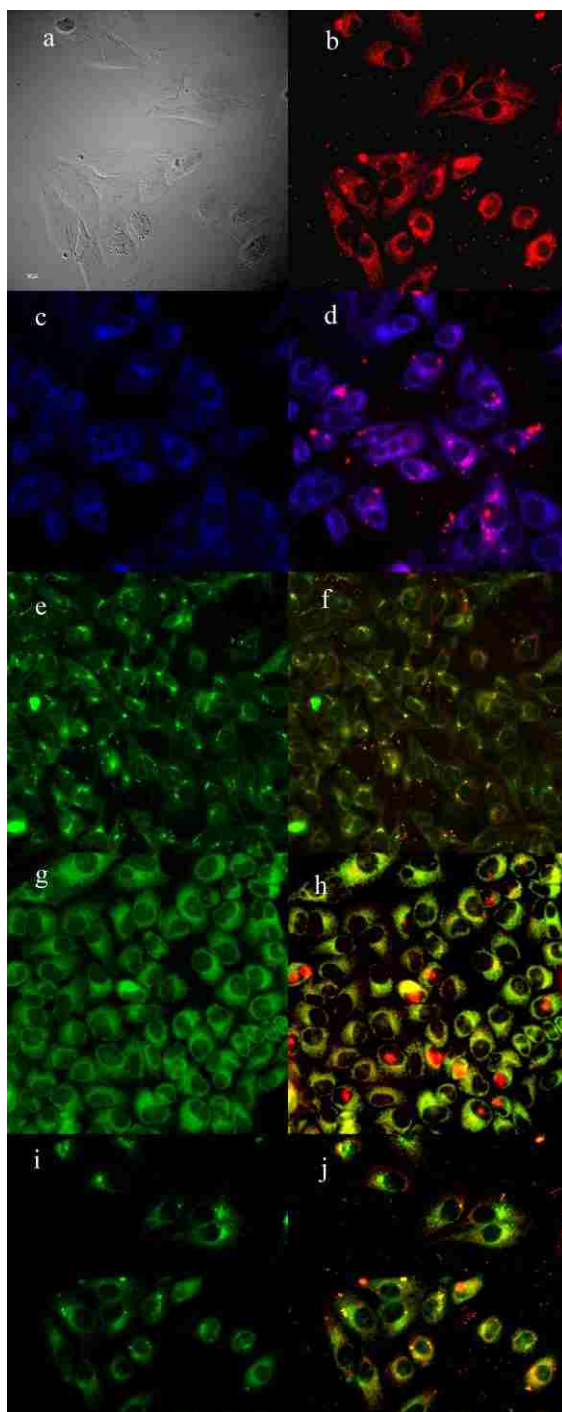


Figure 12. Subcellular fluorescence of conjugate 13 in HEp2 cells at 10  $\mu$ M for 6 h. (a) Phase contrast; (b) overlay of conjugate 13 fluorescence and phase contrast; (c) ER tracker Blue/White fluorescence; (d) overlay of conjugate 13 fluorescence and ER Tracker; (e) BODIPY ceramide; (f) overlay of conjugate 13 fluorescence and BODIPY ceramide; (g) MitoTracker Green fluorescence; (h) overlay of conjugate 13 fluorescence and MitoTracker; (i) LysoSensor Green fluorescence; (j) overlay of conjugate 13 fluorescence and LysoSensor. Scale bar: 10  $\mu$ m.

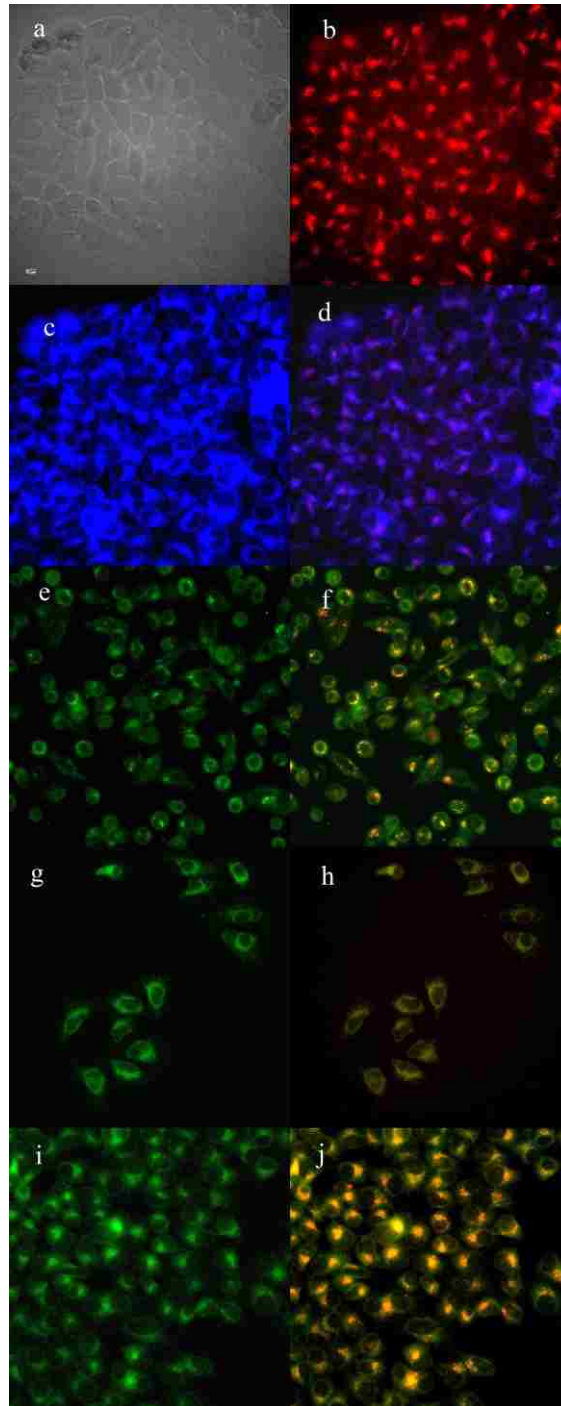


Figure 13. Subcellular fluorescence of conjugate 3-14 in HEp2 cells at 10  $\mu$ M for 6 h. (a) Phase contrast; (b) overlay of conjugate 3-14 fluorescence and phase contrast; (c) ER tracker Blue/White fluorescence; (d) overlay of conjugate 3-14 fluorescence and ER Tracker; (e) BODIPY ceramide; (f) overlay of conjugate 3-14 fluorescence and BODIPY ceramide; (g) MitoTracker Green fluorescence; (h) overlay of conjugate 3-14 fluorescence and MitoTracker; (i) LysoSensor Green fluorescence; (j) overlay of conjugate 3-14 fluorescence and LysoSensor. Scale bar: 10  $\mu$ m

### 3.3 Conclusion

In conclusion, two carboxylic BODIPY dyes were synthesized in a one-pot three step fashion similar to previous studies, however with enhanced reactivity, less impurities, and higher yields. Activation of the carboxylic BODIPY dyes **3-3** and **3-4** were successful, however conjugation with peptides **2-1** and **2-2** were unsuccessful. Strategies to enhance the methods of conjugation were performed, and optimal conditions found were activation of BODIPY **3-3** with TSTU and slow addition of the activated dye to a solution of peptides **2-2**, **2-6**, and **2-7** in .2M NaHCO<sub>3</sub> pH 9.2 at 0C. Conjugates **3-12**, **3-13**, and **3-14** were synthesized over 24 hours in percent yields of 60-75% .All new conjugates were fully characterized using <sup>1</sup>H NMR, HSQC NMR, mass spectrometry (MALDI-TOF and MALDI-TOF MSMS), UV-Vis/fluorescence spectroscopy (Appendix A.3). Spatial Plasmon Resonance was used to determine the affinity of each conjugate for EGFR. Conjugate **3-14** afforded a linear increase in binding affinity for EGFR from 0 to 250 uM concentrations. While conjugates **3-12** and **3-13** showed portions of non-specific binding. Conjugate **3-12** showed a linear increase in affinity up to 200uM and non-specific binding at 250 uM concentration. While conjugate **3-13** showed a linear increase in affinity up to 100uM and non-specific binding at 200 to 250 uM concentration.

Studies in human HEP2 cell lines revealed that all conjugates and precursor dyes were non-toxic to cells in the absence of light (IC<sub>50</sub> > 200 uM). Once cells were treated with 1.5 J/cm<sup>2</sup> irradiation of light, conjugates were still non-toxic to cells (IC<sub>50</sub> > 100 uM) making these beneficial probes for imaging CRC.

Studies in human HEP2 cell lines revealed that all conjugates and precursor dyes were non-toxic to cells in the absence of light (IC<sub>50</sub> > 200 uM). Once cells were treated with 1.5 J/cm<sup>2</sup> irradiation of light, conjugates were still non-toxic to cells (IC<sub>50</sub> > 100 uM) making these beneficial probes for imaging CRC.

With much surprise conjugate **3-13** showed the highest cellular uptake followed by conjugate **3-14**. Conjugate **3-12** had extremely low cellular uptake that followed the uptake noted

in BODIPY **3-3**. Future analyses of the efficacy of these amide conjugates will be determined so that the optimal conjugate is chosen for *in vivo* studies.

### 3.4 Experimental

#### 3.4.1 General Information

Commercial available chemicals were purchased from VWR or Sigma-Aldrich and used without further purifications for the reactions and purifications. Thin layer chromatography (TLC) was performed on the precoated silica gel plates (0.2 mm, 254 indicator, polyester backed, 60Å, Sorbent Technologies) to monitor the reactions. Preparative TLC plates (60G, VWR) and silica gel (60Å, 230-400 mesh, Sorbent Technologies) were used for liquid chromatography and column chromatography. <sup>1</sup>H NMR and <sup>13</sup>C NMR spectra were collected on a Bruker AV-400 liquid, or AV-500 spectrometer at 308K. All the chemical shifts ( $\delta$ ) are provided in parts per million (ppm) in CDCl<sub>3</sub> (7.27 ppm for <sup>1</sup>H NMR and 77.0 ppm for <sup>13</sup>C NMR) and DMSO (2.54 ppm for <sup>1</sup>H NMR). The coupling constants ( $J$ ) are reported in Hz. High-resolution mass spectra (HRMS) and MALDI (TOF) spectra were obtained on a 6210 ESI-TOF Mass Spectrometer (Agilent Technologies) under positive or negative mode and Applied Biosystems QSTAR at the LSU Mass Spectrometry Facility. Reverse-phase HPLC analysis was performed with a Waters 2485 Quaternary Gradient Module, Waters Sample Injector, and 2489 UV/Visible Detector which are controlled by Waters Empower 2 software. Separations were completed on an X-Bridge BEH300 Prep C18 (5  $\mu$ m, 10 x 250 mm) with a X-Bridge BEH300 Prep Guard cartridge 300 Å (5  $\mu$ m, 10 x 10 mm) at a 4 mL/min flow rate with UV detection for peptides at 220 nm, and for BODIPY conjugates at 580 nm. Fractions of HPLC purity (> 95%) with the anticipated mass were combined and lyophilized.

#### 3.4.2 General Procedure for Synthesis of Carboxylic BODIPYs

In an oven dried flask containing a stir bar and/or reflux condenser, 2,4-dimethylpyrrole



(1.67 eq) and anhydride (1 eq) were dissolved in appropriate solvent. Boron trifluoride diethyl etherate may be added to the solution. The reaction is then refluxed/irritated under nitrogen atmosphere for a certain timeframe. The reaction was then allowed to cool to room temperature, and triethylamine (6.7 eq) was added to the solution followed by Boron trifluoride diethyl etherate (6.7 eq). The reaction was then allowed to stir until complexing was complete. The mixture was washed with water three times and extracted with CH<sub>2</sub>Cl<sub>2</sub> three times. The organic layer was dried over MgSO<sub>4</sub> and evaporated under nitrogen gas overnight.

### 3.4.3 Method 1: Conventional Bench-top of BODIPY 3 and 4

**BODIPY 3-3:** In an oven dried flask containing a stirrer and reflux condenser, 2,4-dimethylpyrrole (.856 g, 9 mmol) and glutaric anhydride (.800 g, 5.4 mmol) were dissolved in anhydrous THF (90 mL). Boron trifluoride diethyl etherate (1.53 g, 10.8 mmol) was added drop wise to the solution. The reaction was then refluxed under nitrogen atmosphere for eight hours. The reaction was then allowed to cool to room temperature, and triethylamine (3.64 g, 36 mmol) was added to the solution followed by Boron trifluoride diethyl etherate (3.83 g, 27 mmol). The reaction was then allowed to stir at 50°C for four hours. The mixture was washed with water (3 x 15 mL) and extracted with CH<sub>2</sub>Cl<sub>2</sub> (3 x 100 mL). The organic layer was dried over MgSO<sub>4</sub> and evaporated under nitrogen gas overnight. The resulting oil was purified by running a short plug using CH<sub>2</sub>Cl<sub>2</sub> as the eluent. The resulting residue was purified by silica gel (hexane/EtOAc/HOAc, 80:40:1) and gave 50.8 mg of dye as a red solid. Yield: 3.39% <sup>1</sup>H-NMR (400MHz, CDCl<sub>3</sub>) δ 6.06 (s, 2H, β-pyrrole H), 3.21 (m, 2H, -CH<sub>2</sub>, 6.9 Hz), 3.02 (m, 2H, -CH<sub>2</sub>), 2.53 (s, 6H, -CH<sub>3</sub>), 2.42 (s, 6H, -CH<sub>3</sub>), 1.97 (m, 2H, -CH<sub>2</sub>); MS (ESI-TOF) m/z Calculated for C<sub>17</sub>H<sub>21</sub>BF<sub>2</sub>N<sub>2</sub>O<sub>2</sub>: 334.1664, found <sup>7</sup> 357.1566

**BODIPY 3-4:** In an oven dried flask containing a stirrer and reflux condenser, 2,4-dimethylpyrrole (2.85 g, 30 mmol) and phthalic anhydride (2.22 g, 15 mmol) were dissolved in anhydrous ACN (150 mL). The reaction was then refluxed under nitrogen atmosphere overnight. The reaction was then allowed to cool to room temperature, and triethylamine (9.11 g, 90 mmol) was added to the solution followed by Boron trifluoride diethyl etherate (17.03 g, 120 mmol). The reaction was then

allowed to stir at 50°C for four hours. The mixture was washed with water (3 x 30 mL) and extracted with CH<sub>2</sub>Cl<sub>2</sub> (3 x 100 mL). The organic layer was dried over MgSO<sub>4</sub> and evaporated under nitrogen gas overnight. The resulting oil was purified by running a short plug using CH<sub>2</sub>Cl<sub>2</sub> as the eluent. The resulting residue was purified by silica gel (hexane/EtOAc/MeOH 100:30:3) and gave 23.0 mg of dye as a deep red solid. Yield: 0.42% <sup>1</sup>H-NMR (400MHz, CDCl<sub>3</sub>) δ 8.10 (dd, 1H, 7.9 Hz), 7.59 (dd, 1H, 7.4 Hz), 7.50 (d, 1H, 7.7 Hz) 7.23 (d, 1H, 7.7 Hz), 5.86 (s, 2H, β-pyrrole H), 2.45 (s, 6H, -CH<sub>3</sub>), 1.24 (s, 6H, -CH<sub>3</sub>), MS (ESI-TOF) m/z Calculated for C<sub>20</sub>H<sub>19</sub>BF<sub>2</sub>N<sub>2</sub>O<sub>2</sub>: 368.1508, found [M-H] 367.1435.

#### 3.4.4 Method 2: Microwave Syntheses of BODIPY 3 and 4

**BODIPY 3-3:** In an oven dried flask containing a stirrer, 2,4-dimethylpyrrole (.142 g, 1.5 mmol) and glutaric anhydride (.133 g, 0.9 mmol) were dissolved in anhydrous THF (15 mL). Boron trifluoride diethyl etherate (.255 g, 1.8 mmol) was added drop wise to the solution. The reaction was set to ramp to temperature 110°C at 340 W of power for 5 minutes and held at 340 W and 110°C for 15 minutes. The reaction was cooled to room temperature for 5 minutes. Triethylamine (0.607 g, 6 mmol) was added to the solution followed by Boron trifluoride diethyl etherate (0.638 g, 4.5 mmol). The reaction was then subjected to microwave under a ramp to temperature settings at 70°C 340 W for one minute, and held at these settings for 10 minutes. The reaction was allowed to cool to room temperature for 5 minutes. The mixture was washed with water (3 x 15 mL) and extracted with CH<sub>2</sub>Cl<sub>2</sub> (3 x 100 mL). The organic layer was dried over MgSO<sub>4</sub> and evaporated under nitrogen gas overnight. The resulting oil was purified by running a short plug using CH<sub>2</sub>Cl<sub>2</sub> as the eluent. The resulting residue was purified by thin layer preparative chromatography (hexane/EtOAc/HOAc, 80:40:1) and gave 4.2 mg of the dye as a red solid. Yield: 1.7%

**BODIPY 3-4:** In an oven dried flask containing a stirrer, 2,4-dimethylpyrrole (.190 g, 2 mmol) and phthalic anhydride (.148 g, 1 mmol) were dissolved in anhydrous THF (15 mL). The reaction was subjected to microwave-assistance and set to ramp to temperature 110°C at 340 W of power for 5 minutes and held at 340 W and 110°C for 15 minutes. The reaction was cooled to room temperature

for 5 minutes. Triethylamine (0.607 g, 6 mmol) was added to the solution followed by Boron trifluoride diethyl etherate (0.136 g, 8 mmol). The reaction was then subjected to microwave under a ramp to temperature settings at 70°C 340 W for one minute, and held at these settings for 10 minutes. The reaction was allowed to cool to room temperature for 5 minutes. The mixture was washed with water (3 x 15 mL) and extracted with CH<sub>2</sub>Cl<sub>2</sub> (3 x 100 mL). The organic layer was dried over MgSO<sub>4</sub> and evaporated under nitrogen gas overnight. The resulting oil was purified by running a short plug using CH<sub>2</sub>Cl<sub>2</sub> as the eluent. The resulting residue was purified by thin layer preparative chromatography (hexane/EtOAc/MeOH, 100:30:3) and gave 4.2 mg of dye as a deep red solid. Yield: 1.7%

#### **3.4.5 Method 3: Grignard Syntheses of BODIPY 3-3 and 3-4**

**BODIPY 3-3:** In an oven dried flask containing a stirrer, 2,4-dimethylpyrrole (.171 g, 1.8 mmol) in THF (4ml) and a solution of methyl magnesium chloride in 3M diethyl ether (.237g, 1.98 mmol) were stirred under reflux for 30 minutes. Resulting mixture was allowed to cool to room temperature followed by the addition of glutaric anhydride (.128 g, 1.12 mmol) dissolved in anhydrous THF (1 mL). To this mixture boron trifluoride diethyl etherate (.459 g, 3.24 mmol) was added drop wise over the course of 5 minutes, and allowed to stir at room temperature for 12 hours. Triethylamine (1.122 g, 12 mmol) and Boron trifluoride diethyl etherate (1.27 g, 9 mmol) was added and allowed to stir at 50C for 4 hours. The reaction was quenched with Ammonium chloride. Remaining precipitate dissolved in DCM and added to the aqueous solution. The mixture was washed with water (3 x 15 mL) and extracted with CH<sub>2</sub>Cl<sub>2</sub> (3 x 100 mL). The organic layer was dried over MgSO<sub>4</sub> and evaporated under nitrogen gas overnight. The resulting oil was purified by running a short plug using CH<sub>2</sub>Cl<sub>2</sub> as the eluent. The resulting residue was purified by thin layer preparative chromatography (hexane/EtOAc/HOAc, 80:40:1) and gave 151 mg of the dye as a red solid. Yield: 50.1% <sup>1</sup>H-NMR (400MHz, CDCl<sub>3</sub>).

**BODIPY 3-4:** In an oven dried flask containing a stirrer, 2,4-dimethylpyrrole (.171 g, 1.8 mmol) in THF (4 ml) and a solution of methyl magnesium chloride in 3M diethyl ether (.237g, 1.98 mmol)

were stirred under reflux for 30 minutes. Resulting mixture was allowed to cool to room temperature followed by the addition of phthalic anhydride (.167 g, 1.125 mmol) dissolved in anhydrous THF (1 mL). To this mixture boron trifluoride diethyl etherate (.459 g, 3.24 mmol) was added drop wise over the course of 5 minutes, and allowed to stir at room temperature for 12 hours. Triethylamine (1.09 g, 10.8 mmol) and  $\text{BF}_3\text{OEt}_2$  (2.04 g, 14.4 mmol) was added and allowed to stir at 50°C for 4 hours. The reaction was quenched with Ammonium chloride. Remaining precipitate dissolved in DCM and added to the aqueous solution. The mixture was washed with water (3 x 15 mL) and extracted with  $\text{CH}_2\text{Cl}_2$  (3 x 100 mL). The organic layer was dried over  $\text{MgSO}_4$  and evaporated under nitrogen gas overnight. The resulting residue was purified by thin layer preparative chromatography (hexane/EtOAc/MeOH, 100:30:3) and gave 232 mg of dye as a deep red solid. Yield: 1.7%  $^1\text{H-NMR}$  (400MHz,  $\text{CDCl}_3$ )

#### **3.4.6 Procedure for Activation using N-hydroxylsuccinimide**

**Compound 3-5:** In an oven dried flask with stirrer compound **3** (1.37 g, 4 mmol) is dissolved in anhydrous  $\text{CH}_3\text{CN}$  (130 mL). To this mixture N-hydroxylsuccinimide (.552 g, 4.8 mmol) and dicyclohexylcarbodiimide (2.06 g, 10 mmol) were added and stirred in microwave at 340 W ramped to temperature 60°C for 2 minutes and held at temperature for 15 minutes. The reaction was allowed to cool to room temperature for 5 minutes, and washed with water (3 x 30 mL) and extracted using  $\text{CH}_2\text{Cl}_2$  (3 x 75 mL). The solution was dried over  $\text{MgSO}_4$  and under nitrogen gas overnight. The remaining red solid was then purified using thin layer preparative chromatography (DCM/EtOAc 12:1). And gave 18.7 mg of dye as a red-orange solid. Yield: 10.9% MS (ESI-TOF) m/z Calculated for  $\text{C}_{21}\text{H}_{24}\text{BF}_2\text{N}_3\text{O}_4$ : 431.18, found [M-H] 430.1756.

**Compound 3-6:** In an oven dried flask with stirrer compound **4** (0.029 g, .011 mmol) is dissolved in anhydrous  $\text{CH}_3\text{CN}$  (2 mL). To this mixture N-hydroxylsuccinimide (.004 g, .0355 mmol) and dicyclohexylcarbodiimide (.0153 g, .0740 mmol) were added and stirred in microwave at 340 W ramped to temperature 60°C for 2 minutes and held at temperature for 15 minutes. The reaction was allowed to cool to room temperature for 5 minutes, and washed with water (3 x 15 mL) and

extracted using  $\text{CH}_2\text{Cl}_2$  (3 x 50 mL). The solution was dried over  $\text{MgSO}_4$  and under nitrogen gas overnight. The remaining red solid was then purified using thin layer preparative chromatography (DCM/EtOAc 12:1). And gave 13.8 mg of dye as a red-orange solid. Yield: 84.1 %  $^1\text{H}$ -nmr (400MHz,  $\text{CDCl}_3$ ),  $\delta$  7.12 (d, 2H, 8.3 Hz), 6.81 (d, 2H, 8.0 Hz), 6.06 (s, 2H,  $\beta$ -pyrrole H), 2.53 (s, 6H,  $-\text{CH}_3$ ), 2.43 (s, 4H,  $-\text{CH}_2$ ), 1.25 (s, 6H,  $-\text{CH}_3$ ); MS (MALDI-TOF) m/z Calculated for  $\text{C}_{25}\text{H}_{23}\text{BF}_2\text{N}_2\text{O}_4$ : 464.17, found [M-H]

#### 3.4.7 Procedure for Activation using N,N'-disuccinimidyl carbonate

**Compound 3-5:** In an oven dried flask with stirrer compound **3** (.039 g, .117 mmol) is dissolved in anhydrous DMF (4 mL). To this mixture N,N'-disuccinimidyl carbonate (.045 g, .1757 mmol) and triethylamine (.0889 g, .8784 mmol) were added and stirred in microwave at 340 W ramped to temperature  $60^\circ\text{C}$  for 2 minutes and held at temperature for 15 minutes. The reaction was allowed to cool to room temperature for 5 minutes, and washed with water (3 x 15 mL) and extracted using  $\text{CH}_2\text{Cl}_2$  (3 x 50 mL). The solution was dried over  $\text{MgSO}_4$  and under nitrogen gas overnight. The remaining orange solid was then purified using thin layer preparative chromatography (DCM/EtOAc 12:1). And gave 33.5 mg of dye as a red-orange solid. Yield: 76.3 %  $^1\text{H}$ -nmr (400MHz,  $\text{CDCl}_3$ )  $\delta$  6.06 (s, 2H,  $\beta$ -pyrrole H), 3.09 (m, 2H,  $-\text{CH}_2$ ), 2.80 (m, 2H,  $-\text{CH}_2$ ), 2.51 (s, 6H,  $-\text{CH}_3$ ), 2.41 (s, 4H,  $-\text{CH}_2$ ), 2.16 (s, 6H,  $-\text{CH}_3$ ), 2.07 (dd, 2H,  $-\text{CH}_2$ , 8.62 Hz); MS (ESI-TOF) m/z Calculated for  $\text{C}_{21}\text{H}_{24}\text{BF}_2\text{N}_3\text{O}_4$ : 431.18, found [M-H] 430.1754.

**Compound 3-6:** In an oven dried flask with stirrer compound **4** (.0636 g, .0231 mmol) is dissolved in anhydrous DMF (3 mL). To this mixture N,N'-disuccinimidyl carbonate (.024 g, .095 mmol) and triethylamine (.048 g, .477 mmol) were added and stirred in microwave at 340 W ramped to temperature  $60^\circ\text{C}$  for 2 minutes and held at temperature for 15 minutes. The reaction was allowed to cool to room temperature for 5 minutes, and washed with water (3 x 15 mL) and extracted using  $\text{CH}_2\text{Cl}_2$  (3 x 50 mL). The solution was dried over  $\text{MgSO}_4$  and under nitrogen gas overnight. The remaining orange solid was then purified using thin layer preparative chromatography

(DCM/EtOAc 12:1). And gave 7.5 mg of dye as a red-orange solid. Yield: 25.34 % MS (ESI-TOF)  $m/z$  Calculated for  $C_{21}H_{24}BF_2N_3O_4$ : 464.17, found  $[M+H]$  465.656.

### 3.4.8 General Procedure for Conjugation

To a solution of carboxylic BODIPY dye (1.5 eq) an addition of TSTU (7.5 eq), DIEA (4 eq) were added and stirred for 1 hour, and confirmed by MS for activated BODIPY dye. BODIPY solution was then added drop wise to a vessel containing deprotected peptide in a solution of .2 M  $NaHCO_3$  pH 9.2 buffer previously cooled to 0C for 30 minutes. The combined solution was allowed to come up to 4C in the refrigerator and continual stirring at 4C was permitted for 24 hours. The resulting mixture was then immediately purified using RV-HPLC in varying gradients of acetonitrile (solvent A) and water (solvent B) containing .1% TFA.

**Conjugate 3-12 (BOIDPY-GLARLLT-CONH<sub>2</sub>):** This conjugate was obtained as a red orange solid (6.75 mg, 71%). HPLC (50% A for 1 min, 10% A to 0% A over 18 min, 10% A to 50% A over 2 min at a flow rate of 1 mL/min) and  $t_R = 18.02$  min.  $^1H$  NMR (500 MHz, DMSO- $d_6$ )  $\delta$  8.03 (m, 4H), 7.84 (m, 3H), 7.41 (d,  $J = 8.6$  Hz, 3H), 7.06 (d,  $J = 19.2$  Hz, 5H), 6.48 (s, 3H), 6.23 (s, 3H), 4.86 (d,  $J = 4.8$  Hz, 2H), 4.28 (m, 4H), 4.07 (m, 3H), 3.75 (m, 2H), 3.67 (t,  $J = 6.4$  Hz, 2H), 2.82 (s, 6H), 2.41 (s, 7H), 1.48 (m, 9H), 1.25 (m, 10H), 1.00 (d,  $J = 6.2$  Hz, 4H), 0.86 (m, 18H). MS (MALDI-TOF):  $m/z$  calcd for  $C_{40}H_{78}N_{11}O_{11}$   $[M]^+$  888.588; found 888.542.

**Conjugate 3-13 (BOIDPY-YHWYGYTPQNVI-CONH<sub>2</sub>):** This conjugate was obtained as a red orange solid (8.6 mg, 65 %). HPLC (50% A for 1 min, 10% A to 0% A over 18 min, 10% A to 50% A over 2 min at a flow rate of 1 mL/min) and  $t_R = 18.02$  min.  $^1H$  NMR (500 MHz, DMSO- $d_6$ )  $\delta$  8.09 (s, 5H), 7.64 (m, 4H), 7.21 (m, 14H), 6.98 (d,  $J = 34.8$  Hz, 10H), 6.75 (s, 2H), 6.56 (d,  $J = 65.7$  Hz, 6H), 6.24 (s, 4H), 4.48 (d,  $J = 86.2$  Hz, 10H), 4.05 (m, 7H), 3.67 (t,  $J = 6.4$  Hz, 5H), 2.92 (d,  $J = 19.8$  Hz, 10H), 2.74 (s, 9H), 2.40 (s, 8H), 1.75 (m, 9H), 1.44 (s, 3H), 1.25 (s, 8H), 1.12 (s, 7H), 0.83 (m, 18H). MS(MALDI-TOF):  $m/z$  calcd for  $C_{40}H_{78}N_{11}O_{11}$   $[M]^+$  888.588; found 888.542.

**Conjugate 3-14 (BOIDPY-KLARLLT-CONH<sub>2</sub>):** This conjugate was obtained as a dark red solid (6.5 mg, 73%). HPLC (50% A for 1 min, 10% A to 0% A over 18 min, 10% A to 50% A over 2

min at a flow rate of 1 mL/min) and  $t_R = 18.02$  min  $^1\text{H}$  NMR (500 MHz,  $\text{DMSO-}d_6$ )  $\delta$  8.27 (t,  $J = 5.9$  Hz, 2H), 7.93 (m, 10H), 7.42 (d,  $J = 8.8$  Hz, 2H), 7.06 (s, 2H), 6.49 (s, 5H), 6.23 (s, 3H), 4.27 (m, 5H), 4.06 (m, 6H), 3.67 (t,  $J = 6.4$  Hz, 4H), 3.52 (s, 4H), 2.80 (m, 6H), 2.41 (s, 7H), 1.75 (m, 5H), 1.42 (s, 6H), 1.25 (s, 5H), 1.00 (d,  $J = 6.3$  Hz, 4H), 0.86 (m, 18H).

MS (MALDI-TOF):  $m/z$  calcd for  $\text{C}_{40}\text{H}_{78}\text{N}_{11}\text{O}_{11}$   $[\text{M}]^+$  888.588; found 888.542.

### 3.5 References

1. Kowada, T.; Yamaguchi, S.; Ohe, K., Highly fluorescent BODIPY dyes modulated with spirofluorene moieties. *Organic letters* **2009**, *12* (2), 296-299.
2. Bozdemir, O. A.; Guliyev, R.; Buyukcakir, O.; Selcuk, S.; Kolemen, S.; Gulseren, G.; Nalbantoglu, T.; Boyaci, H.; Akkaya, E. U., Selective manipulation of ICT and PET processes in styryl-bodipy derivatives: applications in molecular logic and fluorescence sensing of metal ions. *Journal of the American Chemical Society* **2010**, *132* (23), 8029-8036.
3. Finikova, O. S.; Cheprakov, A. V.; Beletskaya, I. P.; Carroll, P. J.; Vinogradov, S. A., Novel versatile synthesis of substituted tetrabenzoporphyrins. *The Journal of organic chemistry* **2004**, *69* (2), 522-535.
4. Kowada, T.; Maeda, H.; Kikuchi, K., BODIPY-based probes for the fluorescence imaging of biomolecules in living cells. *Chemical Society Reviews* **2015**, *44* (14), 4953-4972.
5. Liu, B.; Novikova, N.; Simpson, M. C.; Timmer, M. S.; Stocker, B. L.; Söhnel, T.; Ware, D. C.; Brothers, P. J., Lighting up sugars: fluorescent BODIPY–gluco-furanose and–septanose conjugates linked by direct B–O–C bonds. *Organic & biomolecular chemistry* **2016**, *14* (23), 5205-5209.
6. Ni, Y.; Zeng, L.; Kang, N. Y.; Huang, K. W.; Wang, L.; Zeng, Z.; Chang, Y. T.; Wu, J., meso - Ester and Carboxylic Acid Substituted BODIPYs with Far - Red and Near - Infrared Emission for Bioimaging Applications. *Chemistry–A European Journal* **2014**, *20* (8), 2301-2310.
7. Umezawa, K.; Nakamura, Y.; Makino, H.; Citterio, D.; Suzuki, K., Bright, color-tunable fluorescent dyes in the visible– near-infrared region. *Journal of the American Chemical Society* **2008**, *130* (5), 1550-1551.

8. Jang, H. G.; Park, M.; Wishnok, J. S.; Tannenbaum, S. R.; Wogan, G. N., Hydroxyl-specific fluorescence labeling of ABP-deoxyguanosine, PhIP-deoxyguanosine, and AFB1-formamidopyrimidine with BODIPY-FL. *Analytical biochemistry* **2006**, *359* (2), 151-160.
9. Yee, M.-c.; Fas, S. C.; Stohlmeyer, M. M.; Wandless, T. J.; Cimprich, K. A., A cell-permeable, activity-based probe for protein and lipid kinases. *Journal of Biological Chemistry* **2005**, *280* (32), 29053-29059.
10. Skidmore, M.; Guimond, S.; Dumax-Vorzet, A.; Atrih, A.; Yates, E.; Turnbull, J., High sensitivity separation and detection of heparan sulfate disaccharides. *Journal of Chromatography A* **2006**, *1135* (1), 52-56.
11. Aharoni, A.; Weiner, L.; Lewis, A.; Ottolenghi, M.; Sheves, M., Nonisomerizable non-retinal chromophores initiate light-induced conformational alterations in bacterioopsin. *Journal of the American Chemical Society* **2001**, *123* (27), 6612-6616.
12. Lager, E.; Liu, J.; Aguilar-Aguilar, A.; Tang, B. Z.; Pena-Cabrera, E., Novel meso-polyarylamine-BODIPY hybrids: synthesis and study of their optical properties. *The Journal of organic chemistry* **2009**, *74* (5), 2053-2058.
13. Lavis, L. D.; Raines, R. T., Bright ideas for chemical biology. *ACS chemical biology* **2008**, *3* (3), 142-155.
14. Chang, Y.-T.; Escobar, M. V.; Zhai, D.; Kang, N.-Y.; Chandran, Y., Alkylamino BODIPY dyes as selective fluorescent probes for proteins and mouse embryonic stem cells. Google Patents: 2016.
15. Lidström, P.; Tierney, J.; Wathey, B.; Westman, J., Microwave assisted organic synthesis—a review. *Tetrahedron* **2001**, *57* (45), 9225-9283.
16. Rezende, L. C.; Emery, F. S., A review of the synthetic strategies for the development of BODIPY dyes for conjugation with proteins. *Orbital-The Electronic Journal of Chemistry* **2013**, *5* (1), 62-83.
17. Ducheyne, P.; Healy, K.; Hutmacher, D. E.; Grainger, D. W.; Kirkpatrick, C. J., *Comprehensive biomaterials*. Newnes: 2015; Vol. 1.



18. Spicka, K. J., *Design and synthesis of fluorescent dyes for use in proteomic research*. ProQuest: 2008.
19. Lavis, L. D., *Tailoring Fluorescent Molecules for Biological Applications*. ProQuest: 2008.
20. Wang, D.; Fan, J.; Gao, X.; Wang, B.; Sun, S.; Peng, X., Carboxyl BODIPY dyes from bicarboxylic anhydrides: one-pot preparation, spectral properties, photostability, and biolabeling. *The Journal of organic chemistry* **2009**, *74* (20), 7675-7683.
21. de la Hoz, A.; Diaz-Ortiz, A.; Prieto, P., CHAPTER 1 Microwave-Assisted Green Organic Synthesis. In *Alternative Energy Sources for Green Chemistry*, The Royal Society of Chemistry: 2016; pp 1-33.
22. Li, X.; Xu, J., Determination on temperature gradient of different polar reactants in reaction mixture under microwave irradiation with molecular probe. *Tetrahedron* **2016**, *72* (35), 5515-5520.
23. Zhu, S.; Zhang, J.; Vegesna, G.; Luo, F.-T.; Green, S.; Liu, H., Highly Water-soluble Neutral BODIPY Dyes with Controllable Fluorescence Quantum Yields. *Organic Letters* **2011**, *13* (3), 438-441.
24. Williams, T. M.; Sibrian-Vazquez, M.; Vicente, M. G. H., Design and Synthesis of Photosensitizer-Peptide Conjugates for PDT. In *HANDBOOK OF PHOTODYNAMIC THERAPY: Updates on Recent Applications of Porphyrin-Based Compounds*, 2016; pp 45-93.
25. Farber, S. A.; Pack, M.; Ho, S.-Y.; Johnson, I. D.; Wagner, D. S.; Dosch, R.; Mullins, M. C.; Hendrickson, H. S.; Hendrickson, E. K.; Halpern, M. E., Genetic analysis of digestive physiology using fluorescent phospholipid reporters. *Science* **2001**, *292* (5520), 1385-1388.
26. Palomo, J. M.; Lumbierres, M.; Waldmann, H., Efficient Solid - Phase Lipopeptide Synthesis Employing the Ellman Sulfonamide Linker. *Angewandte Chemie* **2006**, *118* (3), 491-495.
27. Valeur, E.; Bradley, M., Amide bond formation: beyond the myth of coupling reagents. *Chemical Society Reviews* **2009**, *38* (2), 606-631.

28. Li, H.; Jiang, X.; Ye, Y.-h.; Fan, C.; Romoff, T.; Goodman, M., 3-(Diethoxyphosphoryloxy)-1,2,3-benzotriazin-4(3H)-one (DEPBT): A New Coupling Reagent with Remarkable Resistance to Racemization. *Organic Letters* **1999**, *1* (1), 91-94.
29. Fontenot, K. Design, Synthesis, Characterization, and Application of peptides in Medicine. Louisiana State University, Dissertation, 2012.
30. Fontenot, K. R.; Ongarora, B. G.; LeBlanc, L. E.; Zhou, Z.; Jois, S. D.; Vicente, M. G. H., Targeting of the epidermal growth factor receptor with mesoporphyrin IX-peptide conjugates. *Journal of porphyrins and phthalocyanines* **2016**, *20* (01n04), 352-366.

## CHAPTER 4. Design and Synthetic Strategies for BODIPY-Peptidic Conjugates for Diagnosis of CRC via Isothiocyanate Chemistry

### 4.1 Introduction

Amide chemistry discussed in chapter 3 demonstrates a “traditional” approach to peptide BODIPY conjugates via amide bond formation reactions. However, conjugation measures using traditional coupling reagents such as TSTU required an additional activation step for at least one hour. Normal amidation procedures of solution phase conjugation proceed for longer reaction times and often yield low amounts of desired compound. However, our approach did proceed for lengthy time periods, but in moderate yields. This increase in percent yield was due to heavy optimization of reaction conditions.

The key component of increasing the yield of peptide-BODIPY conjugates via amidation was determining the best activation component.<sup>1</sup> For amidation the coupling agent TSTU was found to aid in formation of three conjugates. However, the BODIPY scaffold is interestingly tunable and allows for addition of a component that will increase the reactivity of the BODIPY dye before interaction with the biomolecule. One method of tuning the core structure is the introduction of an isothiocyanate moiety on the BODIPY framework as an amino reactive group for conjugation to biomolecules, represents an attractive alternative for the conjugation of BODIPYs to peptides<sup>1</sup>, proteins<sup>2-5</sup>, and other molecules<sup>6-12</sup> as a result of their short reaction times and high product yields.<sup>13-</sup>

14

---

<sup>a</sup> This Chapter originally appeared as Zhao, N.; Williams, T. M.; Zhou, Z.; Fronczek, F. R.; Sibrian-Vazquez, M.; Jois, S. D.; Vicente, M. G. H., Synthesis of BODIPY-Peptide Conjugates for Fluorescence Labeling of EGFR Overexpressing Cells. *Bioconjugate Chemistry* **2017**, 28 (5), 1566-1579. Reprinted with permission from [22] Copyright (2017) American Cancer Society.

Isothiocyanates are natural products that occur widely in nature and are of interest in food science and medicine. The naturally occurring compound belongs to the “cabbage” family or cruciferous vegetable group.<sup>15-16</sup> Vegetables such as broccoli, cauliflower, kale, turnips, collards, bok choy, and horseradish, to name a few, are grouped under the cruciferous class. Most of these vegetables are used in households daily and are eaten raw or cooked. These vegetables tend to be a bit bitter compared to other vegetables.<sup>16-17</sup> Furthermore, naturally occurring isothiocyanates have been found to aid in protection of the body from carcinogens. Isothiocyanates assist the fight against certain cancers, such as lung and esophageal, in three manners: 1) Inhibiting the carcinogens activation by way of enzymes; 2) They promote detoxification of carcinogens from the body; and 3) They neutralize the toxic assets and speed up the elimination of these carcinogens from the body.<sup>15, 18-19</sup> Overall, Isothiocyanates are valued functional groups that are naturally occurring, and possess a wide use of applications in various areas of chemistry including bioconjugation<sup>20</sup>, heterocyclic<sup>21</sup> chemistry, and medicinal chemistry. For these reasons, much effort has been devoted to develop efficient routes for the synthesis of these classes of compounds and attaching biomolecules for further studies.

In this chapter, a description of the effects of conjugating a BODIPY dye bearing a mono NCS moiety is investigated. The mono NCS-BODIPY reactivity towards the addition of pegylated peptides 3PEG-EGFR-L1 (**2-4**) and 3PEG-EGFR-L2-Gly (**2-5**) from chapter 2 is investigated. The effects of each NCS linkage are explored for its efficacy for EGFR binding by way of SPR and docking studies.<sup>22</sup> Finally the performance of each conjugate in human carcinoma HEP2 cells over-expressing EGFR is studied to determine the levels of cellular uptake and cytotoxicity.

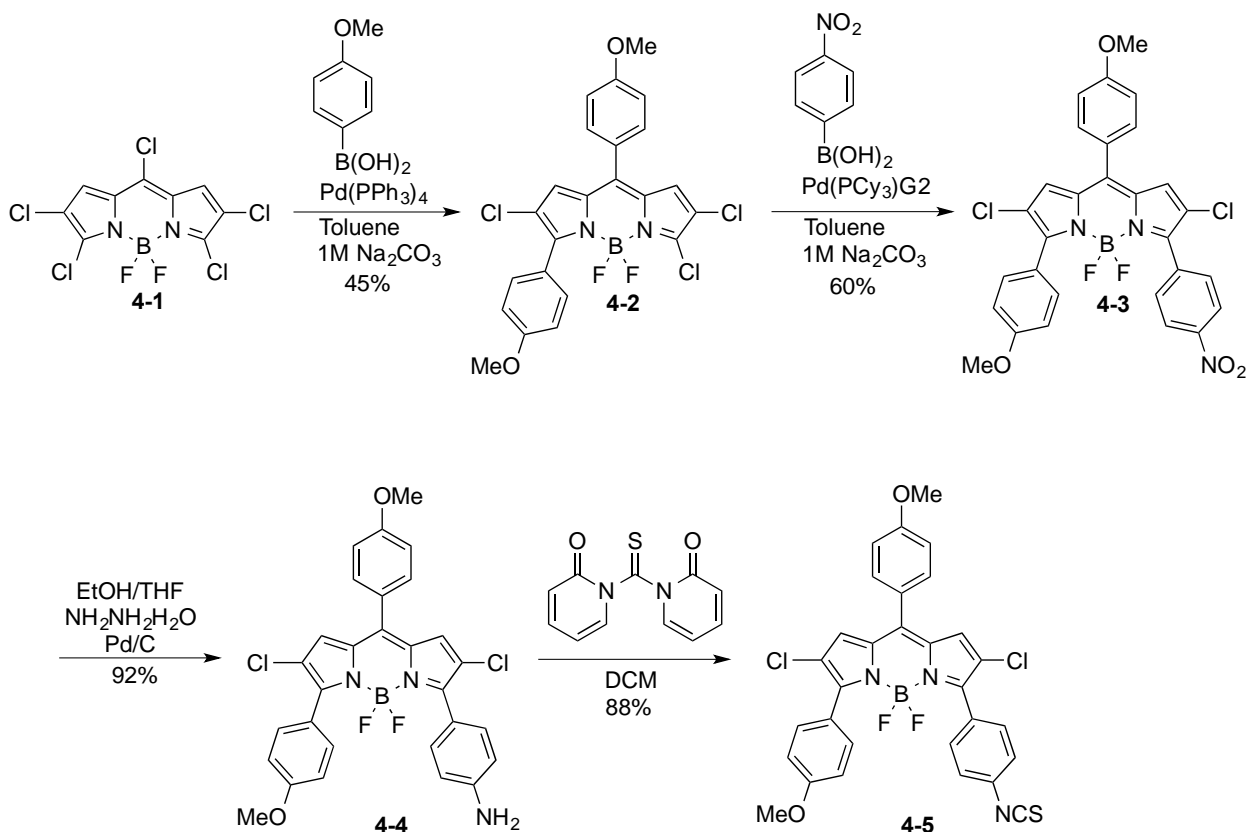
## **4.2 Results and Discussion**

### **4.2.1 BODIPY Synthesis**

We have previously reported the synthesis of flexible polyhalogenated BODIPY platforms, and an investigation of their reactivity under various reaction conditions.<sup>23-26</sup> BODIPY platforms containing halogen moieties with different reactivity, accepting regioselective functionalization of

the BODIPY core using several Pd(0)-catalyzed coupling or nucleophilic elimination/addition reactions. The order of reactivity for the chloro groups in pentachloro-BODIPY **4-1**, was shown to be: 8-Cl > 3,5-Cl > 2,6-Cl, which permits the regioselective functionalization of the 8-position, followed by the 3 and/or 5 positions, and finally the 2 and/or 6 positions of this BODIPY platform in a step-wise manner.<sup>26-27</sup>

This study was determined previously by another colleague of the Vicente group Ning Zhao. Ning was able to modify starting material 2,3,5,6,8-pentachloro-BODIPY **4-1** <sup>26</sup> in four steps. As shown in Scheme 1, Ning was able to tune the BODIPY scaffold through a series of Suzuki-type coupling reactions to give the precursor BODIPY **4-3** bearing a nitro phenyl group. BODIPY **3** was then reduced and treated with 1,1'-thiocarbonyldi-2(1*H*)-pyridone to yield the desired isothiocyanato-BODIPY **4-5** in 88% yield. After purification and characterization of BODIPY **4-5** by MS and NMR studies, Ning contributed the desired starting material for conjugation.



### Scheme 1: Synthesis of NCS-BODIPY 4-5.

A crystal structure of BODIPY 4-5 was obtained and revealed the BODIPY core is reasonably planar, exhibiting a mean deviation of 0.061 Å (**Figure 1**). The 8-methoxyphenyl substituent is turned out of the

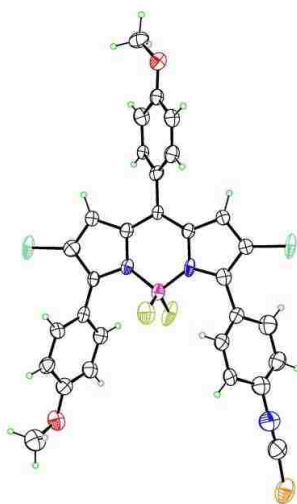


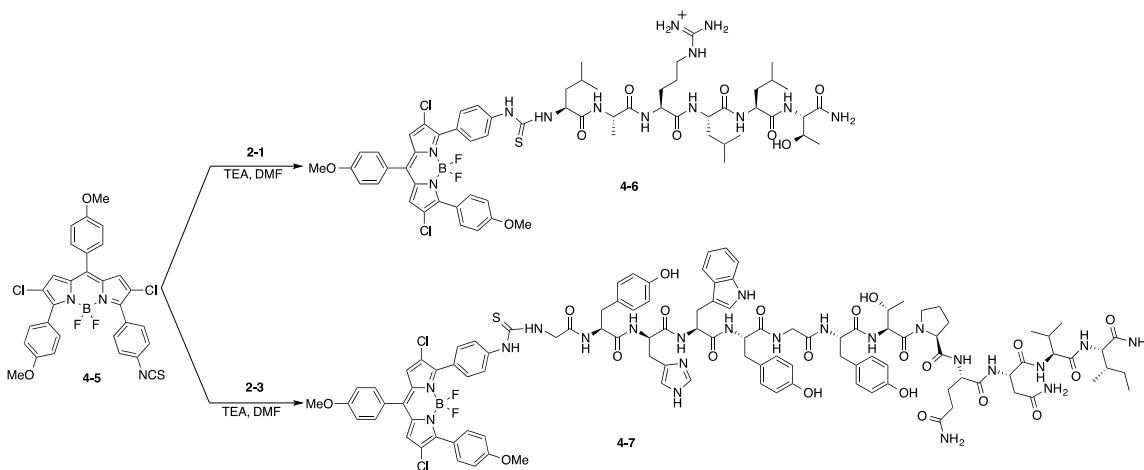
Figure 1. X-ray structure of BODIPY 4-5.

BODIPY plane, where it forms a dihedral angle of 47.4° with the BODIPY core. This behavior is typical of 8-aryl substituents on 1,7-unsubstituted BODIPY dyes. Conversely, the substituents at the 3 and 5 positions exhibit slightly larger dihedral angles with the BODIPY core, the NCS-phenyl has an angle of 54.5° while the OMe-phenyl bears a 62.9° angle. While the average C-Cl distance is 1.706 Å, the NCS group possesses an angle 174(2)° which is nearly linear, however the phenyl group forces the NCS to bend slightly, the angle about N being 168(2)°. This instance causes the NCS to tilt slightly away from the plane of the phenyl group, with the N atom 0.08 Å out of plane, the C atom 0.30 Å and the S atom 0.68 Å.

#### 4.2.2 Conjugation of BODIPY dyes to Peptide Ligands

To establish proof of concept, BODIPY 4-5 was first tested with peptides 2-1 and 2-3 to ensure the reactivity of the peptides amino group would proceed. BODIPY 4-5 was first dissolved in anhydrous DMF followed by the addition of peptide in the presence of triethylamine (TEA). The

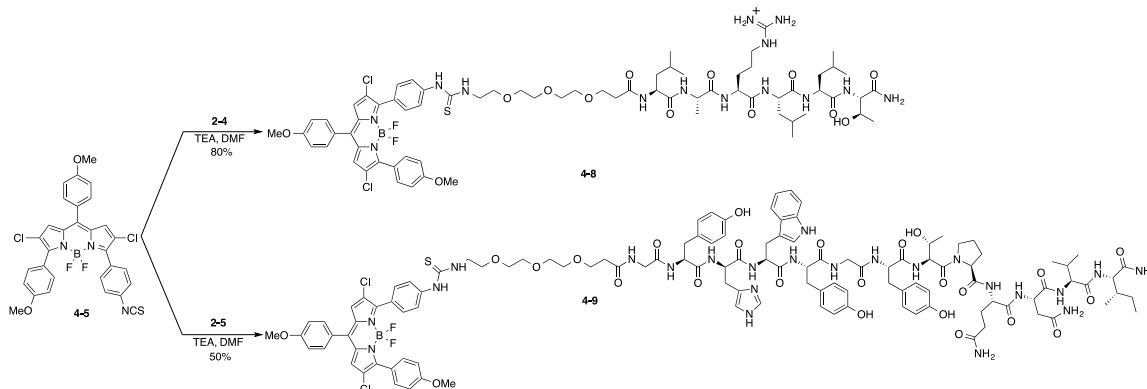
reaction was allowed to stir at room temperature for 18 hours in expectation of achieving conjugates **4-6** and **4-7** (Scheme 2). After 18 hours the reactions were checked via MS to determine their progression. Conjugate **4-7** was present via MALDI-TOF, however no product was confirmed for conjugate **4-6** only starting material of both BODIPY and peptide were returned. This may be due to the N-terminus amine being sterically hindered from the isopropyl group present at the side chain of leucine, and peptide **2-3** having the small amino acid glycine at the N-terminus. To counter these issues incorporation of a small linker or amino acid was considered.



Scheme 2. Synthesis of conjugates 4-6 and 4-7.

Previous reports from the Vicente group suggests that conjugates of EGFR-L1 and EGFR-L2 to a porphyrin<sup>28</sup> and a phthalocyanine<sup>29</sup> macrocycles, using both short (up to 5-atom) and long (up to 20-atom) linkers (Scheme 3) are favorable compound formations. PEG linkers were shown to enhance the solubility and increase the cellular uptake of the conjugates, all while preserving the fluorescent properties of the dye by mediating a distance between the targeting peptides and the fluorescent molecules. This was observed especially in cases where low molecular weight triethylene glycol linkers were used. This phenomenon is mainly due to their relatively low flexibility compared with higher molecular weight PEG groups. Furthermore, PEG linkers have also presented an increase in specificity for affinity based molecules for surface sites.<sup>30</sup> In addition, the triethylene glycol linker is expected to alleviate the steric effects of the leucine at the *N*-terminus

of the peptide with the BODIPY-NCS **4-5**, leading to higher yields of the targeted conjugates. Incorporating a small linker could also afford the conjugates with extended conformation resulting in an enhanced EGFR binding affinity.<sup>29, 31-32</sup>



Scheme 3. Synthesis of conjugate **4-8** and **4-9**.

The pegylated peptides PEG3-EGFR-L1, (**2-4**) and PEG3-EGFR-L2 (**2-5**) reacted with BODIPY-NCS **4-5** in anhydrous DMF and in the presence of TEA, at room temperature for 18 hours (**Scheme 3**). MS showed evidence of compounds and the solvents were removed under vacuum and the blue solid was then purified using RP- HPLC. Conjugates **4-8** and **4-9** were purified and determined to yield 20 and 28 percent, respectively. Although both reactions were able to produce the desired products, further investigation was necessary to optimize the reaction yields. NCS reactions are typically high yielding reactions in the presence of amino groups, however the yields were very low. To determine the effects of reaction time, each desired conjugate was allowed to react at various time points and the results are listed in Table 1.

All studies pointed to reaction conditions of 30 min being the optimal timeframe to provide the corresponding conjugates **8** and **9** in 80 and 50% yields, respectively. Longer reaction times led to lower product yields, required purification of conjugate **8** without the usual .1% TFA normally used in HPLC solvents. The desired molecular weight (MW) of the compound was found as well as two other distinctive molecular weights. Purification using solvents inclusive of TFA showed a continual presence of nagging side products that were difficult to remove.



Table 1: Results of Time Study of synthesis of Conjugates 8 and 9

| Conjugate | Peptide | Reaction Time | % YIELD |
|-----------|---------|---------------|---------|
| 4-8       | 2-4     | 12 h          | 20      |
| 4-8       | 2-4     | 2 h           | 49      |
| 4-8       | 2-4     | 30 min        | 80      |
| 4-9       | 2-5     | 12 h          | 28      |
| 4-9       | 2-5     | 2 h           | 45      |
| 4-9       | 2-5     | 30 min        | 50      |

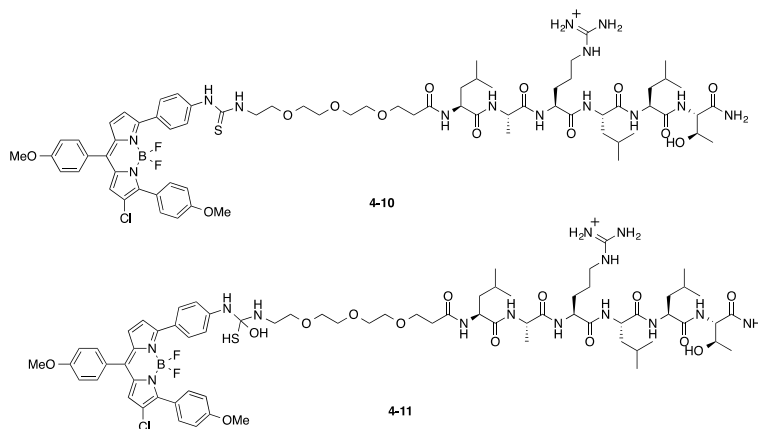


Figure 2. Structure of side products 4-10 and 4-11.

The hypothesized side products **4-10** and **4-11** were both reminiscent of the desired product, however, they both were missing one chloro group. However HPLC purification without the .1% TFA gave cleaner separation and isolation of the desired conjugate **4-8**, and one peak with the corresponding mass for compound **4-10** was able to be isolated (**Figure 2**). Throughout these reaction conditions the BODIPY platform was preserved, as confirmed by <sup>11</sup>B-NMR, which showed triplets for the BF<sub>2</sub> group at  $\delta = 0.368$  and  $0.374$  ppm for **4-8** and **4-9**, respectively (see

Appendix D). The BODIPY-peptide conjugates were further characterized by  $^1\text{H}$  NMR, HSQC, and MALDI-TOF.

### 4.3 Characterization of BODIPY-Peptide Conjugates

#### 4.3.1 Photophysical Studies

The spectroscopic properties were identified for BODIPY **4-5**, and for peptide conjugates **4-8** and **4-9** in DMSO. Specifically, the maximum absorption ( $\lambda_{\text{abs}}$ ) and emission ( $\lambda_{\text{em}}$ ) wavelengths, Stokes shifts, fluorescence quantum yields ( $\Phi_f$ ), and molar extinction coefficients ( $\log \epsilon$ ), were studied and the results are shown below. **Figure 2** shows the normalized absorption and emission spectra for BODIPY **4-5** and the corresponding conjugates. BODIPY **4-5** showed a characteristic strong absorption band and a  $\log \epsilon$  value of 4.5 with an emission at 623 nm in DMSO. This is because of the  $S_0$ - $S_1$  ( $\pi$ - $\pi^*$ ) transition, and the weaker absorption band centered at around 450 nm is due to  $S_0$ - $S_n$  ( $n \geq 2$ ) transition.

Table 2. Spectroscopic properties of BODIPYs in DMSO at room temperature

| Compound   | $\lambda_{\text{abs}}$ | $\lambda_{\text{em}}$ | Stokes shift | $\Phi_f^{[a]}$ | $\log \epsilon$ |
|------------|------------------------|-----------------------|--------------|----------------|-----------------|
| <b>4-5</b> | 575 nm                 | 623 nm                | 48 nm        | 0.16           | 4.5             |
| <b>4-8</b> | 588 nm                 | 634 nm                | 46 nm        | 0.033          | 4.3             |
| <b>4-9</b> | 586 nm                 | 634 nm                | 48 nm        | 0.014          | 4.5             |

<sup>[a]</sup> Cresyl violet (0.5 in ethanol)<sup>33</sup> was used as the standard for compounds **4-5**, **4-8**, and **4-9**.

BODIPY-peptide conjugates **4-8** and **4-9** have similar absorption and emission spectra as their precursor NCS-BODIPY **4-5**, due to their similar BODIPY cores as shown in Table 2 and Figure 3. Small red-shifts (11-13 nm) were observed in the spectra of conjugates **4-8** and **4-9**, compared with BODIPY **4-5**. This may possibly be due to decreased dihedral angles between the BODIPY core and the  $\alpha$ -phenyl groups due to the presence of the peptide group on the *para* position of  $\alpha$ -phenyl group. Both conjugates **4-8** and **4-9** emit closely in the NIR region of the optical spectrum, with minor autofluorescence and absorption by tissues, and with better light penetration,

which makes these two compounds suitable for imaging applications.<sup>34</sup> However, conjugates **4-8** and **4-9** exhibit a 5- and 10-fold decrease in quantum yield from BODIPY **4-5**.

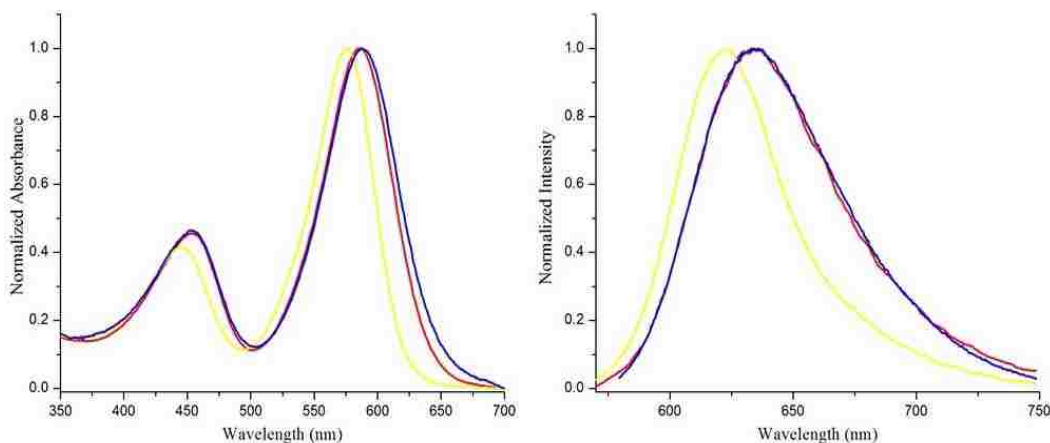


Figure 3. Normalized UV-Vis and fluorescence spectra of BODIPY **4-5** (yellow), BODIPY-peptide conjugate **4-8** (blue), and BODIPY-peptide conjugate **4-9** (red) in DMSO at room temperature.

The difference in quantum yield is thought to be due to the introduced flexibility of the conjugates by way of the small PEG3 linker. Both peptide conjugates have an enhanced interaction between the core of the BODIPY dye and peptides that could possibly lead to increased non-radioactive decay.

#### 4.3.2 SPR of BODIPY-Peptide Conjugates

Compounds **4-8** and **4-9** and NCS-BODIPY **4-5** were evaluated by SPR for their binding affinity for EGFR in a concentration study from 0 to 250  $\mu\text{M}$ . Pegylated peptides **2-4** and **2-5** exhibited binding to EGFR with fast kinetics of association and dissociation are shown in Appendix **B**. For peptide **2-4** at 100  $\mu\text{M}$  the response was observed at approximately 20 units, however for peptide **2-5** at the same concentration the response was about 150 units, suggesting a significantly higher binding affinity for peptide **2-5** compared to the affinity observed with peptide **2-4**.

In the case of binding affinity for conjugates **4-8** and **4-9**, 4% DMSO was used to dissolve the conjugates and diluted with running buffer inclusive of 4% DMSO. Conjugate **4-8** exposed two

methods of binding at concentrations lower than 100  $\mu\text{M}$ , the first observation was an increase in response units were observed by 400 units followed by a level of saturation being met.

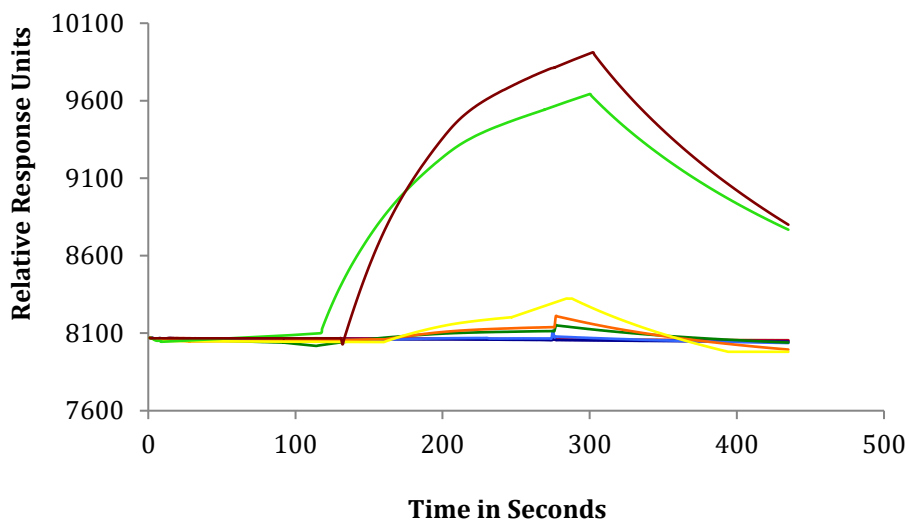


Figure 4. SPR sensogram for conjugate 4-8 at concentrations up to 250  $\mu\text{M}$ . 250 $\mu\text{M}$ (burgundy), 200  $\mu\text{M}$  (lime), 100  $\mu\text{M}$  (yellow), 50  $\mu\text{M}$  (orange), 25  $\mu\text{M}$  (green), 10 $\mu\text{M}$  (royal blue), 1  $\mu\text{M}$  (navy blue), .5  $\mu\text{M}$  (purple), Blank (mint).

Yet, further addition of compound **4-8** at concentrations above 100  $\mu\text{M}$  resulted in a drastic increase of the SPR signal (nearly 2000 units), as seen in **Figure 4**. At higher concentrations, the kinetics of association and dissociation suggest specific binding of **4-8** to EGFR, as seen by a slow increase in the SPR signal.

However, in the case of conjugate **4-9**, the SPR signal showed signs of saturation at the 10  $\mu\text{M}$  concentration, and the relative increase in response was less than 10 units (Figure 5). This sluggish change in response units suggested weak or non-specific binding of conjugate **4-9** to EGFR. As a comparison, BODIPY **4-5** was also used as an analyte in SPR studies to determine if any specificity was pertinent. BODIPY **4-5** also indicated binding similar to conjugate **4-9** (**Figure 6**), showing slow-moving increases in response, and suggesting that the core of the BODIPY dye probably binds to EGFR non-specifically, together with peptide **2-5**. Conversely, peptide **2-5** showed specific binding as shown in Appendix B.

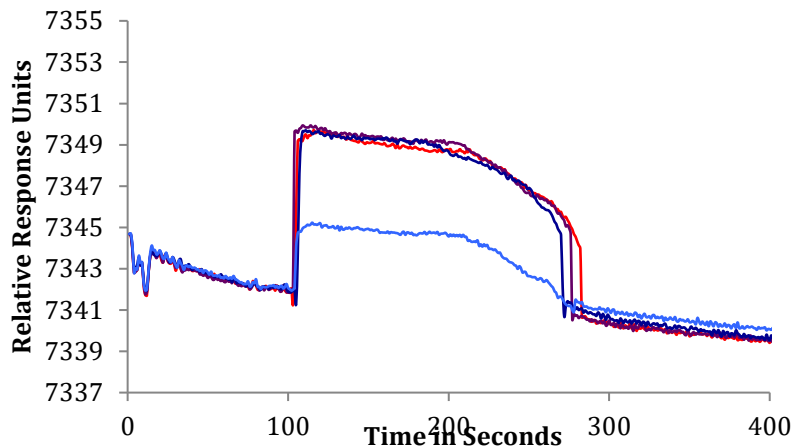


Figure 5. SPR sensogram for conjugate 4-9 at concentrations up to 250  $\mu\text{M}$ . 250 $\mu\text{M}$ (burgundy), 200  $\mu\text{M}$  (lime), 100  $\mu\text{M}$  (yellow), 50  $\mu\text{M}$  (orange), 25  $\mu\text{M}$  (green), 10 $\mu\text{M}$  (royal blue), 1  $\mu\text{M}$  (navy blue), .5  $\mu\text{M}$  (purple), Blank (mint).

Hence, the addition of BODIPY 5 to the hydrophobic sequence of peptide 2-5 appears to reduce the specificity of binding to EGFR.

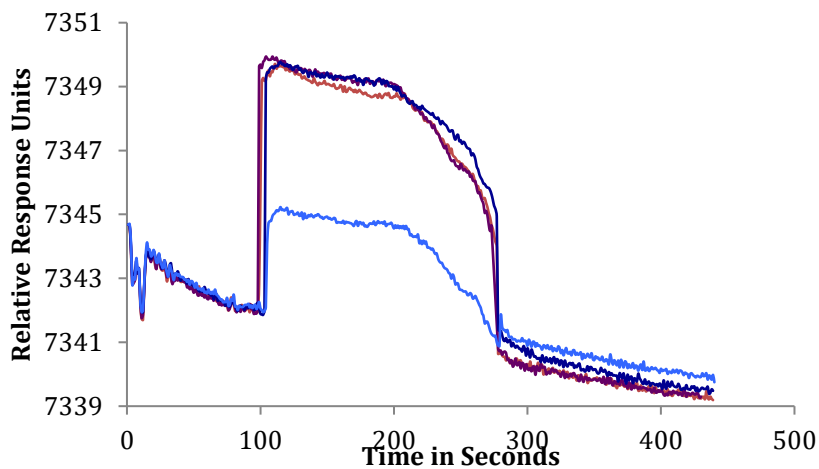


Figure 6. SPR sensograms for BODIPY 4-5 at concentrations up to 250  $\mu\text{M}$ . 250 $\mu\text{M}$ (burgundy), 200  $\mu\text{M}$  (lime), 100  $\mu\text{M}$  (yellow), 50  $\mu\text{M}$  (orange), 25  $\mu\text{M}$  (green), 10 $\mu\text{M}$  (royal blue), 1  $\mu\text{M}$  (navy blue), .5  $\mu\text{M}$  (purple), Blank (mint).

#### 4.3.3 *In vitro* studies

*In vitro* cellular studies were examined against human carcinoma HEP2 cell lines including cellular uptake and cytotoxicity (phototoxicity and dark toxicity), using a Cell Titer Blue (CTB) Assay, a fluorescence-based assay used to measure toxicity of BODIPY 4-5 and BODIPY-peptide conjugates 4-8 and 4-9 which was conducted by Mrs. Zehua Zhou.

#### 4.3.3.1 Cytotoxicity

The phototoxic effect of BODIPY **4-5** and conjugates **4-8** and **4-9** were tested under a low dose of light irradiated at 1.5 J/cm<sup>2</sup>. The dose-dependent survival curves of each compound over a course of 24 hours are shown in Figures **7** and **8**. The results of this test is then expressed in values of IC<sub>50</sub>, the concentration of dye in units of micromolar necessary to kill 50% of the cells as summarized in Table **3**.

The dark- and photo-cytotoxicity (using light dose of 1.5 J/cm<sup>2</sup>) for BODIPY **4-5** and BODIPY-peptide conjugates **4-8** and **9** using HEp2 cell line at concentrations up to 200 μM. Table **3** and Figures **7** and **8** indicate the cytotoxicity results. Dose–response curves of all three compounds were plotted for the determination of IC<sub>50</sub>. BODIPY **4-5** and its peptide conjugates **4-8** and **4-9** were found to be nontoxic in the dark with IC<sub>50</sub> values ≥ 98 μM (Figure **7**).

Table 3. Cytotoxicity results for compounds 5, 8 and 9

| Compound | Dark toxicity (IC <sub>50</sub> , μM) | Phototoxicity (IC <sub>50</sub> , μM) |
|----------|---------------------------------------|---------------------------------------|
| 4-5      | >200                                  | > 100                                 |
| 4-8      | 98                                    | 74                                    |
| 4-9      | 180                                   | > 100                                 |

Moreover, our results showed that there was no photocytotoxic effects of BODIPY **4-5** and BODIPY-peptide conjugate **4-9**, while BODIPY-peptide conjugate **4-8** showed a slightly higher photocytotoxicity with an IC<sub>50</sub> of 74 μM as shown in Figure **8**. This increased phototoxicity may be due to the cationic charge of EGFR-L1 that induces a higher cellular uptake of conjugate **4-8**, compared with BODIPY-peptide conjugate **4-9** and BODIPY **4-5**.<sup>29</sup> This instance was also previously noticed with Pc-PEG-EGFRL1 and Pc-PEG-EGFRL2 conjugates. The observed low cytotoxic effects are good qualities for BODIPY-peptide conjugates use as imaging agents of colorectal cancer cells.

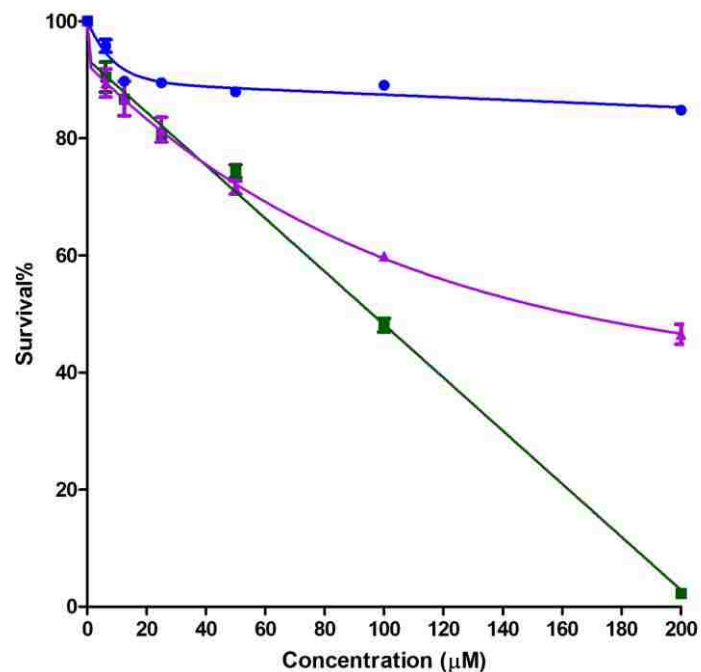


Figure 7. Dark toxicity of BODIPYs 4-5 (blue), 4-8 (green) and 4-9 (purple) in HEp2 cells using the CTB assay.

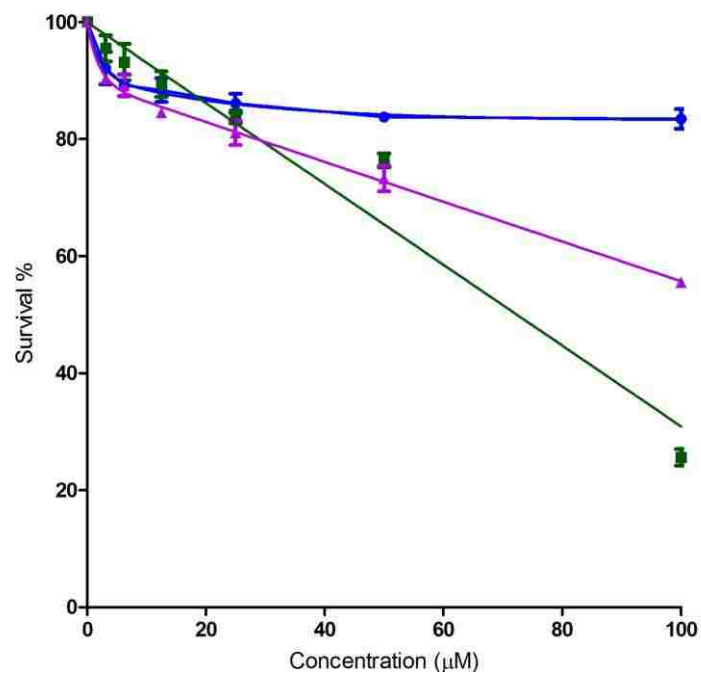


Figure 8. Photo toxicity ( $\sim 1.5 \text{ J/cm}^2$ ) of BODIPYs 4-5 (blue), 4-8 (green) and 4-9 (purple) in HEp2 cells using a CTB assay.

#### 4.3.3.2 Time Dependent Cellular Uptake.

The time-dependent cellular uptakes for all three compounds were performed at the 10  $\mu$ M concentration in HEp2 cells, and the results are indicated in Figure 9. After 24 h, conjugates **4-8** and **4-9** accrued  $\sim$ 30-fold more than BODIPY **4-5** in the HEp2 cell line. Additionally, each conjugate accumulated much faster than BODIPY **4-5**. As observed in Table 4, conjugates **4-8** and **4-9** accumulated approximately 90- and 60-fold more than the precursor **4-5** at 1h, and approximately 55- and 35-fold more at 2 h, respectively. Various factors may cause an enhanced uptake of conjugates at a rapid speed: (1) enhanced aqueous solubility from PEG linker, and (2) the potential EGFR targeting effect from EGFR-peptides, as previously observed.<sup>35</sup>

On the other hand, BODIPY-peptide conjugate **4-8** accumulated around 2-fold faster than conjugate **9**, which can be due to the charged arginine amino acid of the peptide sequence of conjugate **4-8**. The charged amino acid may also aid the PEG3 linker with increasing the solubility.

Table 4. Cellular Uptake for Compounds at Various Timeframes

| Compound   | Cellular uptake at 1 h (nM/cell) | cellular uptake at 2 h (nM/cell) | cellular uptake at 4 h (nM/cell) | cellular uptake at 8 h (nM/cell) | cellular uptake at 24 h (nM/cell) |
|------------|----------------------------------|----------------------------------|----------------------------------|----------------------------------|-----------------------------------|
| <b>4-5</b> | 0.00028                          | 0.00063                          | 0.00073                          | 0.00090                          | <b>0.0016</b>                     |
| <b>4-8</b> | 0.0254                           | 0.0344                           | 0.0398                           | 0.0424                           | <b>0.0431</b>                     |
| <b>4-9</b> | <b>0.016</b>                     | <b>0.0224</b>                    | <b>0.0287</b>                    | <b>0.036</b>                     | <b>0.0485</b>                     |



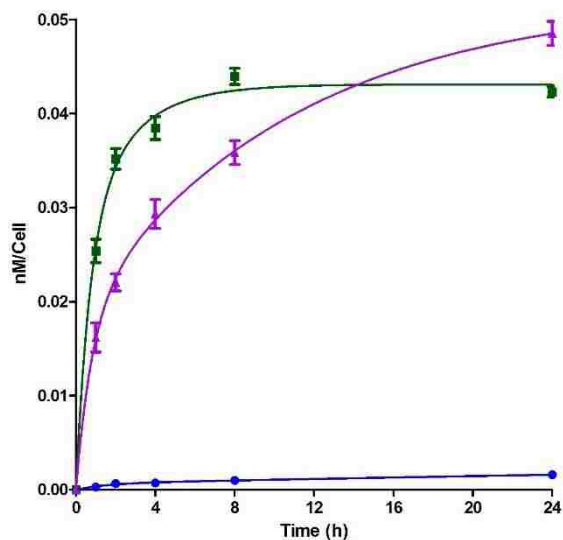


Figure 9. Time-dependent cellular uptake of BODIPYs 4-5 (blue), 4-8 (green) and 4-9 (purple) at 10  $\mu$ M in human HEP2 cells.

#### 4.3.3.3 Fluorescence Microscopy

To determine the subcellular sites of localization of BODIPY **4-5** and conjugates **4-8** and **4-9** in the HEP2 cell line, fluorescence microscopy was used. The results are summarized in Table **5** as well as Figures **10-12**. During co-localization experiments, organelle-specific probes were used, including ER Tracker Blue/White (ER), BODIPY Ceramide (Golgi), MitoTracker Green (mitochondria), and LysoSensor Green (lysosomes). All compounds were found to preferably localize in the cell ER, as identified in Figures **10-12**, which is confirmed within previous studies.<sup>36-37</sup> Additionally, small amounts of localization were determined in the Golgi apparatus, while conjugates **4-8** and **4-9** were also found in the lysosomes to a moderate extent. However, very trace localization of the conjugates was observed in the mitochondria.

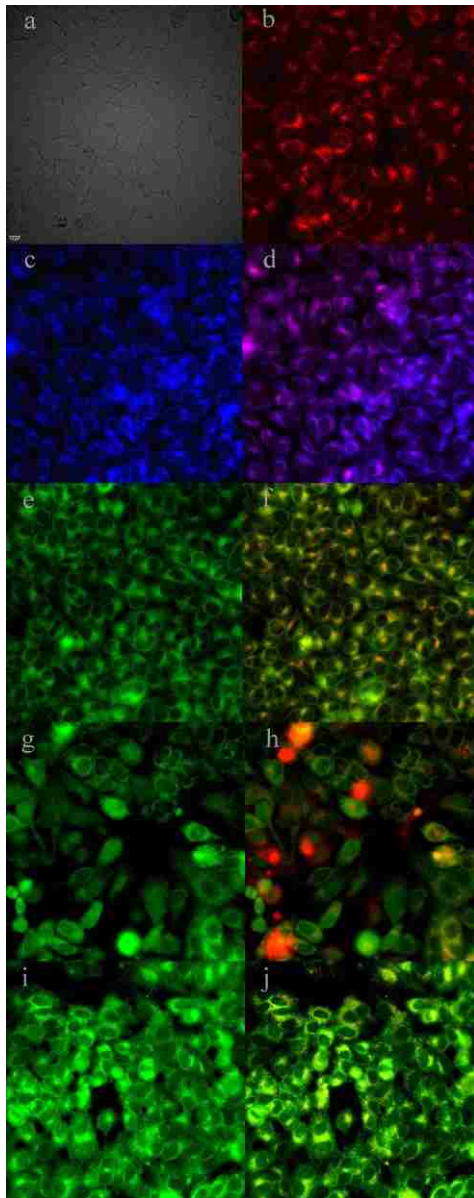


Figure 10. Subcellular fluorescence of BODIPY 4-5 in HEp2 cells at 10  $\mu$ M for 6 h. (a) Phase contrast; (b) overlay of BODIPY 4-5 fluorescence and phase contrast; (c) ER tracker Blue/White fluorescence; (d) overlay of BODIPY 4-5 fluorescence and ER Tracker; (e) BODIPY ceramide; (f) overlay of BODIPY 4-5 fluorescence and BODIPY ceramide; (g) MitoTracker Green fluorescence; (h) overlay of BODIPY 4-5 fluorescence and MitoTracker; (i) LysoSensor Green fluorescence; (j) overlay of BODIPY 4-5 fluorescence and LysoSensor. Scale bar: 10  $\mu$ m.

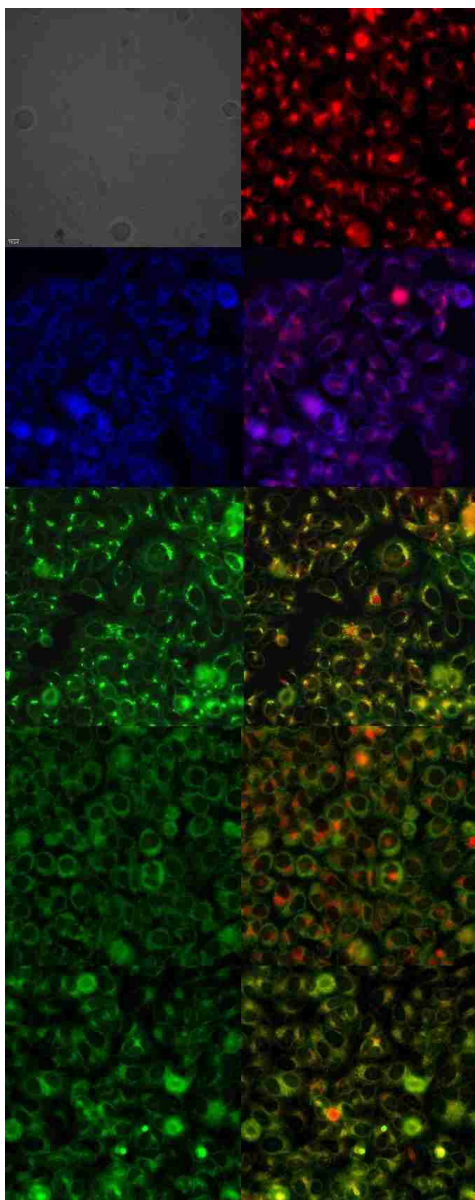


Figure 11. Subcellular fluorescence of conjugate 4-8 in HEp2 cells at 10  $\mu$ M for 6 h. (a) Phase contrast; (b) overlay of conjugate 4-8 fluorescence and phase contrast; (c) ER tracker Blue/White fluorescence; (d) overlay of conjugate 4-8 fluorescence and ER Tracker; (e) BODIPY ceramide; (f) overlay of conjugate 4-4-8 fluorescence and BODIPY ceramide; (g) MitoTracker Green fluorescence; (h) overlay of conjugate 4-8 fluorescence and MitoTracker; (i) LysoSensor Green fluorescence; (j) overlay of conjugate 4-8 fluorescence and LysoSensor. Scale bar: 10  $\mu$ m.

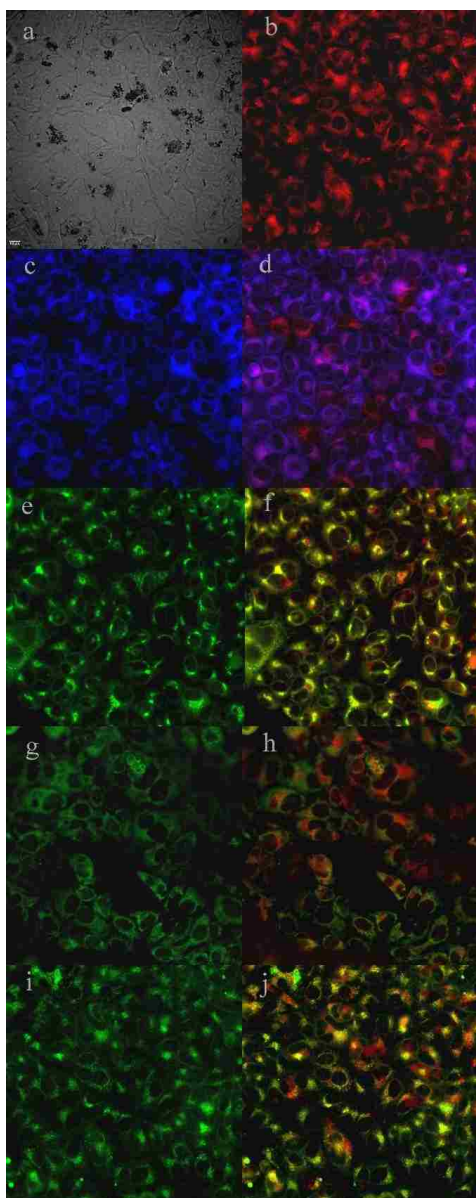


Figure 12. Subcellular fluorescence of conjugate 4-9 in HEp2 cells at 10  $\mu$ M for 6 h. (a) Phase contrast; (b) overlay of conjugate 4-9 fluorescence and phase contrast; (c) ER tracker Blue/White fluorescence; (d) overlay of conjugate 4-9 fluorescence and ER Tracker; (e) BODIPY ceramide; (f) overlay of conjugate 4-9 fluorescence and BODIPY ceramide; (g) MitoTracker Green fluorescence; (h) overlay of conjugate 4-9 fluorescence and MitoTracker; (i) LysoSensor Green fluorescence; (j) overlay of conjugate 4-9 fluorescence and LysoSensor. Scale bar: 10  $\mu$ m.

Table 5. Subcellular localization of BODIPY 4-5 and Conjugates 4-8 and 4-9

| Compound | Major sites of localization |
|----------|-----------------------------|
| 4-5      | ER                          |
| 4-8      | ER, Golgi                   |
| 4-9      | ER, Golgi, Lyso             |

#### 4.3.3.4 Modeling and Docking

To accurately account for the binding interaction of conjugates **4-8** and **4-9** with EGFR, three-dimensional structures of the compounds were pursued using InsightII molecular modeling software by collaborator Dr. Seetharama Jois. The 3D structures of each conjugate was docked to the EGFR structure using Autodock software (Figure **13**).<sup>38</sup> The parent peptide sequence (LARLLT) of conjugate **4-8** is known to bind to EGFR near domain I, as observed in previous studies.<sup>29, 39</sup> The lowest energy docked structure of conjugate **4-8** is found in Figure **13A** with docking energy of -4.19 kcal/mol. In the docked structure three interactions of hydrogen bonding can be observed: the -NH of L5 of the peptide sequence hydrogen bonded with the carbonyl group of Ser222 from EGFR; -NH of L1 hydrogen bonds with carbonyl group of Gln59; and oxygen of the 3PEG bonded with Asn119 of EGFR. The core of the BODIPY dye formed a hydrophobic interaction with Leu186, Pro171, Lys185 side chain, Ile189 and 190 of EGFR. The conjugate exhibited an extended confirmation with the BODIPY dye pointing away from the peptide sequence. This confirmation allowed for the BODIPY and binding pocket to form a non-specific hydrophobic interaction with the surface of EGFR.

In figure **13B** the binding of conjugate **4-9** with EGFR near the EGF binding pocket was observed.<sup>40</sup> Compound **4-9** was found to bind at the lower side of the binding pocket with a docking energy of -6.07 kcal/mol equipped with three hydrogen bonding interactions as well. The side chains of G6 and T8 of the peptide sequence of conjugate **4-9** formed hydrogen-bonding interactions with the side chain of Arg310 from EGFR. Y2 of the hydrogen bonded with Val312 of

EGFR. Conjugate **4-9** did not exhibit a hydrogen bond with the 3PEG moiety. This instance is due to the folded loop structure of the PEG group to block any and hydrogen bonding interaction with the receptor. The BODIPY scaffold of conjugate **4-9** was suppressed in the hydrophobic pocket near Phe335 and His334 of EGFR. One of the methoxy phenyl groups of the dye was also found buried in the hydrophobic pocket of EGFR. This immersion into the hydrophobic pocket leads to stabilizing the compound in binding pocket of EGFR. Still, the BODIPY core was extended out of the pocket with the peptide part buried in the inside of EGF binding site.

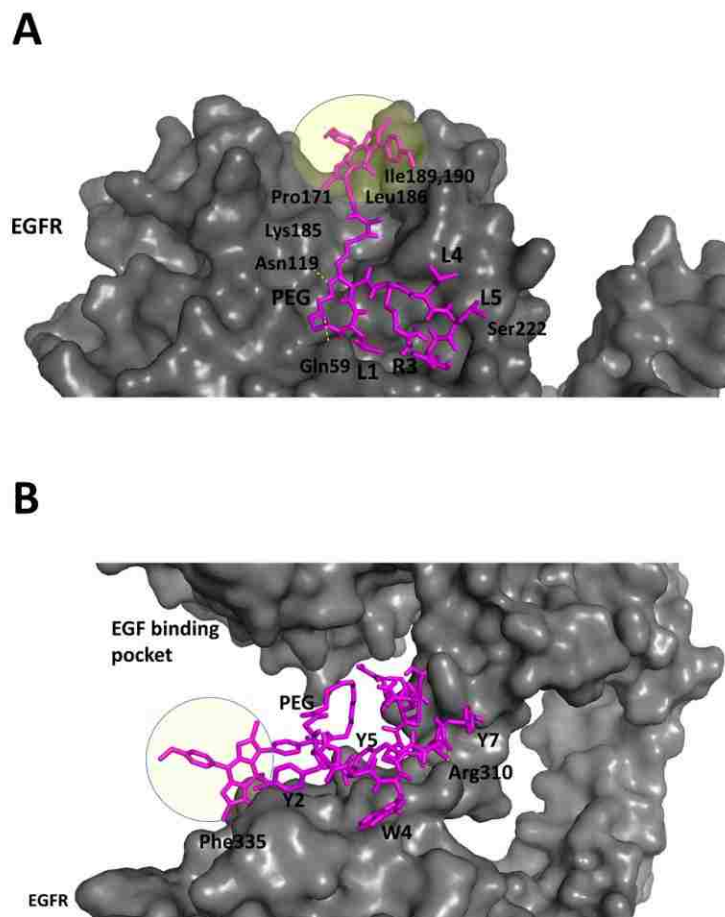


Figure 13. Proposed model of interaction of EGFR with A) conjugate 4-8 and B) conjugate 4-9. BODIPY is highlighted. Amino acids from peptide are represented by single letter code and amino acids from the protein are represented with three-letter code. EGFR is shown in surface representation. Reprinted with permission from [22] Copyright (2017) American Cancer Society.

From SPR and docking studies it is clear the conjugate **4-8** binds specifically to EGFR away from the EGF binding pocket. However, conjugate **4-9** binds near EGF binding pocket with BODIPY buried in the hydrophobic pocket. Previous studies by Li et al.,<sup>40</sup> suggest that peptide YHWYGYTPQNVI binds near EGF binding pocket, and the EGF binding pocket is partially overlapped with the peptide binding pocket. Dr. Jois' docking studies demonstrate that conjugate **4-9** binds to the lower side of EGFR in the EGF pocket. Furthermore, SPR studies indicated that compound **4-5** binds to EGFR non-specifically (Figure 6) and conjugate **4-9** (Figure 5) binding seems to be non-specific at higher concentration. This may be due to the binding of BODIPY to the hydrophobic pocket near EGF binding pocket. Furthermore, modeling studies indicated that in the case of conjugate **4-8**, PEG and BODIPY part of the molecule did not block the efficient groups (amino acid side chains) of the peptide needed for bonding interactions, whereas in compound **4-9** the 3PEG moiety twisted structure onto the peptide surface covering some of the side chains in the peptide (Figures 13 A and B). Consequently, looking at specific binding to EGFR, conjugate **4-8** may be a better choice for EGFR binding.

#### 4.4 Conclusion

In conclusion, NCS-BODIPY **4-5** was designed and successfully synthesized from pentachloro-BODIPY **4-1** in several steps. BODIPY **4-5** was confirmed by <sup>1</sup>H, <sup>13</sup>C, and <sup>11</sup>B NMR, HRMS, and X-ray analysis. The quick and clean conjugation reactions between isothiocyanate group of BODIPY **4-5** and EGFR-peptides **2-4** and **2-5** were investigated for the first time, and each conjugation exhibits percent yields up to 80%. The formation of BODIPY-peptide conjugates **4-8** and **4-9** was confirmed using <sup>1</sup>H and <sup>11</sup>B NMR, HSQC, and MALDI-TOF. Each conjugate was further characterized by spectroscopic studies, which showed that conjugates **4-8** and **4-9** observed similar spectroscopic properties, both emitting > 630 nm in DMSO. BODIPY **4-5** and conjugate **4-9** (at higher concentrations) showed a non-specific binding to EGFR, while conjugate **4-8** displayed an apparent specific binding to EGFR. Computational studies were conducted by Dr.

Seetharama Jois to further reveal the binding ways of conjugates **8-9** to EGFR. Cell studies conducted by Mrs. Zehua Zhou results, compared with precursor **4-5**, conjugates **4-8** and **4-9** showed faster ( $> 50$  fold) accumulation in the human HEP2 cells; conjugates **4-8** and **4-9** also showed low dark toxicity ( $IC_{50} \geq 98 \mu M$ ) and phototoxicity ( $IC_{50} \geq 74$ ). Those properties above suggest BODIPY-peptide conjugates **4-8** and **4-9** are suitable EGFR targeting agents for imaging CRC.

## 4.5 Experimental

### 4.5.1 General Information

Commercially available chemicals were purchased from VWR or Sigma-Aldrich and used without further purifications for the reactions and purifications. Thin layer chromatography (TLC) was performed on the precoated silica gel plates (0.2 mm, 254 indicator, polyester backed, 60Å, Sorbent Technologies) to monitor the reactions. Preparative TLC plates (60G, VWR) and silica gel (60Å, 230-400 mesh, Sorbent Technologies) were used for liquid chromatography and column chromatography.  $^1H$  NMR and  $^{13}C$  NMR spectra were collected on a Bruker AV-400 liquid, or AV-500 spectrometer at 300K. All the chemical shifts ( $\delta$ ) are provided in parts per million (ppm) in  $CDCl_3$  (7.27 ppm for  $^1H$  NMR and 77.0 ppm for  $^{13}C$  NMR) and DMSO (2.54 ppm for  $^1H$  NMR). The coupling constants ( $J$ ) are reported in Hz. High-resolution mass spectra (HRMS) and MALDI (TOF) spectra were obtained on a 6210 ESI-TOF Mass Spectrometer (Agilent Technologies) under negative mode and Applied Biosystems QSTAR at the LSU Mass Spectrometry Facility. Normal-phase HPLC was performed on Dionex system (organics system) including a P680 pump with a UVD 340 detector and a fraction collector III. This system is connected to a Dynamax axial compression column in the packing of irregular silica gel (Rainin 60 Å). Reverse-phase HPLC analysis was performed with a Waters 2485 Quaternary Gradient Module, Waters Sample Injector, and 2489 UV/Visible Detector, which are controlled by Waters Empower 2 software. Separations were completed on an X-Bridge BEH300 Prep C18 (5  $\mu m$ , 10 x 250 mm) with a X-Bridge BEH300 Prep Guard cartridge 300 Å (5  $\mu m$ , 10 x 10 mm) at a 4 mL/min flow rate with UV detection for



peptides at 220 nm, and for BODIPY conjugates at 580 nm. Fractions of HPLC purity (> 95%) with the anticipated mass were combined and lyophilized.

#### 4.5.2 Synthesis of NCS BODIPY 4-5

##### BODIPY 4-5

Into a 25 mL round-bottomed flask were added BODIPY **4-4** (10.2 mg, 0.018 mmol), 1,1'-thiocarbonyldi-2(1*H*)-pyridone (20.9 mg, 0.09 mmol), and dichloromethane (2 mL). The mixture was stirred at room temperature for 2 h. The reaction was stopped when the starting material was completely consumed, according to TLC. The organic solvent was removed, and the residue was subjected to prep TLC using ethyl acetate/hexanes 1:2 for elution to provide the desired product **5** (9.6 mg, 88%). mp 247-249 oC; <sup>1</sup>H NMR (400 MHz, CDCl<sub>3</sub>) δ 7.64-7.69 (m, 4H), 7.54-7.56 (d, *J* = 8.7 Hz, 2H), 7.27-7.29 (s, 2H), 7.09-7.11 (d, *J* = 8.7 Hz, 1H), 6.96-6.98 (m, 3H), 6.90 (s, 1H), 3.95 (s, 1H), 3.86 (s, 1H); <sup>13</sup>C NMR (125 MHz, CDCl<sub>3</sub>) δ 162.2, 161.1, 155.8, 151.0, 144.1, 136.7, 133.3, 132.8, 132.4, 132.3, 131.9, 131.7, 129.2, 128.6, 127.4, 125.8, 125.3, 123.6, 121.7, 121.3, 114.3, 113.6, 55.6, 55.2; <sup>11</sup>B NMR (128 MHz, CDCl<sub>3</sub>) δ 0.518 (t, *J* = 30.3 Hz); HRMS (ESI-TOF) *m/z* calcd for C<sub>30</sub>H<sub>20</sub>BCl<sub>2</sub>F<sub>2</sub>N<sub>3</sub>O<sub>2</sub>S [M]<sup>-</sup> 604.0756; found 604.0734.

#### 4.5.3 Procedure for peptide conjugation

Into a 4 mL vial were added the pegylated peptides (1.5eq) and triethylamine (7.5 eq). The mixture was stirred at room temperature for 5 min. BODIPY **4-5** (1 eq) was added into the vial, and the final mixture was stirred at room temperature for 30 min. TLC was used to monitor the reaction. H<sub>2</sub>O (0.5 mL) was added to quench the reaction, and the solvent was removed using pressure. The residue was then subjected to HPLC (CH<sub>3</sub>CN/H<sub>2</sub>O as the eluents for conjugate **4-8**; CH<sub>3</sub>CN and H<sub>2</sub>O including 0.1% TFA as the eluents for conjugate **9**) to afford the desired BODIPY-peptide conjugates **4-8** and **4-9**.

**Conjugate 4-8** (BODIPY-3PEG-LARLLT-NH<sub>2</sub>): Yield: 5.91 mg, 80%. HPLC (50% A for 5 min, 10% A to 0% A over 13 minutes, 0% A to 50% A over 2 min at a flow rate of 4 mL/min) and *t<sub>R</sub>* = 11.00 min. <sup>1</sup>H NMR (500 MHz, DMSO) δ 9.87 (s, 2H), 8.16 (s, 2H), 8.03 (s, 4H), 7.91 (d, *J* = 8.1

Hz, 1H), 7.72 (d,  $J = 8.7$  Hz, 2H), 7.68 (d,  $J = 8.6$  Hz, 2H), 7.51 (dd,  $J = 14.9, 8.7$  Hz, 4H), 7.40 (d,  $J = 7.8$  Hz, 2H), 7.19 (dd,  $J = 23.7, 9.7$  Hz, 5H), 7.05 (m, 4H), 6.48 (s, 1H), 4.27 (m, 5H), 4.05 (m, 2H), 3.92 (s, 3H), 3.82 (s, 3H), 3.67 (s, 2H), 3.52 (m, 14H), 3.09 (d,  $J = 6.0$  Hz, 2H), 1.58 (m, 4H), 1.48 (m, 8H), 1.21 (m, 7H), 1.00 (d,  $J = 6.3$  Hz, 3H), 0.87 (m, 18H);  $^{11}\text{B}$  NMR (128 MHz, DMSO)  $\delta$  0.368 (t,  $J = 30.2$  Hz); MS (MALDI-TOF):  $m/z$  calcd for  $\text{C}_{70}\text{H}_{98}\text{BCl}_2\text{F}_2\text{N}_{14}\text{O}_{11}\text{S}$   $[\text{M}]^+$  1493.659; found 1493.726.

**Conjugate 4-9** (BODIPY-3PEG-GYHWYGYTPQNVI-NH<sub>2</sub>): Yield: 5.95 mg, 50%. HPLC (50% A for 5 min, 10% A to 0% A over 13 minutes, 0% A to 50% A over 2 min at a flow rate of 4 mL/min) and  $t_{\text{R}} = 11.99$  min.  $^1\text{H}$  NMR (500 MHz, DMSO)  $\delta$  13.99 (s, 1H), 10.74 (s, 1H), 9.89 (s, 2H), 9.15 (s, 3H), 8.90 (s, 1H), 8.09 (m, 12H), 7.70 (dd,  $J = 26.4, 8.5$  Hz, 5H), 7.51 (dd,  $J = 14.2, 8.7$  Hz, 4H), 7.43 (s, 1H), 7.22 (m, 6H), 7.03 (m, 8H), 6.79 (s, 1H), 6.62 (d,  $J = 4.2$  Hz, 5H), 6.54 (s, 3H), 4.58 (dd,  $J = 12.0, 5.6$  Hz, 4H), 4.38 (t,  $J = 7.0$  Hz, 5H), 4.16 (m, 2H), 4.08 (t,  $J = 7.8$  Hz, 2H), 3.92 (s, 4H), 3.81 (s, 3H), 3.59 (m, 16H), 3.13 (m, 3H), 2.90 (s, 4H), 2.67 (m, 3H), 2.37 (m, 2H), 1.99 (m, 11H), 1.45 (m, 3H), 1.16 (m, 14H), 0.83 (m, 9H);  $^{11}\text{B}$  NMR (128 MHz, DMSO)  $\delta$  0.374 (t,  $J = 30.2$  Hz); MS (MALDI-TOF):  $m/z$ . calcd for  $\text{C}_{116}\text{H}_{139}\text{BCl}_2\text{F}_2\text{N}_{23}\text{O}_{25}\text{S}^+$   $[\text{M}+\text{H}]^+$  2405.950; found 2406.018.

#### 4.5.4 Spectroscopic Studies

A Varian Cary spectrophotometer and a Perkin Elmer LS55 spectrophotometer were used to determine the UV-Visible and emission spectra at room temperature. Quartz cuvettes (1 cm path length) were used for both measurements. The plots of integrated absorbance vs. the corresponding solution concentrations were used to determine the extinction coefficients ( $\epsilon$ ) at the maximum absorption. Different dilute BODIPY solutions with absorbance values between 0.03-0.1 at  $\lambda = 550$  nm or 580 nm were selected and used for the determination of the relative fluorescence quantum yields. Crystal violet perchlorate (0.50 in ethanol) and methylene blue (0.03 in methanol) were used as the external standards.<sup>33</sup> Relative fluorescence quantum yields ( $\Phi_{\text{f}}$ ) were calculated using the following equation:<sup>41</sup>

$$\Phi_x = \Phi_{\text{std}} \times (\text{Grad}_x / \text{Grad}_{\text{std}}) \times (n_x^2 / n_{\text{std}}^2)$$

Where  $\Phi$  refers to the fluorescence quantum yields;  $n$  represents the refractive indexes of the solvents used for the measurement; Grad refers to the gradient of integrated fluorescence intensity vs. the corresponding absorbance; subscript  $x$  and  $\text{std}$  represent the tested samples and the external standards, respectively.

#### **4.5.5 Surface Plasmon Resonance**

SPR was achieved using Biacore X100 from GE Health Sciences. Pure recombinant protein EGFR was obtained from Leinco Technologies (St. Louis, MO). HBS-EP+ buffer and 100 mM glycine at pH 4, 4.5, 5, 5.5 were purchased from GE Health Science. The extracellular domain of EGFR protein was immobilized on a CM5 sensor chip (GE Healthcare Biosciences) at a rate of 10  $\mu\text{L}/\text{min}$  using a customary amine coupling procedure. The carboxyl groups on the CM5 chip were initiated using a solution containing 0.2 M N-ethyl N-(dimethylaminopropyl) carbodiimide (EDC) and 0.05 M N-hydroxysuccinimide (NHS) (35  $\mu\text{L}$  solution, with a flow rate of 5  $\mu\text{L}/\text{min}$ ). The running buffer for peptides was HBS-EP+ buffer diluted 10 times, including 0.01 M HEPES, 0.15 M NaCl, 3 mM EDTA, and 0.005% surfactant P20 at pH 7.5. Peptides dissolved in buffer were used as analytes. The running buffer for the BODIPY conjugates was HBS-EP+ buffer diluted 10 times, also containing 0.01 M HEPES, 0.15 M NaCl, 3mM EDTA, 0.005% surfactant P20 at pH 7.5, but brought to a 4% DMSO concentration. BODIPY **5** and conjugates **8** and **9** were dissolved in 4% DMSO buffer solutions and used as the analytes. SPR sensorgrams were attained and the association and dissociation rates were obtained from 0 to 250  $\mu\text{M}$  concentrations.

#### **4.5.6 Cell Studies**

The human HEp2 cell line was purchased from ATCC, and maintained in a DMEM/AMEM (50:50) mixture supplemented with FBS (5%) and Primocin antibiotic. All other commercial available reagents used in the cell studies were purchased from Life Technologies.

##### *4.5.6.1 Dark Cytotoxicity*

A Stock solution (32 mM) of BODIPYs **4-5** and conjugates **8** and **9** was prepared using 100% DMSO. Working solutions with concentrations of 0, 6.25, 12.5, 25, 50, and 100  $\mu\text{M}$  were prepared from the stock solutions. The HEp2 cells were exposed to each of the solutions of desired compounds up to 100  $\mu\text{M}$  and incubated overnight (5%  $\text{CO}_2$ , 95% humidity, 37  $^\circ\text{C}$ ). The loading medium solution was removed, and the cells were washed with PBS solution. Medium (20% Cell Titer Blue from Promega) was added and the cells incubated for another 4 h. BMG FLUOstar Optima microplate reader was used to measure the dark toxicity by reading the medium fluorescence at 570/615 nm. The fluorescence intensity of the untreated cells was normalized to 100%.

#### *4.5.6.2 Phototoxicity*

The HEp2 cells were exposed to the different working solutions of BODIPYs **4-5**, **4-8** and **4-9** up to 100  $\mu\text{M}$  and incubated overnight (5%  $\text{CO}_2$ , 95% humidity, 37  $^\circ\text{C}$ ). The loading medium solution was removed, and the cells were washed with PBS solution. New medium was added and the cells were then exposed to a halogen lamp (600 W) as the light source, prepared with a water filter (transmits radiation 250–950 nm) and a beam turning mirror (200 nm to 30  $\mu\text{m}$  spectral range, Newport), for 20 min. The total light dose used was  $\approx 1.5 \text{ J/cm}^2$ . The cells were then incubated for another 24 h, followed by the measurement of cell viability as previously described.

#### *4.5.6.3 Time-Dependent Cellular Uptake*

The HEp2 cells were exposed to 10  $\mu\text{M}$  concentration solutions of BODIPYs **4-5**, **4-8** and **4-9** for different periods of time (0, 1, 2, 4, 8, and 24 h). The loading medium solution was removed, and the cells were washed with PBS solution. The cells were then dissolved in 0.25% Triton X-100 in PBS solution. BODIPY solutions with concentrations of 10, 5, 2.5, 1.25, 0.625, and 0.3125  $\mu\text{M}$  were prepared by diluting 400  $\mu\text{M}$  of each compound with 0.25% Triton X-100 (Sigma-Aldrich) in PBS solution, and used to obtain the standard curves. The concentration of the compounds was determined using a BMG FLUOstar Optima microplate reader at 570/615 nm.

#### *4.5.6.4 Microscopy*

The human HEp2 cells were incubated in a six-well plate (MatTek), and allowed to grow overnight. The cells were exposed to each compound at a concentration of 10  $\mu$ M, and incubated for 6 h (5% CO<sub>2</sub>, 95% humidity, 37 °C). The following organelle trackers (Invitrogen) were added to the cells: ER Tracker Blue/White (100 nM), BODIPY FL C5 Ceramide (50 nM), MitoTracker Green (250 nM), LysoSensor Green (50 nM). The cells were incubated with each compound and trackers for half an hour, and washed with PBS solution three times before imaging. A Leica DMRXA2 upright microscope equipped with a water immersion objective, and DAPI, GFP, and Texas Red filter cubes (Chroma Technologies) was used to acquire the images.

#### 4.5.7 Computational Modeling

The 3D structures of conjugates **4-8** and **4-9** were built using InsightII (BIOVIA San Diego, CA) molecular modeling software. The BODIPY structure was obtained from the coordinates of the crystal structure of **5** described above. For the EGFR receptor 3D structure, the pdb file 1nql<sup>42</sup> that represents EGFR in a closed conformation was downloaded from the protein data bank. Conjugates **4-8** and **4-9** contain a boron atom in the BODIPY core and forcefield parameters were not defined in the Autodock default parameters file. Parameters for boron can be obtained from the literature,<sup>43</sup> however, for docking calculations the boron atom was replaced with a carbon atom, as boron atom is not calibrated in docking studies using Autodoc. Docking was performed using Autodock 4.<sup>38</sup> The lowest energy docked structure was represented using PyMol software (Schrodinger LLC, Portland, OR).

#### 4.6 Reference

1. Karlsson, I.; Samuelsson, K.; Ponting, D. J.; Törnqvist, M.; Ilag, L. L.; Nilsson, U., Peptide Reactivity of Isothiocyanates – Implications for Skin Allergy. *Scientific Reports* **2016**, *6*, 21203.
2. Poty, S.; Gourni, E.; Désogère, P.; Boschetti, F.; Goze, C.; Maecke, H. R.; Denat, F., AMD3100: A Versatile Platform for CXCR4 Targeting 68Ga-Based Radiopharmaceuticals. *Bioconjugate Chem.* **2016**, *27* (3), 752-761.

3. Sutton, J. M.; Clarke, O. J.; Fernandez, N.; Boyle, R. W., Porphyrin, Chlorin, and Bacteriochlorin Isothiocyanates: Useful Reagents for the Synthesis of Photoactive Bioconjugates. *Bioconjugate Chem.* **2002**, *13* (2), 249-263.
4. Hudson, R.; Carcenac, M.; Smith, K.; Madden, L.; Clarke, O. J.; Pelegrin, A.; Greenman, J.; Boyle, R. W., The development and characterisation of porphyrin isothiocyanate-monoclonal antibody conjugates for photoimmunotherapy. *Br. J. Cancer* **2005**, *92* (8), 1442-1449.
5. Maindron, N.; Ipuý, M.; Bernhard, C.; Lhenry, D.; Moreau, M.; Carme, S.; Oudot, A.; Collin, B.; Vrigneaud, J.-M.; Provent, P.; Brunotte, F.; Denat, F.; Goze, C., Near-Infrared-Emitting BODIPY-trisDOTA111In as a Monomolecular Multifunctional Imaging Probe: From Synthesis to In Vivo Investigations. *Chem. Eur. J.* **2016**, *22* (36), 12670-12674.
6. Brizet, B.; Goncalves, V.; Bernhard, C.; Harvey, P. D.; Denat, F.; Goze, C., DMAP-BODIPY Alkynes: A Convenient Tool for Labeling Biomolecules for Bimodal PET–Optical Imaging. *Chem. Eur. J.* **2014**, *20* (40), 12933-12944.
7. Lhenry, D.; Larrouy, M.; Bernhard, C.; Goncalves, V.; Raguin, O.; Provent, P.; Moreau, M.; Collin, B.; Oudot, A.; Vrigneaud, J.-M.; Brunotte, F.; Goze, C.; Denat, F., BODIPY: A Highly Versatile Platform for the Design of Bimodal Imaging Probes. *Chem. Eur. J.* **2015**, *21* (37), 13091-13099.
8. Dumont, Y.; Gaudreau, P.; Mazzuferi, M.; Langlois, D.; Chabot, J.-G.; Fournier, A.; Simonato, M.; Quirion, R., BODIPY®-conjugated neuropeptide Y ligands: new fluorescent tools to tag Y1, Y2, Y4 and Y5 receptor subtypes. *Br. J. Pharmacol.* **2005**, *146* (8), 1069-1081.
9. Kondo, N.; Temma, T.; Deguchi, J.; Sano, K.; Ono, M.; Saji, H., Development of PEGylated peptide probes conjugated with 18F-labeled BODIPY for PET/optical imaging of MT1-MMP activity. *J. Controlled Release* **2015**, *220*, Part A, 476-483.
10. Liu, L.; Fu, L.; Jing, T.; Ruan, Z.; Yan, L., pH-Triggered Polypeptides Nanoparticles for Efficient BODIPY Imaging-Guided Near Infrared Photodynamic Therapy. *ACS Applied Materials & Interfaces* **2016**, *8* (14), 8980-8990.
11. Verwilst, P.; David, C. C.; Leen, V.; Hofkens, J.; de Witte, P. A. M.; De Borggraeve, W. M., Synthesis and in vitro evaluation of a PDT active BODIPY–NLS conjugate. *Bioorg. Med. Chem. Lett.* **2013**, *23* (11), 3204-3207.

12. Malatesti, N.; Hudson, R.; Smith, K.; Savoie, H.; Rix, K.; Welham, K.; Boyle, R. W., Isothiocyanato Boron Dipyrromethenes—The First BODIPY Analogues of Fluorescein Isothiocyanate. *Photochem. Photobiol.* **2006**, *82* (3), 746-749.
13. Boas, U.; Gertz, H.; Christensen, J. B.; Heegaard, P. M. H., Facile synthesis of aliphatic isothiocyanates and thioureas on solid phase using peptide coupling reagents. *Tetrahedron Lett.* **2004**, *45* (2), 269-272.
14. Sureshbabu, V. V.; Naik, S. A.; Hemantha, H. P.; Narendra, N.; Das, U.; Guru Row, T. N., N-Urethane-Protected Amino Alkyl Isothiocyanates: Synthesis, Isolation, Characterization, and Application to the Synthesis of Thioureidopeptides. *J. Org. Chem.* **2009**, *74* (15), 5260-5266.
15. Drewnowski, A.; Gomez-Carneros, C., Bitter taste, phytonutrients, and the consumer: a review. *The American journal of clinical nutrition* **2000**, *72* (6), 1424-1435.
16. Cinciripini, P. M.; Hecht, S. S.; Henningfield, J. E.; Manley, M. W.; Kramer, B. S., Tobacco addiction: implications for treatment and cancer prevention. *Journal of the National Cancer Institute* **1997**, *89* (24), 1852-1867.
17. Edens, N. K., REPRESENTATIVE COMPONENTS OF FUNCTIONAL FOOD SCIENCE. *Nutrition Today* **1999**, *34* (4), 152-154.
18. Fahey, J. W.; Zhang, Y.; Talalay, P., Broccoli sprouts: an exceptionally rich source of inducers of enzymes that protect against chemical carcinogens. *Proceedings of the National Academy of Sciences* **1997**, *94* (19), 10367-10372.
19. Zhang, Y.; Talalay, P.; Cho, C.-G.; Posner, G. H., A major inducer of anticarcinogenic protective enzymes from broccoli: isolation and elucidation of structure. *Proceedings of the national academy of sciences* **1992**, *89* (6), 2399-2403.
20. Fernández, J. G.; Mellet, C. O.; Blanco, J. J.; Mota, J. F.; Gadelle, A.; Coste-Sarguet, A.; Defaye, J., Isothiocyanates and cyclic thiocarbamates of  $\alpha$ ,  $\alpha'$ -trehalose, sucrose, and cyclomaltooligosaccharides. *Carbohydrate research* **1995**, *268* (1), 57-71.
21. Mukerjee, A. K.; Ashare, R., Isothiocyanates in the chemistry of heterocycles. *Chemical Reviews* **1991**, *91* (1), 1-24.

22. Zhao, N.; Williams, T. M.; Zhou, Z.; Fronczek, F. R.; Sibrian-Vazquez, M.; Jois, S. D.; Vicente, M. G. H., Synthesis of BODIPY-Peptide Conjugates for Fluorescence Labeling of EGFR Overexpressing Cells. *Bioconjugate Chemistry* **2017**, *28* (5), 1566-1579.
23. Wang, H.; Fronczek, F. R.; Vicente, M. G. H.; Smith, K. M., Functionalization of 3,5,8-Trichlorinated BODIPY Dyes. *J. Org. Chem.* **2014**, *79* (21), 10342-10352.
24. Zhao, N.; Vicente, M. G. H.; Fronczek, F. R.; Smith, K. M., Synthesis of 3,8-Dichloro-6-ethyl-1,2,5,7-tetramethyl-BODIPY from an Asymmetric Dipyrroketone and Reactivity Studies at the 3,5,8-Positions. *Chem. Eur. J.* **2015**, *21*, 6181-6192.
25. Zhao, N.; Xuan, S.; Byrd, B.; Fronczek, F. R.; Smith, K. M.; Vicente, M. G. H., Synthesis and regioselective functionalization of perhalogenated BODIPYs. *Org. Biomol. Chem.* **2016**, *14*, 6184-6188.
26. Zhao, N.; Xuan, S.; Fronczek, F. R.; Smith, K. M.; Vicente, M. G. H., Stepwise Polychlorination of 8-Chloro-BODIPY and Regioselective Functionalization of 2,3,5,6,8-Pentachloro-BODIPY. *J. Org. Chem.* **2015**, *80* (16), 8377-8383.
27. Xuan, S.; Zhao, N.; Ke, X.; Zhou, Z.; Fronczek, F. R.; Kadish, K. M.; Smith, K. M.; Vicente, M. G. H., Synthesis and Spectroscopic Investigation of a Series of Push-Pull Boron Dipyrromethenes (BODIPYs). *J. Org. Chem.* **2017**.
28. Fontenot, K. R.; Ongarora, B. G.; LeBlanc, L. E.; Zhou, Z.; Jois, S. D.; Vicente, M. G. H., Targeting of the epidermal growth factor receptor with mesoporphyrin IX-peptide conjugates. *J. Porphyrins Phthalocyanines* **2016**, *20* (01n04), 352-366.
29. Ongarora, B. G.; Fontenot, K. R.; Hu, X.; Sehgal, I.; Satyanarayana-Jois, S. D.; Vicente, M. G. H., Phthalocyanine-Peptide Conjugates for Epidermal Growth Factor Receptor Targeting. *J. Med. Chem.* **2012**, *55* (8), 3725-3738.
30. Hermanson, G. T., *Bioconjugate techniques*. Academic press: 2013.
31. Sibrian-Vazquez, M.; Jensen, T. J.; Hammer, R. P.; Vicente, M. G. H., Peptide-Mediated Cell Transport of Water Soluble Porphyrin Conjugates. *J. Med. Chem.* **2006**, *49* (4), 1364-1372.



32. Sibrian-Vazquez, M.; Ortiz, J.; Nesterova, I. V.; Fernández-Lázaro, F.; Sastre-Santos, A.; Soper, S. A.; Vicente, M. G. H., Synthesis and Properties of Cell-Targeted Zn(II)–Phthalocyanine–Peptide Conjugates. *Bioconjugate Chem.* **2007**, *18* (2), 410-420.
33. Olmsted, J., Calorimetric determinations of absolute fluorescence quantum yields. *J. Phys. Chem.* **1979**, *83* (20), 2581-2584.
34. Ntziachristos, V., Going deeper than microscopy: the optical imaging frontier in biology. *Nat Meth* **2010**, *7* (8), 603-614.
35. Sibrian-Vazquez, M.; Jensen, T. J.; Vicente, M. G. H., Influence of the number and distribution of NLS peptides on the photosensitizing activity of multimeric porphyrin-NLS. *Org. Biomol. Chem.* **2010**, *8* (5), 1160-1172.
36. Uppal, T.; Bhupathiraju, N. V. S. D. K.; Vicente, M. G. H., Synthesis and cellular properties of Near-IR BODIPY–PEG and carbohydrate conjugates. *Tetrahedron* **2013**, *69* (23), 4687-4693.
37. Xuan, S.; Zhao, N.; Zhou, Z.; Fronczek, F. R.; Vicente, M. G. H., Synthesis and in Vitro Studies of a Series of Carborane-Containing Boron Dipyrromethenes (BODIPYs). *J. Med. Chem.* **2016**, *59* (5), 2109-2117.
38. Morris, G. M.; Huey, R.; Lindstrom, W.; Sanner, M. F.; Belew, R. K.; Goodsell, D. S.; Olson, A. J., AutoDock4 and AutoDockTools4: Automated docking with selective receptor flexibility. *J. Comput. Chem.* **2009**, *30* (16), 2785-2791.
39. Song, S.; Liu, D.; Peng, J.; Deng, H.; Guo, Y.; Xu, L. X.; Miller, A. D.; Xu, Y., Novel peptide ligand directs liposomes toward EGF-R high-expressing cancer cells in vitro and in vivo. *The FASEB Journal* **2009**, *23* (5), 1396-1404.
40. Li, Z.; Zhao, R.; Wu, X.; Sun, Y.; Yao, M.; Li, J.; Xu, Y.; Gu, J., Identification and characterization of a novel peptide ligand of epidermal growth factor receptor for targeted delivery of therapeutics. *The FASEB Journal* **2005**, *19* (14), 1978-1985.
41. Gorke, A. P.; Nani, R. R.; Zhu, J.; Mackem, S.; Schnermann, M. J., A Near-IR Uncaging Strategy Based on Cyanine Photochemistry. *J. Am. Chem. Soc.* **2014**, *136* (40), 14153-14159.

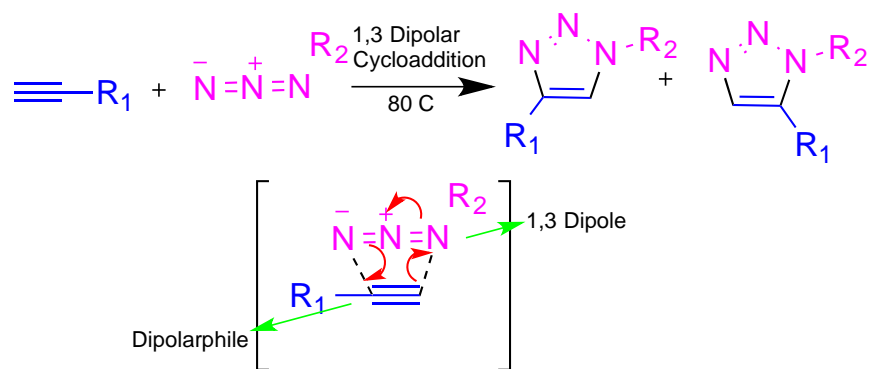
42. Ferguson, K. M.; Berger, M. B.; Mendrola, J. M.; Cho, H.-S.; Leahy, D. J.; Lemmon, M. A., EGF Activates Its Receptor by Removing Interactions that Autoinhibit Ectodomain Dimerization. *Mol. Cell* **2003**, *11* (2), 507-517.

43. Tafi, A.; Agamennone, M.; Tortorella, P.; Alcaro, S.; Gallina, C.; Botta, M., AMBER force field implementation of the boronate function to simulate the inhibition of  $\beta$ -lactamases by alkyl and aryl boronic acids. *European Journal of Medicinal Chemistry* **2005**, *40* (11), 1134-1142.

## CHAPTER 5. Design and Synthetic Strategies for BODIPY-Peptidic Conjugates for Diagnosis of CRC via Click Chemistry

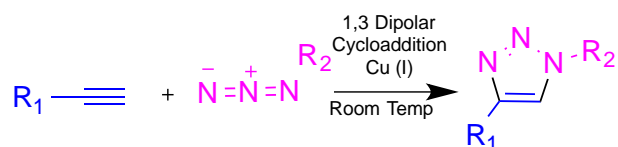
### 5.1 Introduction

Nobel Laureate Dr. Barry Sharpless first introduced a novel 1,3-dipolar cycloaddition between a terminal alkyne and an azide in 2001. This cycloaddition also known as the azide/alkyne-“Click”-reaction or “CuAAC reaction” is a very unique reaction that has gained popularity due to its varied utility in diverse fields. Click chemistry consists of a group of reactions that are clean, fast, and efficient. Click chemistry can be very versatile in the method of connecting two compounds, as well as providing a regiospecific manner during connection<sup>1</sup>. There are several reaction types that use this concept such as the mentioned cycloadditions, nucleophilic ring opening, non-aldol carbonyl chemistry, and addition to carbon-carbon multiple bonds to name a few. Of those mentioned reactions, cycloadditions in particular the copper-catalyzed Huisgen 1,3-dipolar cycloaddition of azides and terminal alkynes, abbreviated as CuAAC (Copper-catalyzed azide alkyne cycloaddition) is the best known click reaction.<sup>2</sup> Rolf Huisgen contribution to the azide/alkyne cycloadditions required the alkyne to behave as a dipolarophile ready for the addition of an azide moiety or 1,3-dipole in concerted fashions<sup>3</sup> by heating, to produce a mixture of 1,4- and 1,5-triazoles (Scheme 1).



Scheme 1. 1,3-Dipolar cycloaddition of an 1,3-dipole and dipolarophile discovered by Rolf Huisgen.<sup>3</sup>

The heating of these reactions to induce cycloaddition was considered harsh reaction conditions requiring improvements. The desired changes were considerably moderated by the use of a copper catalyst, which accelerates the rate of the reaction by 7 orders of magnitude.<sup>4</sup> This phenomenon was revealed by Sharpless and Meldal groups opposing Huisgen's uncatalyzed conditions, where the addition of copper (I) salts safeguards the restricted 1,2,3-triazole regioselective formation of the 1,4- regioisomer (Scheme 2).<sup>4</sup>



Scheme 2. Copper catalyzed 1,3-dipolar cycloaddition by Sharpless/Meldal.

Copper (I) catalyzed cycloaddition reactions have a multitude of desirable characteristics including simple reaction conditions, short reaction time, simple purification, and robust under various reaction conditions, such as air and moisture. These benefits have allowed this 1,3-dipolar cycloaddition to catch the eye of researchers in biomolecule conjugation for use in multiple areas such as photodynamic therapy and imaging. This cycloaddition is especially suitable for gentle components such as peptides, carbohydrates, and nucleotides.<sup>2</sup> The continual attraction of the click chemistry is ingrained in its selectivity, productivity, and adaptability.<sup>5</sup> The click reaction is often quantitative and highly desirable due to its robust behavior and insensitivity to various environments.<sup>6</sup> The triazole formed is a strong entity that is stable to conditions such as acid and base hydrolysis, reductive and oxidative environments, and is quite resistant to proteolytic cleavages.<sup>7</sup>

Thus, cycloadditions have been used in various conjugation attempts in probe developments including BODIPY dyes as the fluorophore of choice, and a targeting moiety for appreciation in *in vivo* imaging. Wolfbeis et al.<sup>8</sup> reported *in vivo* cellular labeling of biomolecules by way of copper free and copper-mediated click chemistry. Clickable BODIPY fluorophores were

designed for labeling of the azide modified surface glycans of CHO cells. Akkaya et al.<sup>9</sup> reported the use of click chemistry in the synthesis of a bay region BODIPY dye appended to a perylenediimide (PDI). The molecule is suited for light-harvesting and allows a large cross-section for the absorption of light in the visible range. The excitation energy was shown to efficiently channel the perylenediimide core structures.<sup>9</sup> Overkleeft et al.<sup>10</sup> synthesized three acetylene functionalized BODIPY dyes that are used to identify an azido- bearing epoxomicin analogue by fluorescence. This identification was performed through the Huisgen 1,3-dipolar cycloaddition, which resulted in a collection of fluorescent epoxomicin derived proteasome probes.<sup>10</sup>

The growing success of the CuAAC reaction is ingrained in its selectivity, efficiency and versatility. The CuAAC reaction is a virtually quantitative, very robust, insensitive to the environment, and with the orthogonal ligation reaction, suitable for various bimolecular pairing and *in vivo* labeling. The triazole formed is stable to acid and base hydrolysis, reductive and oxidative environments, and is quite resilient to metabolic degradation.<sup>2</sup> Several other functionalized BODIPYs were conjugated to peptides or proteins for imaging applications using “click” reactions.<sup>11-14</sup>

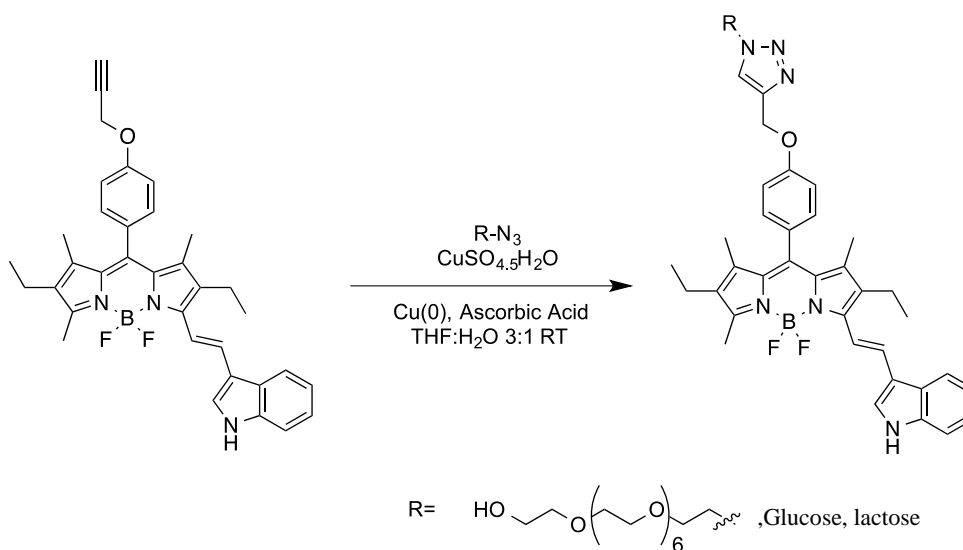
As a result, this chapter will focus on utilizing click chemistry as the desired method for conjugating peptides to alkynyl BODIPY dyes. The use of click chemistry is not only due to the facile synthetic processes surrounding the methodology, but also due to the: (1) resourcefulness of the reaction (2) moderate reaction conditions that could be well endured by the BODIPY and peptide scaffolds, and (3) ease of purification.<sup>15 15-16</sup>

## 5.2 Results and Discussion

The drive of this work was to make use of the versatile cycloaddition reactions to design and synthesize a sequence of new fluorescent bioconjugates appended to L1 peptide derivatives. This group of bioconjugates would consist of a BODIPY fluorophore bearing a durable 1,2,3-triazole ring, linked to a peptide moiety that targets EGFR for a specific accumulation of fluorescent

dye at the site of CRC. Furthermore, the ultimate goal would not be complete unless the entire probe possessed moieties that would promote a red-shift of the emission wavelength into the red and NIR region through a classical Knoevenagel condensation approach, along with useful Sharpless alkyne/azide cycloaddition potentials.

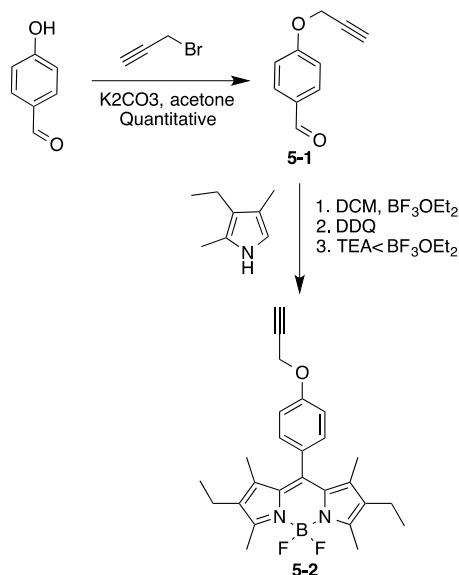
The strategies employed for development of the desired BODIPY-peptide conjugates, has been formerly investigated on different fluorophores including porphyrins and related macrocycles.<sup>17-20</sup> However, similar work has been noted with identical BODIPY dyes that were conjugated to biomolecule moieties PEG (for linkage to biomolecules) and carbohydrates (as a targeting moiety) (Scheme 3).<sup>21</sup> This work was noted by a former member of the Vicente's group Timsy Uppal.



Scheme 3. Copper catalyzed 1,3-dipolar cycloaddition of BODIPY dyes with PEG and carbohydrates moiety.<sup>21</sup>

A thorough study of BODIPY-conjugates generated via click chemistry implied that the 1,3-cycloaddition labeling of biomolecules is generally completed on the functionalized macrocycle.<sup>2</sup> Thus, a comparable practice was implemented for the work described hereon. Vicente et al. mentioned the most important stage as the development of the terminal alkyne “handle” on the BODIPY fluorophore, to generate the so-called “clickable BODIPY fluorophores”.<sup>22</sup> To

replicate Timsy's work of installing this alkyne arm while creating the BODIPYs core, a literature procedure was followed that used *p*-hydroxy benzaldehyde which then could be O-alkylated through a Williamson reaction, using propargyl bromide and potassium carbonate in acetone to generate *p*-propargyloxy-benzaldehyde **5-1** in a near quantitative manner (Scheme 4.4).<sup>23</sup> This starting material is greatly desired due to the establishment of the desired alkyne arm very early on in the BODIPY synthesis. To develop the meso-phenyl-BODIPY **5-2** bearing the desired alkyne, a cascade of reactions took place in a classical one-pot, three-step approach. This synthesis began with the *p*-propargyloxy-benzaldehyde **5-1** and two equivalents of 3-ethyl-2,4-dimethyl pyrrole, in the presence of a catalytic amount of BF<sub>3</sub>OEt<sub>2</sub> and dry dichloromethane as solvent (Scheme 4).



Scheme 4. Synthetic route to desired BODIPY **5-2**.

The final reaction mixture was allowed to stir under inert conditions while being monitored by TLC until completion. The resulting mixture was allowed to cool down to 0 °C in an ice bath, and treated with 1.2 equiv. of DDQ oxidant to form the dipyrromethene component. After stirring for 20 min., triethylamine was added in a dropwise manner while remaining at 0 °C. After 20 min. stirring, the reaction mixture was treated with BF<sub>3</sub>OEt<sub>2</sub> and the resulting reaction mixture was stirred at room temperature under nitrogen. The progress of the reaction was closely monitored by TLC until completion. To remove the majority of oxidized dipyrromethene, unwanted side

products, and residual DDQ, the reaction mixture was then filtered through a short plug of silica gel to separate the desired product and byproducts. The solvent was removed under vacuum to afford the crude mixture of BODIPY **5-2**. This residue was then dissolved in a mixture of dichloromethane and water and stirred overnight to decompose any unreacted  $\text{BF}_3\text{OEt}_2$ . The consequent reaction mixture in DCM was then extracted with .1M HCl to ensure all DDQ is removed. The organic layers are then combined and dried over sodium sulfate and the solvent removed under vacuum.

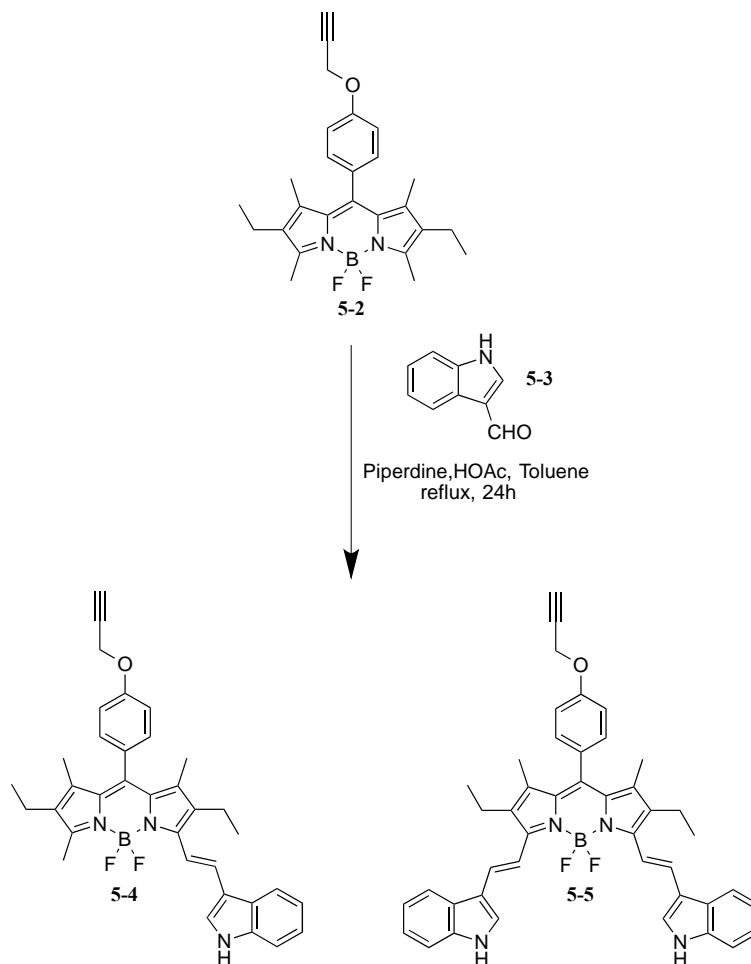
The crude result was purified on a silica gel column with a solvent mixture of dichloromethane/hexane in a 1:1 ratio as the eluting solvent. The desired product is an orange-green fluorescent band, and is the first compound to elute off the column. The product was collected and the solvent was evaporated to afford the desired BODIPY **5-2** in 40% overall yield over three steps. Unlike the high yields received in the previous work of our group, the yield was moderate. This is could be in part due to the purity of the 3-ethyl-2,4-dimethyl pyrrole used. The pyrrole was slightly discolored hinting at possible oxidized products inclusive in the mixture. Nevertheless, BODIPY **5-2** was then confirmed by H-NMR and MS (MALDI) .

BODIPY **5-2** possesses acidic methyl groups at the 3- and 5- positions on the BODIPY core, and an attempt to create a BODIPY dye with the desired alkyne while red shifting the absorption and emission of the molecule was investigated using Knoevenagel condensation. It is known that styryl-derived BODIPY compounds display red-shifted fluorescence emissions due to extension of the  $\pi$ -conjugation, and their emission wavelengths vary according to the styryl moieties.<sup>24</sup> The insertion of one or two styryl groups on BODIPY **5-2** was accomplished with electron-rich indole-3-carbaldehyde **5-3** by classical Knoevenagel condensation, using piperidine and acetic acid while refluxing in toluene. The use of a Dean-Stark apparatus was essential in previous work for removing any water formed during the reaction to push the reaction towards double condensation;<sup>25</sup> however, in this work the desired product was mono conjugation and no significant difference was noted for the production of mono condensation when using the Dean-



Stark apparatus. The key component for pushing the reaction forward for mono condensation was noted at the concentration of the reagents. The more concentrated the reaction mixture was the more product was achieved, and the less double condensation was noted. The use of indole-3-carbaldehyde **5-3** for the integration of styryl groups was based on results previously published in our group.<sup>21</sup> Additionally, the incorporation of “indole” moieties have been admired for their biological incorporation with tryptophan.<sup>26</sup> Tryptophan is a naturally occurring amino acid and an important component of many enzymes, peptides, and proteins, such as EGFR-L2 found in chapter 2.<sup>27-28</sup> It is expected that by attaching the styryl group on the BODIPYs’ core the product will not only exhibit the desired bathochromic shift, but have further increased biological efficacy for our desired receptor EGFR.

BODIPY **5-2** was added to a mixture of dry toluene, glacial acetic acid and piperidine followed by the addition of compound **5-3** in a 1:3 ratio. The advancement of the reaction was monitored by TLC analysis, a slightly blue spot corresponding to the monostyryl-BODIPY derivative **5-4** was noticeable as early as 4 hours (Scheme 5). However, a larger spot on TLC indicated the presence of starting material, therefore the reaction was left to stir overnight. Although starting material was still present, the reaction was stopped after 14 hours to minimize the amount of distyryl compound formed. The reaction mixture was then allowed to cool to room temperature and removal of the solvent was performed under vacuum. The crude material was purified by silica gel chromatography using an eluent mixture of dichloromethane/hexane in 2:1. In this purification, three distinct bands were obtained. The orange-green band corresponding to starting material BODIPY **5-2** was the first to elute, followed by the blue-red band of the desired mono- styryl BODIPY **5-4**, and finally a dark green band is eluted corresponding to the di-styryl BODIPY **5-5**.



Scheme 5. Synthetic route to BODIPYs 5-4 and 5-5.

Each band was collected and the solvent was removed under vacuum. The starting material BODIPY **5-2** was then reused to develop more of BODIPY **5-4**. The desired product **5-4** was isolated in 28% yield. Mass spectrometry MALDI-TOF and proton NMR were used to characterize BODIPYs **5-2** and **5-4**.

Two peptides previously discussed in chapter 2 with azide functionalities were ideal for cycloaddition to BODIPYs **5-2** and **5-4**. Peptide **2-9** has a linear sequence that displayed good binding affinity to EGFR; however, it may be prone to proteolytic cleavage *in vivo* due to its linear structure. While peptide **cycloL1.1** is a cyclic peptide, it also exhibited high binding affinity for EGFR, and it is less likely to undergo enzymatic cleavage due to the cyclic structure of the backbone

of the sequence. With these two azido peptides and alkynyl BODIPY dyes **5-2** and **5-4**, 1,3-cycloaddition reactions were studied.

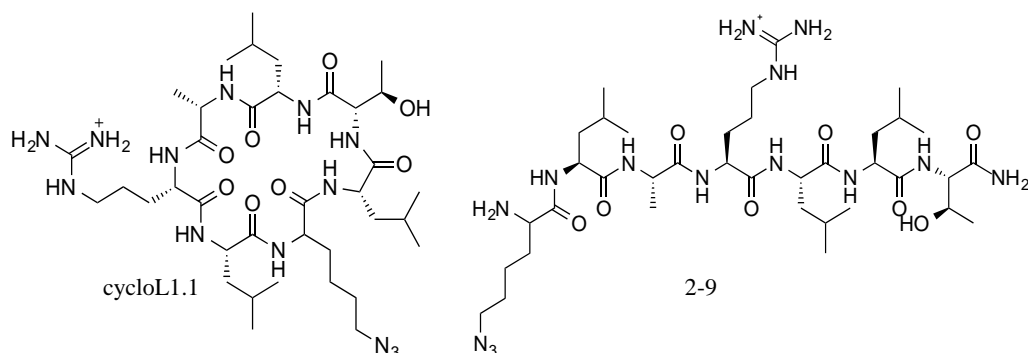
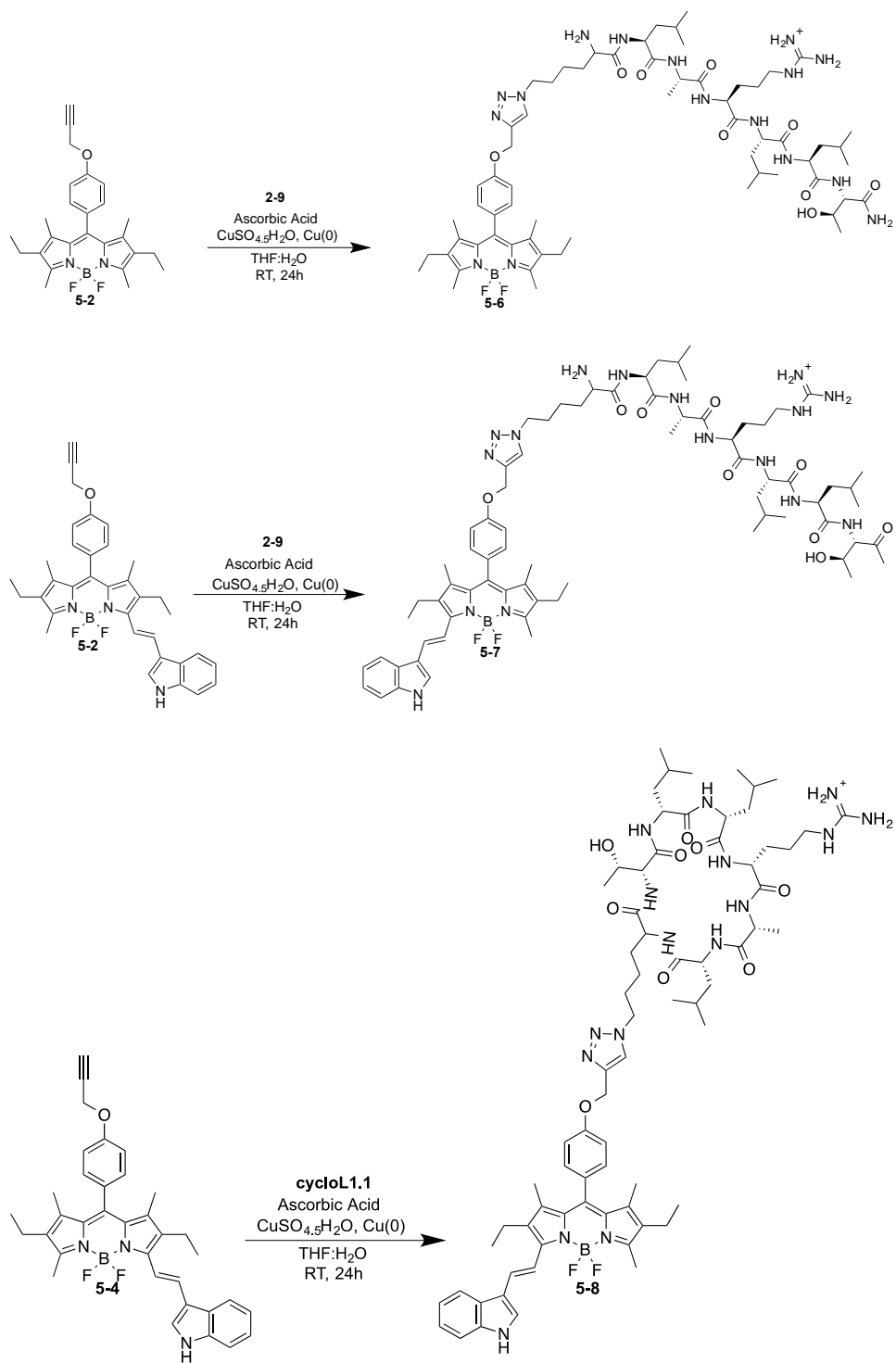


Figure 1. Azido peptides cycloL1.1 and 2-9 .

To employ “click chemistry,” the reaction was performed in the presence of  $\text{CuSO}_4 \cdot \text{H}_2\text{O}$ ,  $\text{Cu} (0)$  , and ascorbic acid in THF/water (3:1), as shown in Scheme 5.6. The meso-alkynylphenyl-BODIPY **5-2** was dissolved in THF/water, and to this solution azido-peptide **2-9** (1.5 equiv) dissolved in DMSO was added. A catalytic amount of  $\text{Cu} (0)$  (1 equiv) was added to the resulting mixture followed by the addition of  $\text{CuSO}_4 \cdot 5\text{H}_2\text{O}$  (1 equiv) and L- ascorbic acid (1 equiv.) in distilled water. A catalytic amount of the essential copper metal was added as a suitable reductant for  $\text{Cu}(\text{II})$  in an aqueous solution to produce  $\text{Cu}(\text{I})$ , which is a potent stimulus for the formation of 1,2,3-triazoles.<sup>29</sup> The reaction mixture was allowed to stir for 24 hours and monitored by MALDI-TOF for the desired product. Once the reaction was complete, the mixture was then quenched with water. To purify the resulting conjugate a molecular weight cut off (MWCO) of 1,000 Da was used to retain the conjugate, as the molecular weight for this conjugate was 1273.91, and remove any starting materials remaining in the mixture.



Scheme 6. Generic synthetic route to BODIPY conjugates 5-6 ,5-7, and 5-8.

After removal of solvents the mixtures were purified using RP-HPLC, eluting with a gradient of 10:90 to 0:100 .1% TFA in H<sub>2</sub>O/ .1% TFA in CH<sub>3</sub>CN to afford 1,2,3-triazole cycloadduct **5-6** in 82% yield. The reaction conditions used with BODIPY **5-2** and azido-peptide **2-9** were repeated to determine the efficacy of peptide **2-9** in the click reaction with BODIPY **5-4**. The meso-alkynylphenyl-BODIPY **5-4** was dissolved in THF/water, to this solution azido-peptide **2-9** (1.5 equiv) dissolved in DMSO was added. A catalytic amount of Cu (0) (1.0 eq) was added to the resulting mixture, followed by the addition of CuSO<sub>4</sub> · 5H<sub>2</sub>O (1 equiv) and L- ascorbic acid (1 equiv) in distilled water (Scheme 4-7). This reaction yielded the desired cycloadduct **5-7** in 70% yield. Thus, the most bulky azido peptide **cycloL1.1** was then subjected to cycloaddition with the reddest shifted BODIPY dye **5-4** under the same conditions with peptide **cycloL1.1** to produce conjugate **5-89** in a percent yield of 80% as shown in Scheme 5.6.

All cycloadducts were formed in good yields as shown in Table 1. Compound **5-6** was synthesized in the highest percent yield of 82%. Cycloadduct **5-8** was isolated in a percent yield of 80% which is an excellent yield, considering the bulkiness of the cyclic backbone structure of the peptide **cycloL1.1**, and the larger size of BODIPY **5-4**, however this is one of the attractive features of click chemistry.

Table 1: Results of Peptide BODIPY Conjugates via Click Chemistry

| Compound   | Molecular Weight (g/mol) | Peptide   | Percent Yield |
|------------|--------------------------|-----------|---------------|
| <b>4-6</b> | 1273.79                  | 2-9       | 82%           |
| <b>4-7</b> | 1400.89                  | 2-9       | 70%           |
| <b>4-8</b> | 1383.81                  | cycloL1.1 | 80%           |

### 5.2.1 *In Vitro* Studies

Preliminary *in vitro* cellular studies, including photo cytotoxicity and cellular uptake were investigated against human carcinoma HEP2 cell lines in order to determine the biological efficacy of the peptide-functionalized BODIPY-conjugates.

**5.2.1.1 Time Dependent Cellular Uptake.** The cellular uptake of all compounds were obtained by Mrs. Zehua Zhou in a time-dependent manner. At a 10  $\mu$ M concentration against HEP2 cells cellular uptake was determined over a 24 hour period. The results are shown in Figure 2. To compare the uptake of the conjugates, BODIPYs **5-2** and **5-4** were also investigated. At the 10  $\mu$ M concentration, both BODIPYs were found to be nontoxic under a CTB assay, and displayed a similar cellular uptake. The kinetics showed a rapid accumulation of the dyes at short time points of less than 4 hours, after the addition of BODIPY to the cells. The addition of one indole moiety to the core of the BODIPY **5-4** dye gave a faster uptake into cells. However, when compared to the conjugates, there is a significant difference in the cellular uptake observed. Conjugates with linear peptide sequences cycloadducts **5-6** and **5-7** showed a significant difference in the behavior of uptake into the cells. Cycloadduct **5-7** was not only taken up in to the cells faster than cycloadduct **5-6**, but more of the compound was taken into the cells. Essentially, cycloadduct **5-6** was taken up into the HEP2 cell line with the least amount when compared to all compounds. This may be due to the lack of styryl components that may aid in increasing the amount of conjugate taken up into HEP2 cells. Cycloadduct **5-8** surprisingly accrued in cells slower than all of the other conjugates; however, between 4 and 8 hours an increase in the amount of compound taken up into cells was observed. This instance may be noted by the increased stability of the cyclic structure allowing for a sustained conjugate uptake within cells, but entering at a slower rate when compared to the linear sequences.

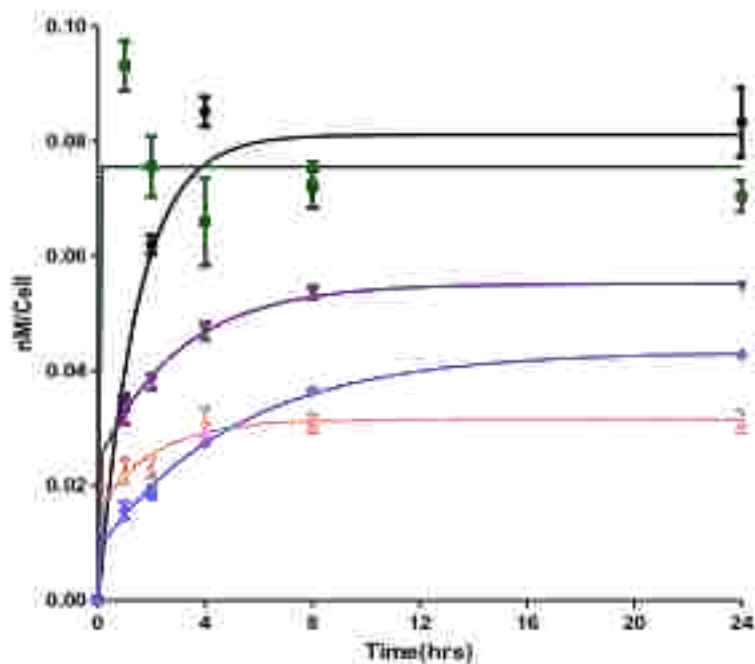


Figure 2. Time dependent cellular uptake of BODIPYs 5-2 (Black), 5-4 (Green), 5-6 (Pink), 5-7 (Purple), 5-8 (Blue).

**5.2.1.2 Phototoxicity.** The phototoxic effect of BODIPYs and conjugates were tested under a low dose of light irradiated at  $1 \text{ J/cm}^2$ . The dose-dependent survival curves of each compound over a course of 24 hours are shown in Figure 3. All compounds proved nontoxic in the presence of light with  $\text{IC}_{50}$  values greater than  $100 \mu\text{M}$ . It is observed that all BODIPY dyes are indeed nontoxic in the presence of light. The cycloadduct **5-6** follows strongly in suit with the BODIPY dyes. However, conjugates **5-7** and **5-8** show a slight increase in phototoxicity when compared to the other conjugate, but overall, the conjugates are non-toxic to the cells. This slight increase in phototoxicity is probably due to the increase in cellular uptake that was noted for the compounds against the HEP2 cell line still less than BODIPYs **5-2** and **5-4**. The increase in cellular uptake paired with the charge observed in the sequence of both peptides might explain the results observed.

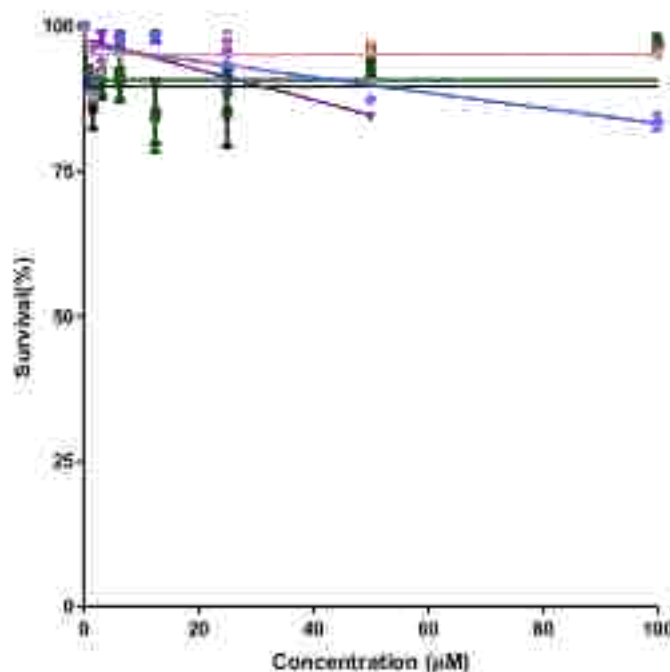


Figure 3. Phototoxicity of BODIPYs 5-2 (Black), 5-4 (Green), 5-6 (Pink), 5-7 (Purple), 5-8 (Blue).

### 5.3 Conclusion and Future Work

Two BODIPY dyes **5-2** and **5-4** were synthesized, one bearing one indolyl styryl arm inclusive of a meso-alkynyl functionalization point for click chemistry. These BODIPY dyes were characterized by  $^1\text{H-NMR}$  and mass spectrometry (MALDI-TOF). Cu(I)-catalyzed azide-alkyne Huisgen cycloaddition (also referred to as “click chemistry”) was used to successfully synthesized conjugates **5-6**, **5-7** and **5-8** in a convenient, quick and proficient method to offer percent yields of 70-80 %. Of the conjugates, compounds **5-7** and **5-8** bearing an additional mono-styryl group, and conjugate **5-8** was the only conjugate to bear a cyclic peptide **cycloL1.1**. Preliminary in vitro studies using human carcinoma HEP2 cells indicated all the BODIPYconjugates were cell permeable, non-cytotoxic with high cellular uptake. The monoindolyl styryl-BODIPY conjugate (**5-7**) conjugated to the linear peptide **2-9** was the most efficiently taken up by the HEP2 cells, accumulating more than the other conjugates, but less than what was seen for the BODIPY dyes alone. This supple



versatile synthetic strategy is anticipated to provide a resourceful platform for vast arrays of functionalized BODIPYs possessing potential utility in *in vivo* imaging for conjugation of various biomolecules.

## 5.4 Experimental

### 5.4.1: General Information

All reagents are commercially available were purchased from Sigma-Aldrich Co. Canada and VWR International. All solvents and reagents used in the synthesis of conjugates were performed with reagents purchased from Sigma Aldrich peptide synthesis grade. Required amino acids were purchased from either Anaspec, AAPPTec or Applied Biosystems. All reactions were performed under argon atmosphere in oven-dried glassware unless otherwise noted. Analytical thin-layer-chromatography (TLC) was performed on polyester backed TLC plates 254 (pre-coated, 200  $\mu\text{m}$ , Sorbent Technologies). Column chromatography was performed on silica gel (Sorbent Technologies, 60  $\text{\AA}$ , 40-63  $\mu\text{m}$ ).  $^1\text{H}$  NMR and HSQC spectra were recorded using a Bruker AVIII-500 spectrometer (operating at 500MHz for  $^1\text{H}$  NMR and HSQC) in DMSO- $d_6$ . All chemical shifts are given in parts per millions (ppm) relative to tetramethylsilane (TMS, 0 ppm); multiplicities are indicated as br (broad), s (singlet), d (doublet), t (triplet), q (quartet) and m (multiplet). All spectra were recorded at 308 K and coupling constants (J values) are given in Hz. High resolution mass spectra were obtained at the LSU Department of Chemistry Mass Spectrometry Facility using Bruker Omnix MALDI Time-of-Flight Mass Spectrometer. The absorption measurements were carried out on a Varian 212 Cary 50 UV/Vis spectrophotometer and the steady-state fluorescence spectroscopic studies were performed on a PTI Quantum Master4/2006SE spectrofluorometer. All spectras were recorded at 298 K using non-degassed samples, spectroscopic grade solvents and a 10 mm quartz cuvette.

#### 5.4.2: Synthesis of 4-(prop-2-ynoxy)-benzaldehyde (5-1)

4-hydroxybenzaldehyde, 1, (2.00 g, 16.38 mmol) and propargyl bromide (7.79 g, 65.51 mmol,) were added to a solution of potassium carbonate (13.58 g, 98.3 mmol) in 100 mL acetone. The reaction mixture was heated to reflux overnight and then cooled to room temperature. The heterogeneous solution was filtered off to remove solid potassium carbonate and the solvent was removed under vacuum. The crude product was dissolved in dichloromethane (20 mL) and washed successively with water twice (20 mL), 5% NaHCO<sub>3</sub> (20 mL) and brine (20 mL) once each. The organic extracts were combined, dried over Na<sub>2</sub>SO<sub>4</sub> and concentrated under vacuum. The resulting crude product was purified by column chromatography using pure dichloromethane as the eluent to afford 2.28 g of the compound 2 as pale yellow solid (quantitative). <sup>1</sup>H NMR (500 MHz, Chloroform-*d*) δ 9.92 (d, *J* = 1.4 Hz, 1H), 7.87 (d, *J* = 8.8 Hz, 2H), 7.11 (d, *J* = 8.8 Hz, 2H), 4.80 (d, *J* = 2.4 Hz, 2H), 2.59 (t, *J* = 2.4 Hz, 1H).MALDI-TOF *m/z* 161.059; calcd. for C<sub>10</sub>H<sub>8</sub>O<sub>2</sub>: 160.52.

#### 5.4.3: Synthesis of BODIPY 5-2

**Compound 5-1** (0.6490 g, 4.0584 mmol, 1 equiv.) and 3-ethyl-2,4-dimethyl pyrrole (3.51 g, 28.47 mmole) were dissolved in dry dichloromethane (281 mL) under the inert gas atmosphere. Two drops of BF<sub>3</sub>OEt<sub>2</sub> were added and the reaction mixture was stirred overnight at room temperature. When the aldehyde was consumed (monitored by TLC), a solution of DDQ (3.88 g, 17.08 mmole) in dry dichloromethane (35 mL) was added via syringe at 0°C. After stirring for 20 min at room temperature, triethylamine (13.89 mL, 7 equiv.) was added dropwise and the reaction mixture was stirred for another 30 min at room temperature. Further, BF<sub>3</sub>OEt<sub>2</sub> (19.32 mL, 11 equiv.) was added dropwise at 0°C and the mixture was stirred for 10h at room temperature. Once TLC indicated reaction completion, the reaction mixture was passed through a short plug of silica gel to get rid of the oxidized dipyrromethene derivatives and starting materials. The solvent was removed under reduced pressure and the residue was taken up in dichloromethane (100 mL) and kept for overnight stirring at room temperature to decompose any unreacted BF<sub>3</sub>OEt<sub>2</sub>. The

subsequent reaction mixture was extracted with 0.1M HCl (2 x 100mL) to remove excess DDQ, brine (1 x 100 mL). The organic extracts were collected, dried over Na<sub>2</sub>SO<sub>4</sub> and the solvent was evaporated. The crude product was purified by column chromatography using Hexane/dichloromethane (1/1, v/v) as eluent. The orange-green fluorescent fraction containing the desired BODIPY 4 was collected and recrystallized from dichloromethane/hexane mixtures to yield the title compound as lustrous orange-red solid. Yield: 2.41 g, 39%. <sup>1</sup>H NMR (400 MHz, Chloroform-*d*) δ 7.22 (d, *J* = 8.7 Hz, 2H), 7.11 (d, *J* = 8.7 Hz, 2H), 4.79 (d, *J* = 2.4 Hz, 2H), 2.58 (t, *J* = 2.4 Hz, 1H), 2.55 (s, 5H), 2.33 (q, *J* = 7.6 Hz, 4H), 1.35 (s, 5H), 1.28 (s, 2H), 1.01 (t, *J* = 7.6 Hz, 5H), 0.91 (t, *J* = 13.6 Hz, 1H). MALDI-TOF *m/z* 434.10; calcd. for C<sub>26</sub>H<sub>29</sub>BF<sub>2</sub>N<sub>2</sub>O: 434.23.

#### 5.4.4: Synthesis of BODPY 5-4

BODIPY 5-2 (0.0122 g, 0.02809 mmol) and indole-3-carbaldehyde (0.01223 g, .08427 mmol) were added to a 150 mL triple necked round bottom flask containing a mixture of dry toluene (20 ml), piperidine (0.032 ml) and glacial acetic acid (0.019 ml). The mixture was refluxed overnight. After completion of the reaction (monitored via thin-layer chromatography), the mixture was cooled to room temperature and the solvent was removed under vacuum. The residue was purified by silica gel column chromatography using dichloromethane/hexane (2/1, v/v) as eluent. (BODIPY 5-4): The first fraction with red fluorescence was dried in vacuo, affording (BODIPY 5-4): The first fraction with red fluorescence was dried in vacuo, affording BODIPY 5-4 as a red-blue solid (4.4 mg, yield 28%). <sup>1</sup>H NMR (400 MHz, (CD<sub>3</sub>)<sub>2</sub>CO): δ; 10.72 (s, NH), 8.16 (m, 1H), 7.91 (d, *J* = 8.1 Hz, 1H), 7.74 (d, 1H), 7.65 (d, *J* = 8.1 Hz, 1H), 7.49–7.51 (m, 2H), 7.20-7.32 (m, 6H), 4.89 (d, *J* = 2.0 Hz, 2H), 3.13 (t, *J* = 2.0 Hz, 1H), 2.69 (q, *J* = 7.6 Hz, 2H), 2.56 (s, 3H), 2.36 (q, *J* = 7.6 Hz, 2H), 1.41 (s, 3H), 1.38 (s, 3H), 1.19 (t, *J* = 7.6 Hz, 3H), 0.99 (t, *J* = 7.6 Hz, 3H); <sup>13</sup>C NMR (100MHz, (CD<sub>3</sub>)<sub>2</sub>CO): δ; 158.3, 152.1, 151.4, 129.8, 128.7, 128.2, 125.3, 122.5, 120.9, 120.7, 120.2, 115.8, 115.7, 115.6, 112.0, 78.5, 76.4 55.7, 18.0, 16.6, 14.1, 13.5, 11.8, 11.1, 10.9; MALDI-TOF *m/z* 561.28; calcd. for C<sub>35</sub>H<sub>34</sub>BF<sub>2</sub>N<sub>3</sub>O: 561.35.

#### 5.4.5: General Procedure for 1,3 cycloaddition

Meso-alkynylphenyl-BODIPY 5-2 and azido-peptide (1.5 equiv) were dissolved in a mixture of THF:H<sub>2</sub>O (1.8 mL, 3:1), followed by addition of Cu (0) (1.0 equiv). Next, a solution of CuSO<sub>4</sub> · 5H<sub>2</sub>O (1 equiv) and L-ascorbic acid (1 equiv.) in H<sub>2</sub>O was added to the reaction mixture. The solution was allowed to stir at room temperature for 24 hours. Once the reaction was complete, the mixture was quenched with water and lyophilized. The fluffy product was then purified by RP-HPLC under varying gradients of water (with .1% TFA) and Acetonitrile (with .1% TFA).

**Conjugate 5-6 (BOIDPY-K(N<sub>3</sub>)LARLLT-CONH<sub>2</sub>):** This conjugate was obtained as a redish orange solid (4.8 mg, 82%). MALDI-TOF m/z 1274.59; calc. for C<sub>63</sub>H<sub>100</sub>BF<sub>2</sub>N<sub>16</sub>O<sub>9</sub><sup>+</sup>: 1273.79.

**Conjugate 5-7 (BOIDPY-K(N<sub>3</sub>)LARLLT-CONH<sub>2</sub>):** This conjugate was obtained as a dark blue solid (3.49 mg, 70%). MALDI-TOF m/z 1274.59; calc. for C<sub>73</sub>H<sub>106</sub>BF<sub>2</sub>N<sub>16</sub>O<sub>9</sub><sup>+</sup>: 1399.93.

**Conjugate 5-8 (BOIDPY-K(N<sub>3</sub>)LARLLT-CONH<sub>2</sub>):** This conjugate was obtained as a deep blue solid (6.1 mg, 80%). MALDI-TOF m/z 1367.497; calc. for C<sub>72</sub>H<sub>102</sub>BF<sub>2</sub>N<sub>16</sub>O<sub>9</sub><sup>+</sup>: 1383.80.

#### 5.5 References

1. Hein, C. D.; Liu, X.-M.; Wang, D., Click chemistry, a powerful tool for pharmaceutical sciences. *Pharmaceutical research* **2008**, *25* (10), 2216-2230.
2. Dumoulin, F.; Ahsen, V., Click chemistry: the emerging role of the azide-alkyne Huisgen dipolar addition in the preparation of substituted tetrapyrrolic derivatives. *Journal of Porphyrins and Phthalocyanines* **2011**, *15* (07n08), 481-504.
3. Fehlhhammer, W. P.; Beck, W., Azide Chemistry—An Inorganic Perspective, Part II [‡][3+ 2] - Cycloaddition Reactions of Metal Azides and Related Systems. *Zeitschrift für anorganische und allgemeine Chemie* **2015**, *641* (10), 1599-1678.
4. Meldal, M.; Tornøe, C. W., Cu-catalyzed azide–alkyne cycloaddition. *Chemical reviews* **2008**, *108* (8), 2952-3015.
5. Best, M. D., Click chemistry and bioorthogonal reactions: unprecedented selectivity in the labeling of biological molecules. *Biochemistry* **2009**, *48* (28), 6571-6584.

6. Hoyle, C. E.; Bowman, C. N., Thiol–ene click chemistry. *Angewandte Chemie International Edition* **2010**, *49* (9), 1540-1573.
7. Tron, G. C.; Pirali, T.; Billington, R. A.; Canonico, P. L.; Sorba, G.; Genazzani, A. A., Click chemistry reactions in medicinal chemistry: Applications of the 1, 3 - dipolar cycloaddition between azides and alkynes. *Medicinal research reviews* **2008**, *28* (2), 278-308.
8. Kele, P.; Li, X.; Link, M.; Nagy, K.; Herner, A.; Lőrincz, K.; Béni, S.; Wolfbeis, O. S., Clickable fluorophores for biological labeling—with or without copper. *Organic & biomolecular chemistry* **2009**, *7* (17), 3486-3490.
9. Yilmaz, M. D.; Bozdemir, O. A.; Akkaya, E. U., Light Harvesting and Efficient Energy Transfer in a Boron-dipyrrin (BODIPY) Functionalized Peryleneimide Derivative. *Organic Letters* **2006**, *8* (13), 2871-2873.
10. Verdoes, M.; Hillaert, U.; Florea, B. I.; Sae-Heng, M.; Risseuw, M. D. P.; Filippov, D. V.; van der Marel, G. A.; Overkleeft, H. S., Acetylene functionalized BODIPY dyes and their application in the synthesis of activity based proteasome probes. *Bioorganic & Medicinal Chemistry Letters* **2007**, *17* (22), 6169-6171.
11. Hansen, A. M.; Sewell, A. L.; Pedersen, R. H.; Long, D.-L.; Gadegaard, N.; Marquez, R., Tunable BODIPY derivatives amenable to ‘click’ and peptide chemistry. *Tetrahedron* **2013**, *69* (39), 8527-8533.
12. Verwilt, P.; David, C. C.; Leen, V.; Hofkens, J.; de Witte, P. A. M.; De Borggraeve, W. M., Synthesis and in vitro evaluation of a PDT active BODIPY–NLS conjugate. *Bioorg. Med. Chem. Lett.* **2013**, *23* (11), 3204-3207.
13. Kamkaew, A.; Burgess, K., Double-Targeting Using a TrkC Ligand Conjugated to Dipyrrrometheneboron Difluoride (BODIPY) Based Photodynamic Therapy (PDT) Agent. *J. Med. Chem.* **2013**, *56* (19), 7608-7614.
14. Maindron, N.; Ipu, M.; Bernhard, C.; Lhenry, D.; Moreau, M.; Carme, S.; Oudot, A.; Collin, B.; Vrigneaud, J.-M.; Provent, P.; Brunotte, F.; Denat, F.; Goze, C., Near-Infrared-Emitting BODIPY-trisDOTA<sup>111</sup>In as a Monomolecular Multifunctional Imaging Probe: From Synthesis to In Vivo Investigations. *Chem. Eur. J.* **2016**, *22* (36), 12670-12674.

15. Binder, W. H.; Sachsenhofer, R., 'Click' chemistry in polymer and materials science. *Macromolecular Rapid Communications* **2007**, *28* (1), 15-54.
16. Kolb, H. C.; Sharpless, K. B., The growing impact of click chemistry on drug discovery. *Drug discovery today* **2003**, *8* (24), 1128-1137.
17. Palacin, T.; Khanh, H. L.; Joussetme, B.; Jegou, P.; Filoramo, A.; Ehli, C.; Guldi, D. M.; Campidelli, S., Efficient functionalization of carbon nanotubes with porphyrin dendrons via click chemistry. *Journal of the American Chemical Society* **2009**, *131* (42), 15394-15402.
18. Hao, E.; Jensen, T. J.; Vicente, M. G. H., Synthesis of porphyrin-carbohydrate conjugates using "click" chemistry and their preliminary evaluation in human HEP2 cells. *Journal of Porphyrins and Phthalocyanines* **2009**, *13* (01), 51-59.
19. Juríček, M.; Kouwer, P. H.; Reháček, J.; Sly, J.; Rowan, A. E., A novel modular approach to triazole-functionalized phthalocyanines using click chemistry. *The Journal of organic chemistry* **2008**, *74* (1), 21-25.
20. Verwilt, P.; David, C. C.; Leen, V.; Hofkens, J.; de Witte, P. A.; De Borggraeve, W. M., Synthesis and in vitro evaluation of a PDT active BODIPY-NLS conjugate. *Bioorganic & medicinal chemistry letters* **2013**, *23* (11), 3204-3207.
21. Uppal, T.; Bhupathiraju, N. D. K.; Vicente, M. G. H., Synthesis and cellular properties of Near-IR BODIPY-PEG and carbohydrate conjugates. *Tetrahedron* **2013**, *69* (23), 4687-4693.
22. Uppal, T. K. Synthesis and Characterization of Red and Near-Infrared BODIPY-based fluorophores for various Biological Applications. University of Delhi, India, 2012.
23. Giguère, J.-B.; Thibeault, D.; Cronier, F.; Marois, J.-S.; Auger, M.; Morin, J.-F., Synthesis of [2]- and [3] rotaxanes through Sonogashira coupling. *Tetrahedron Letters* **2009**, *50* (39), 5497-5500.
24. Lee, J.-S.; Kang, N.-y.; Kim, Y. K.; Samanta, A.; Feng, S.; Kim, H. K.; Vendrell, M.; Park, J. H.; Chang, Y.-T., Synthesis of a BODIPY library and its application to the development of live cell glucagon imaging probe. *Journal of the American Chemical Society* **2009**, *131* (29), 10077-10082.

25. Deniz, E.; Isbasar, G. C.; Bozdemir, O. A.; Yildirim, L. T.; Siemiarczuk, A.; Akkaya, E. U., Bidirectional switching of near IR emitting boradiazaindacene fluorophores. *Organic letters* **2008**, *10* (16), 3401-3403.
26. Sinha, D.; Tiwari, A. K.; Singh, S.; Shukla, G.; Mishra, P.; Chandra, H.; Mishra, A. K., Synthesis, characterization and biological activity of Schiff base analogues of indole-3-carboxaldehyde. *European journal of medicinal chemistry* **2008**, *43* (1), 160-165.
27. Ahmad, A.; A Sakr, W.; Wahidur Rahman, K., Anticancer properties of indole compounds: mechanism of apoptosis induction and role in chemotherapy. *Current drug targets* **2010**, *11* (6), 652-666.
28. Kaushik, N. K.; Kaushik, N.; Attri, P.; Kumar, N.; Kim, C. H.; Verma, A. K.; Choi, E. H., Biomedical importance of indoles. *Molecules* **2013**, *18* (6), 6620-6662.
29. Wang, Q.; Chan, T. R.; Hilgraf, R.; Fokin, V. V.; Sharpless, K. B.; Finn, M., Bioconjugation by copper (I)-catalyzed azide-alkyne [3+ 2] cycloaddition. *Journal of the American Chemical Society* **2003**, *125* (11), 3192-3193.

## APPENDIX A: Characterization of Chapter 2 Compounds

### HPLC of Compounds in Chapter 2

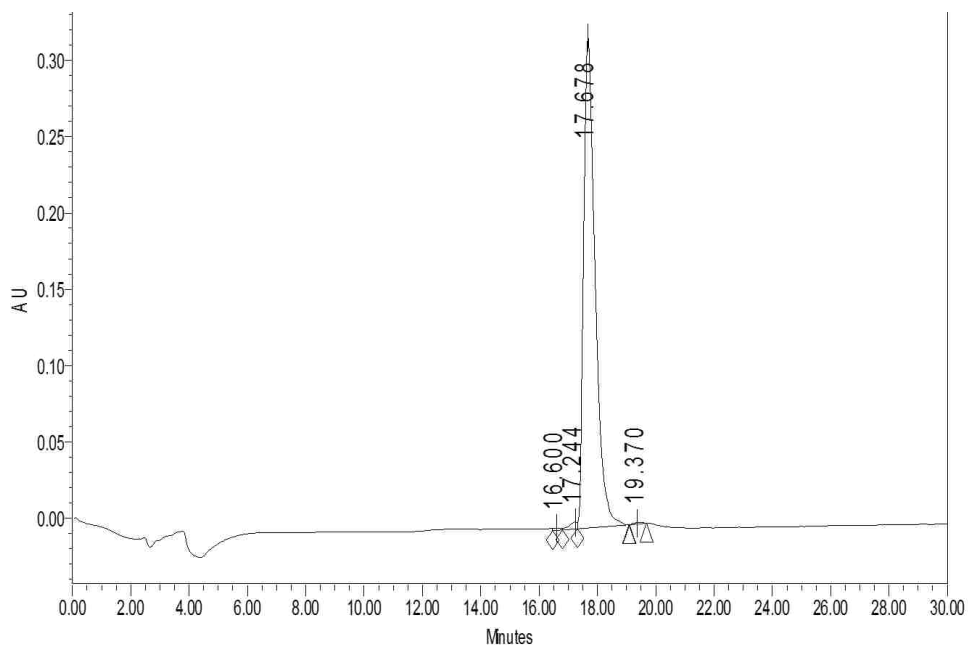


**Figure A.1:** The gradient used for chromatogram of 2-1 using RP-HPLC with a C18 column is listed below.

| <i>Table 1 HPLC Gradient for peptide 2-1</i> |                       |                   |                            |                 |
|--|-----------------------|-------------------|----------------------------|-----------------|
| <i>#</i>                                     | <i>Time (minutes)</i> | <i>Flow</i>       | <i>%A (H<sub>2</sub>O)</i> | <i>%B (ACN)</i> |
| <i>0</i>                                     | <i>0</i>              | <i>4.0 ml/min</i> | <i>90</i>                  | <i>10</i>       |
| <i>1</i>                                     | <i>5</i>              | <i>4.0 ml/min</i> | <i>90</i>                  | <i>10</i>       |
| <i>2</i>                                     | <i>8</i>              | <i>4.0 ml/min</i> | <i>30</i>                  | <i>70</i>       |
| <i>3</i>                                     | <i>18</i>             | <i>4.0 ml/min</i> | <i>10</i>                  | <i>90</i>       |
| <i>4</i>                                     | <i>25</i>             | <i>4.0 ml/min</i> | <i>90</i>                  | <i>10</i>       |
| <i>5</i>                                     | <i>30</i>             | <i>4.0 ml/min</i> | <i>90</i>                  | <i>10</i>       |



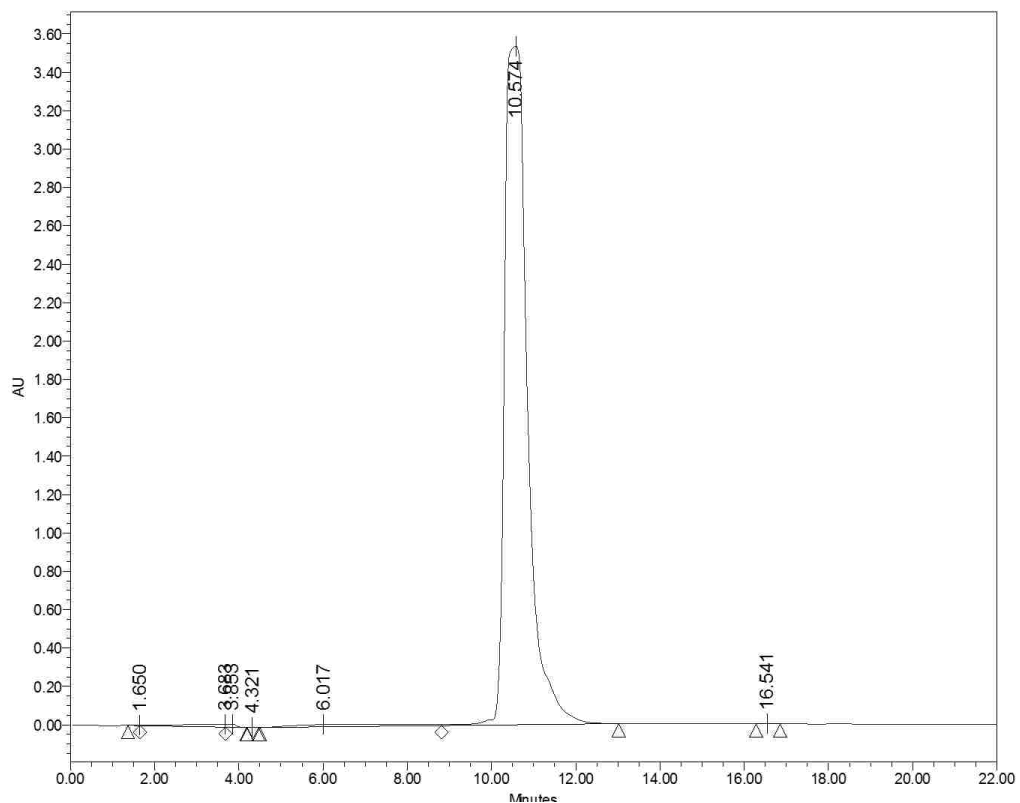


**Figure A.2:** The gradient used for chromatogram of 2-3 using RP-HPLC with a C18 column is listed below.

| <b>#</b> | <b>Time (minutes)</b> | <b>Flow</b> | <b>%A (H<sub>2</sub>O)</b> | <b>%B (ACN)</b> |
|----------|-----------------------|-------------|----------------------------|-----------------|
| 0        | 0                     | 4.0 ml/min  | 90                         | 10              |
| 1        | 5                     | 4.0 ml/min  | 90                         | 10              |
| 2        | 8                     | 4.0 ml/min  | 30                         | 70              |
| 3        | 16                    | 4.0 ml/min  | 10                         | 90              |
| 4        | 18                    | 4.0 ml/min  | 90                         | 10              |
| 5        | 22                    | 4.0 ml/min  | 90                         | 10              |

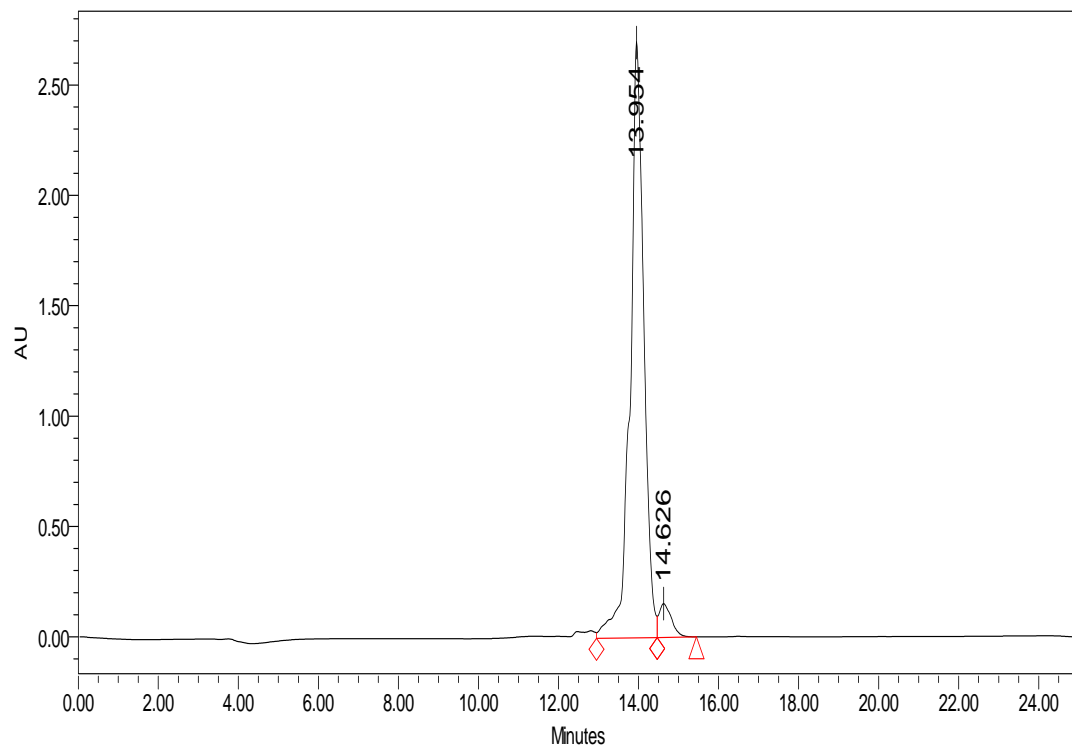


**Figure A.3:** The gradient used for chromatogram of 2-4 using RP-HPLC with a C18 column is listed below.

| <i>Table 1 HPLC Gradient for peptide 2-4</i> |                       |                   |                            |                 |
|--|-----------------------|-------------------|----------------------------|-----------------|
| <i>#</i>                                     | <i>Time (minutes)</i> | <i>Flow</i>       | <i>%A (H<sub>2</sub>O)</i> | <i>%B (ACN)</i> |
| <i>0</i>                                     | <i>0</i>              | <i>4.0 ml/min</i> | <i>90</i>                  | <i>10</i>       |
| <i>1</i>                                     | <i>5</i>              | <i>4.0 ml/min</i> | <i>90</i>                  | <i>10</i>       |
| <i>2</i>                                     | <i>8</i>              | <i>4.0 ml/min</i> | <i>30</i>                  | <i>70</i>       |
| <i>3</i>                                     | <i>18</i>             | <i>4.0 ml/min</i> | <i>10</i>                  | <i>90</i>       |
| <i>4</i>                                     | <i>20</i>             | <i>4.0 ml/min</i> | <i>90</i>                  | <i>10</i>       |
| <i>5</i>                                     | <i>25</i>             | <i>4.0 ml/min</i> | <i>90</i>                  | <i>10</i>       |

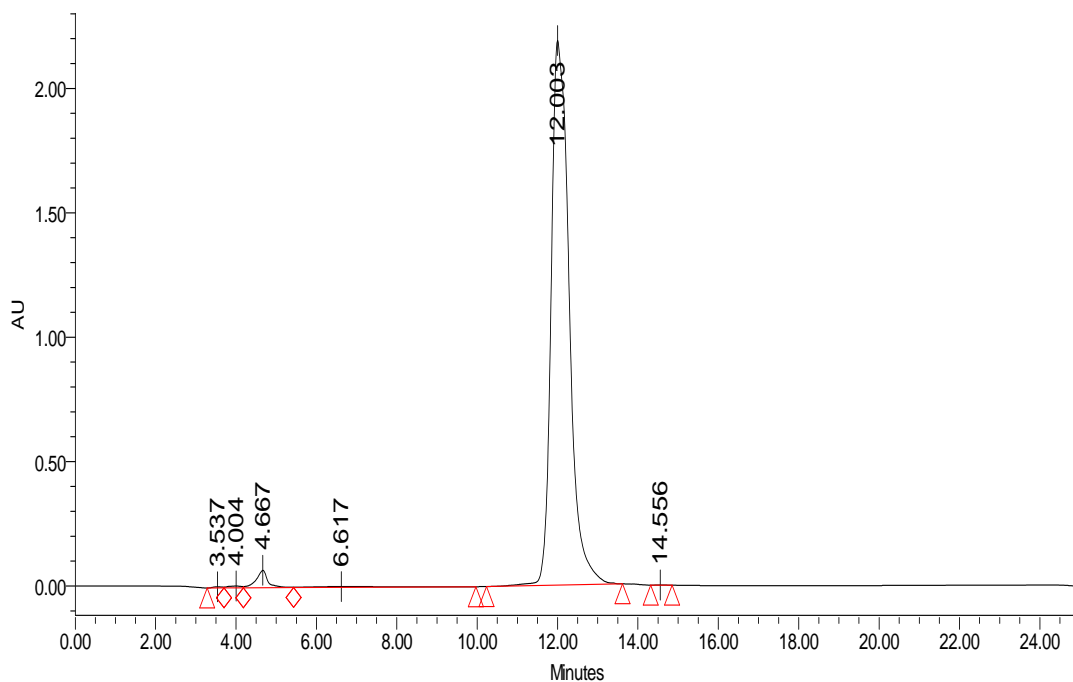


**Figure A.4:** The gradient used for chromatogram of 2-5 using RP-HPLC with a C18 column is listed below.

| <i>Table 1 HPLC Gradient for peptide 2-5</i> |                       |                   |                            |                 |
|--|-----------------------|-------------------|----------------------------|-----------------|
| <i>#</i>                                     | <i>Time (minutes)</i> | <i>Flow</i>       | <i>%A (H<sub>2</sub>O)</i> | <i>%B (ACN)</i> |
| <i>0</i>                                     | <i>0</i>              | <i>4.0 ml/min</i> | <i>90</i>                  | <i>10</i>       |
| <i>1</i>                                     | <i>5</i>              | <i>4.0 ml/min</i> | <i>90</i>                  | <i>10</i>       |
| <i>2</i>                                     | <i>8</i>              | <i>4.0 ml/min</i> | <i>30</i>                  | <i>70</i>       |
| <i>3</i>                                     | <i>18</i>             | <i>4.0 ml/min</i> | <i>10</i>                  | <i>90</i>       |
| <i>4</i>                                     | <i>20</i>             | <i>4.0 ml/min</i> | <i>90</i>                  | <i>10</i>       |
| <i>5</i>                                     | <i>25</i>             | <i>4.0 ml/min</i> | <i>90</i>                  | <i>10</i>       |

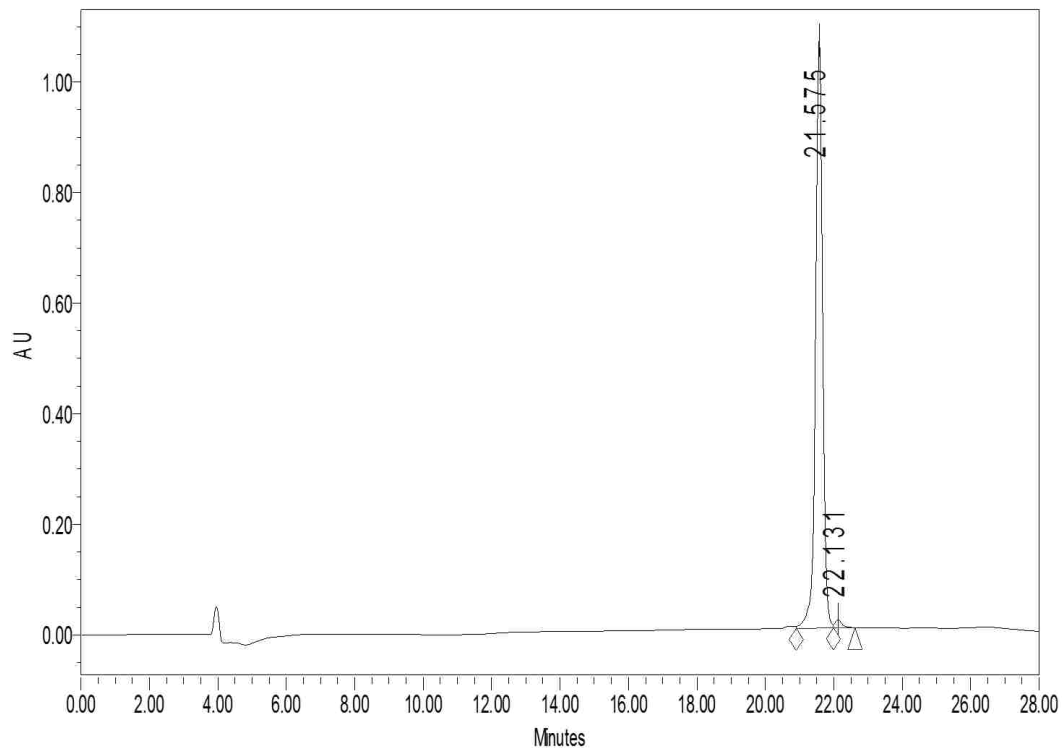


**Figure A.5:** The gradient used for chromatogram of 2-6 using RP-HPLC with a C18 column is listed below.

| <i>Table 1 HPLC Gradient for peptide 2-6</i> |                       |                   |                            |                 |
|--|-----------------------|-------------------|----------------------------|-----------------|
| <i>#</i>                                     | <i>Time (minutes)</i> | <i>Flow</i>       | <i>%A (H<sub>2</sub>O)</i> | <i>%B (ACN)</i> |
| <i>0</i>                                     | <i>0</i>              | <i>4.0 ml/min</i> | <i>90</i>                  | <i>10</i>       |
| <i>1</i>                                     | <i>5</i>              | <i>4.0 ml/min</i> | <i>90</i>                  | <i>10</i>       |
| <i>2</i>                                     | <i>8</i>              | <i>4.0 ml/min</i> | <i>30</i>                  | <i>70</i>       |
| <i>3</i>                                     | <i>18</i>             | <i>4.0 ml/min</i> | <i>10</i>                  | <i>90</i>       |
| <i>4</i>                                     | <i>20</i>             | <i>4.0 ml/min</i> | <i>90</i>                  | <i>10</i>       |
| <i>5</i>                                     | <i>25</i>             | <i>4.0 ml/min</i> | <i>90</i>                  | <i>10</i>       |

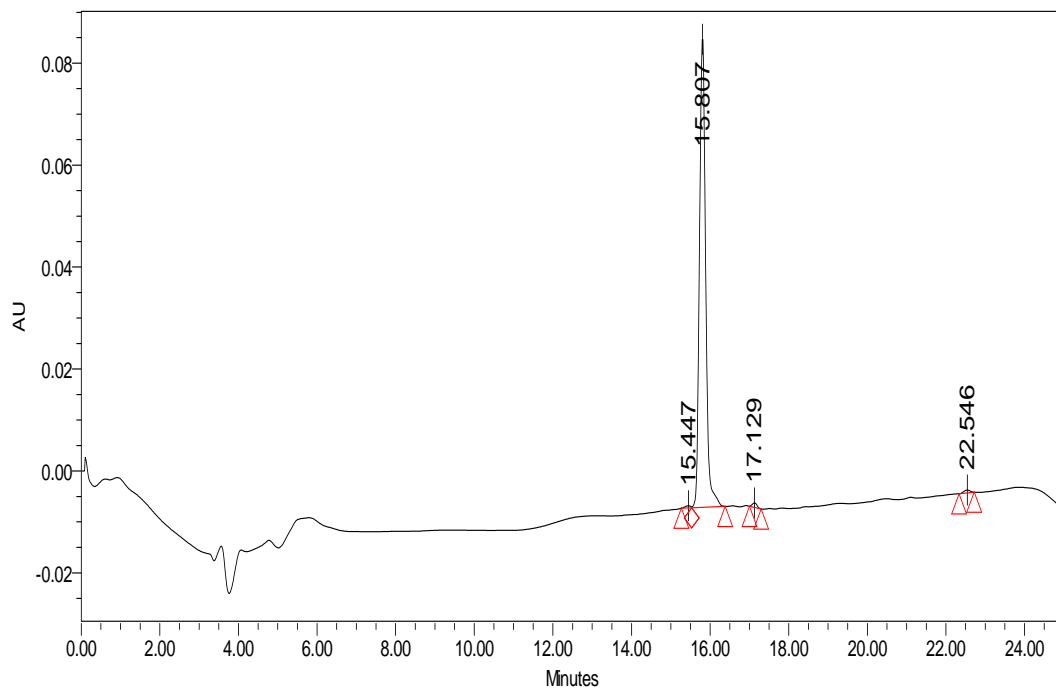


**Figure A.6:** The gradient used for chromatogram of 2-7 using RP-HPLC with a C18 column is listed below.

| <i>Table 1 HPLC Gradient for peptide 2-7</i> |                       |                   |                            |                 |
|--|-----------------------|-------------------|----------------------------|-----------------|
| <i>#</i>                                     | <i>Time (minutes)</i> | <i>Flow</i>       | <i>%A (H<sub>2</sub>O)</i> | <i>%B (ACN)</i> |
| <i>0</i>                                     | <i>0</i>              | <i>4.0 ml/min</i> | <i>90</i>                  | <i>10</i>       |
| <i>1</i>                                     | <i>5</i>              | <i>4.0 ml/min</i> | <i>90</i>                  | <i>10</i>       |
| <i>2</i>                                     | <i>8</i>              | <i>4.0 ml/min</i> | <i>30</i>                  | <i>70</i>       |
| <i>3</i>                                     | <i>18</i>             | <i>4.0 ml/min</i> | <i>10</i>                  | <i>90</i>       |
| <i>4</i>                                     | <i>20</i>             | <i>4.0 ml/min</i> | <i>90</i>                  | <i>10</i>       |
| <i>5</i>                                     | <i>25</i>             | <i>4.0 ml/min</i> | <i>90</i>                  | <i>10</i>       |

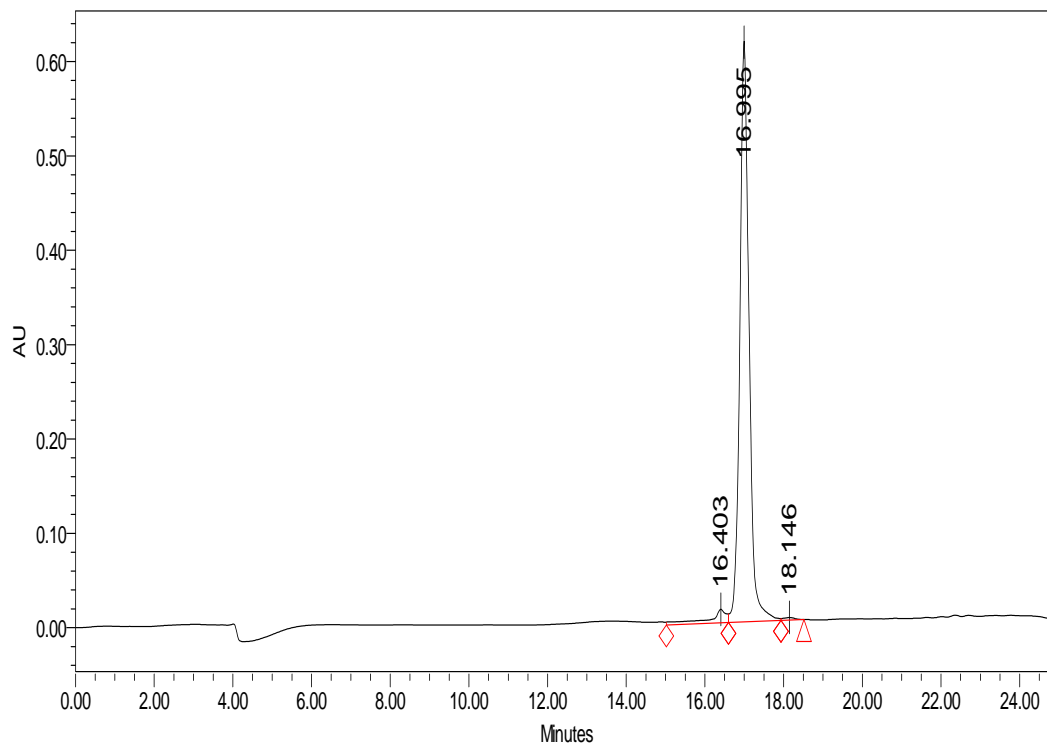


**Figure A.7:** The gradient used for chromatogram of 2-8 using RP-HPLC with a C18 column is listed below.

| <i>Table 1 HPLC Gradient for peptide 2-8</i> |                       |                   |                            |                 |
|--|-----------------------|-------------------|----------------------------|-----------------|
| <i>#</i>                                     | <i>Time (minutes)</i> | <i>Flow</i>       | <i>%A (H<sub>2</sub>O)</i> | <i>%B (ACN)</i> |
| <i>0</i>                                     | <i>0</i>              | <i>4.0 ml/min</i> | <i>90</i>                  | <i>10</i>       |
| <i>1</i>                                     | <i>5</i>              | <i>4.0 ml/min</i> | <i>90</i>                  | <i>10</i>       |
| <i>2</i>                                     | <i>8</i>              | <i>4.0 ml/min</i> | <i>30</i>                  | <i>70</i>       |
| <i>3</i>                                     | <i>18</i>             | <i>4.0 ml/min</i> | <i>10</i>                  | <i>90</i>       |
| <i>4</i>                                     | <i>20</i>             | <i>4.0 ml/min</i> | <i>90</i>                  | <i>10</i>       |
| <i>5</i>                                     | <i>25</i>             | <i>4.0 ml/min</i> | <i>90</i>                  | <i>10</i>       |

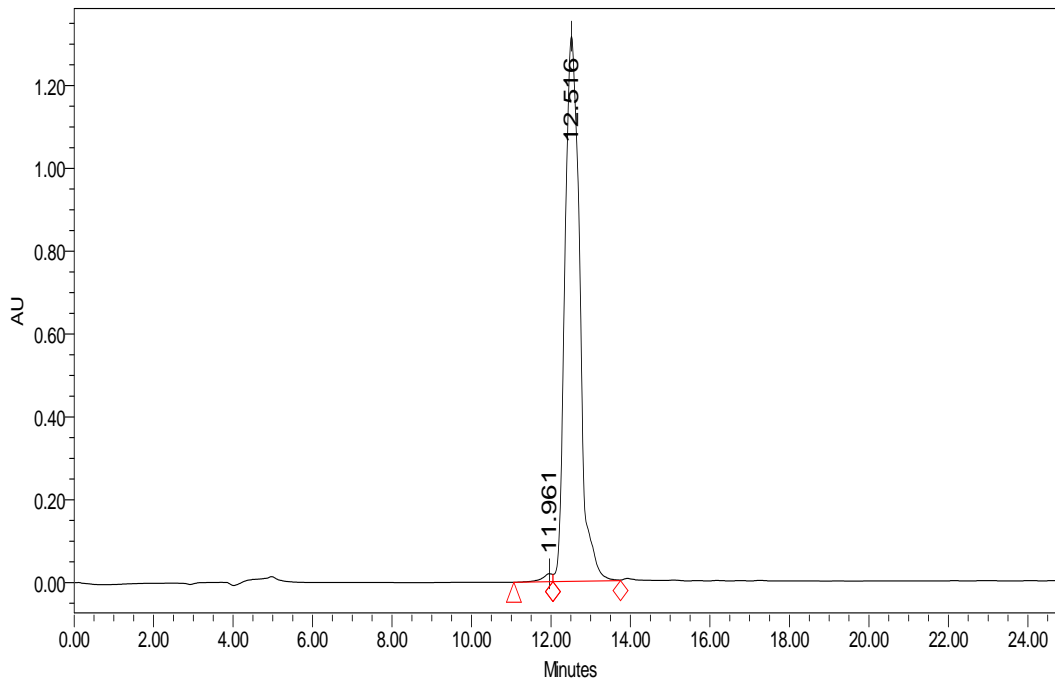


**Figure A.8:** The gradient used for chromatogram of 2-9 using RP-HPLC with a C18 column is listed below.

| <b>Table 1 HPLC Gradient for peptide 2-9</b> |                       |             |                            |                 |
|--|-----------------------|-------------|----------------------------|-----------------|
| <b>#</b>                                     | <b>Time (minutes)</b> | <b>Flow</b> | <b>%A (H<sub>2</sub>O)</b> | <b>%B (ACN)</b> |
| 0  | 0                     | 4.0 ml/min  | 90                         | 10              |
| 1  | 5                     | 4.0 ml/min  | 90                         | 10              |
| 2  | 8                     | 4.0 ml/min  | 30                         | 70              |
| 3  | 18                    | 4.0 ml/min  | 10                         | 90              |
| 4  | 20                    | 4.0 ml/min  | 90                         | 10              |
| 5  | 25                    | 4.0 ml/min  | 90                         | 10              |

# MALDI of Compounds in Chapter 2

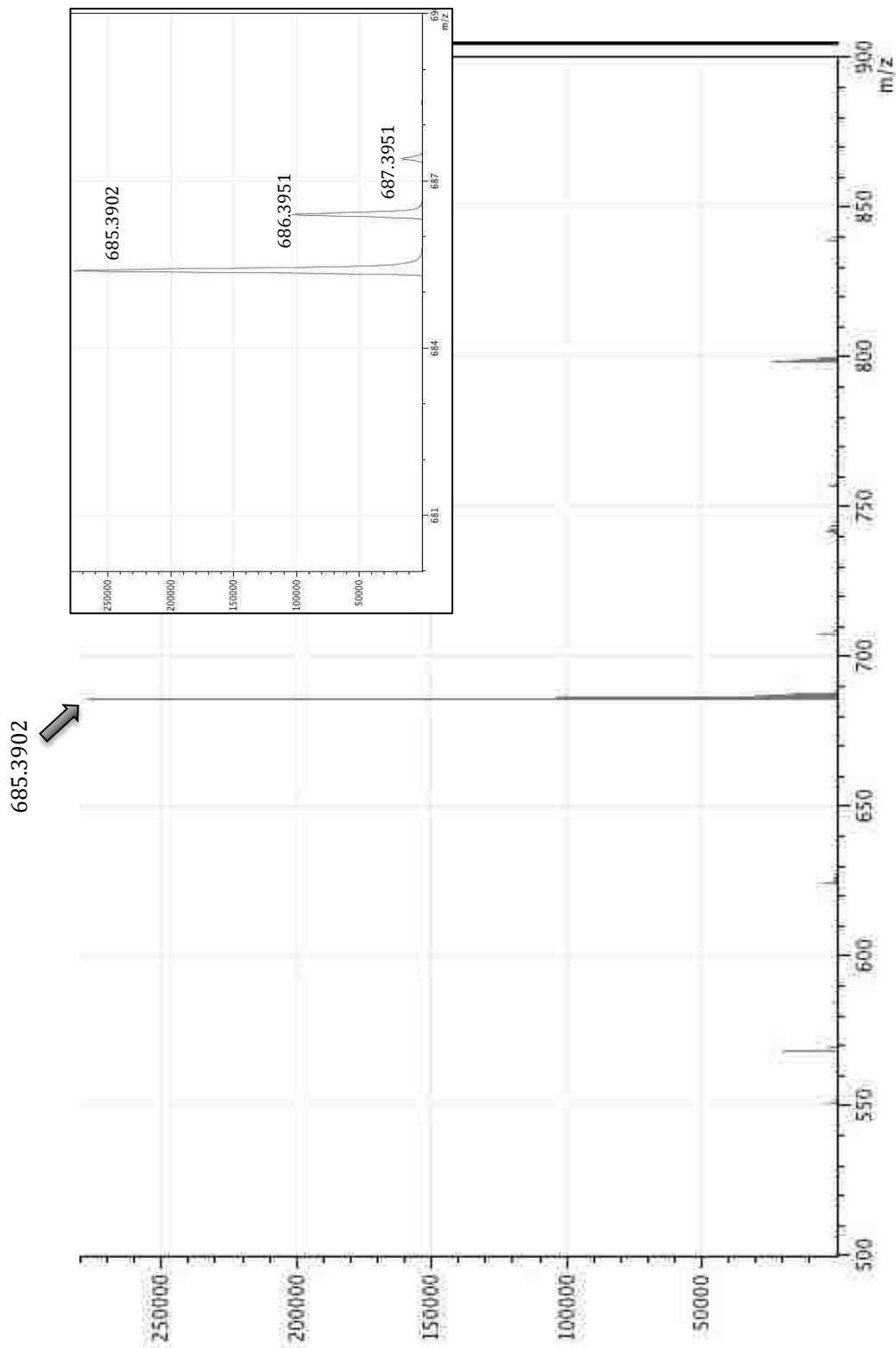


Figure A.9. MALDI-TOF of peptide 2-1



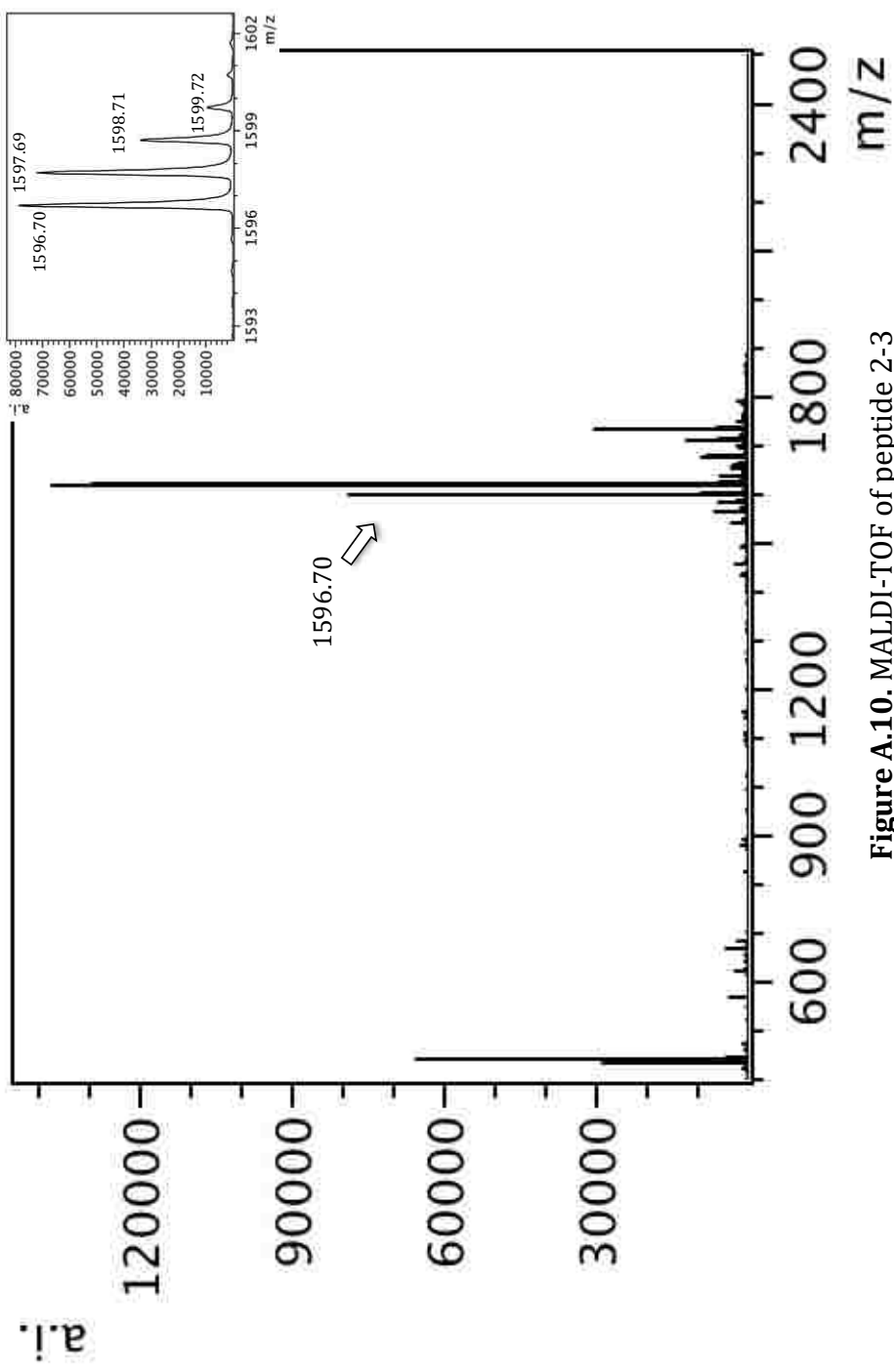


Figure A.10. MALDI-TOF of peptide 2-3

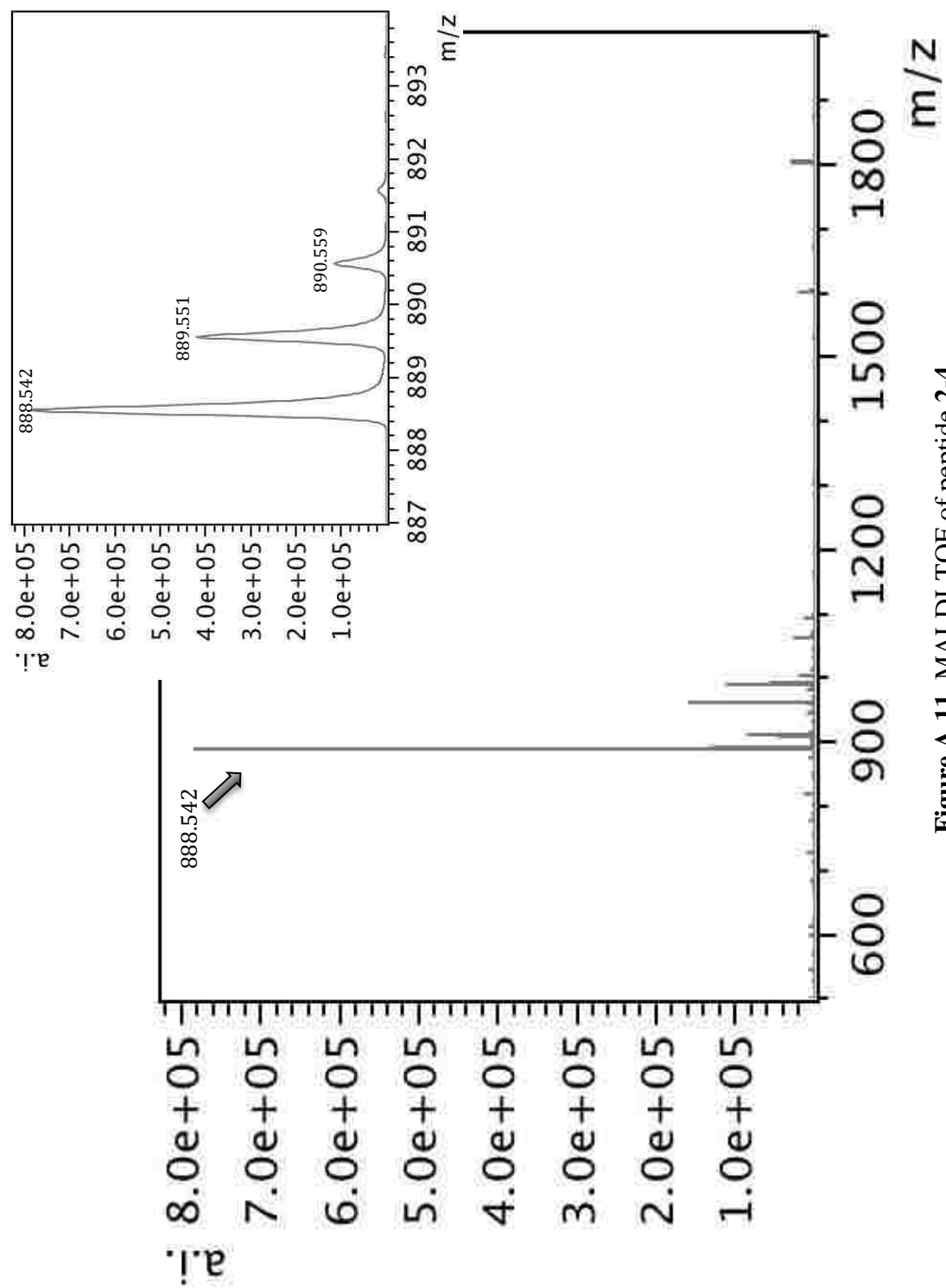


Figure A.11. MALDI-TOF of peptide 2-4

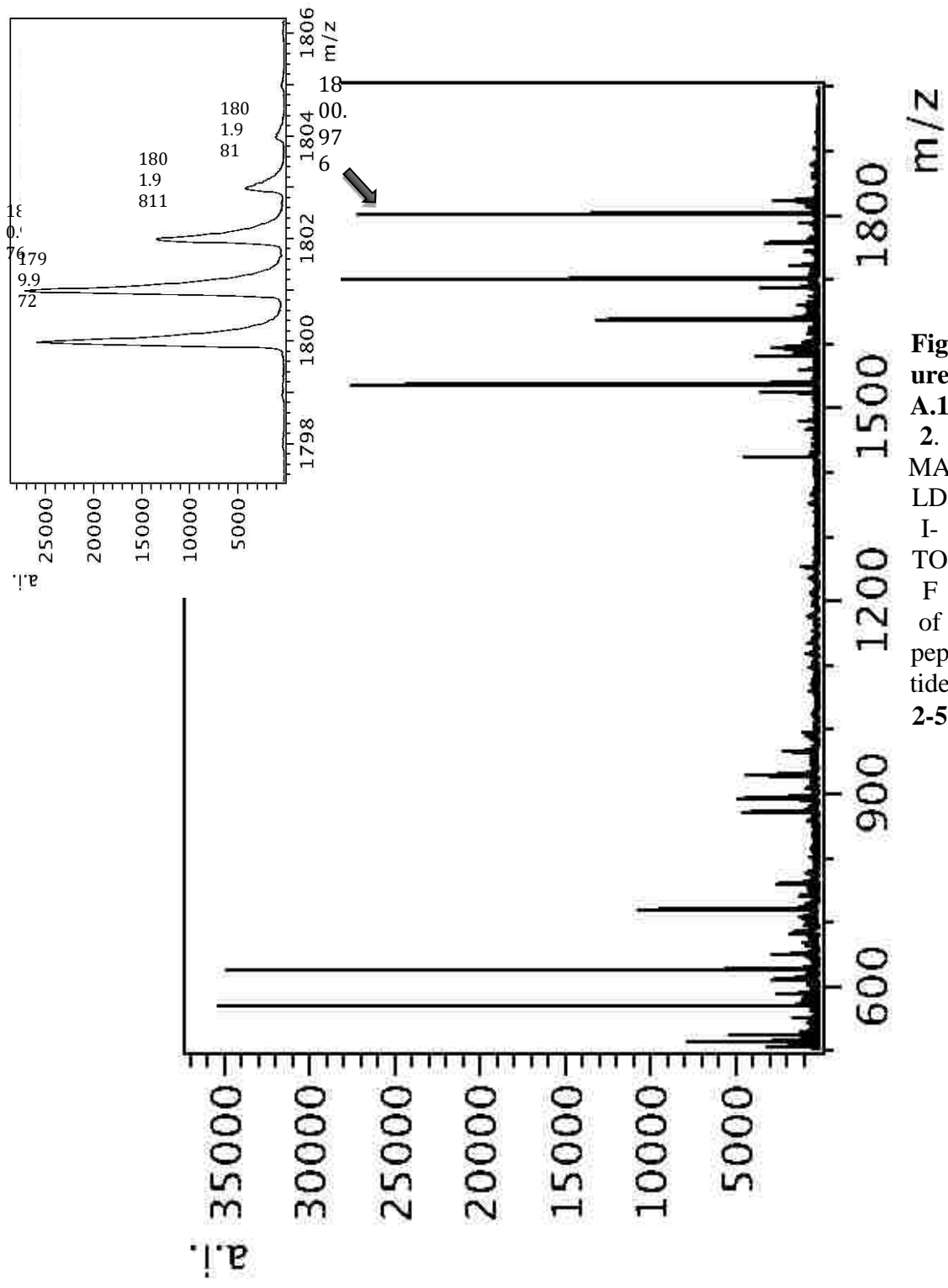


Figure A.1 2. MALDI-TOF of peptide 2-5

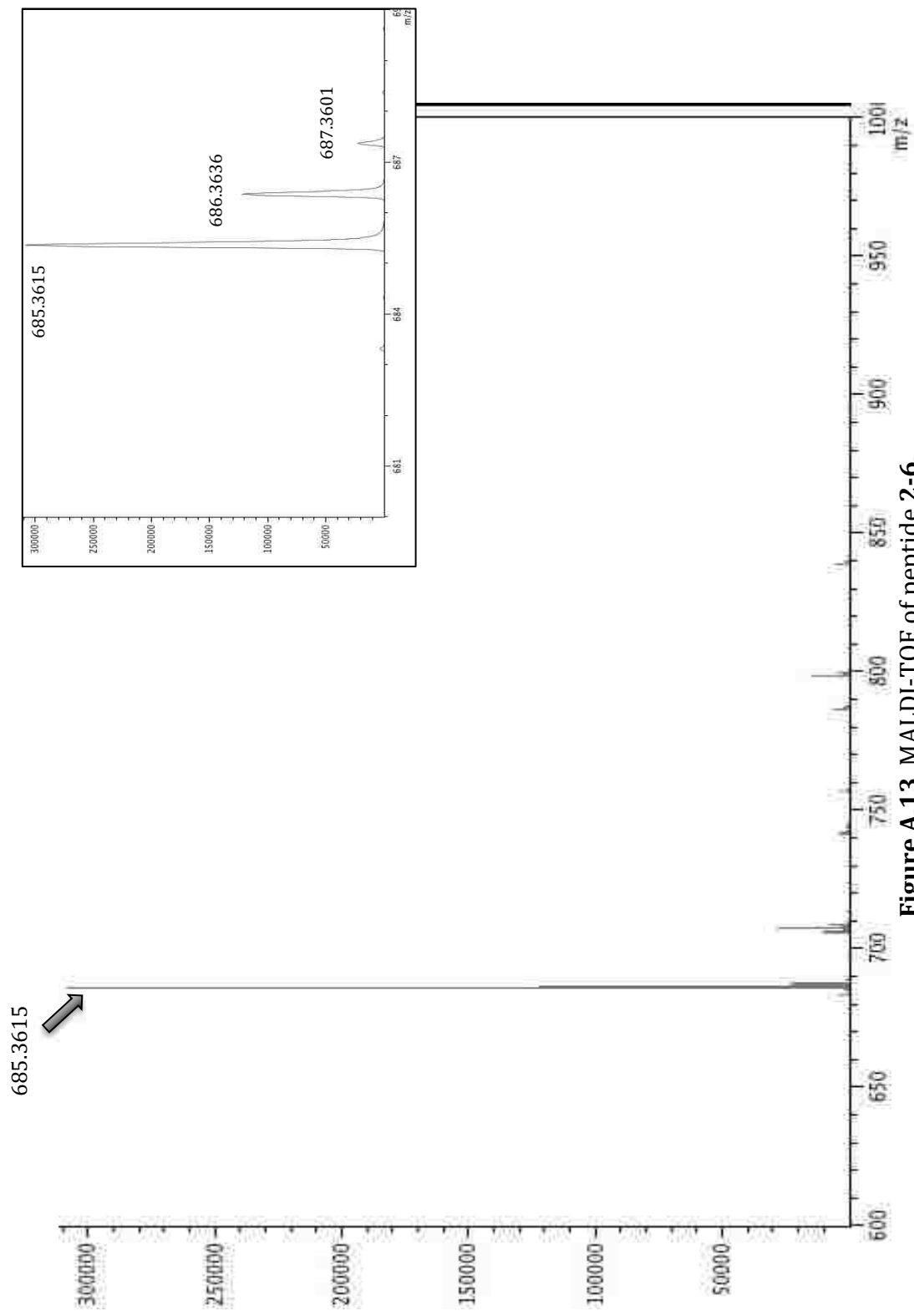


Figure A.13. MALDI-TOF of peptide 2-6.

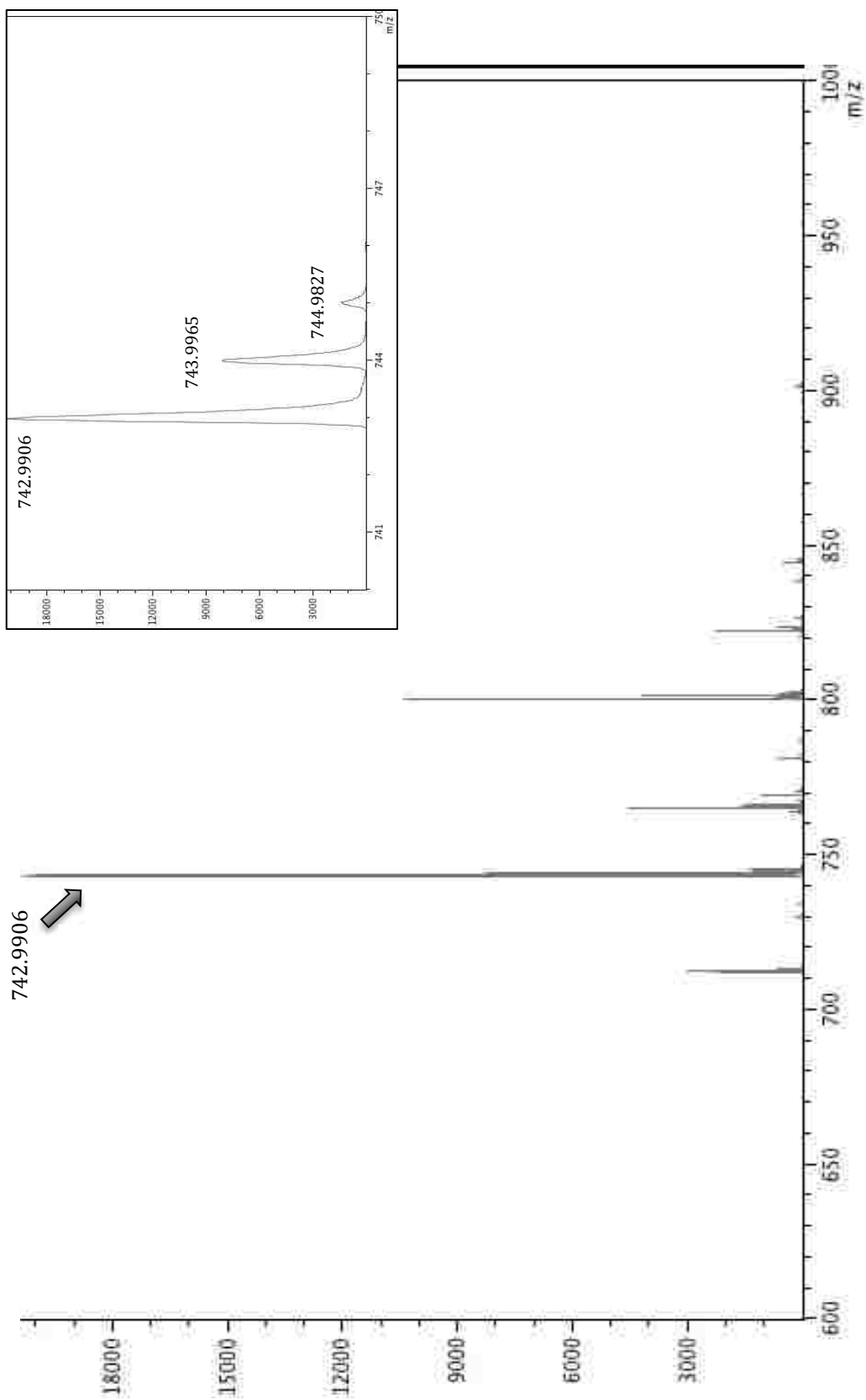
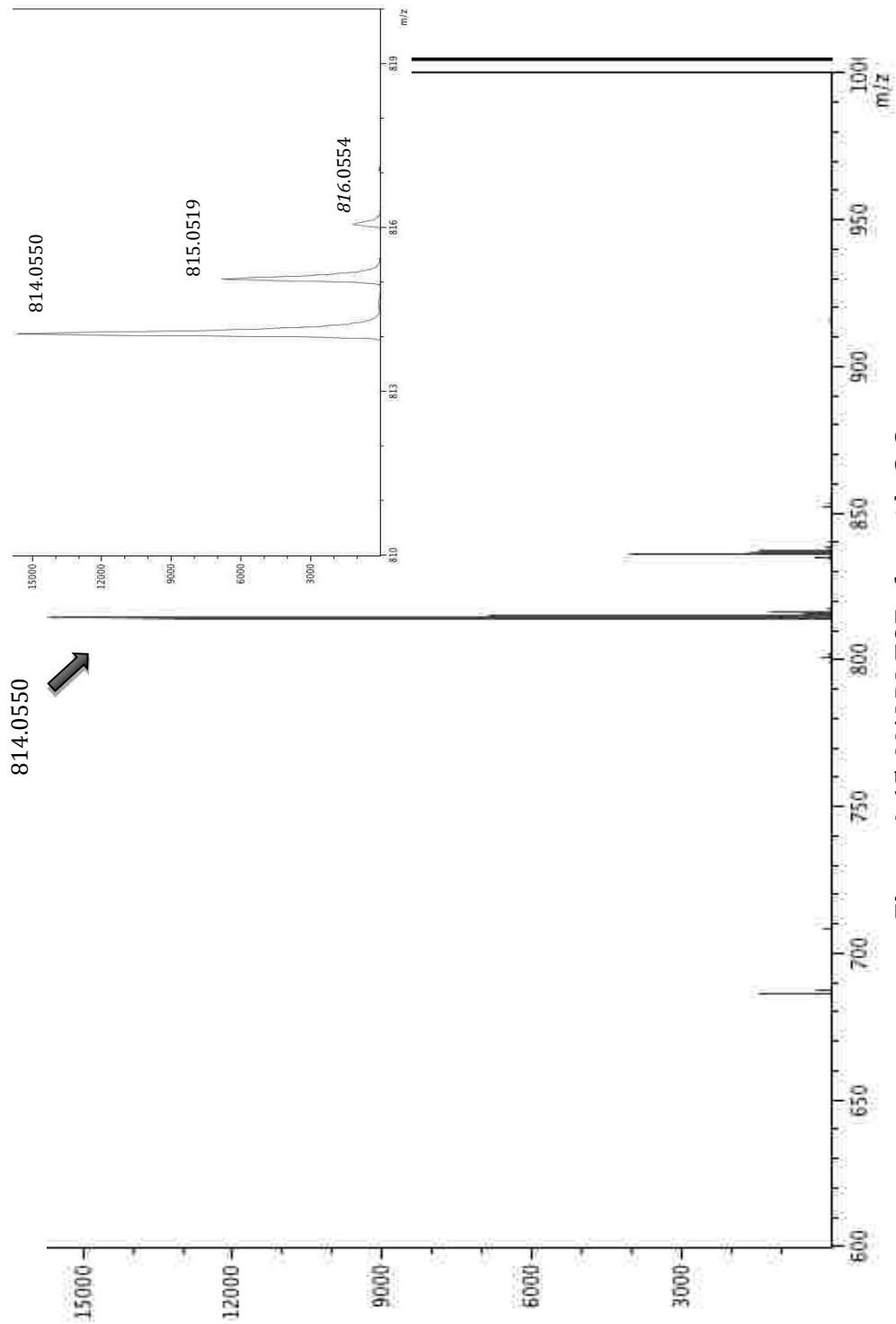


Figure A.14. MALDI-TOF of peptide 2-7.



**Figure A.15.** MALDI-TOF of peptide 2-8.

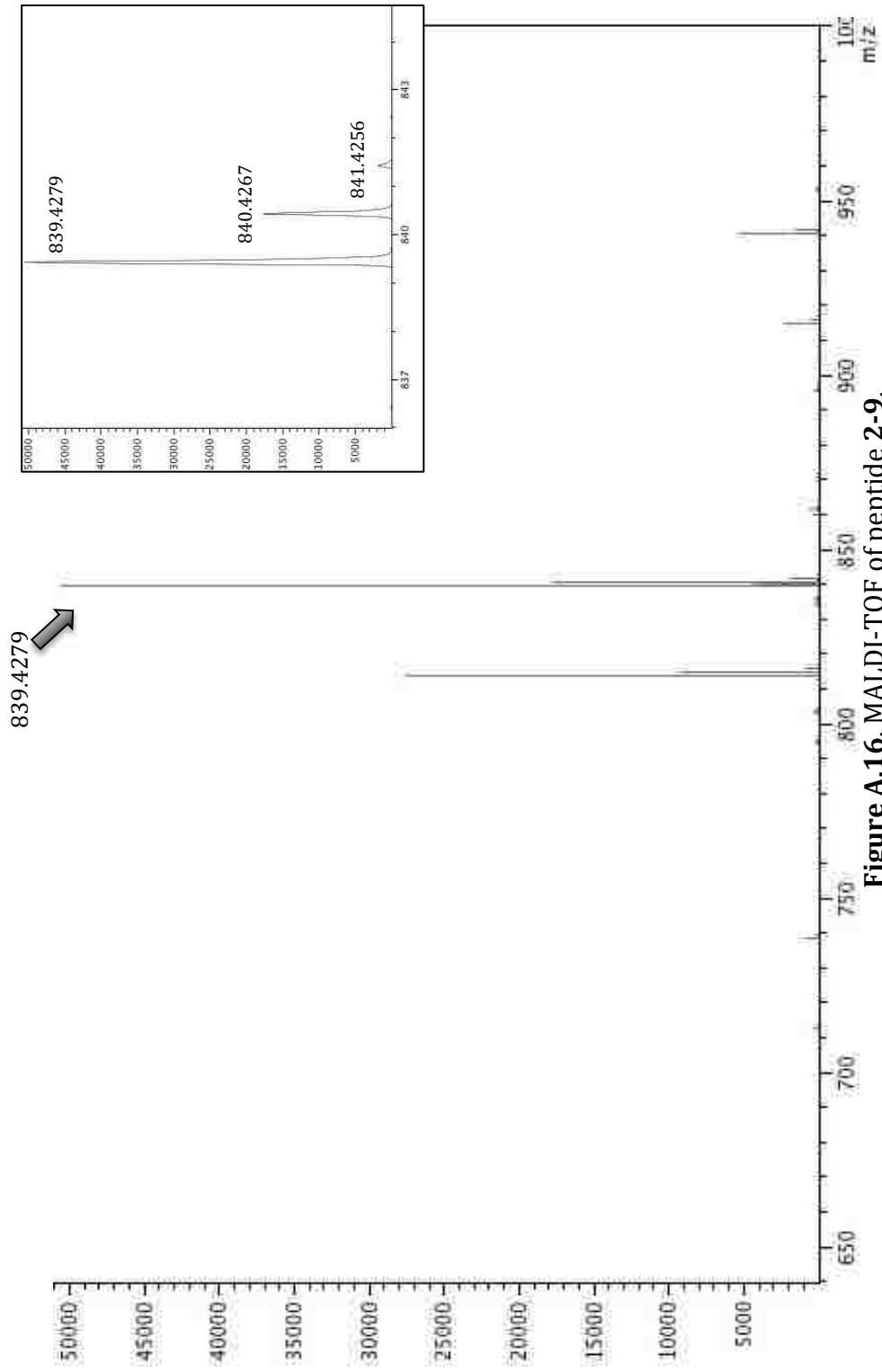
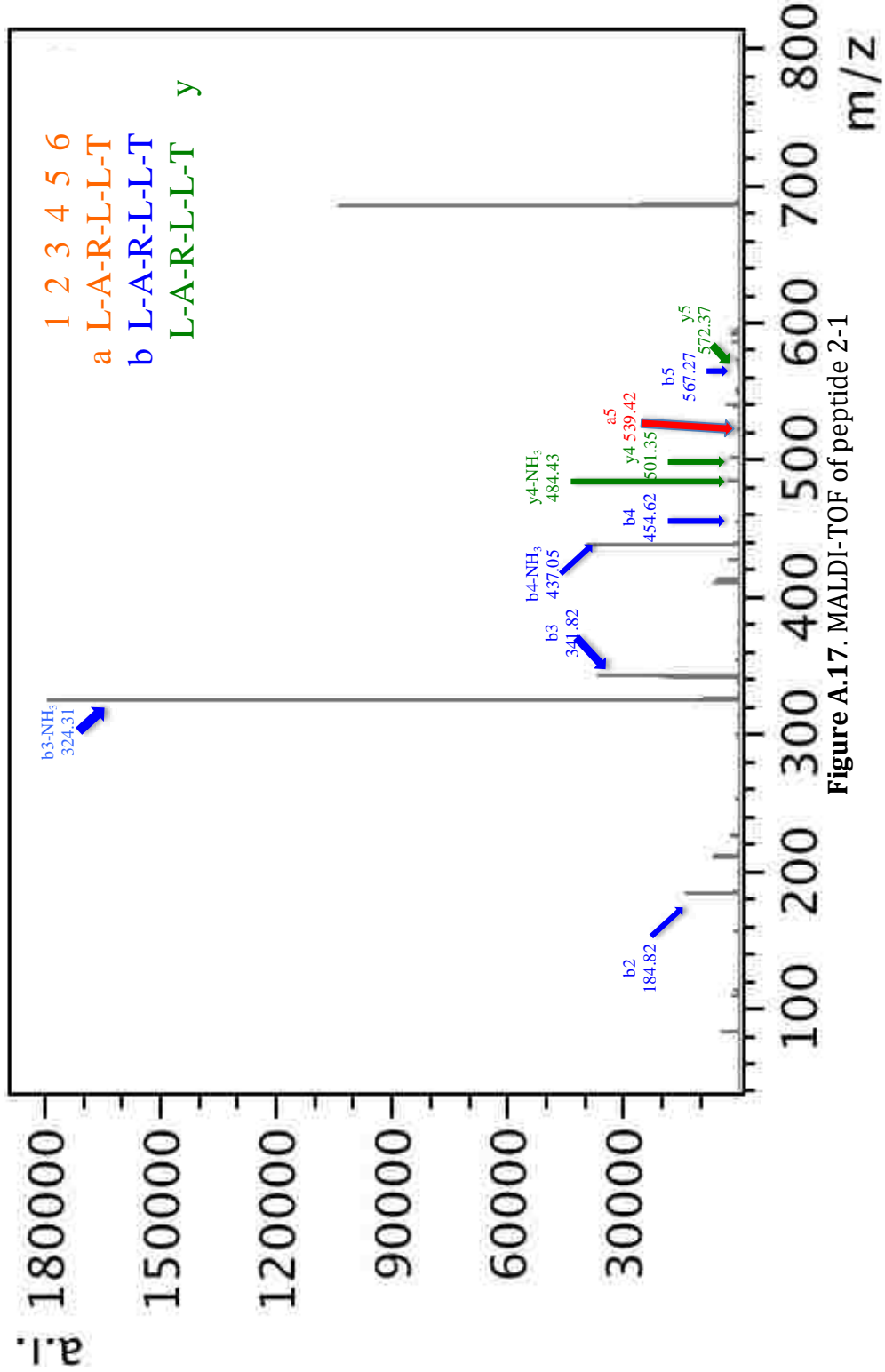


Figure A.16. MALDI-TOF of peptide 2-9.

MALDI MSMS of Compounds in Chapter 2





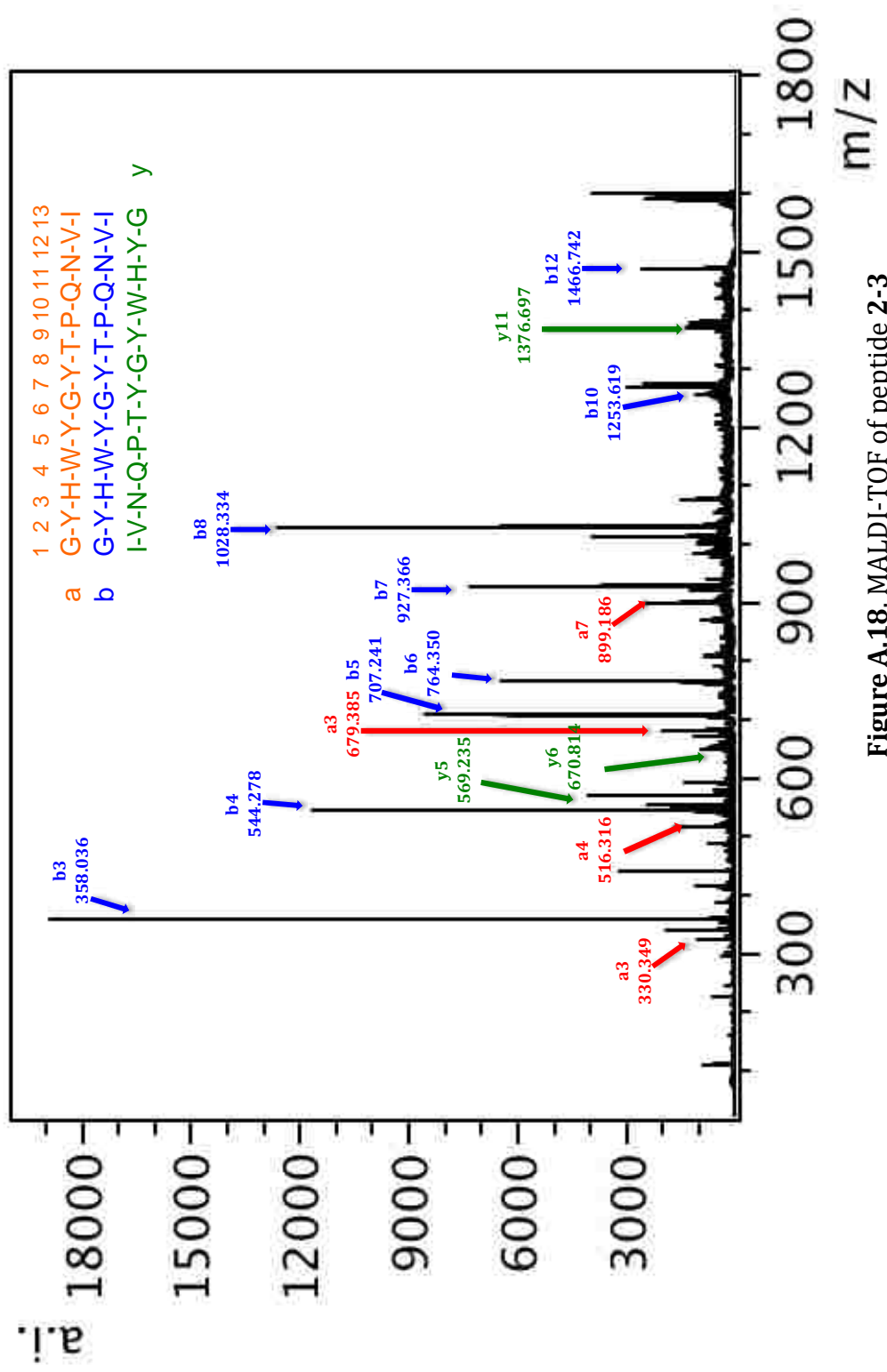


Figure A.18. MALDI-TOF of peptide 2-3

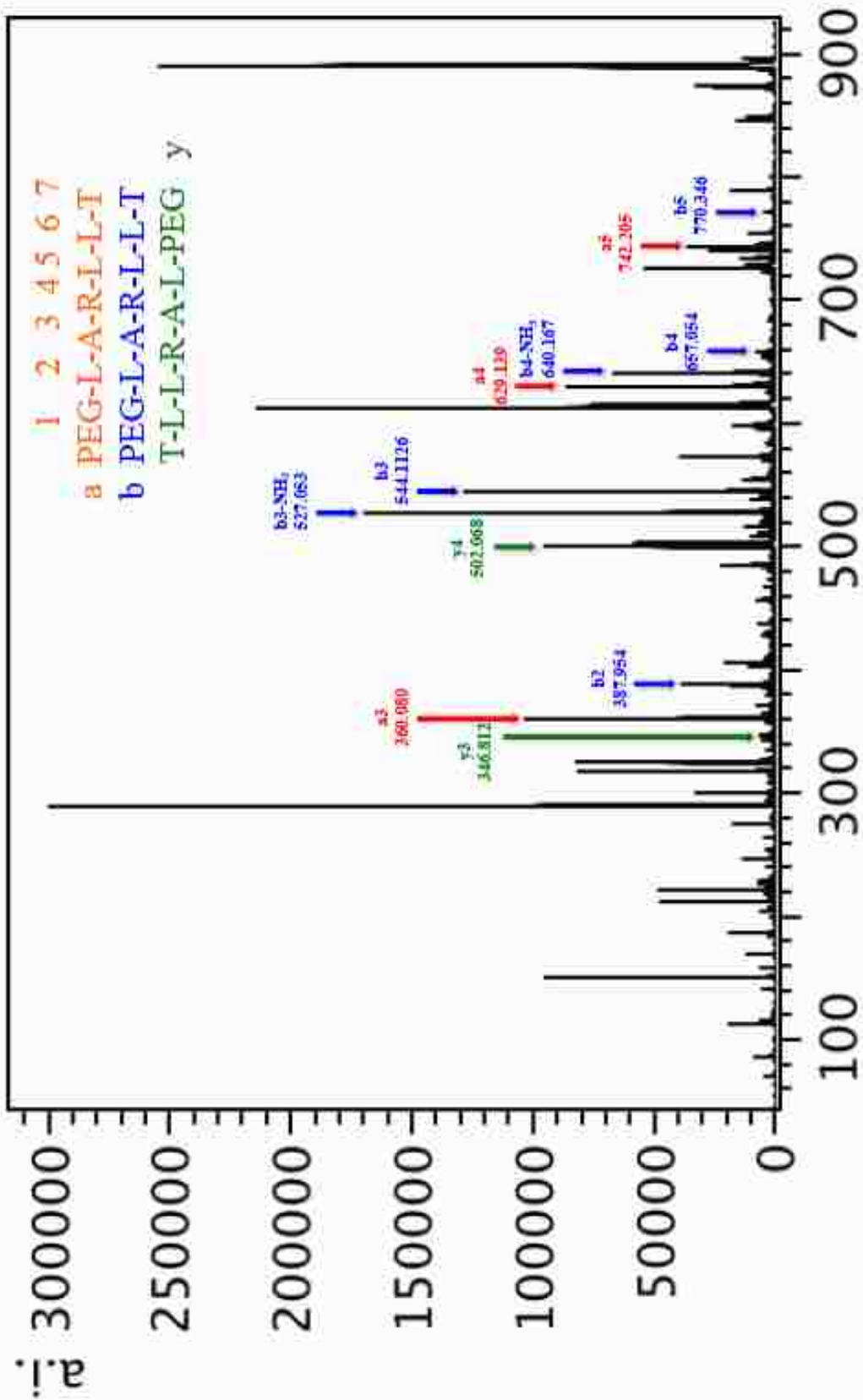


Figure A.19. MALDI-TOF of peptide 2-4

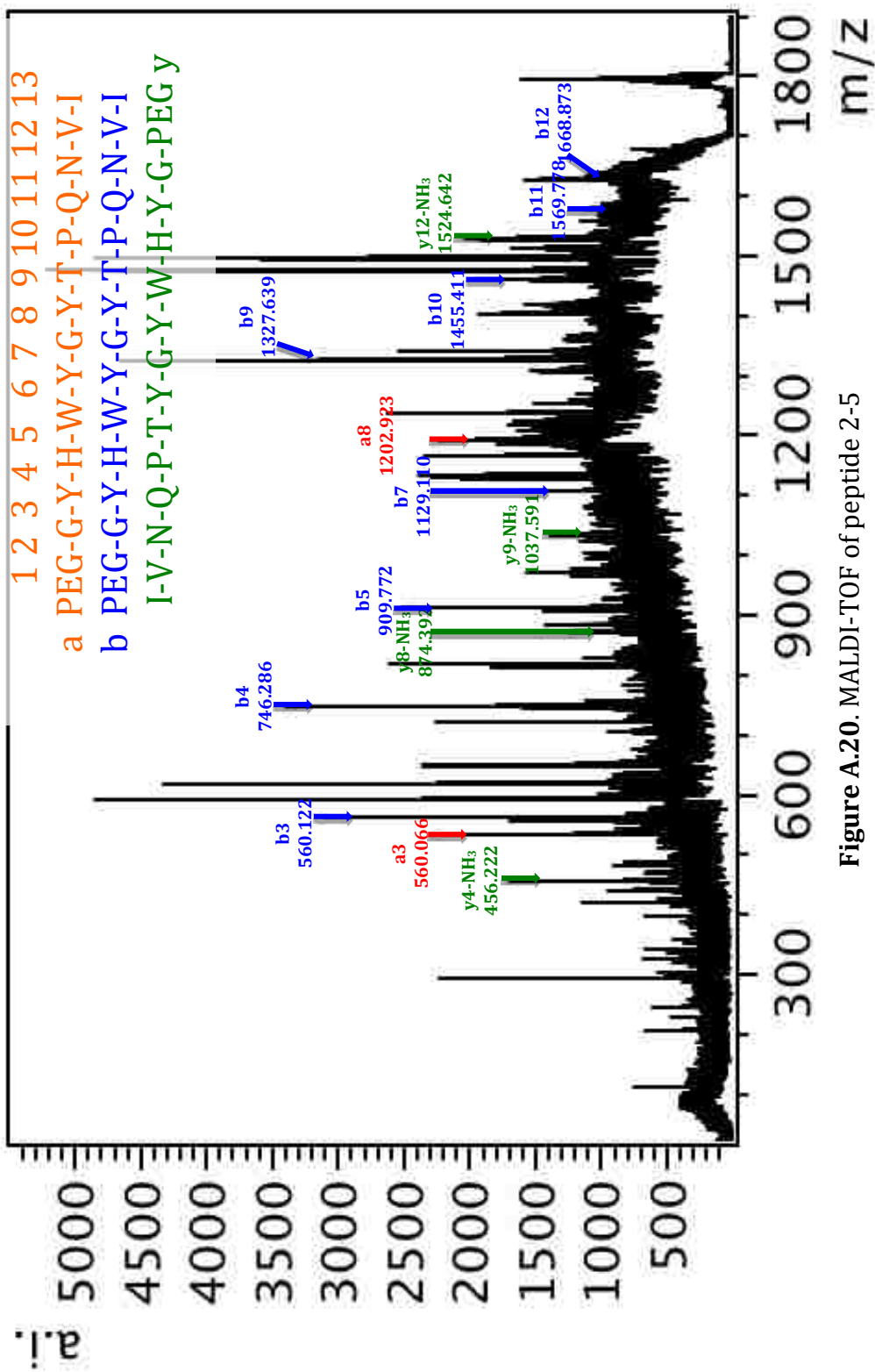


Figure A.20. MALDI-TOF of peptide 2-5

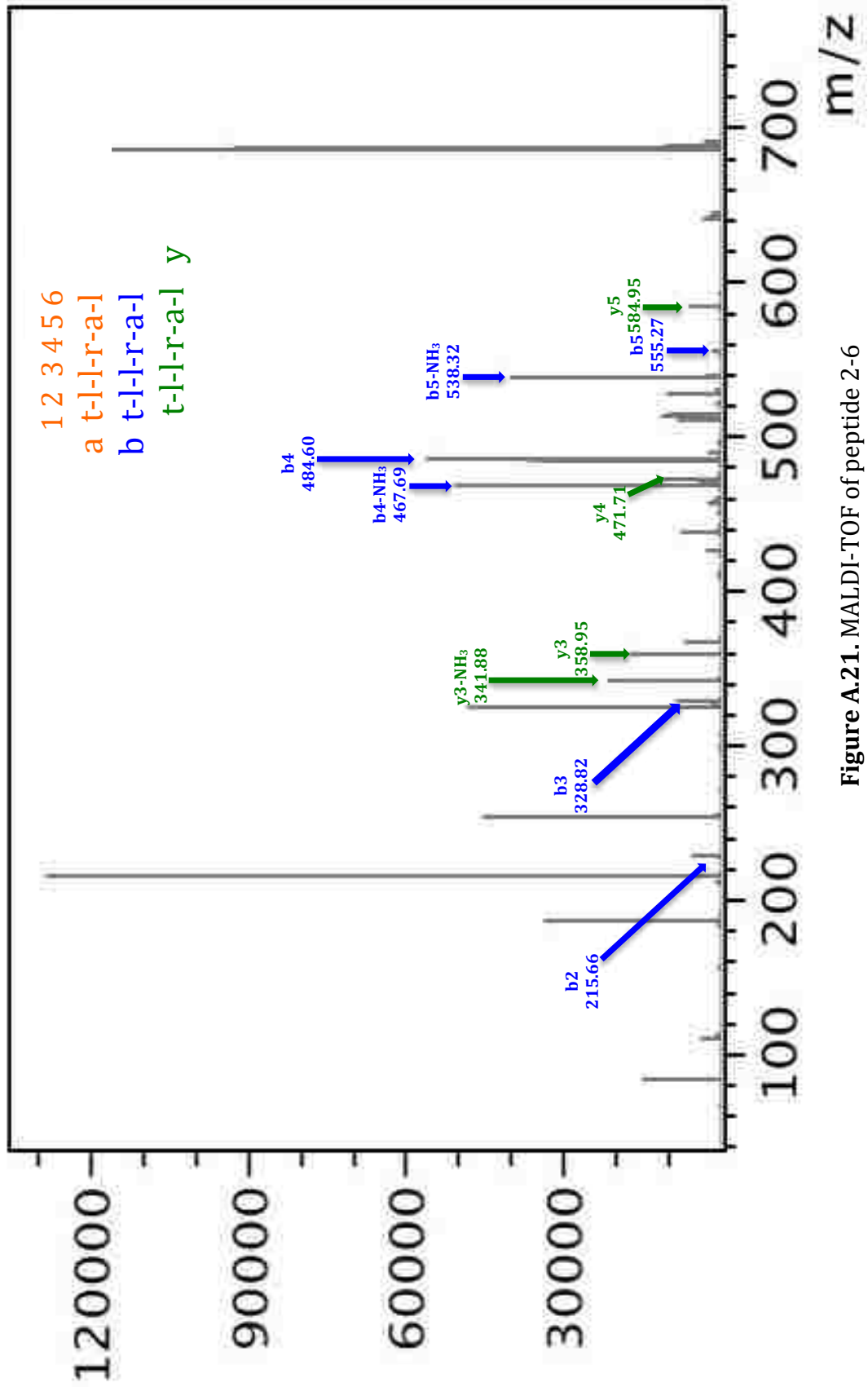


Figure A.21. MALDI-TOF of peptide 2-6

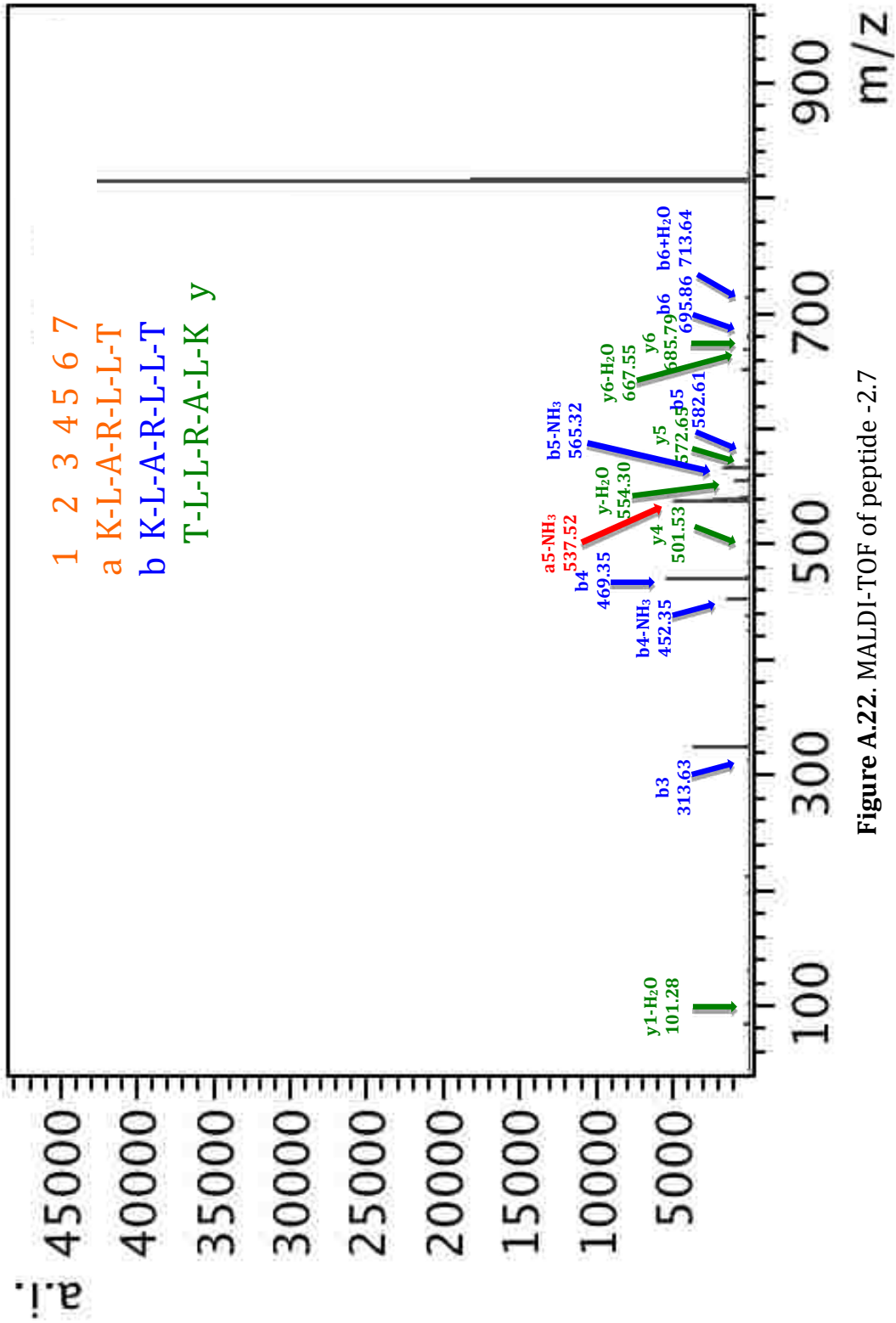


Figure A.22. MALDI-TOF of peptide -2.7

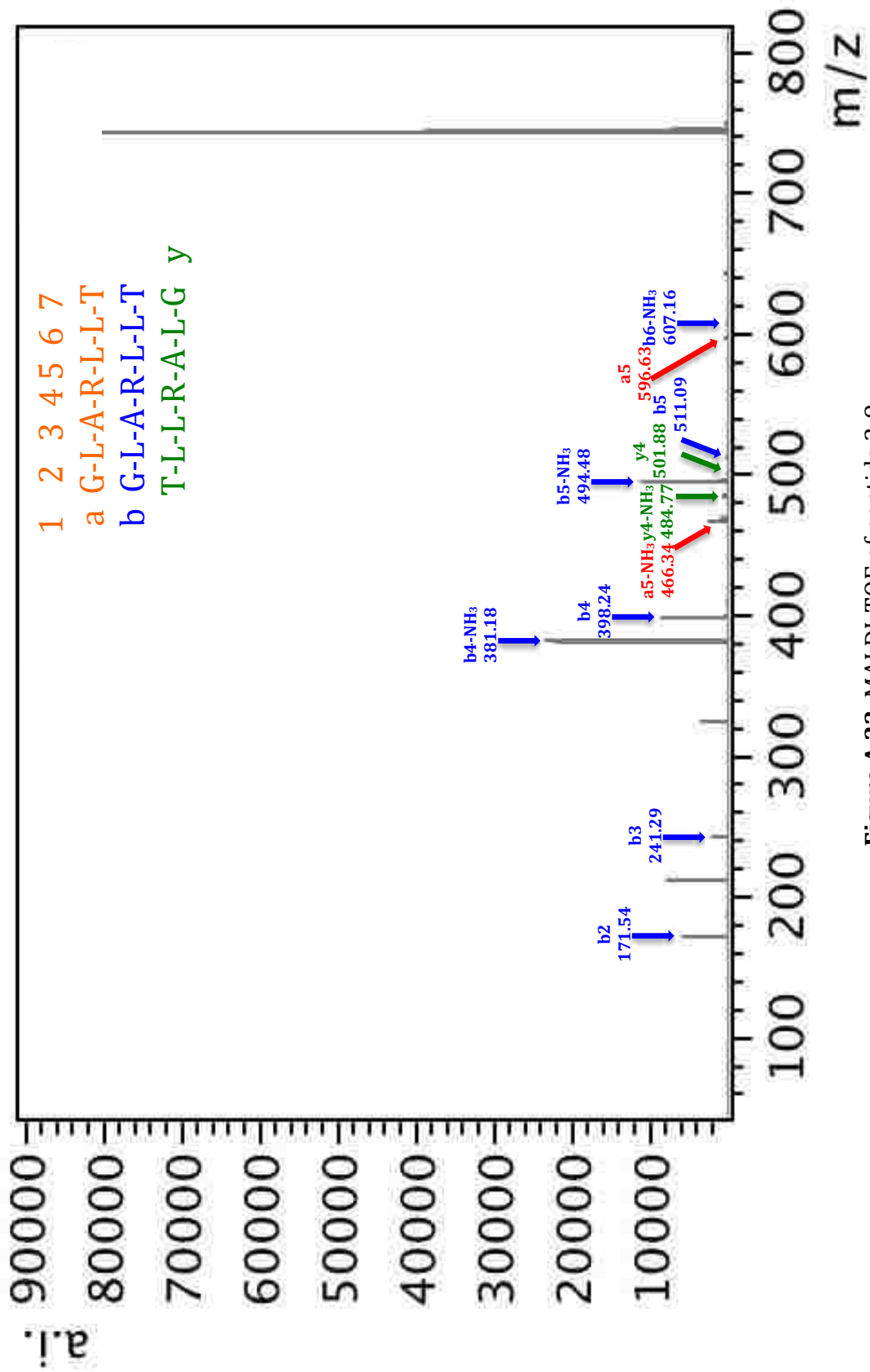


Figure A.23. MALDI-TOF of peptide 2-8

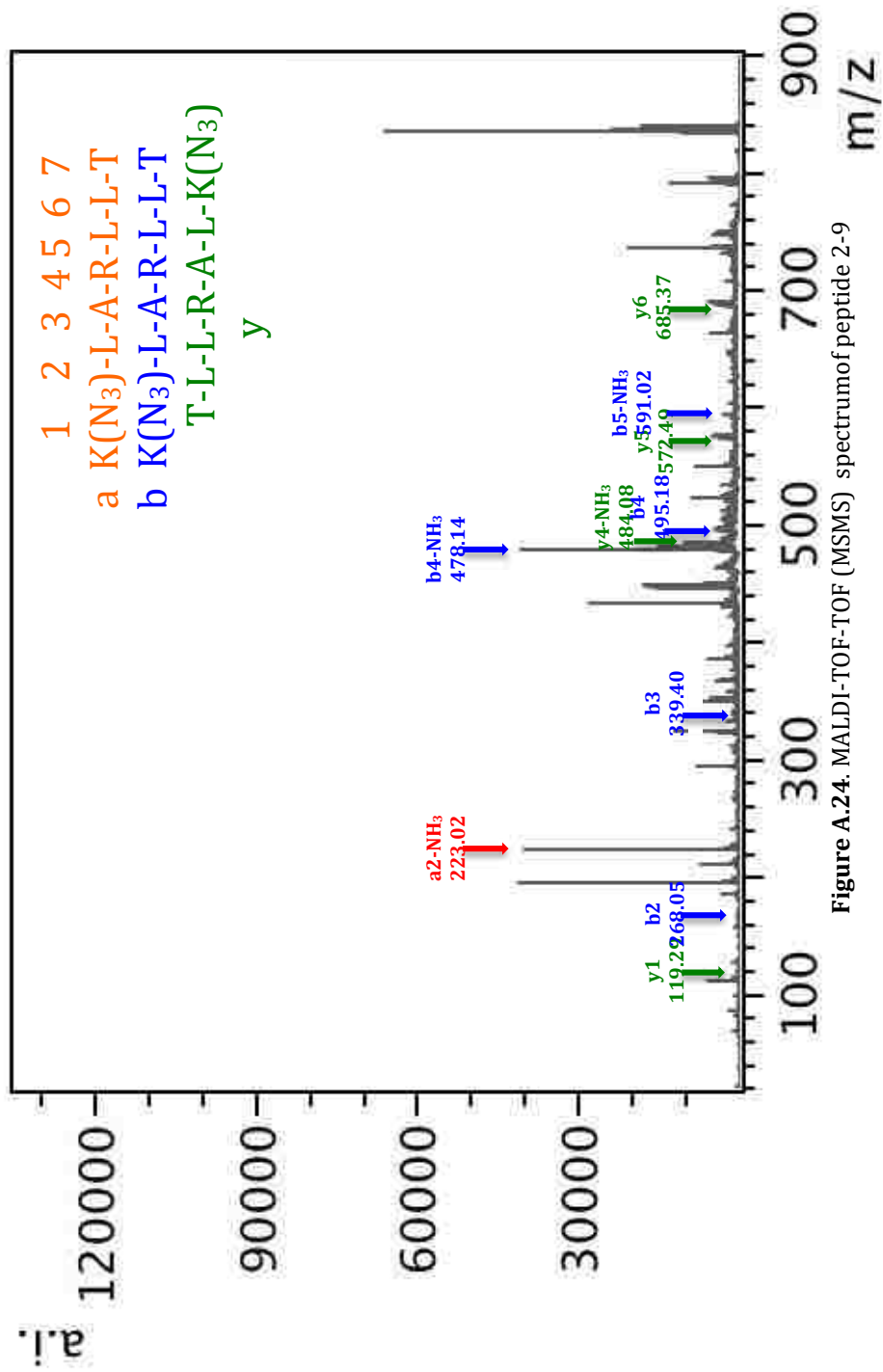


Figure A.24. MALDI-TOF-TOF (MSMS) spectrum of peptide 2-9

## Proton NMR of Compounds in Chapter 2

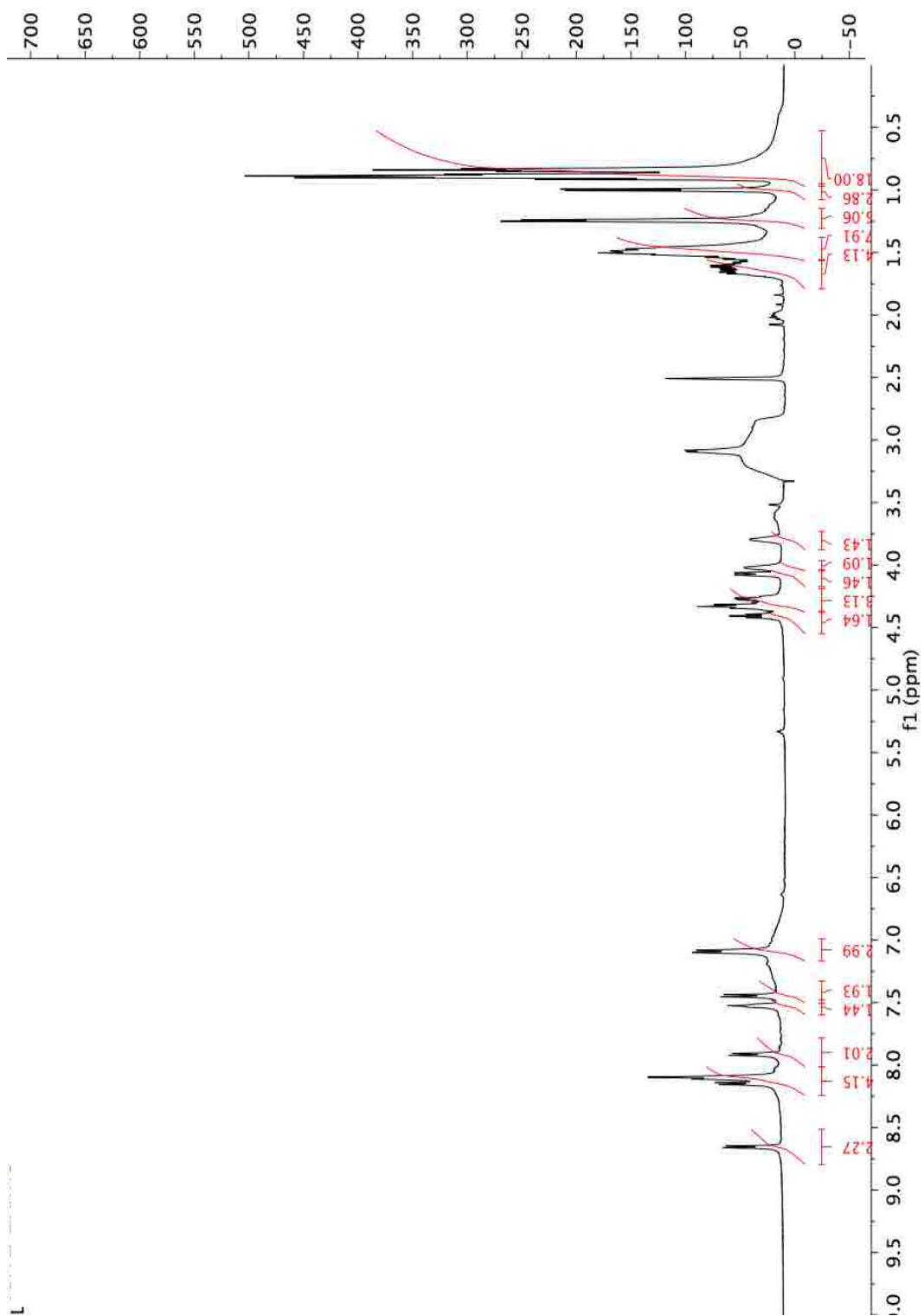
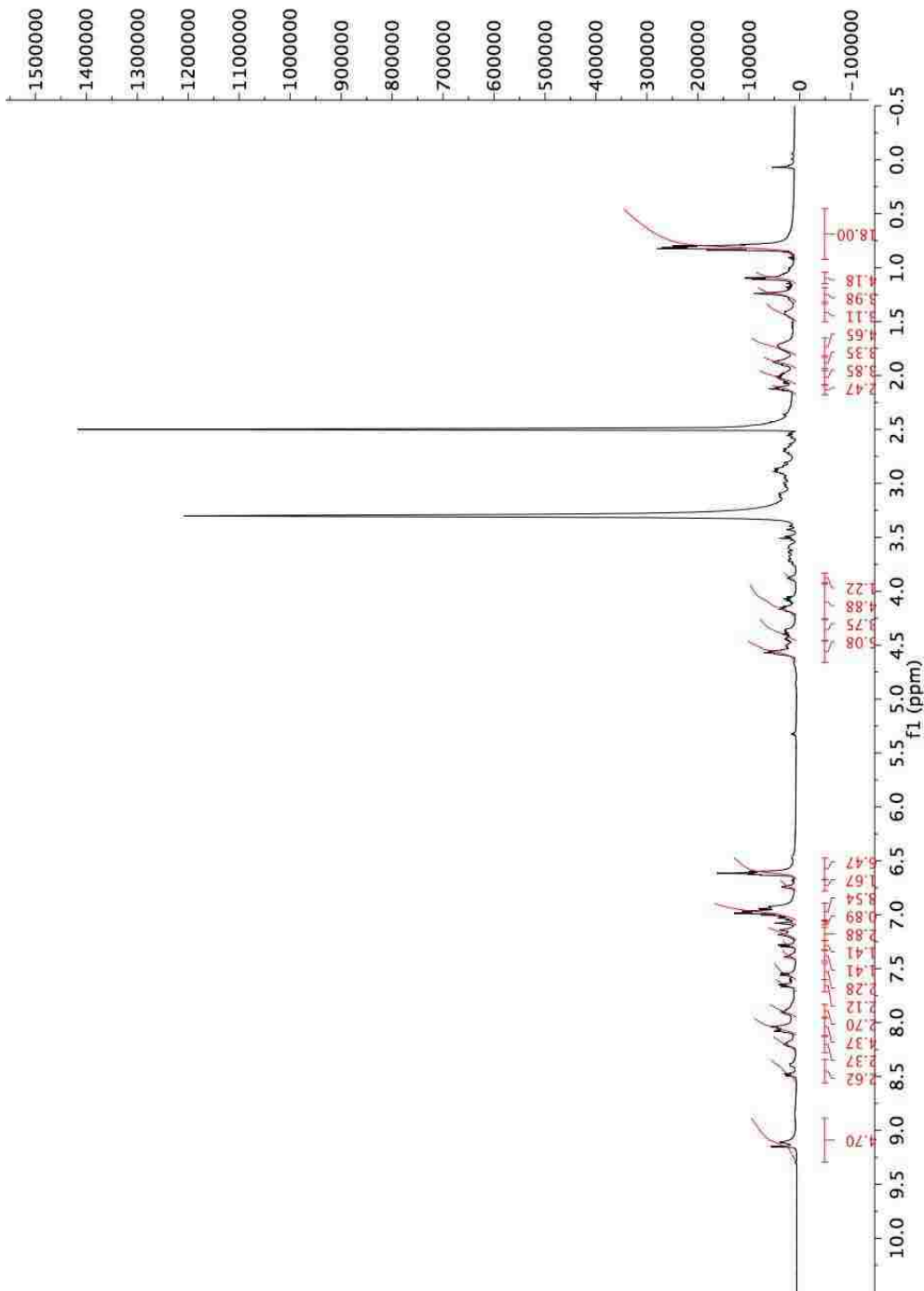
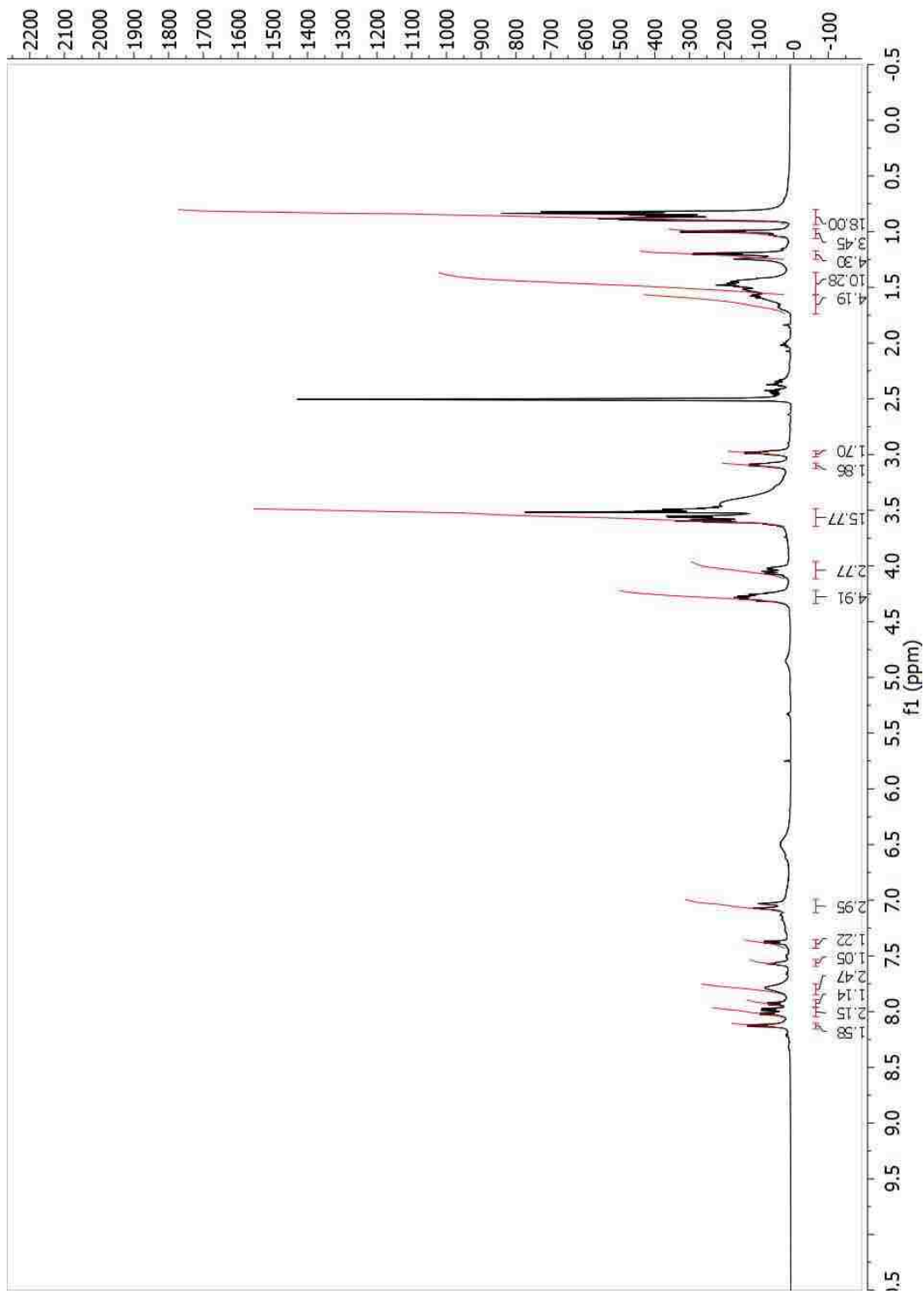


Figure A.25. MALDI-TOF of peptide 2-1







**Figure A.27.** MALDI-TOF of peptide 2-4

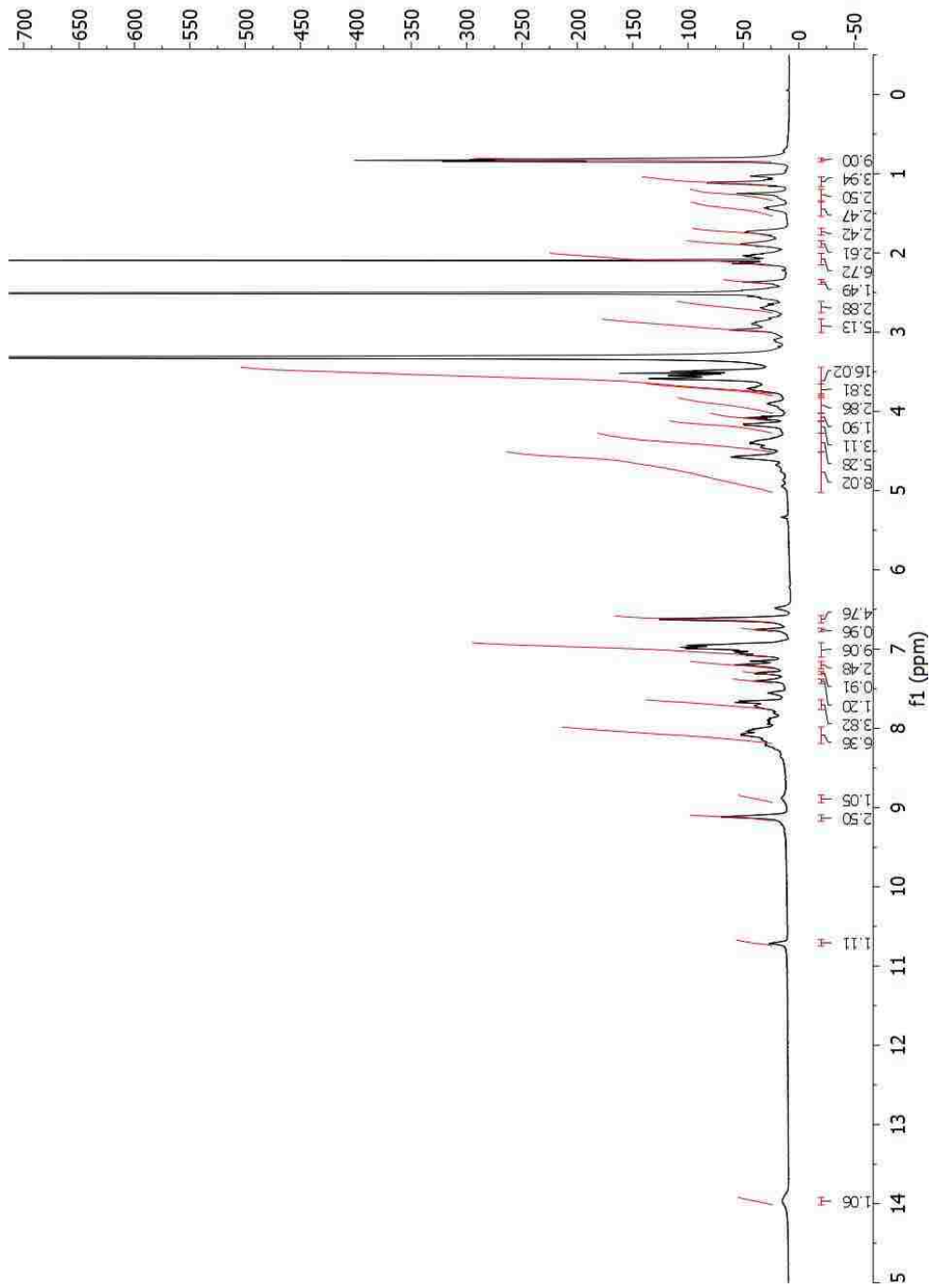


Figure A.28. MALDI-TOF of peptide 2-5

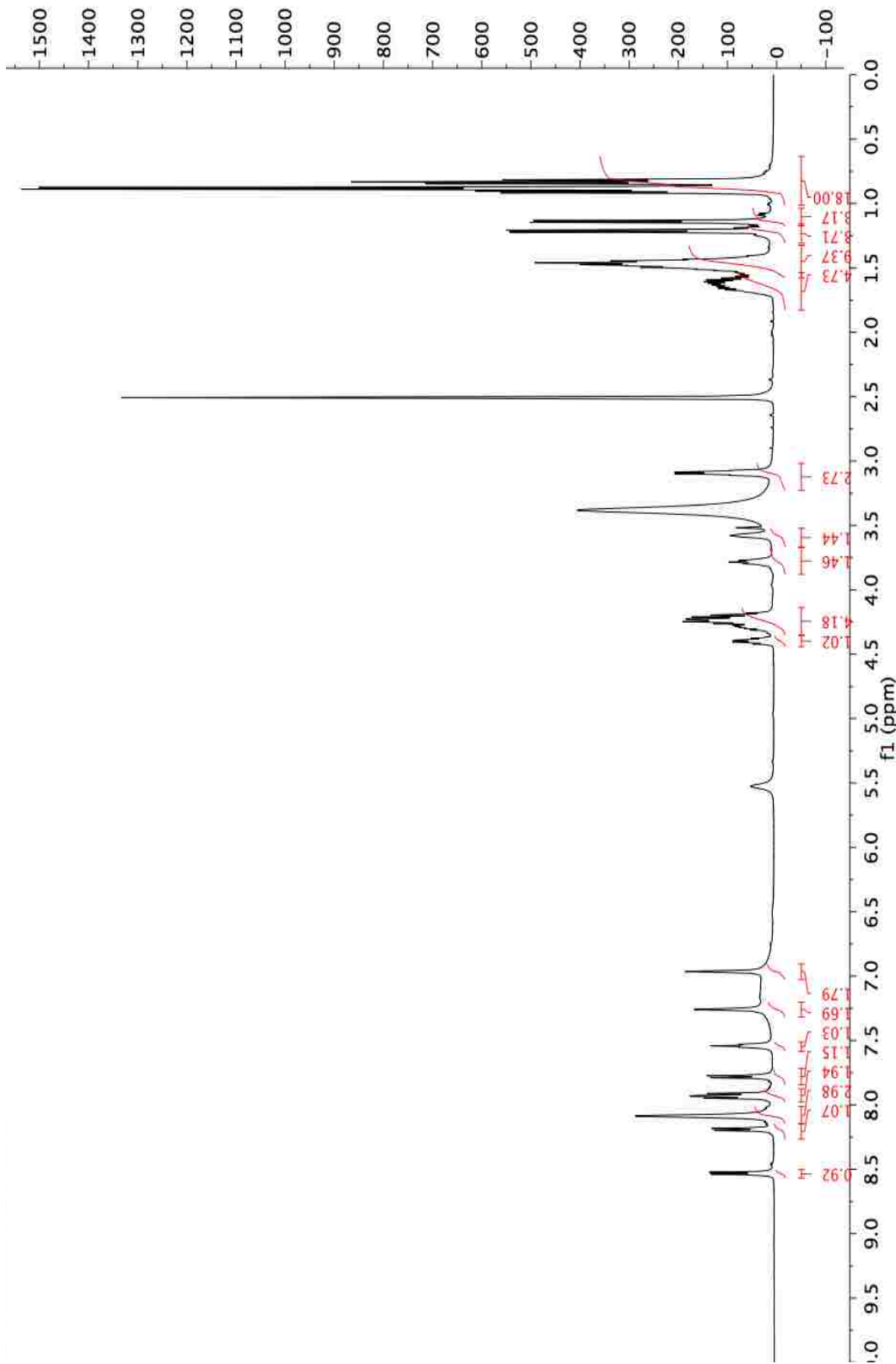


Figure A.29. <sup>1</sup>H NMR spectrum for peptide 2-6

KLARLLT-TMW -052016/7  
KLARLLT-TMW 052016 PROTON

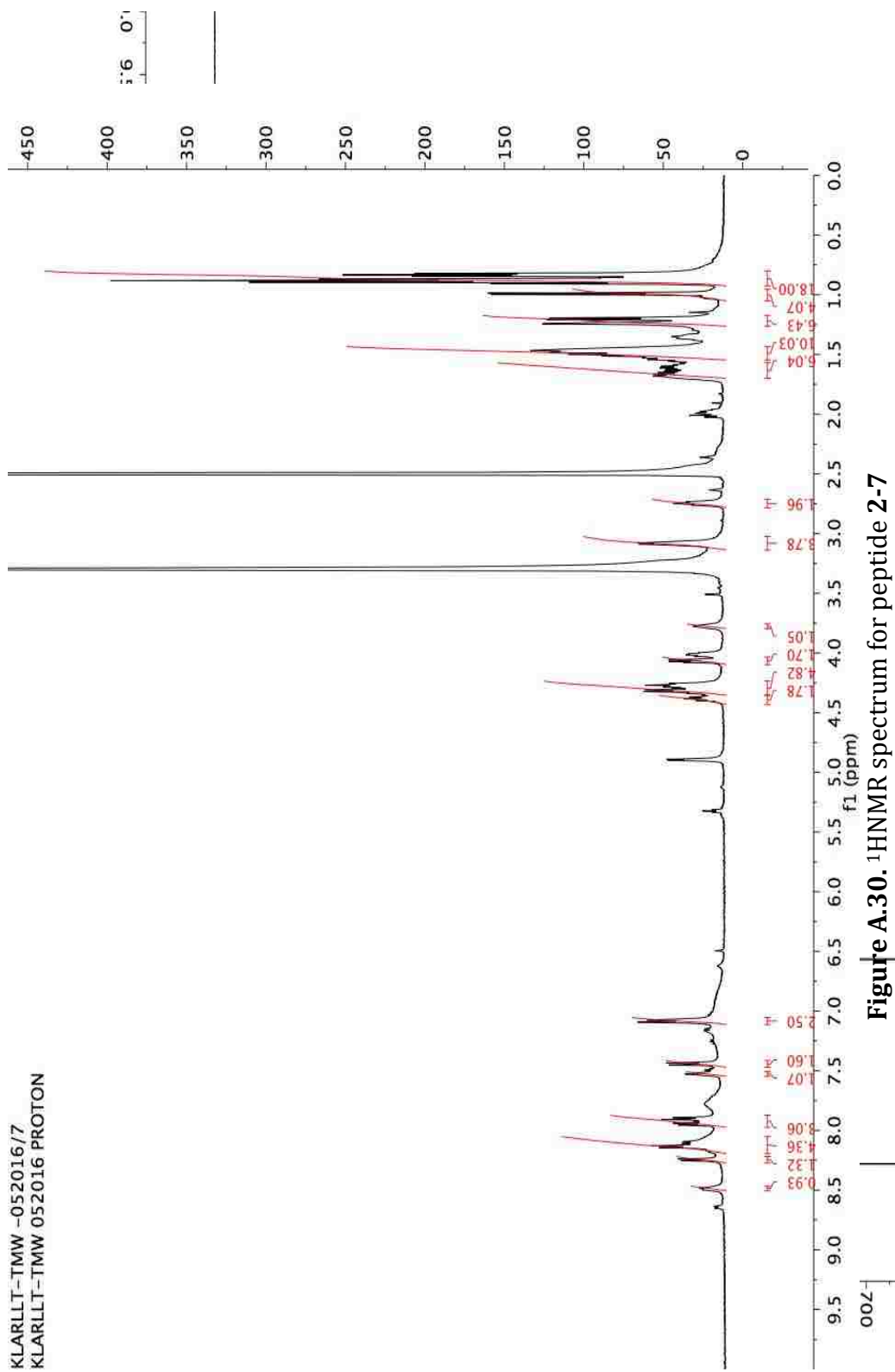


Figure A.30. <sup>1</sup>H NMR spectrum for peptide 2-7

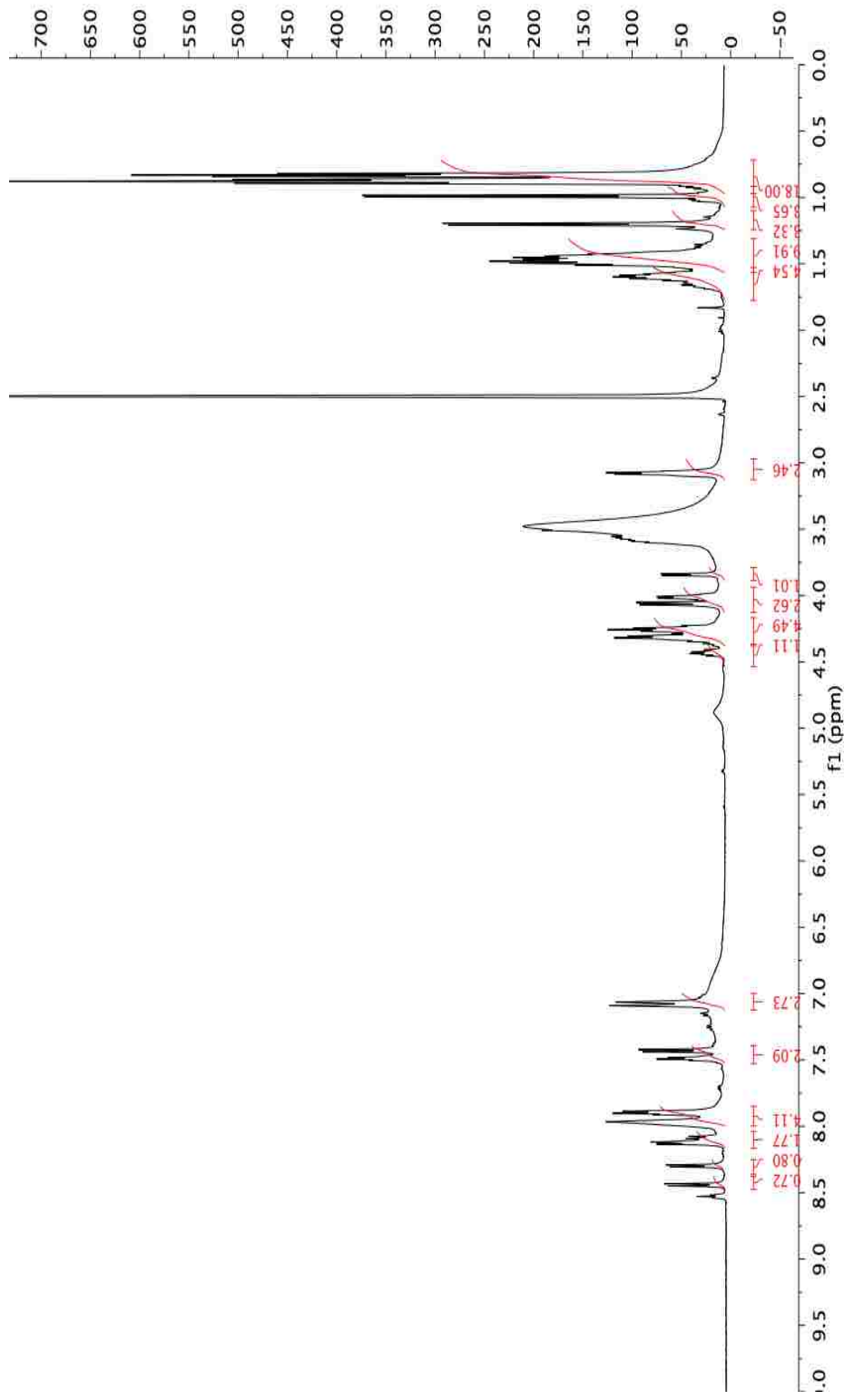


Figure A.31. <sup>1</sup>H NMR spectrum for peptide 2-8

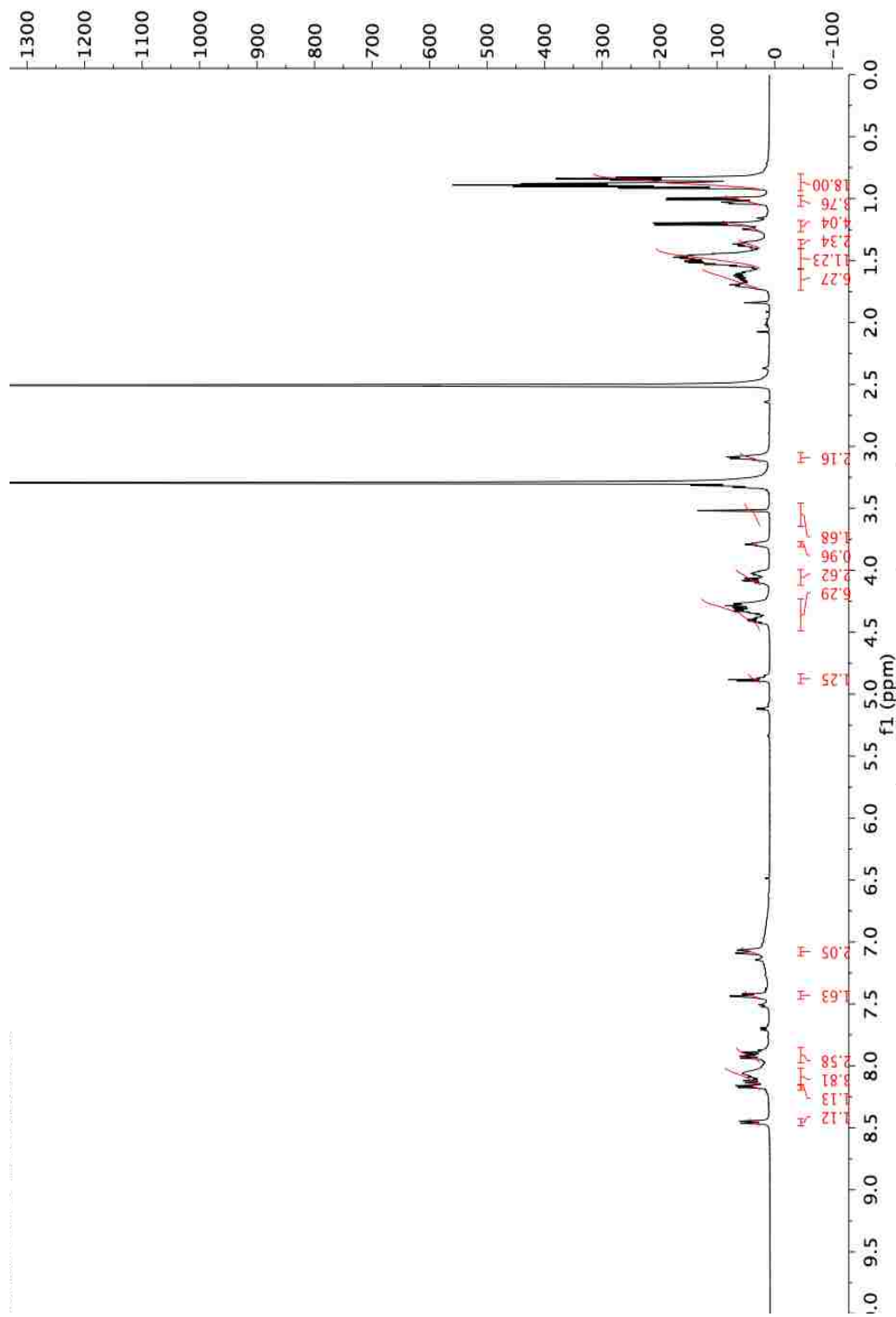
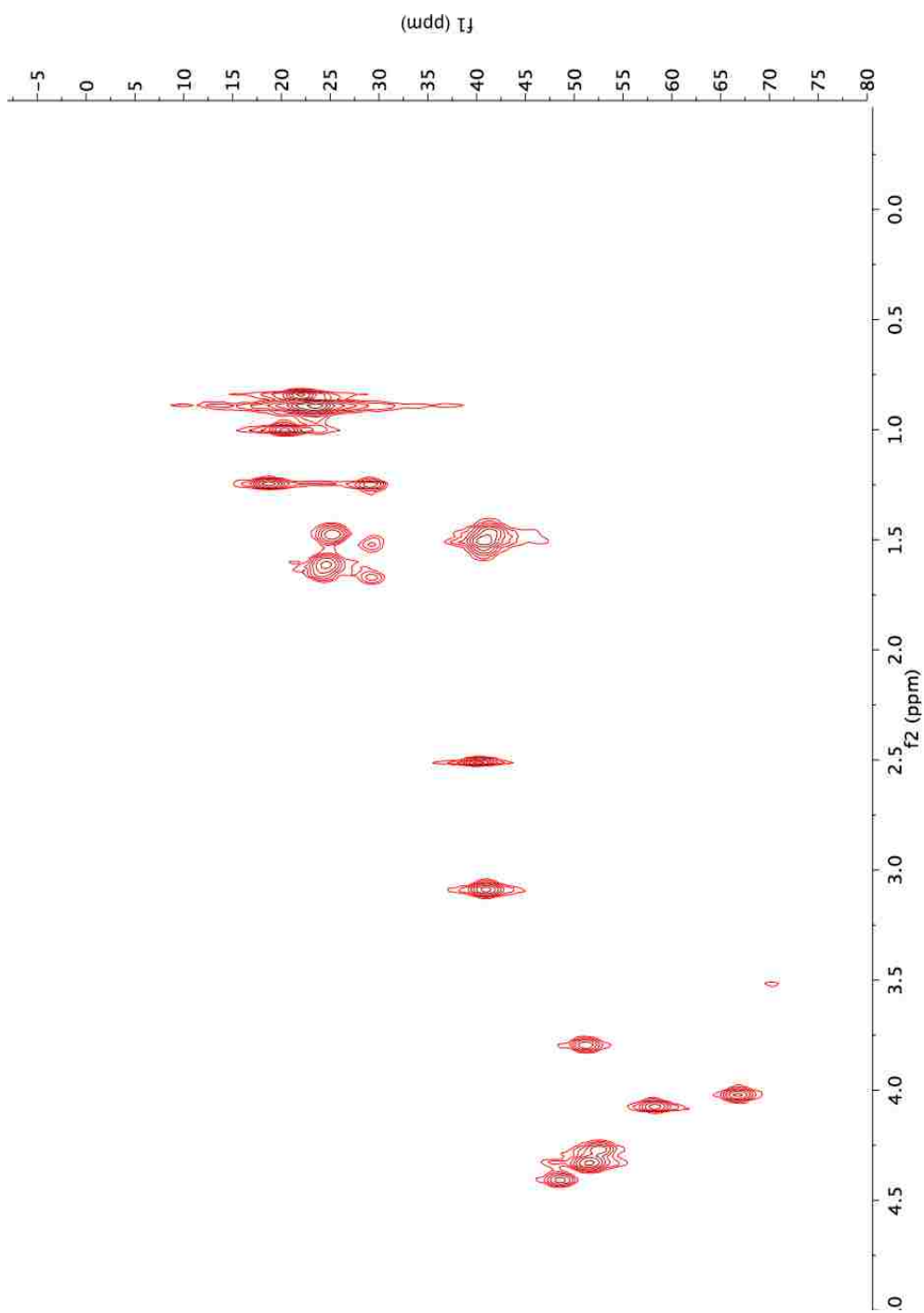


Figure A.32. <sup>1</sup>H NMR spectrum for peptide 2-9.

## HSQC NMR of Compounds in Chapter 2



**Figure A.33.** HSQC NMR spectrum for peptide 2-1



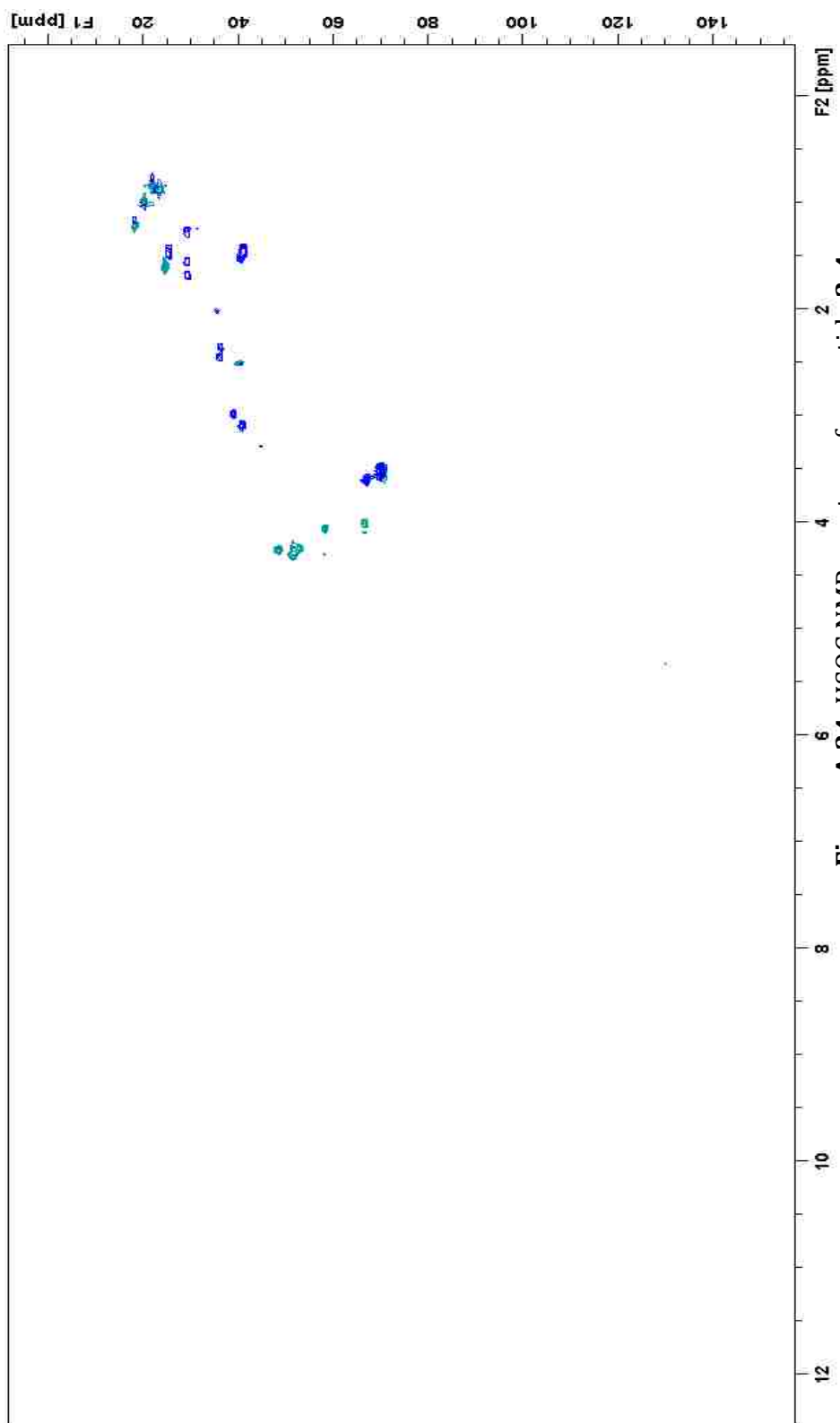


**Figure A.34.** HSQC NMR spectrum for peptide 2-4

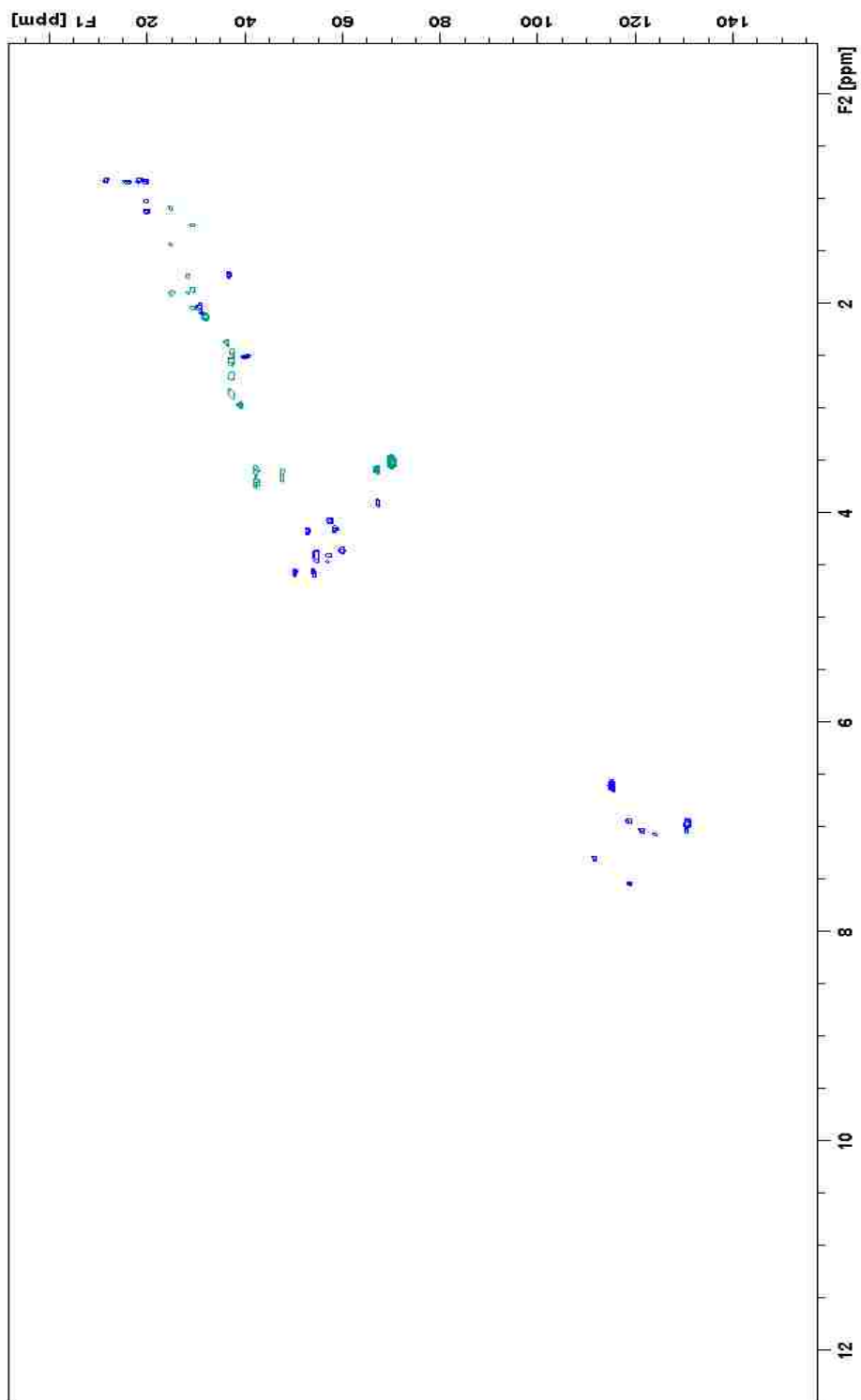
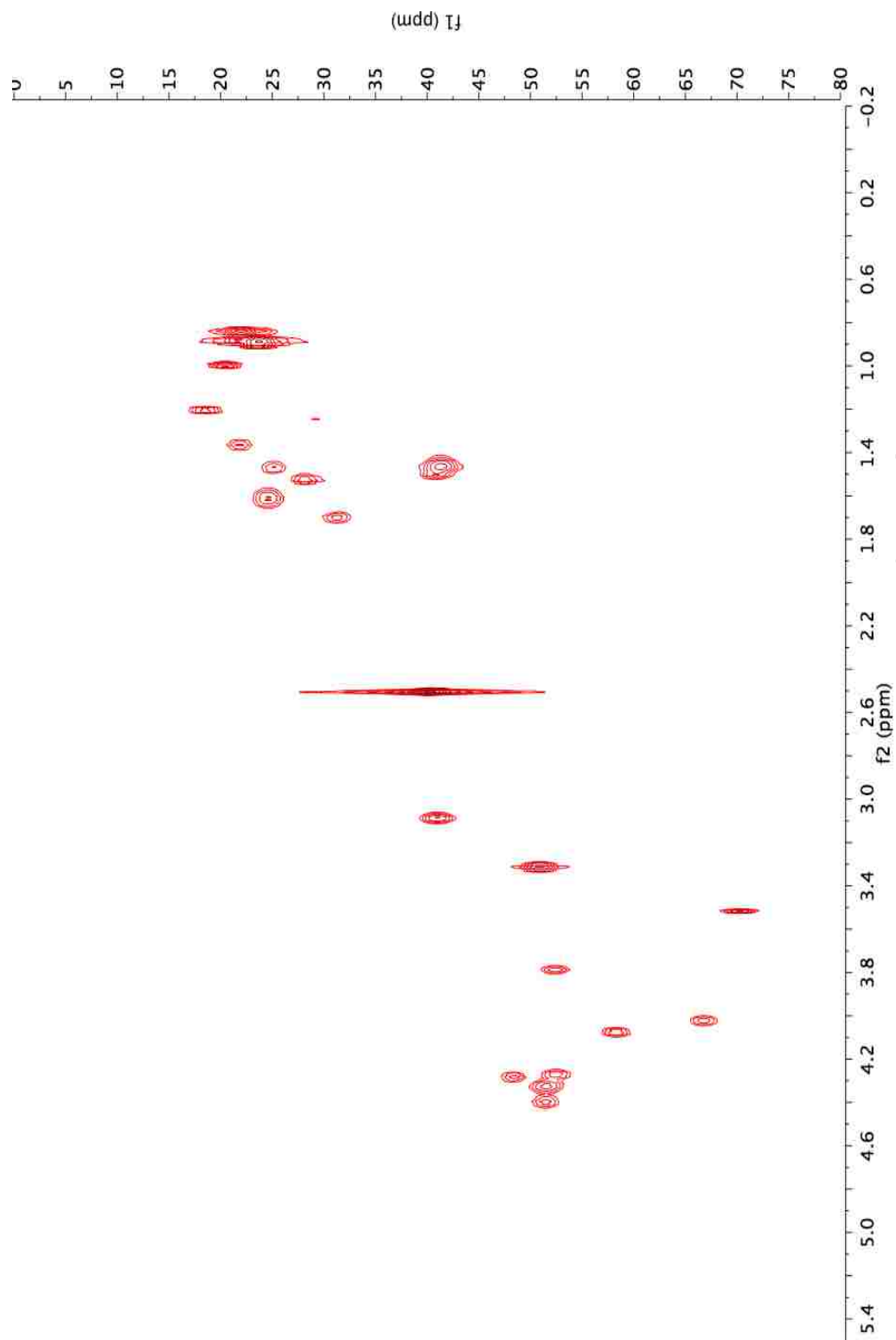


Figure A.35. HSQC NMR spectrum for peptide 2-5



**Figure A.36.** HSQC spectrum for peptide 2-9.

## SPR Sensograms of Compounds in Chapter 2

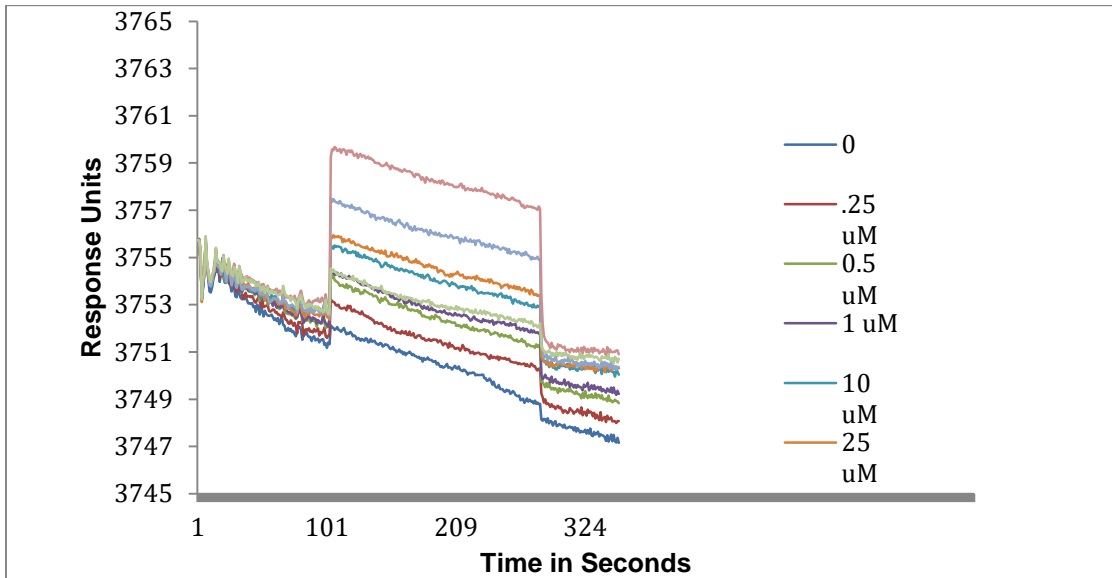


Figure A.37. SPR sensogram of peptide 2-1

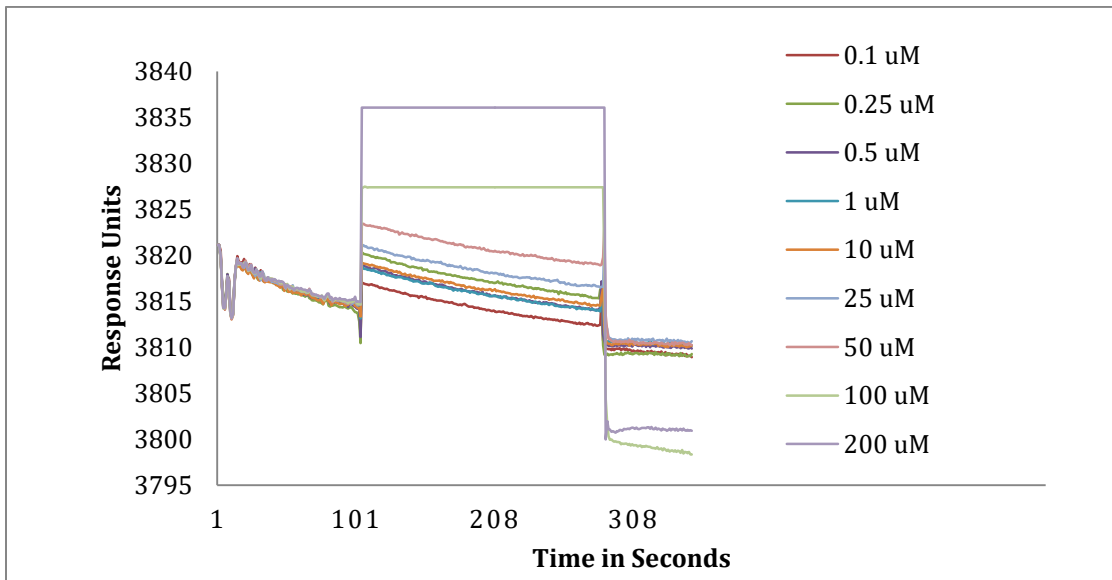
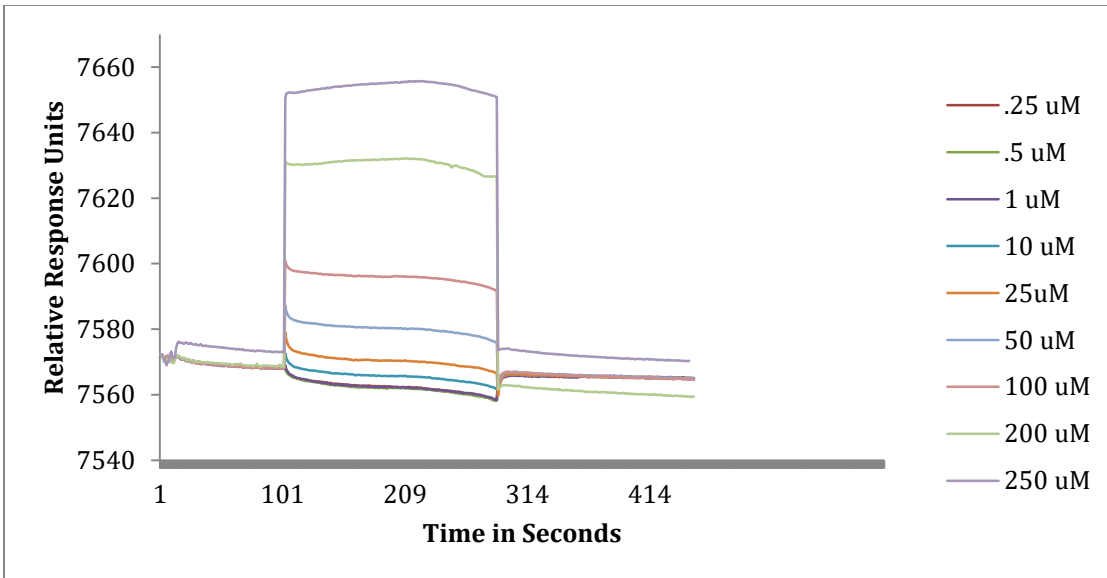
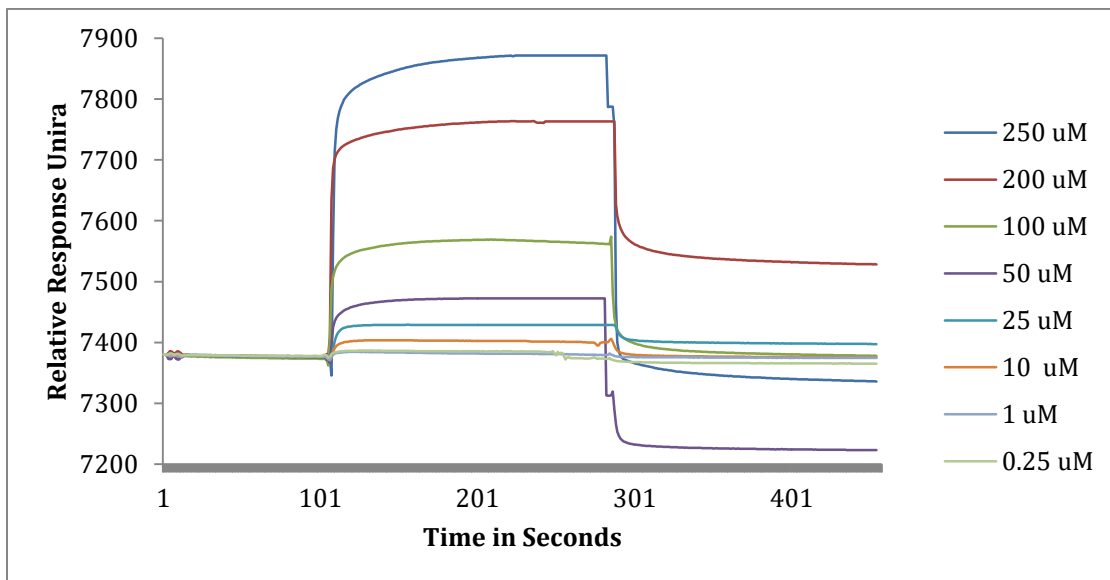


Figure A.38. SPR sensogram of peptide 2-3



**Figure A.39.** SPR sensogram of peptide 2-4



**Figure A.40.** SPR sensogram of peptide 2-5

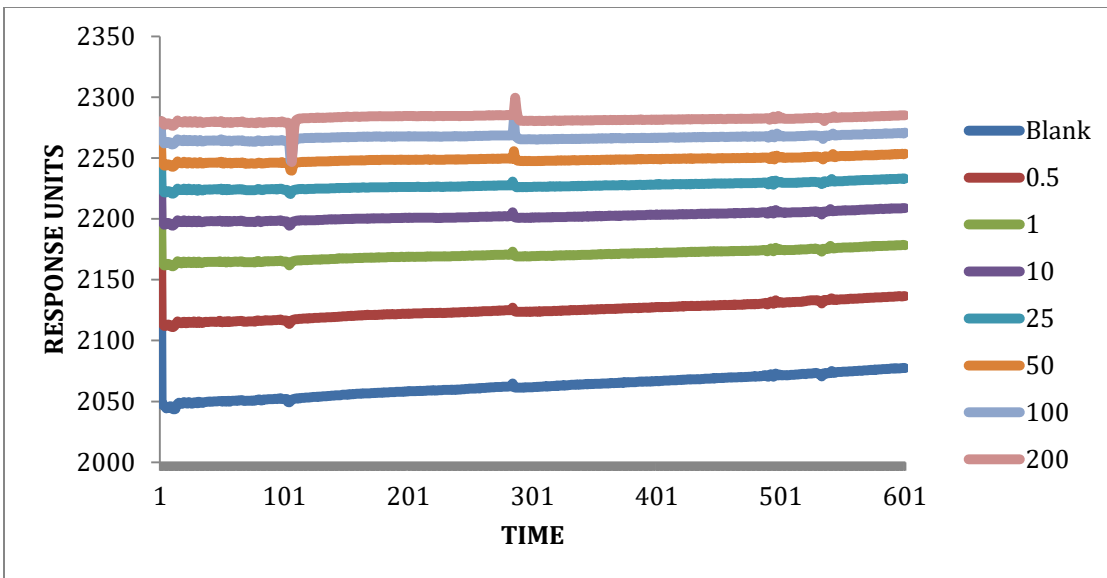


Figure A.41. SPR sensogram of peptide 2-6

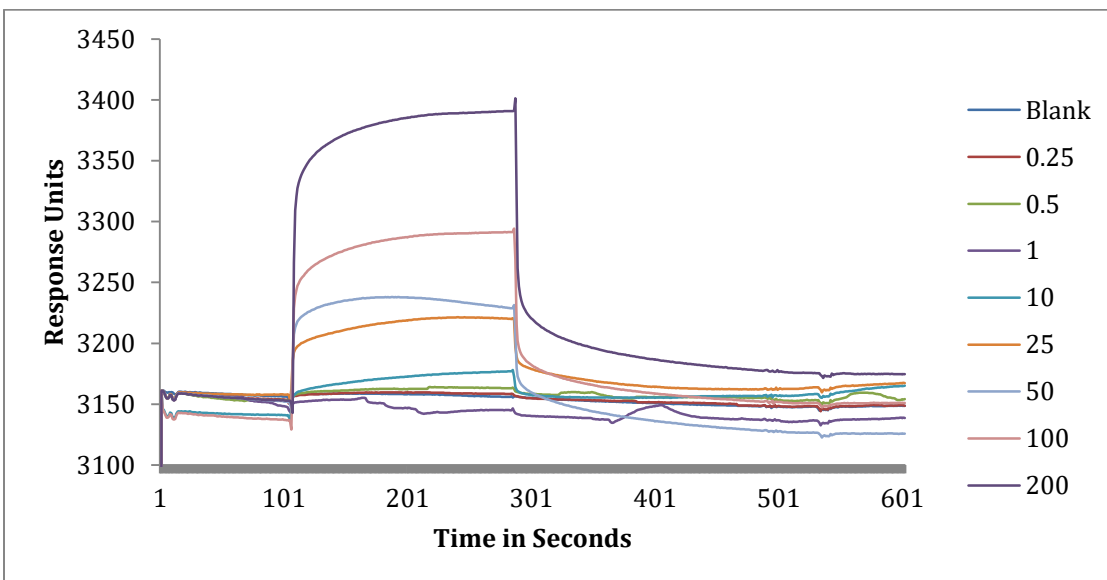


Figure A.42. SPR sensogram of peptide 2-7

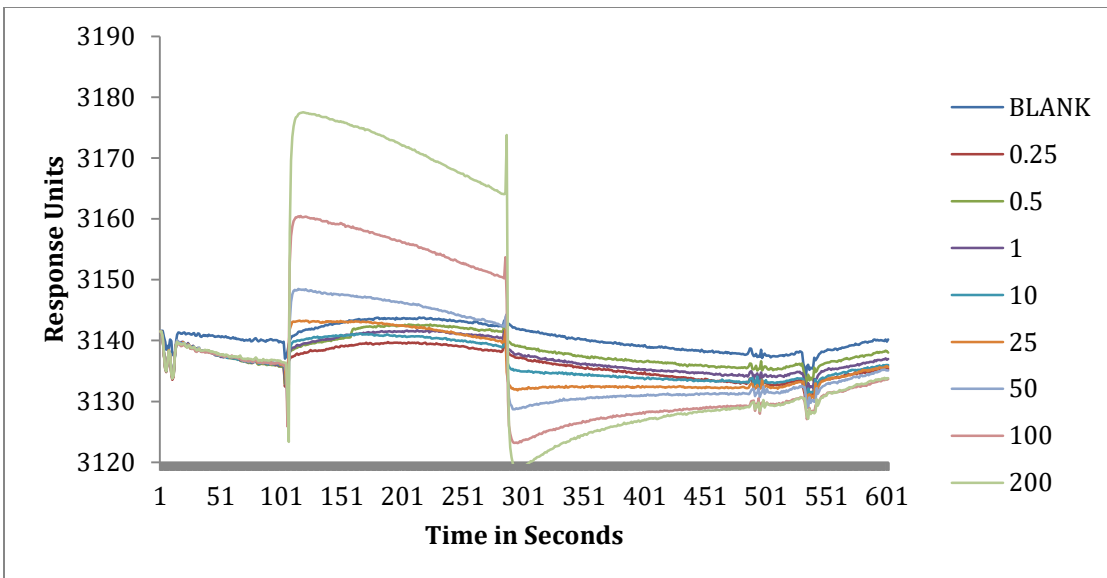


Figure A.43. SPR sensogram of peptide 2-8

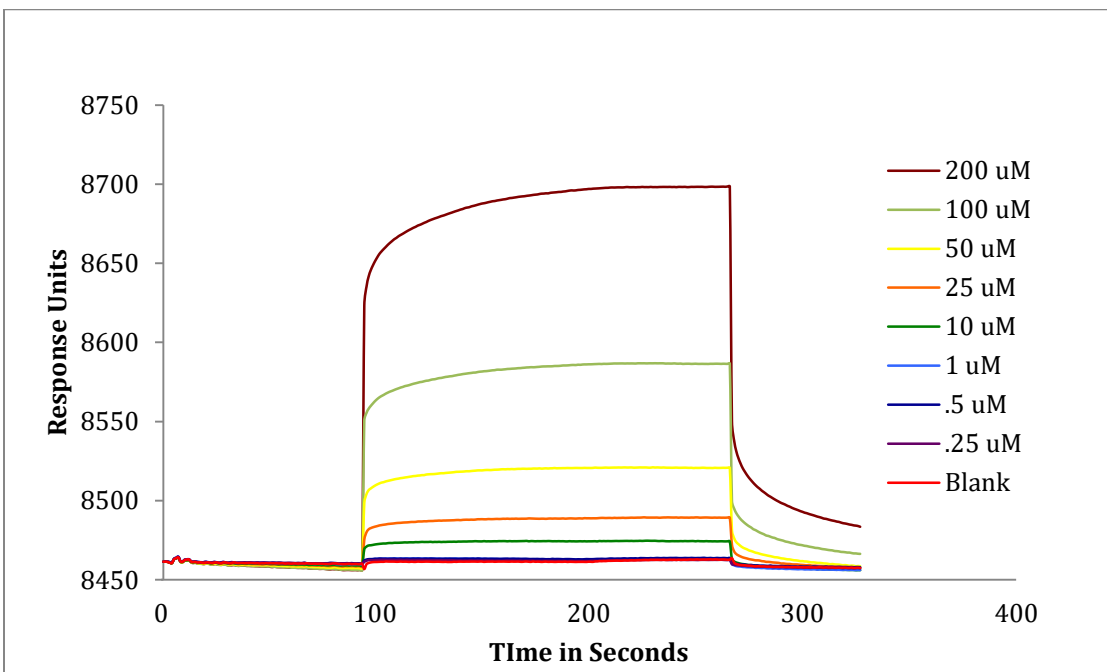
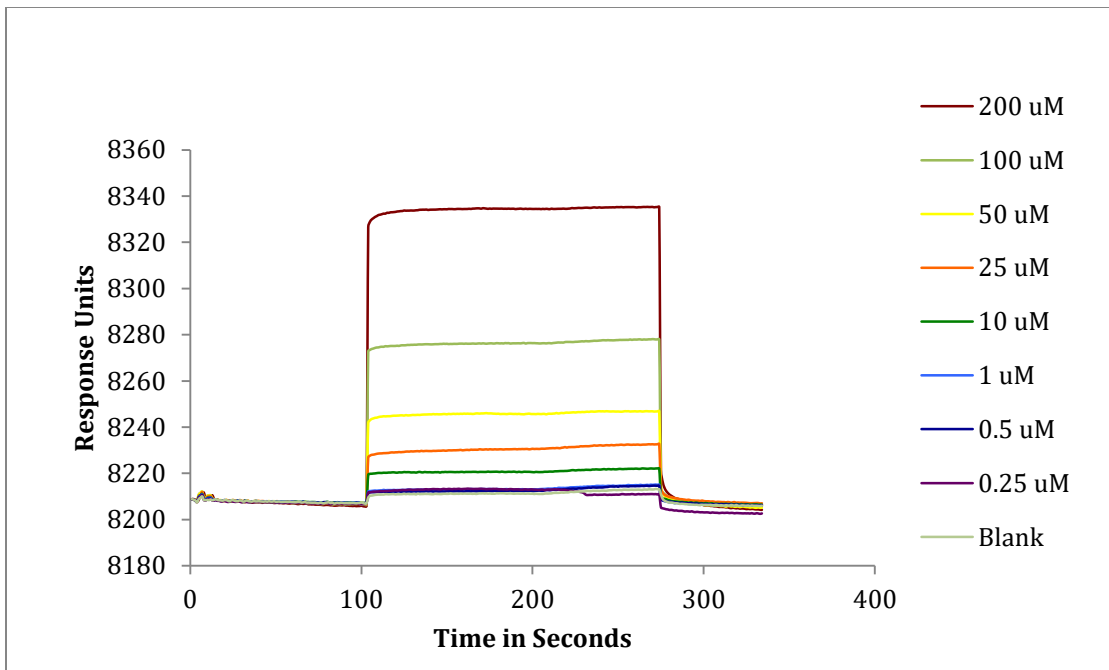


Figure A.44. SPR sensogram of peptide 2-9



**Figure A.45.** SPR sensogram of peptide cycloL1.1



## APPENDIX B: Characterization of Chapter 3 Compounds

### HPLC of Compounds in Chapter 3

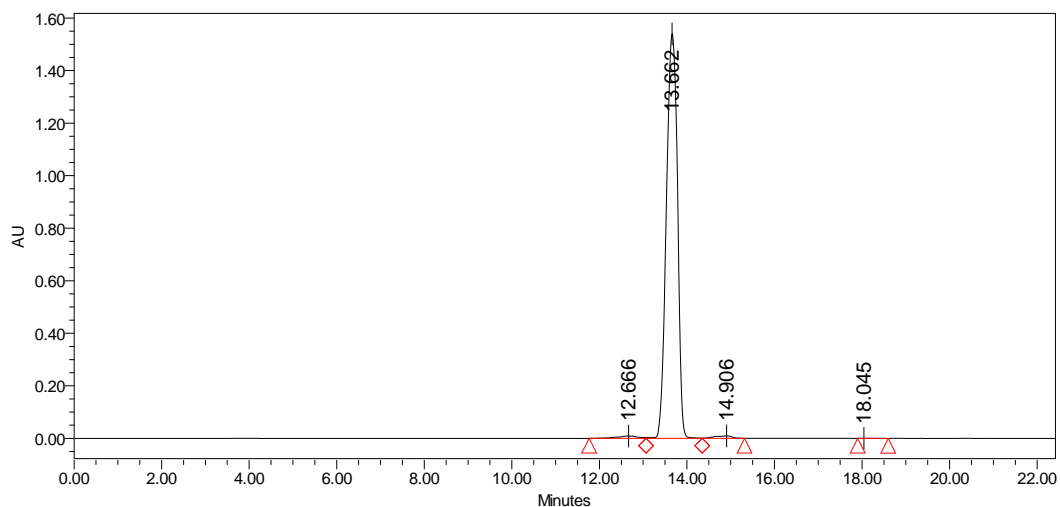


**Figure B.1:** The gradient used for chromatogram of 3-3 using RP-HPLC with a C18 column is listed below.

| # | Time (minutes) | Flow       | %A (H <sub>2</sub> O) | %B (ACN) |
|---|----------------|------------|-----------------------|----------|
| 0 | 0              | 4.0 ml/min | 50                    | 50       |
| 1 | 5              | 4.0 ml/min | 50                    | 50       |
| 2 | 8              | 4.0 ml/min | 10                    | 90       |
| 3 | 18             | 4.0 ml/min | 0                     | 100      |
| 4 | 20             | 4.0 ml/min | 50                    | 50       |
| 5 | 25             | 4.0 ml/min | 50                    | 50       |
|   |                |            |                       |          |

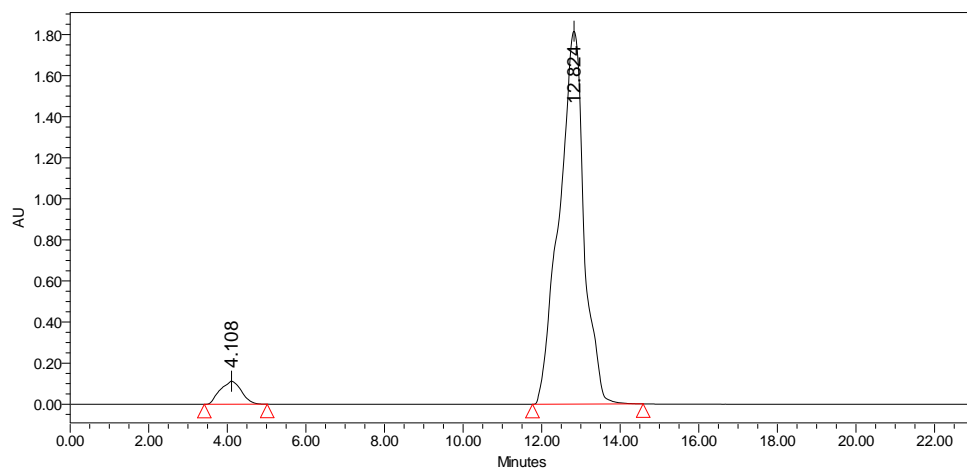


**Figure B.2:** The gradient used for chromatogram of 3-12 using RP-HPLC with a C18 column is listed below.

| <i>Table 1 HPLC Gradient for Conjugate 3-12</i> |                       |                   |                            |                 |
|---|-----------------------|-------------------|----------------------------|-----------------|
| <i>#</i>  | <i>Time (minutes)</i> | <i>Flow</i>       | <i>%A (H<sub>2</sub>O)</i> | <i>%B (ACN)</i> |
| <i>0</i>  | <i>0</i>              | <i>4.0 ml/min</i> | <i>50</i>                  | <i>50</i>       |
| <i>1</i>  | <i>5</i>              | <i>4.0 ml/min</i> | <i>50</i>                  | <i>50</i>       |
| <i>2</i>  | <i>8</i>              | <i>4.0 ml/min</i> | <i>10</i>                  | <i>90</i>       |
| <i>3</i>  | <i>18</i>             | <i>4.0 ml/min</i> | <i>0</i>                   | <i>100</i>      |
| <i>4</i>  | <i>20</i>             | <i>4.0 ml/min</i> | <i>50</i>                  | <i>50</i>       |
| <i>5</i>  | <i>25</i>             | <i>4.0 ml/min</i> | <i>50</i>                  | <i>50</i>       |
|   |                       |                   |                            |                 |

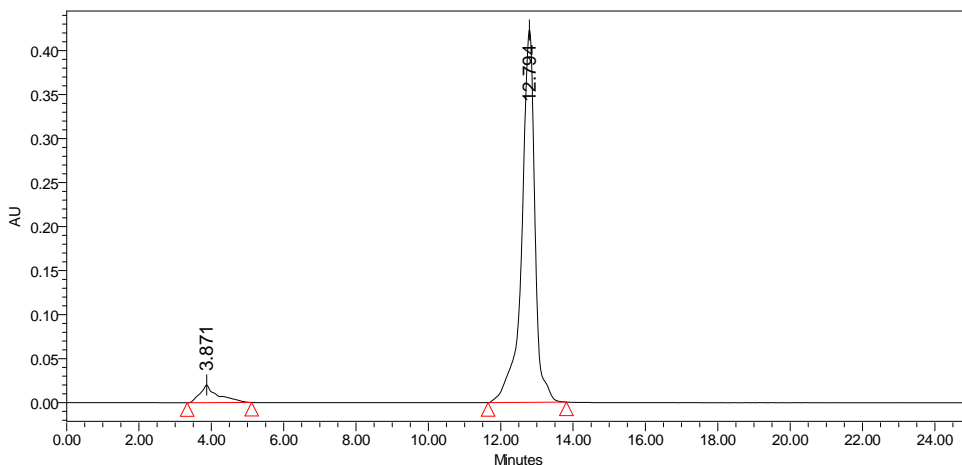


**Figure B.3:** The gradient used for chromatogram of 3-13 using RP-HPLC with a C18 column is listed below.

| <i>Table 1 HPLC Gradient for Conjugate 3-13</i> |                       |                   |                            |                 |
|---|-----------------------|-------------------|----------------------------|-----------------|
| <i>#</i>  | <i>Time (minutes)</i> | <i>Flow</i>       | <i>%A (H<sub>2</sub>O)</i> | <i>%B (ACN)</i> |
| <i>0</i>  | <i>0</i>              | <i>4.0 ml/min</i> | <i>50</i>                  | <i>50</i>       |
| <i>1</i>  | <i>5</i>              | <i>4.0 ml/min</i> | <i>50</i>                  | <i>50</i>       |
| <i>2</i>  | <i>8</i>              | <i>4.0 ml/min</i> | <i>10</i>                  | <i>90</i>       |
| <i>3</i>  | <i>18</i>             | <i>4.0 ml/min</i> | <i>0</i>                   | <i>100</i>      |
| <i>4</i>  | <i>20</i>             | <i>4.0 ml/min</i> | <i>50</i>                  | <i>50</i>       |
| <i>5</i>  | <i>25</i>             | <i>4.0 ml/min</i> | <i>50</i>                  | <i>50</i>       |
|   |                       |                   |                            |                 |

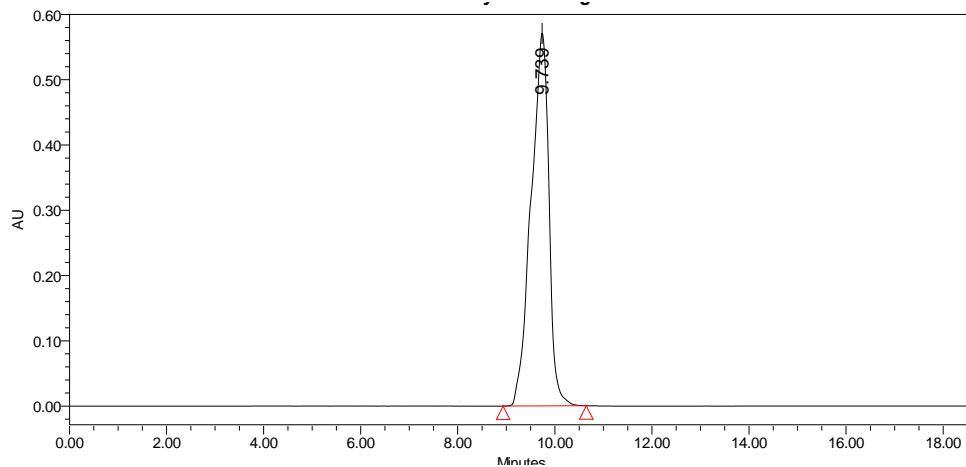


**Figure B.4:** The gradient used for chromatogram of 3-14 using RP-HPLC with a C18 column is listed below.

| <i>Table 1 HPLC Gradient for Conjugate 3-14</i> |                       |                   |                            |                 |
|---|-----------------------|-------------------|----------------------------|-----------------|
| <i>#</i>  | <i>Time (minutes)</i> | <i>Flow</i>       | <i>%A (H<sub>2</sub>O)</i> | <i>%B (ACN)</i> |
| <i>0</i>  | <i>0</i>              | <i>4.0 ml/min</i> | <i>50</i>                  | <i>50</i>       |
| <i>1</i>  | <i>5</i>              | <i>4.0 ml/min</i> | <i>50</i>                  | <i>50</i>       |
| <i>2</i>  | <i>8</i>              | <i>4.0 ml/min</i> | <i>10</i>                  | <i>90</i>       |
| <i>3</i>  | <i>18</i>             | <i>4.0 ml/min</i> | <i>0</i>                   | <i>100</i>      |
| <i>4</i>  | <i>20</i>             | <i>4.0 ml/min</i> | <i>50</i>                  | <i>50</i>       |
| <i>5</i>  | <i>25</i>             | <i>4.0 ml/min</i> | <i>50</i>                  | <i>50</i>       |
|   |                       |                   |                            |                 |

### MALDI of Compounds in Chapter 3

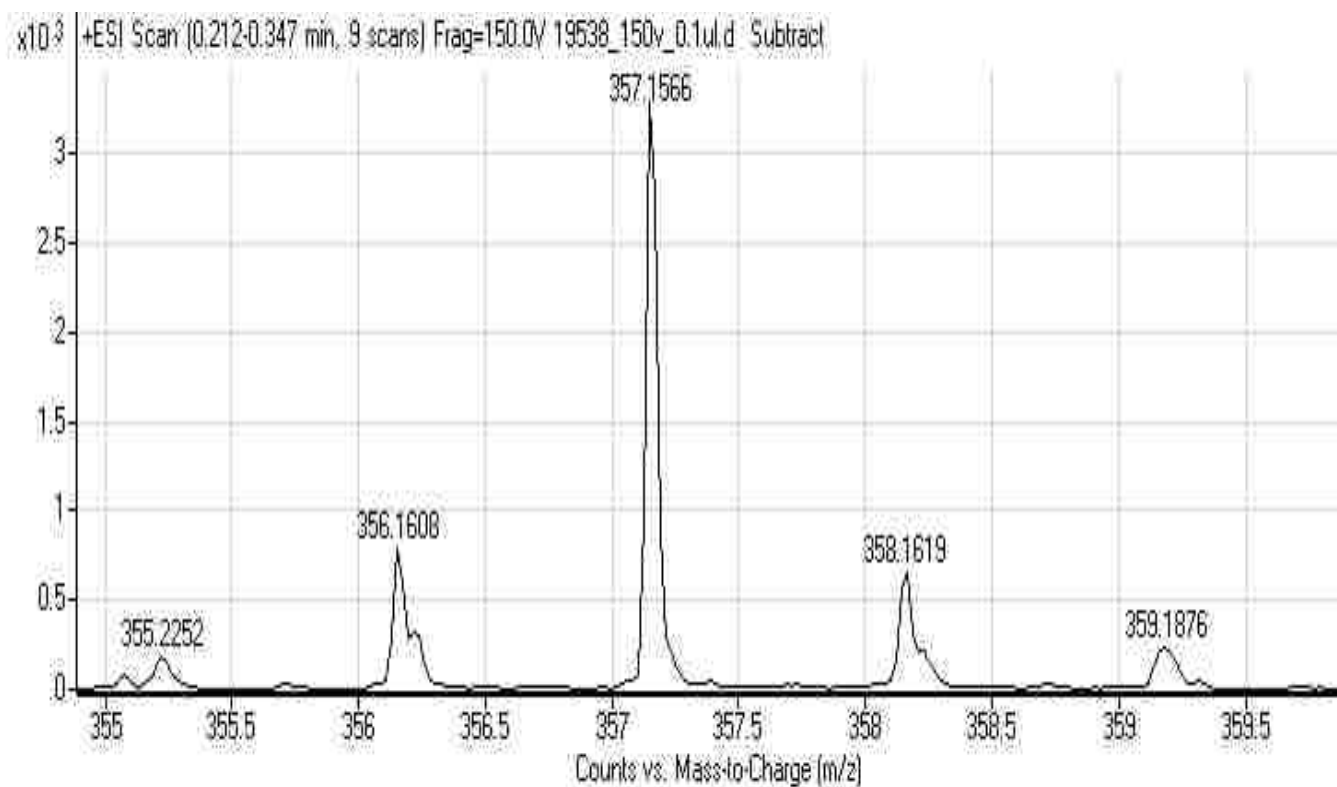


**Figure B.5.** ESI spectrum of BODIPY 3-3 .

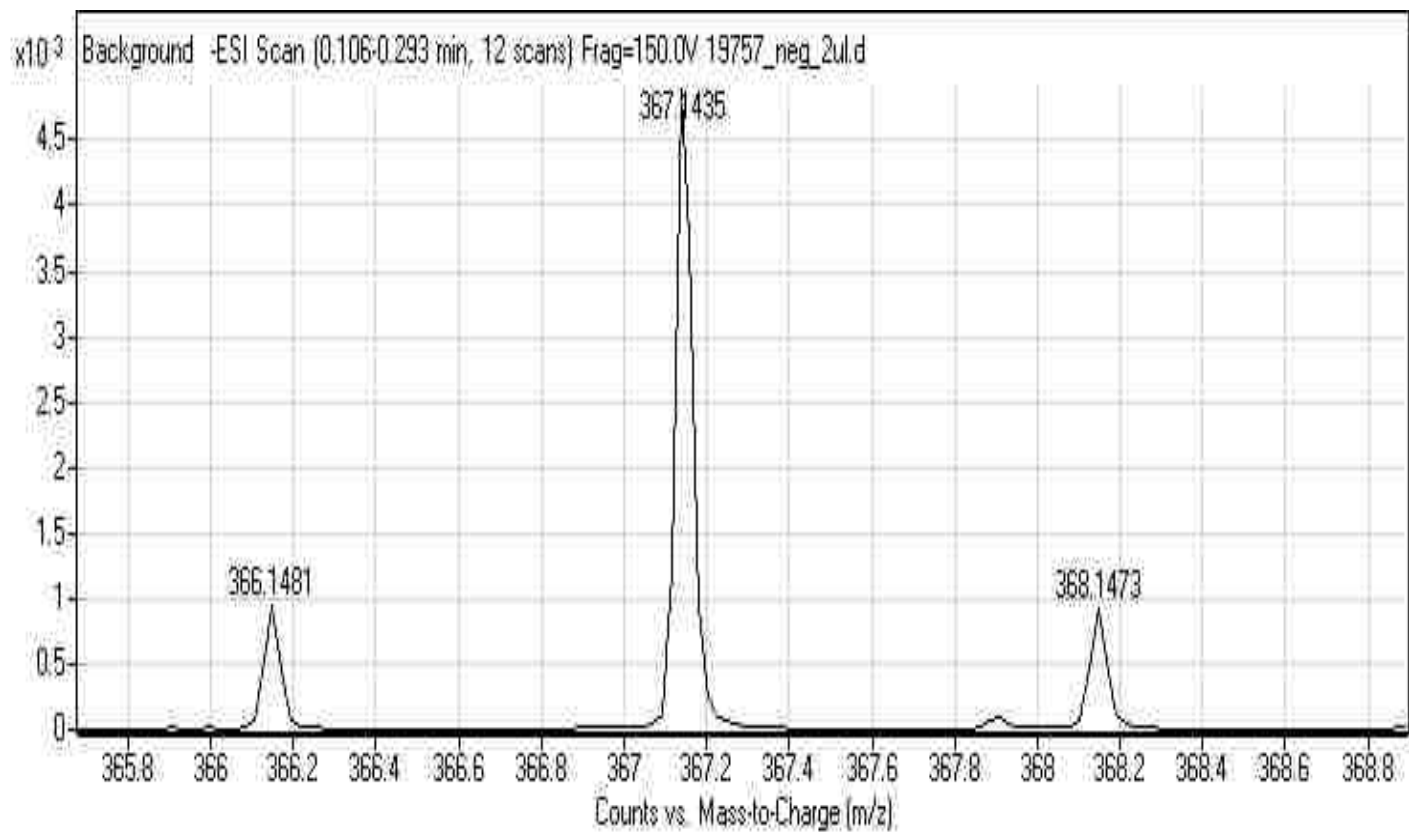


**Figure B.6.** ESI spectrum of BODIPY 3-4 .

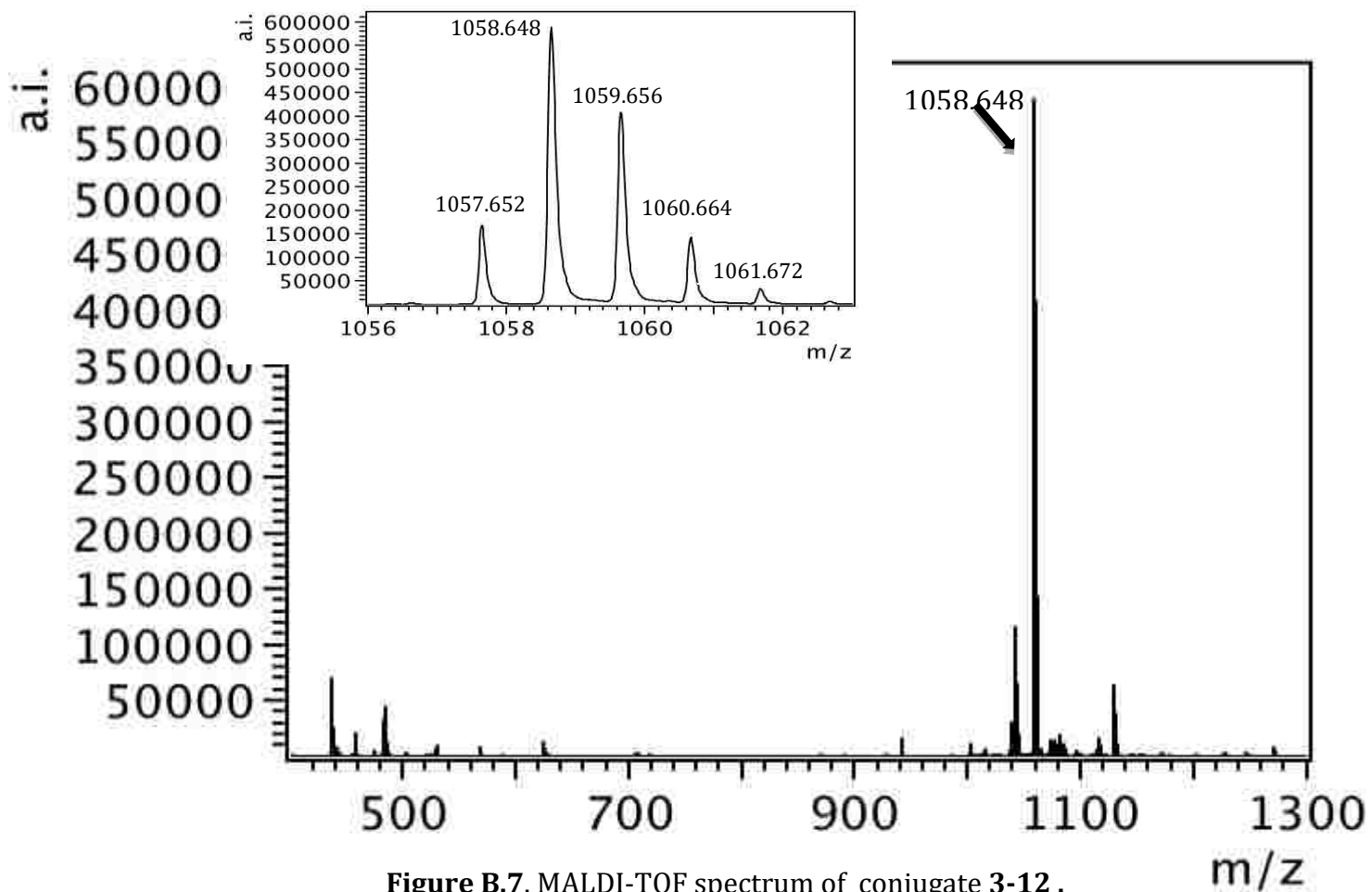
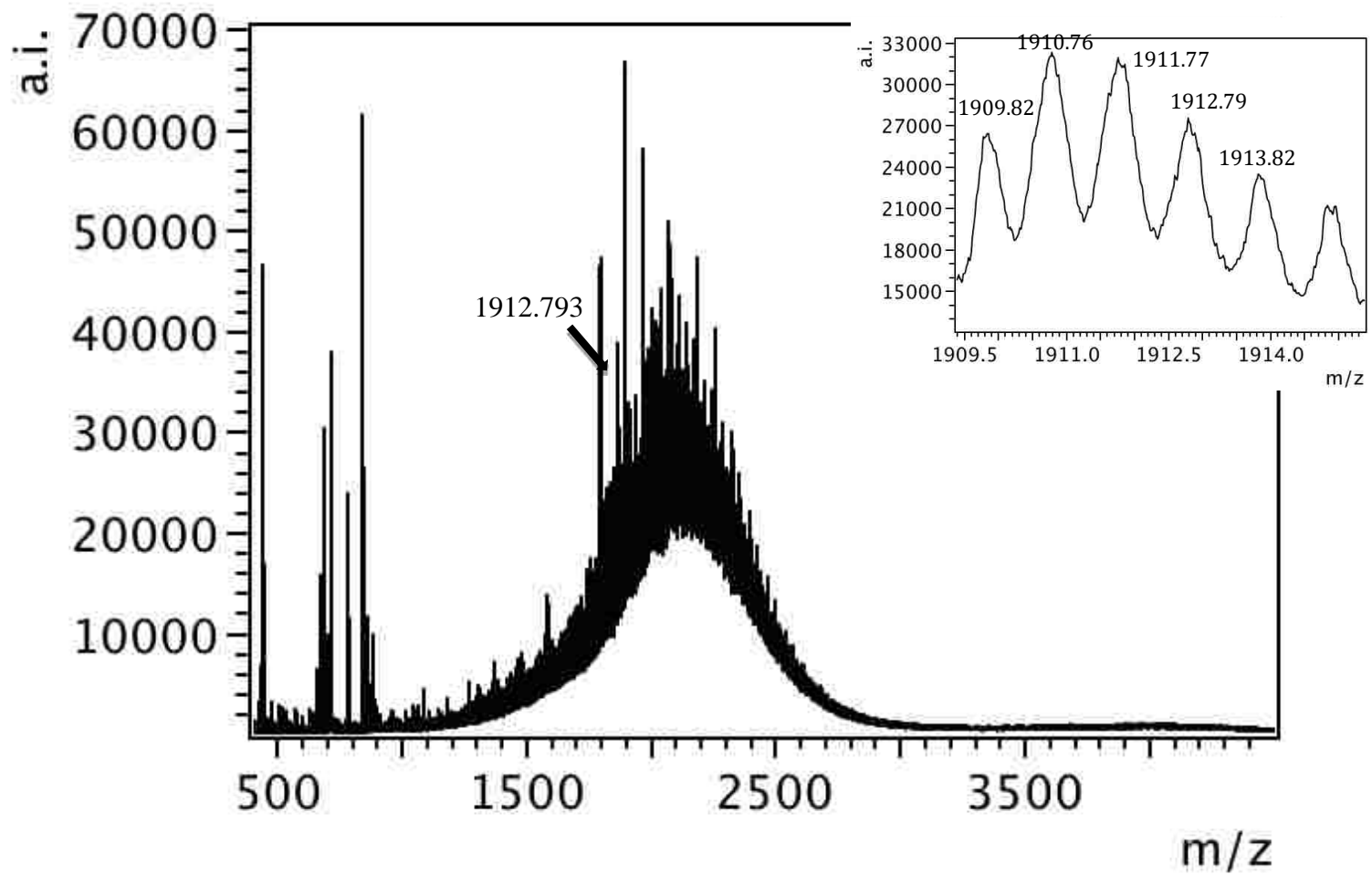
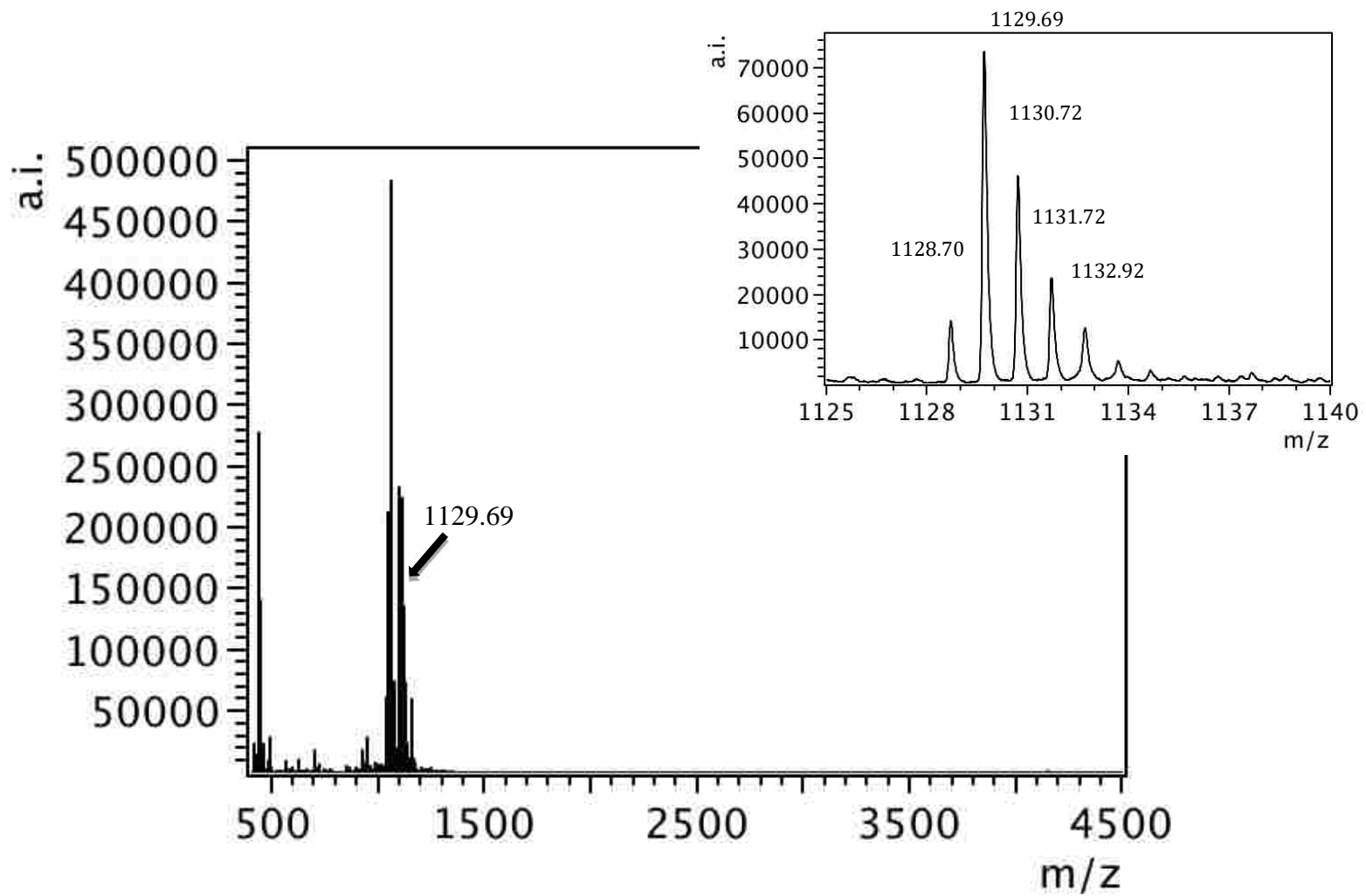


Figure B.7. MALDI-TOF spectrum of conjugate 3-12 .



**Figure B.8.** MALDI spectrum of conjugate 3-13 .





**Figure B.9.** MALDI spectrum conjugate 3-14 .

MALDI MSMS of Compounds in Chapter 3

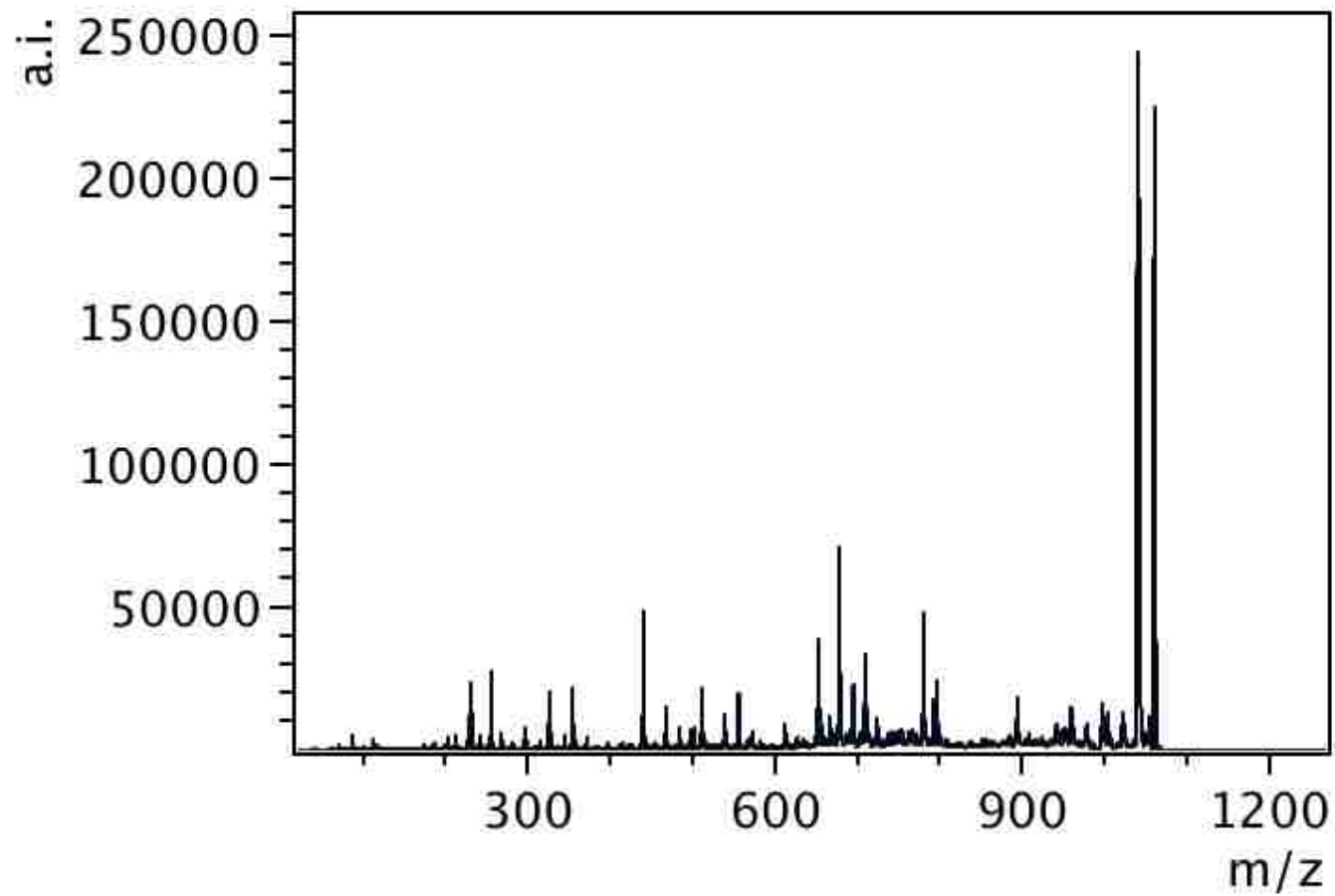
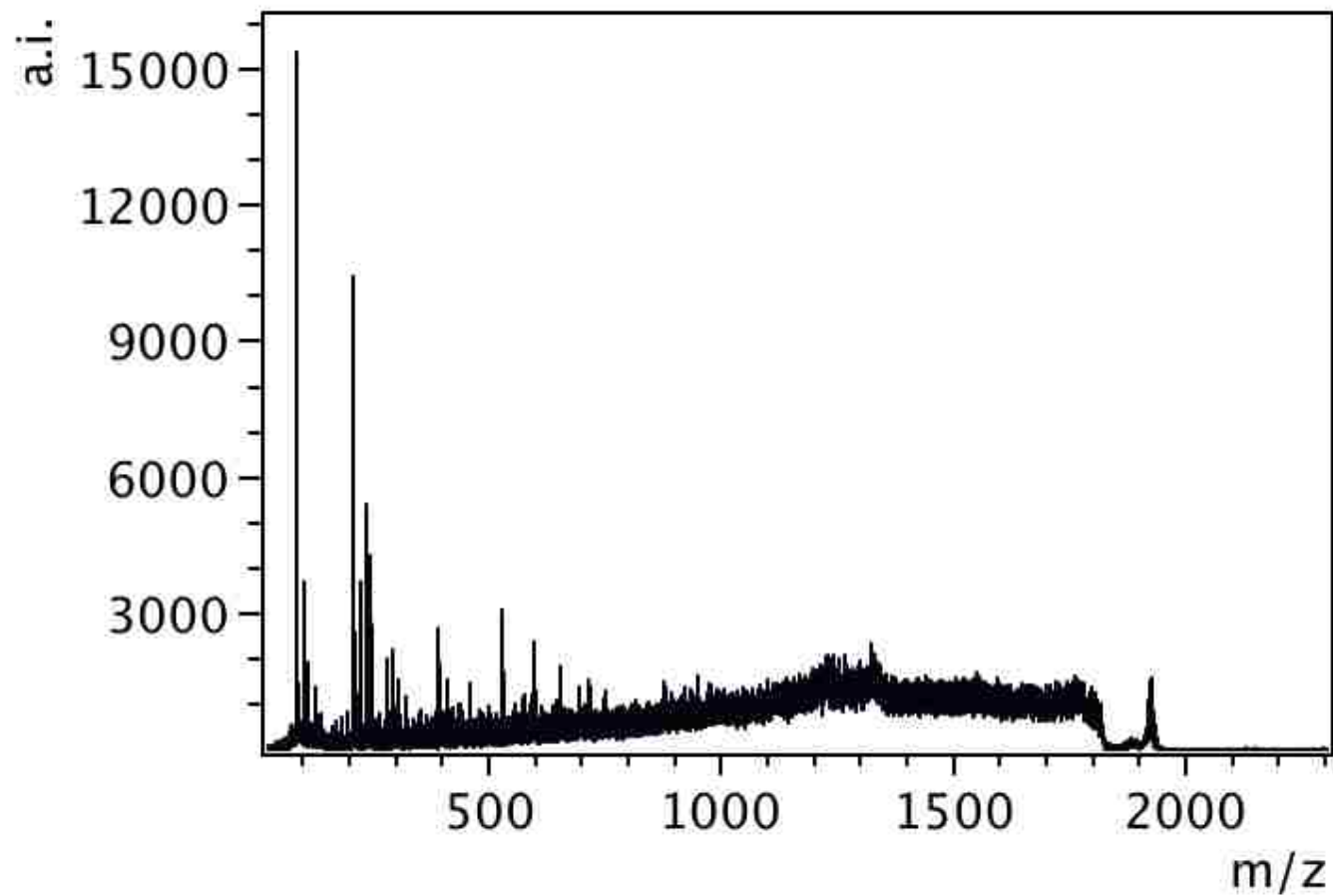
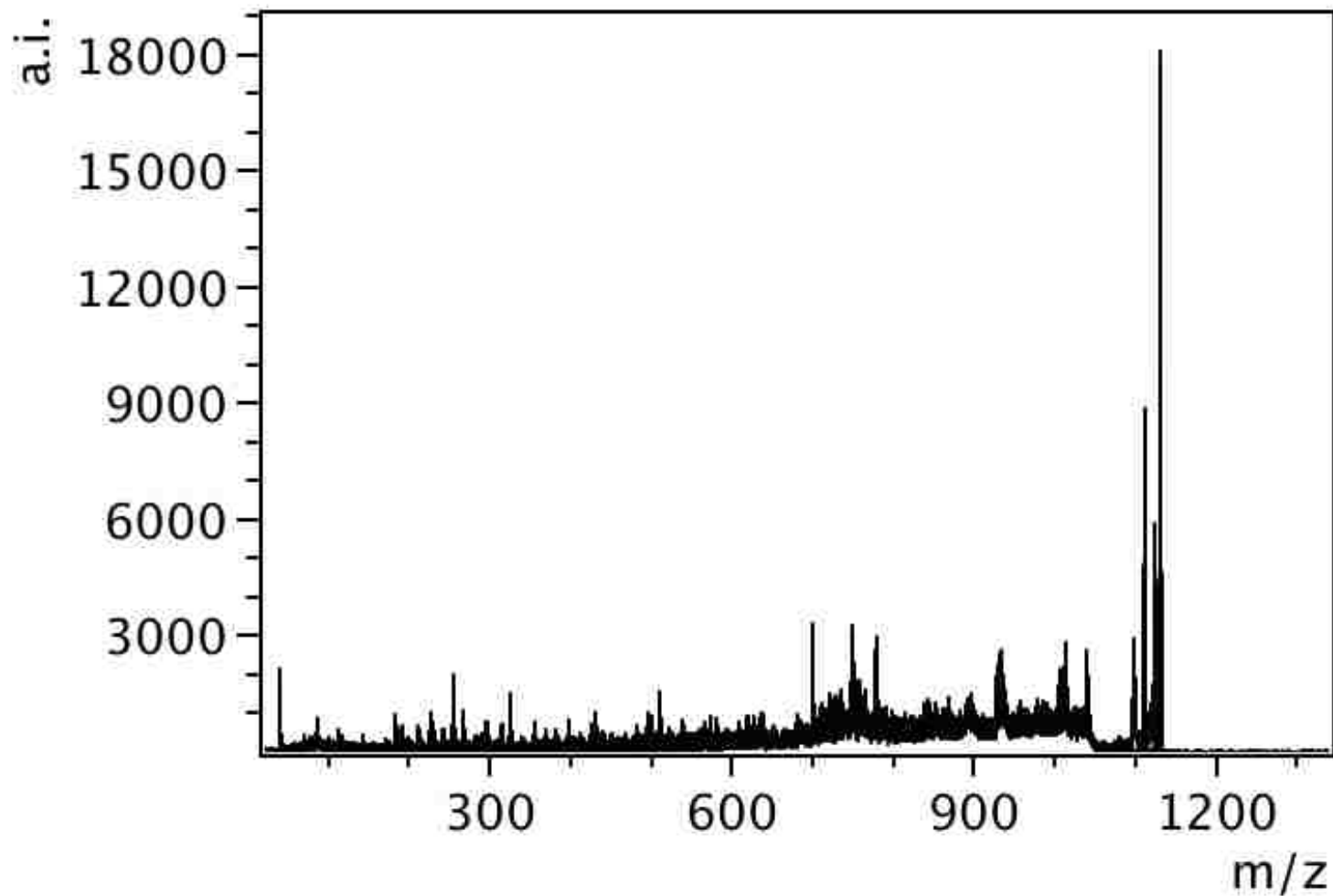


Figure B.10. MALDI MSMS spectrum of conjugate 3-12.



**Figure B.11.** MALDI MSMS spectrum of conjugate 3-13.



**Figure B.12.** MALDI MSMS spectrum of conjugate 3-14.

### Proton NMR of Compounds in Chapter 3

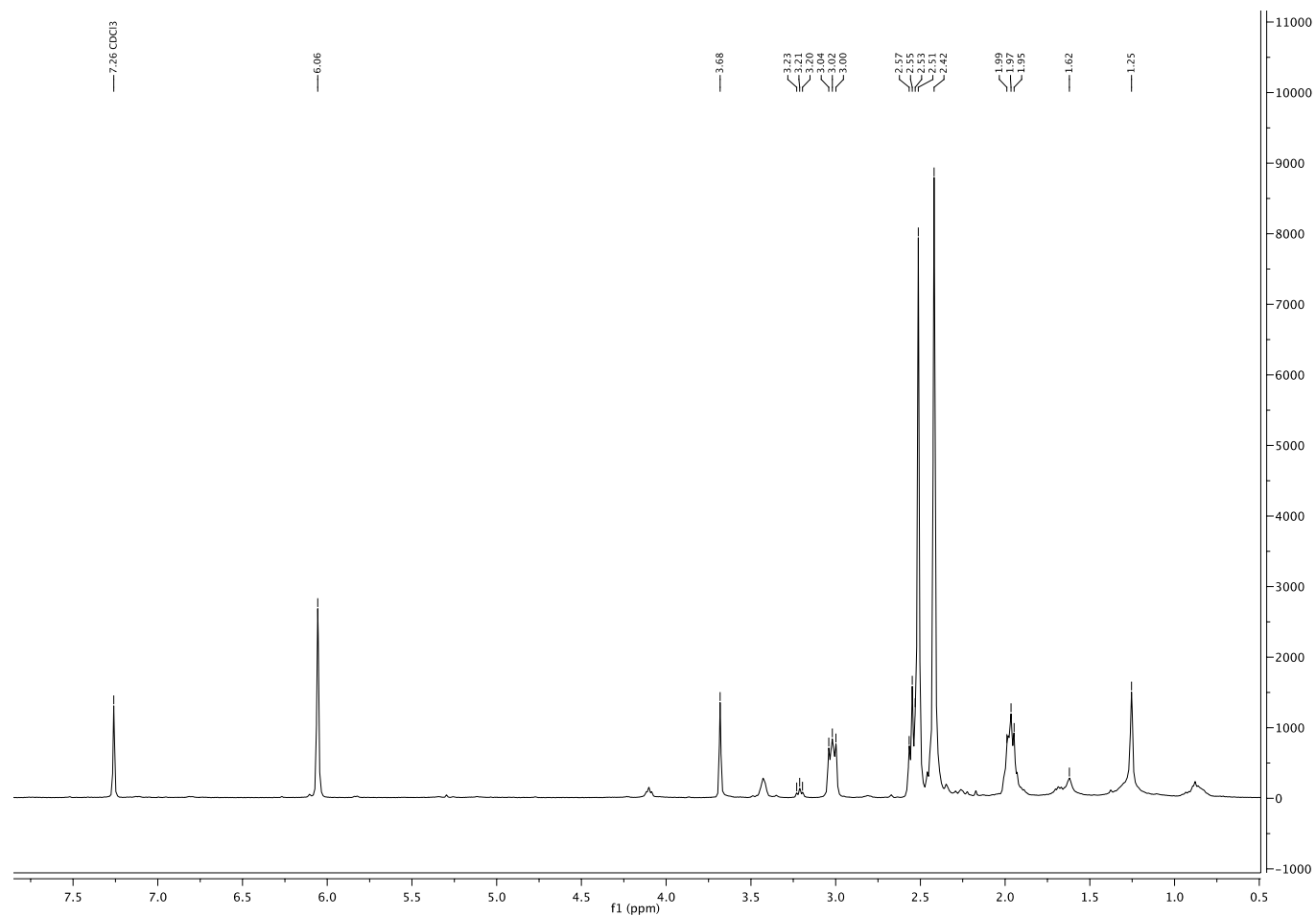


**Figure B.14.** Proton NMR spectrum of BODIPY 3-3 .

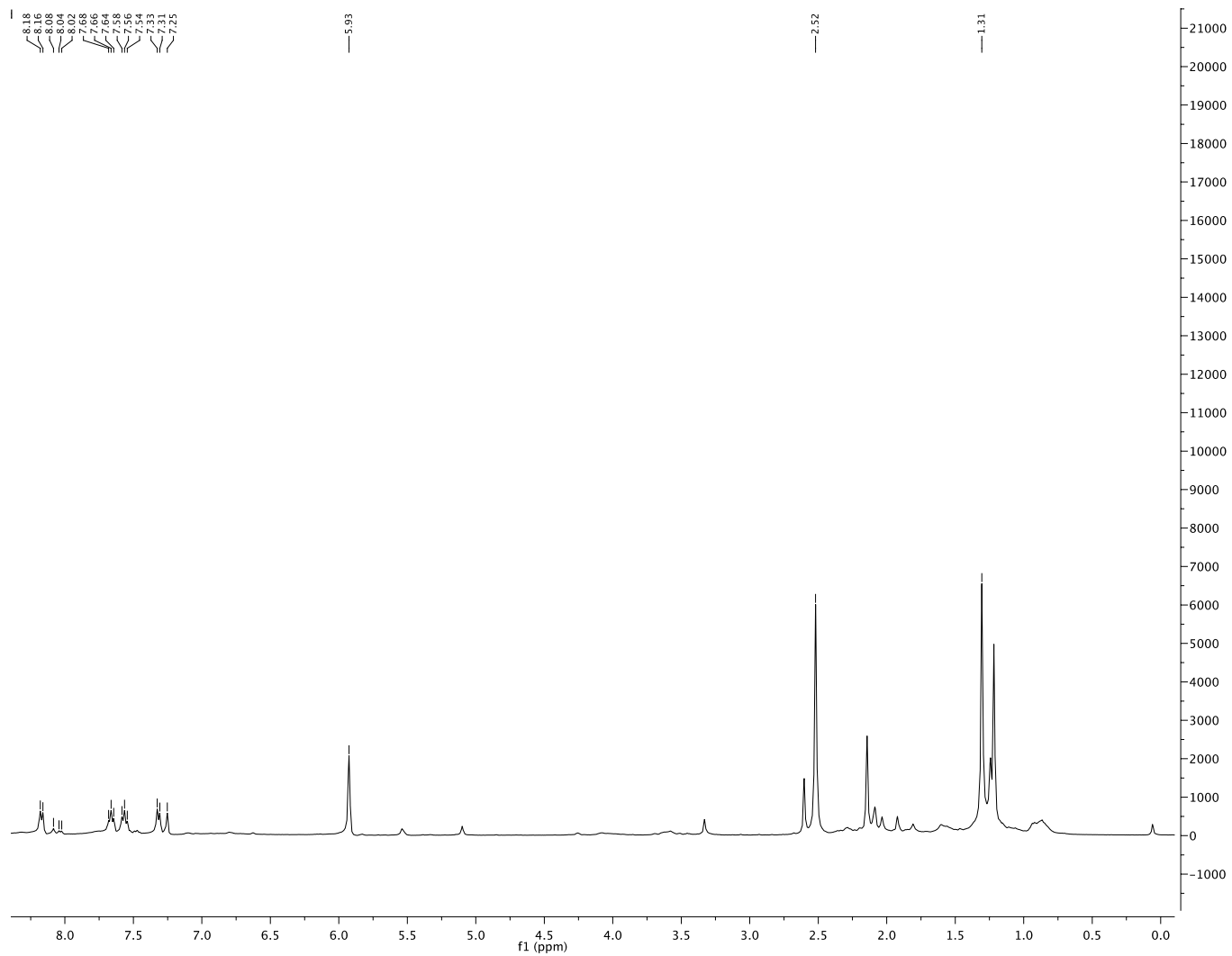


**Figure B.15.** Proton NMR spectrum of BODIPY 3-4.

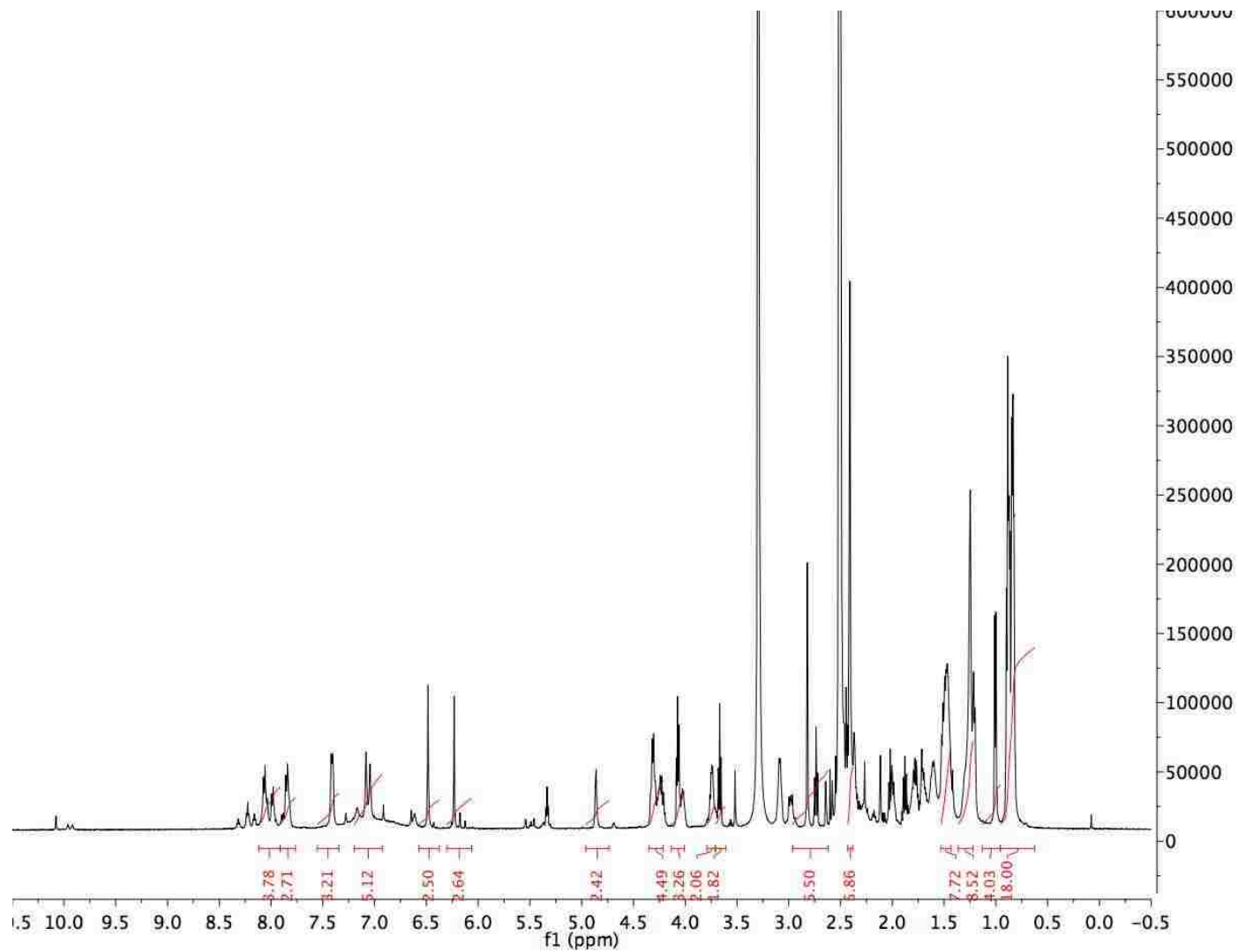


**Figure B.16.** Proton NMR spectrum of conjugate 3-12.

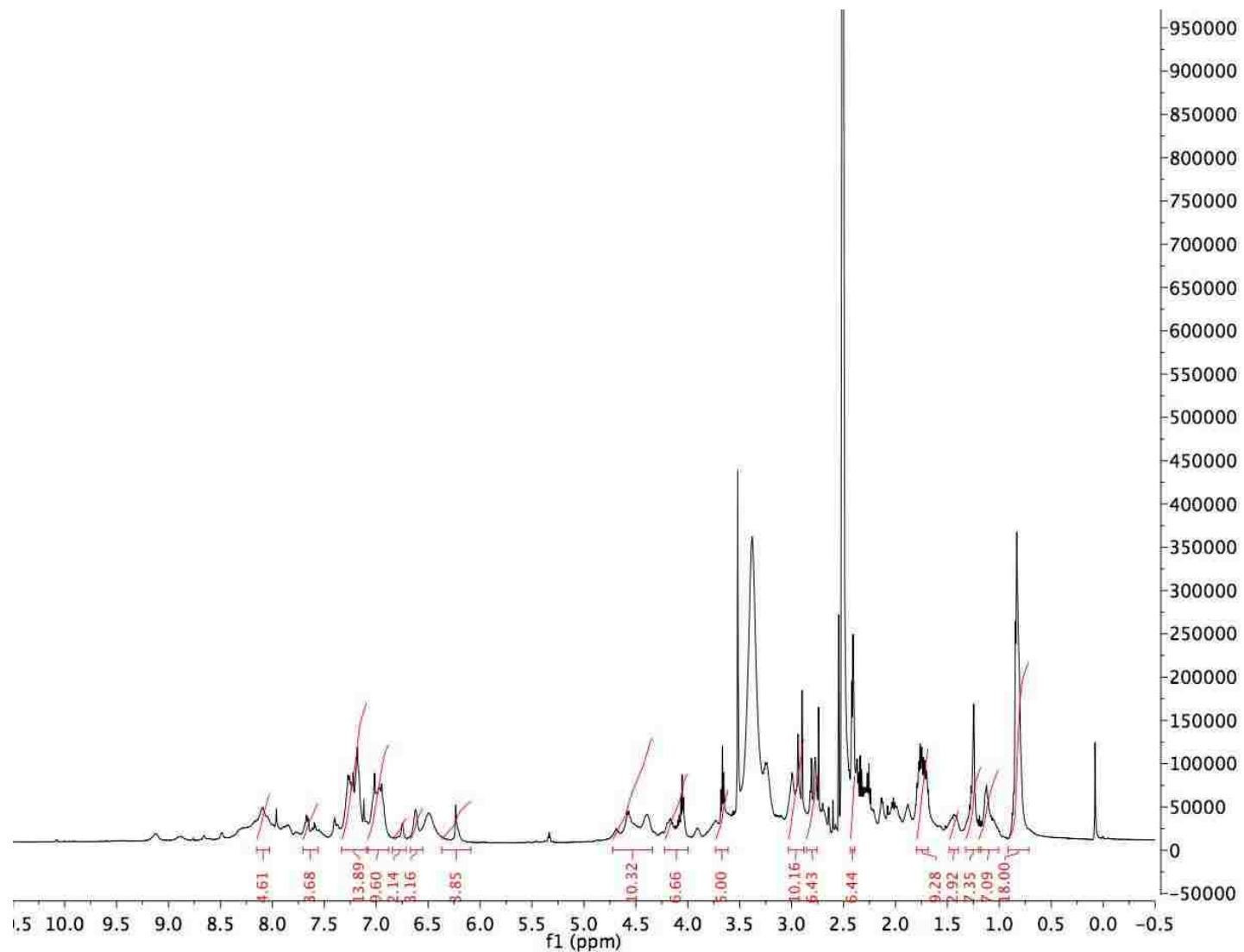


**Figure B.17.** Proton NMR spectrum of conjugate 3-13.



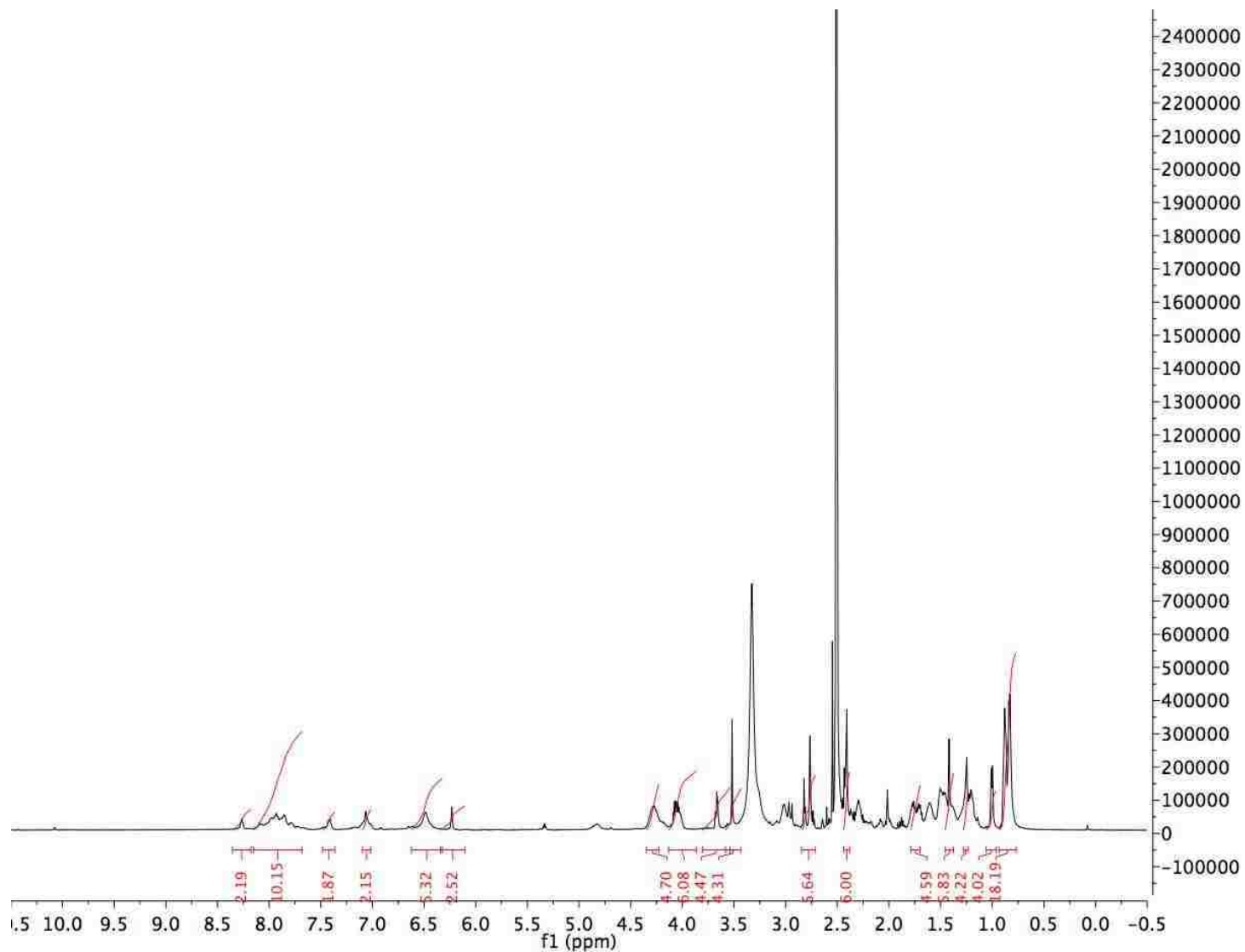


**Figure B.18.** Proton NMR spectrum of conjugate 3-14 .

### HSQC NMR of Compounds in Chapter 3

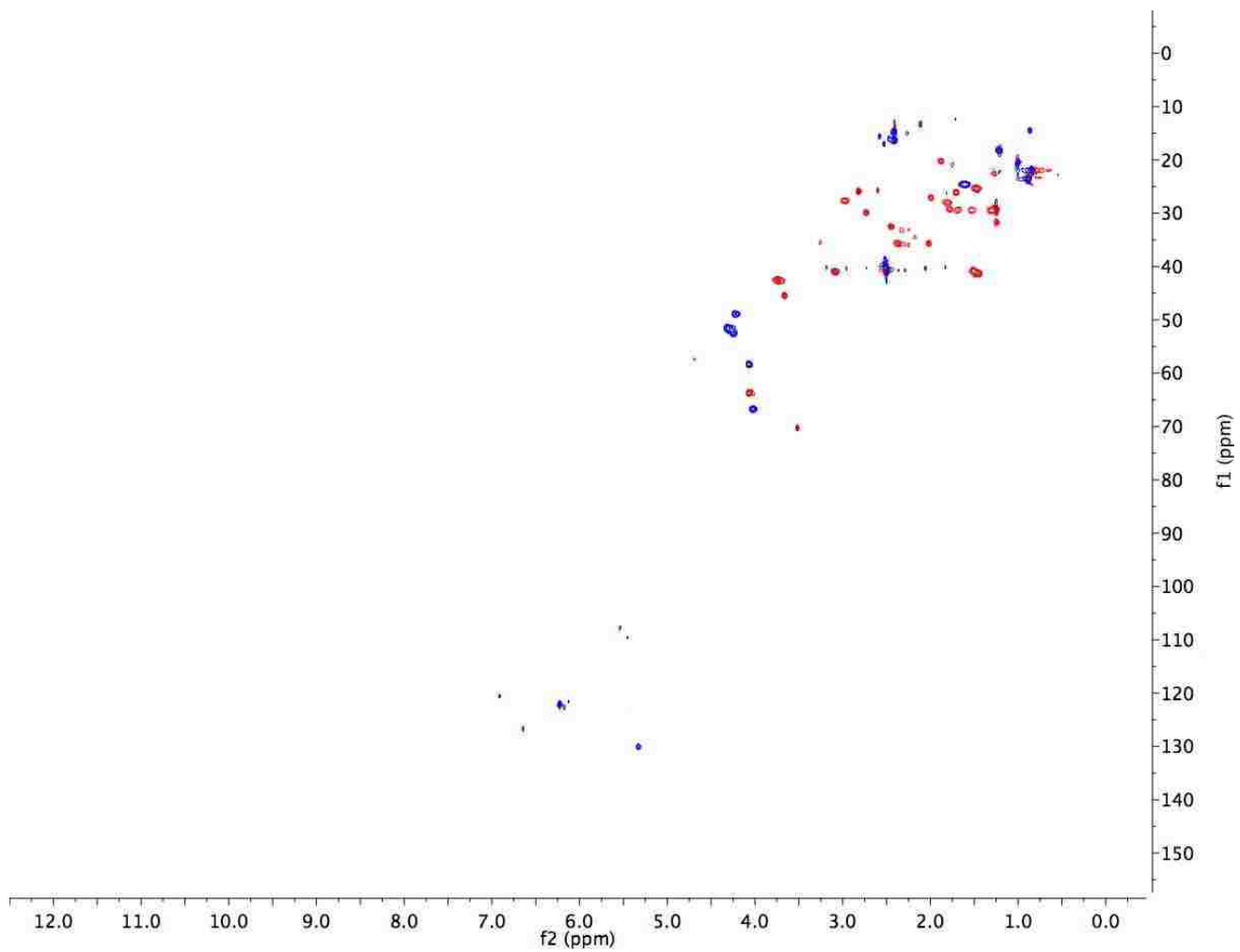


**Figure B.19.** HSQC NMR spectrum of conjugate **3-12** .

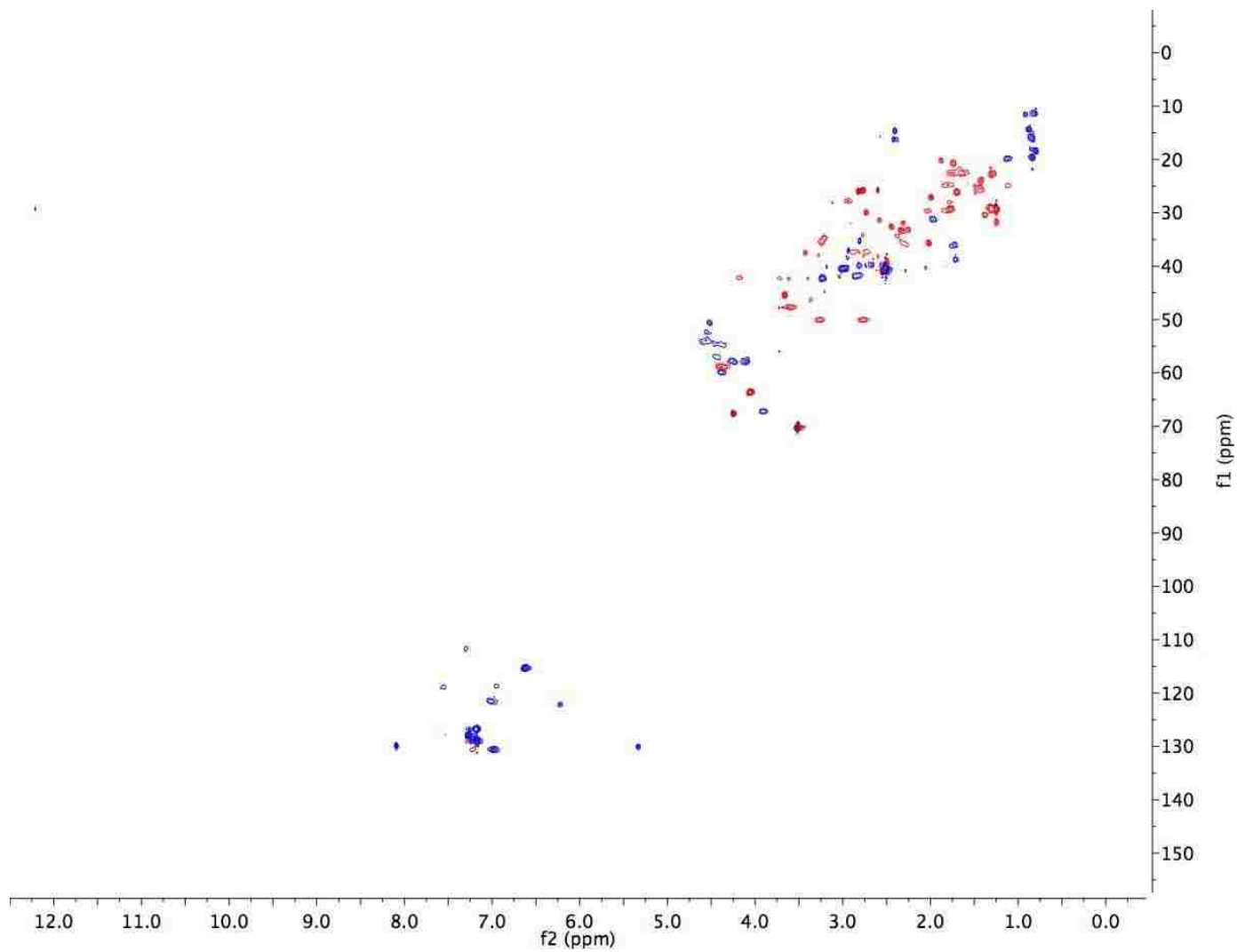


**Figure B.20.** HSQC NMR spectrum of conjugate **3-13** .

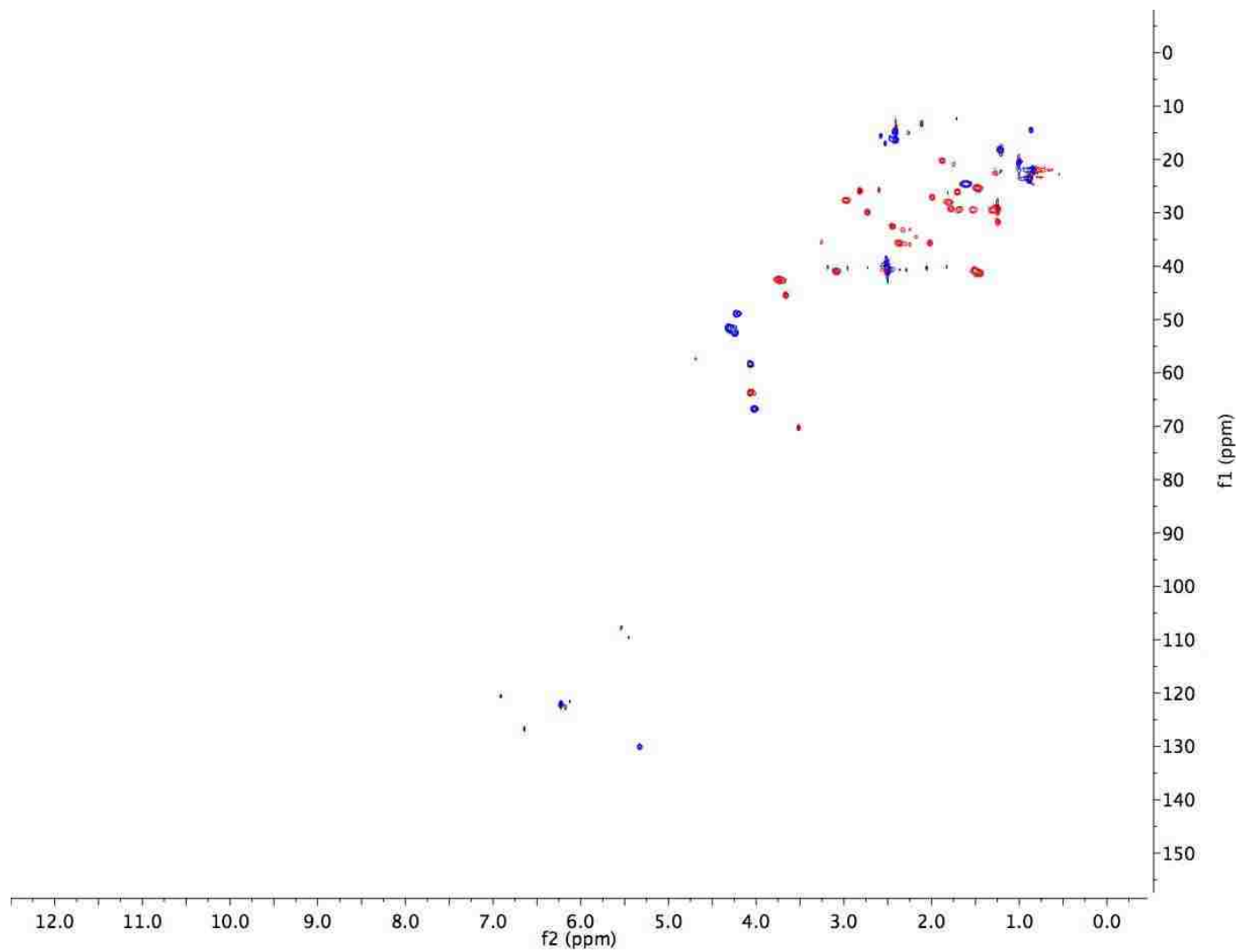


**Figure B.21.** HSQC NMR spectrum of conjugate 3-14.

### Boron NMR of Compounds in Chapter 3

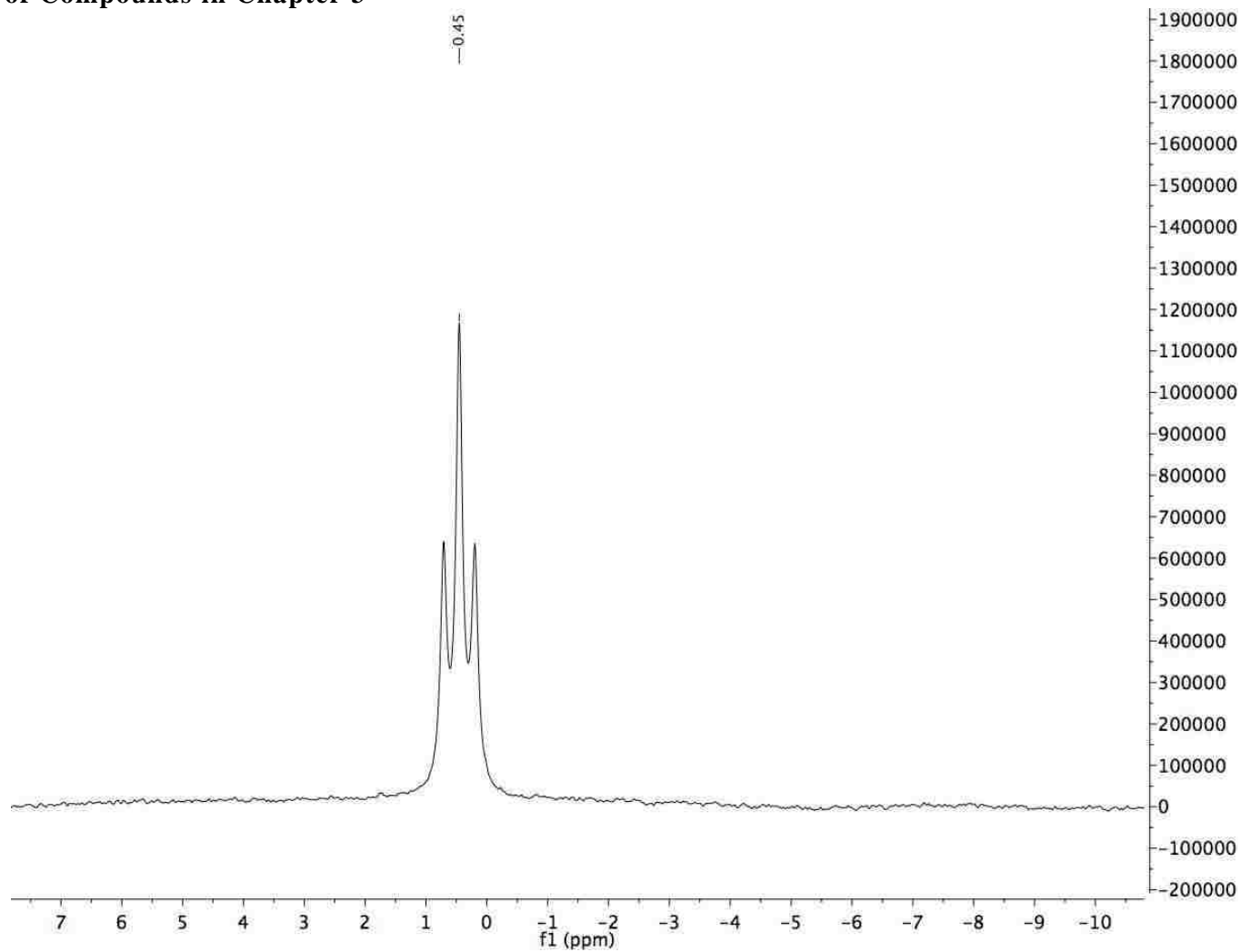


**Figure B.22.** Boron NMR spectrum of BODIPY 3-3.

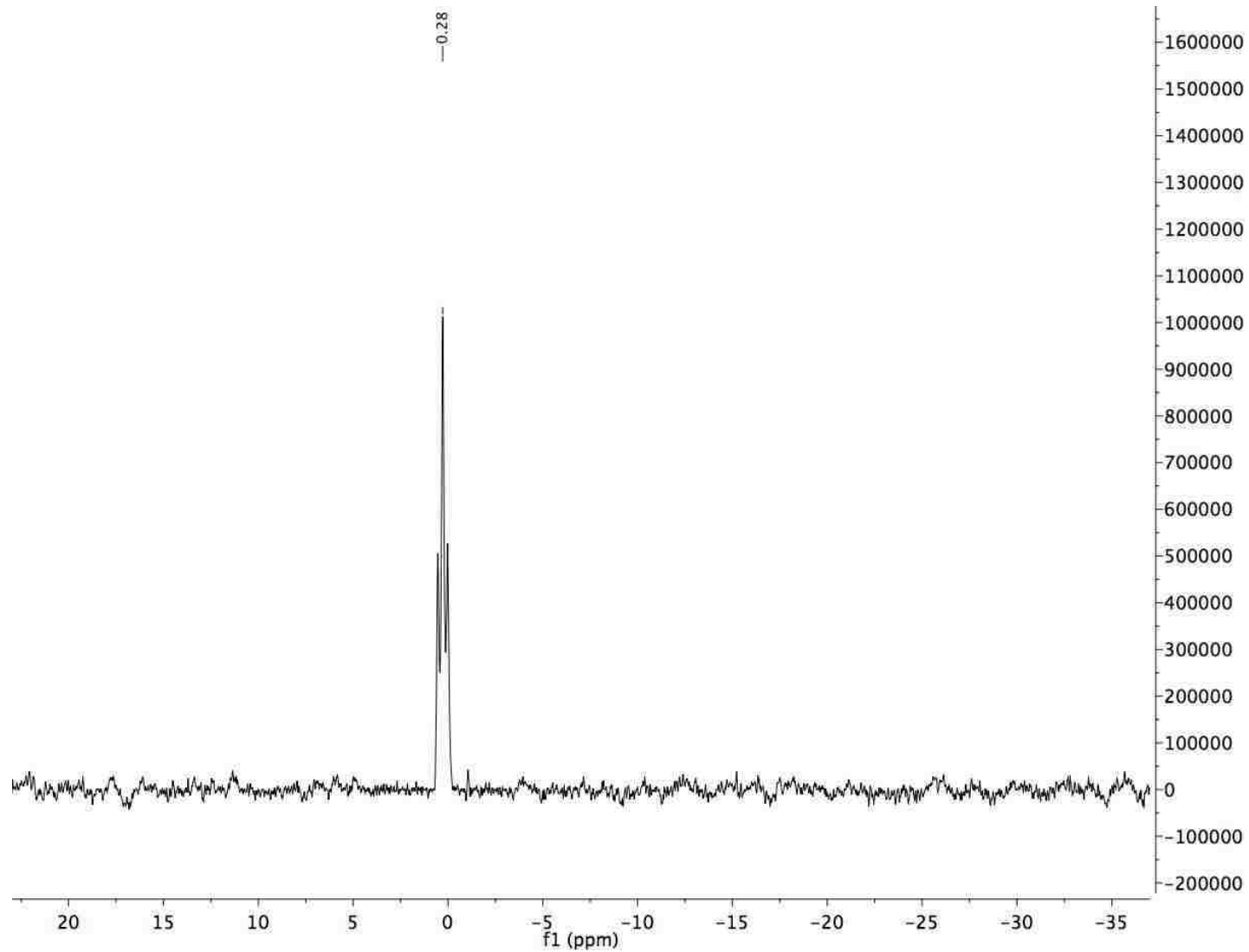


**Figure B.23.** Boron NMR spectrum of conjugate 3-12.

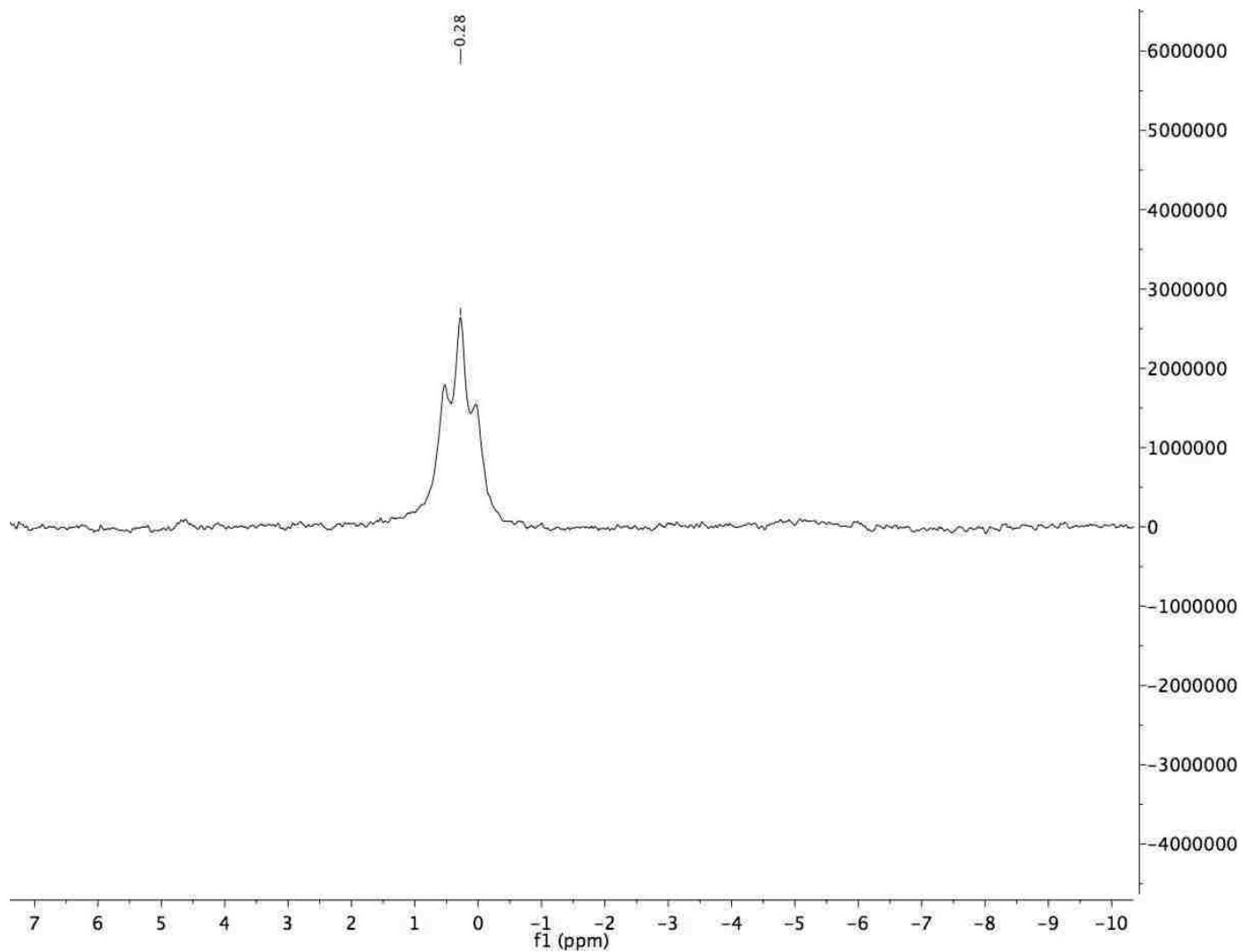


**Figure B.24.** Boron NMR spectrum of conjugate 3-13.

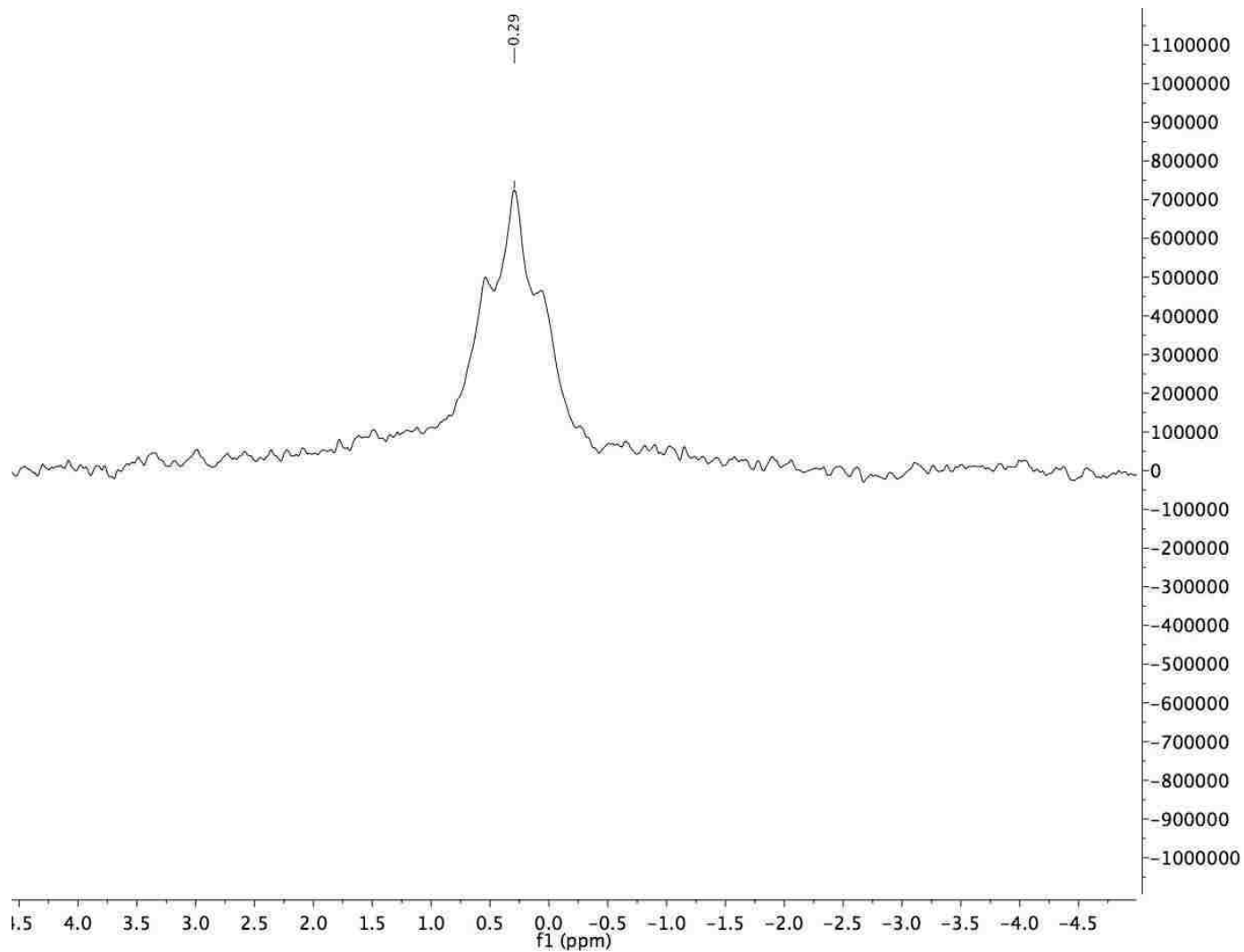


**Figure B.25.** Boron NMR spectrum of conjugate 3-14



## APPENDIX C: Characterization of Chapter 4 Compounds

### HPLC of Compounds in Chapter 4

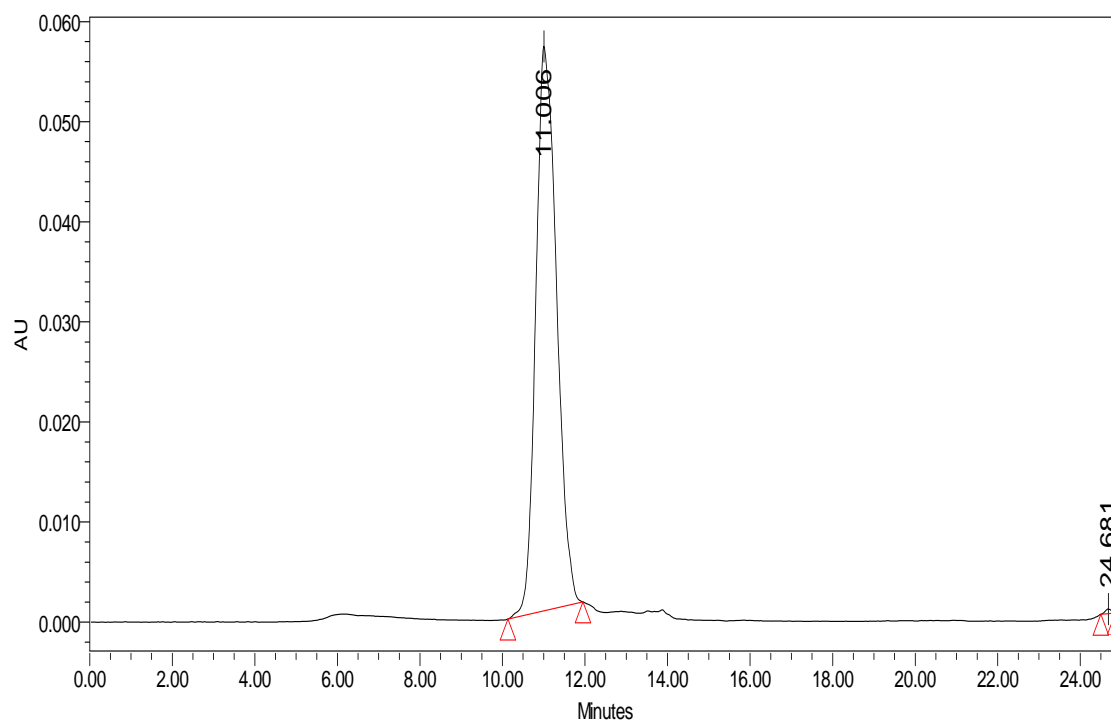


**Figure C.1.** The gradient used for chromatogram of 4-8 using RP-HPLC with a C18 column is listed below.

| # | Time (minutes) | Flow       | %A (H <sub>2</sub> O) | %B (ACN) |
|---|----------------|------------|-----------------------|----------|
| 0 | 0              | 4.0 ml/min | 50                    | 50       |
| 1 | 5              | 4.0 ml/min | 50                    | 50       |
| 2 | 8              | 4.0 ml/min | 10                    | 90       |
| 3 | 18             | 4.0 ml/min | 0                     | 100      |
| 4 | 20             | 4.0 ml/min | 50                    | 50       |
| 5 | 25             | 4.0 ml/min | 50                    | 50       |

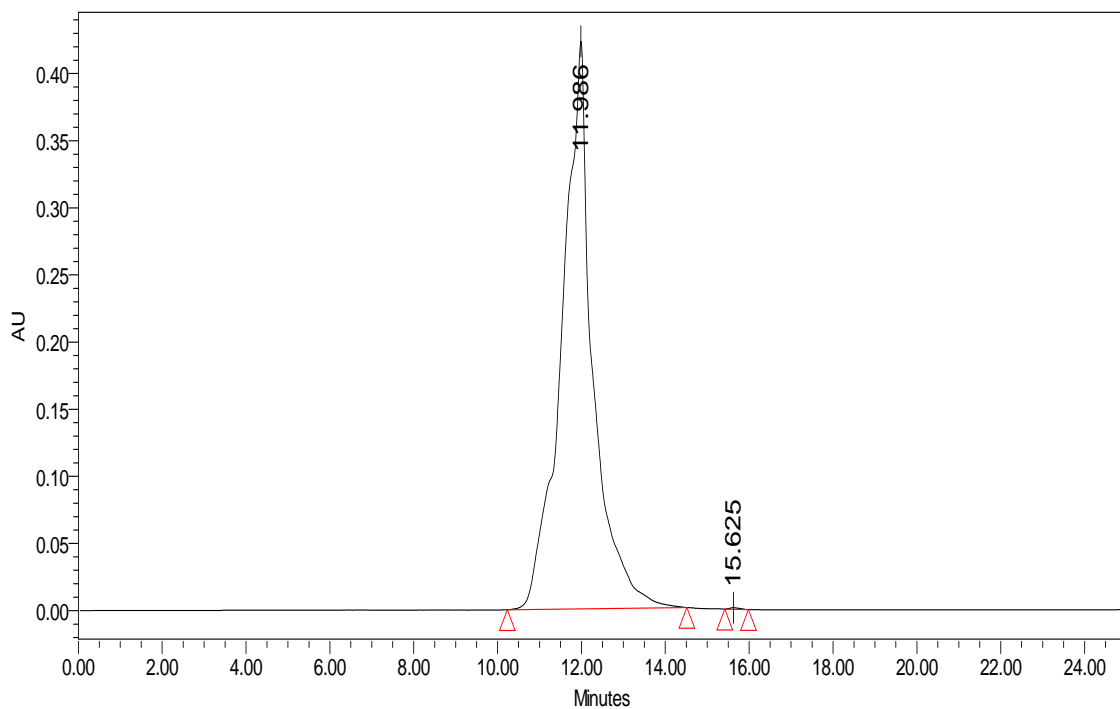


**Figure C.2.** The gradient used for chromatogram of 4-9 using RP-HPLC with a C18 column is listed below.

| <i>Table 1 HPLC Gradient for peptide 4-9</i> |                       |                   |                            |                 |
|--|-----------------------|-------------------|----------------------------|-----------------|
| <i>#</i>                                     | <i>Time (minutes)</i> | <i>Flow</i>       | <i>%A (H<sub>2</sub>O)</i> | <i>%B (ACN)</i> |
| <i>0</i>                                     | <i>0</i>              | <i>4.0 ml/min</i> | <i>50</i>                  | <i>50</i>       |
| <i>1</i>                                     | <i>5</i>              | <i>4.0 ml/min</i> | <i>50</i>                  | <i>50</i>       |
| <i>2</i>                                     | <i>8</i>              | <i>4.0 ml/min</i> | <i>10</i>                  | <i>90</i>       |
| <i>3</i>                                     | <i>18</i>             | <i>4.0 ml/min</i> | <i>0</i>                   | <i>100</i>      |
| <i>4</i>                                     | <i>20</i>             | <i>4.0 ml/min</i> | <i>50</i>                  | <i>50</i>       |
| <i>5</i>                                     | <i>25</i>             | <i>4.0 ml/min</i> | <i>50</i>                  | <i>50</i>       |

# MALDI of Compounds in Chapter 4

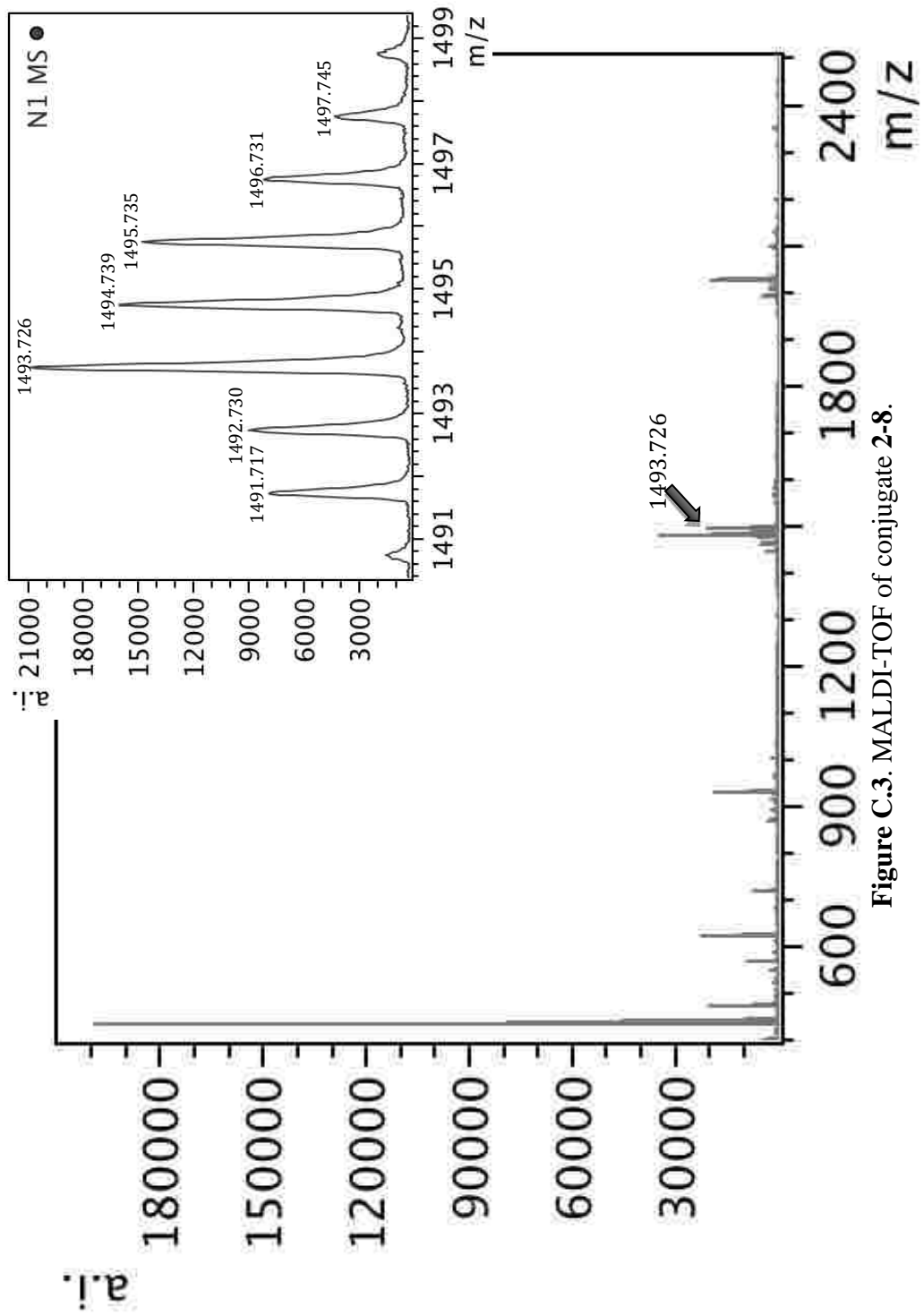


Figure C.3. MALDI-TOF of conjugate 2-8.

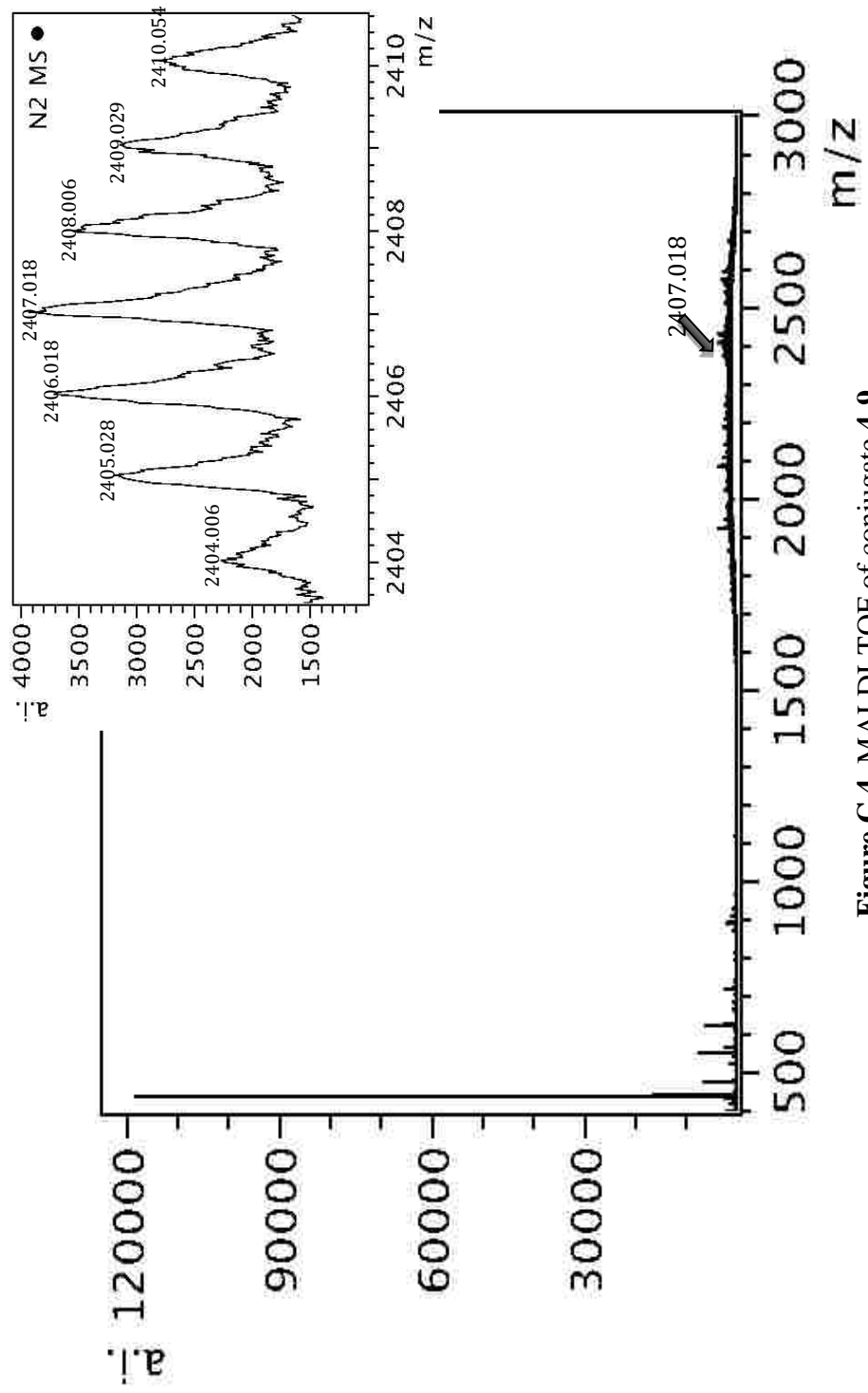


Figure C.4. MALDI-TOF of conjugate 4-9.

# MALDI MSMS of Compounds in Chapter 4

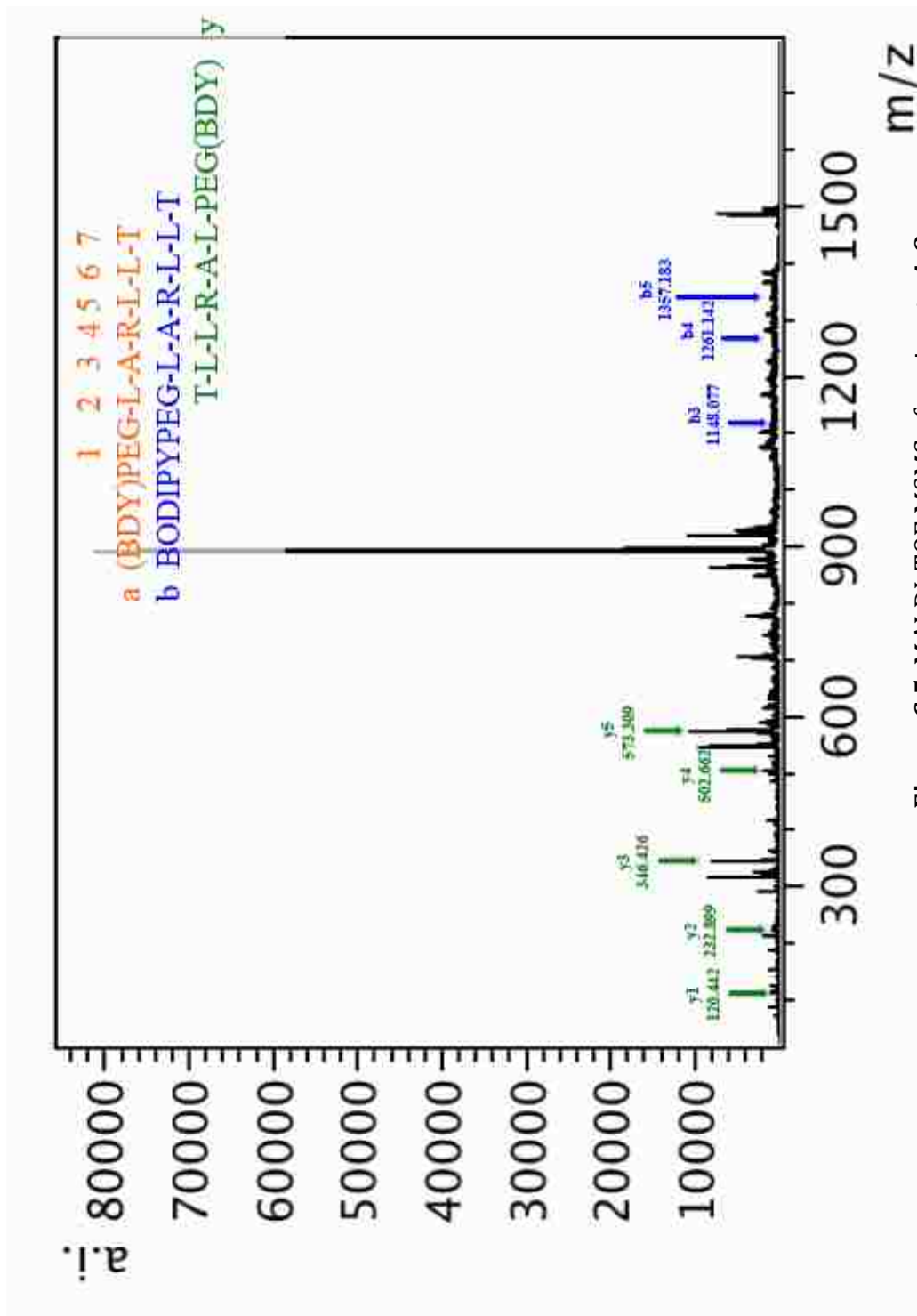


Figure C.5. MALDI-TOF MSMS of conjugate 4-8.

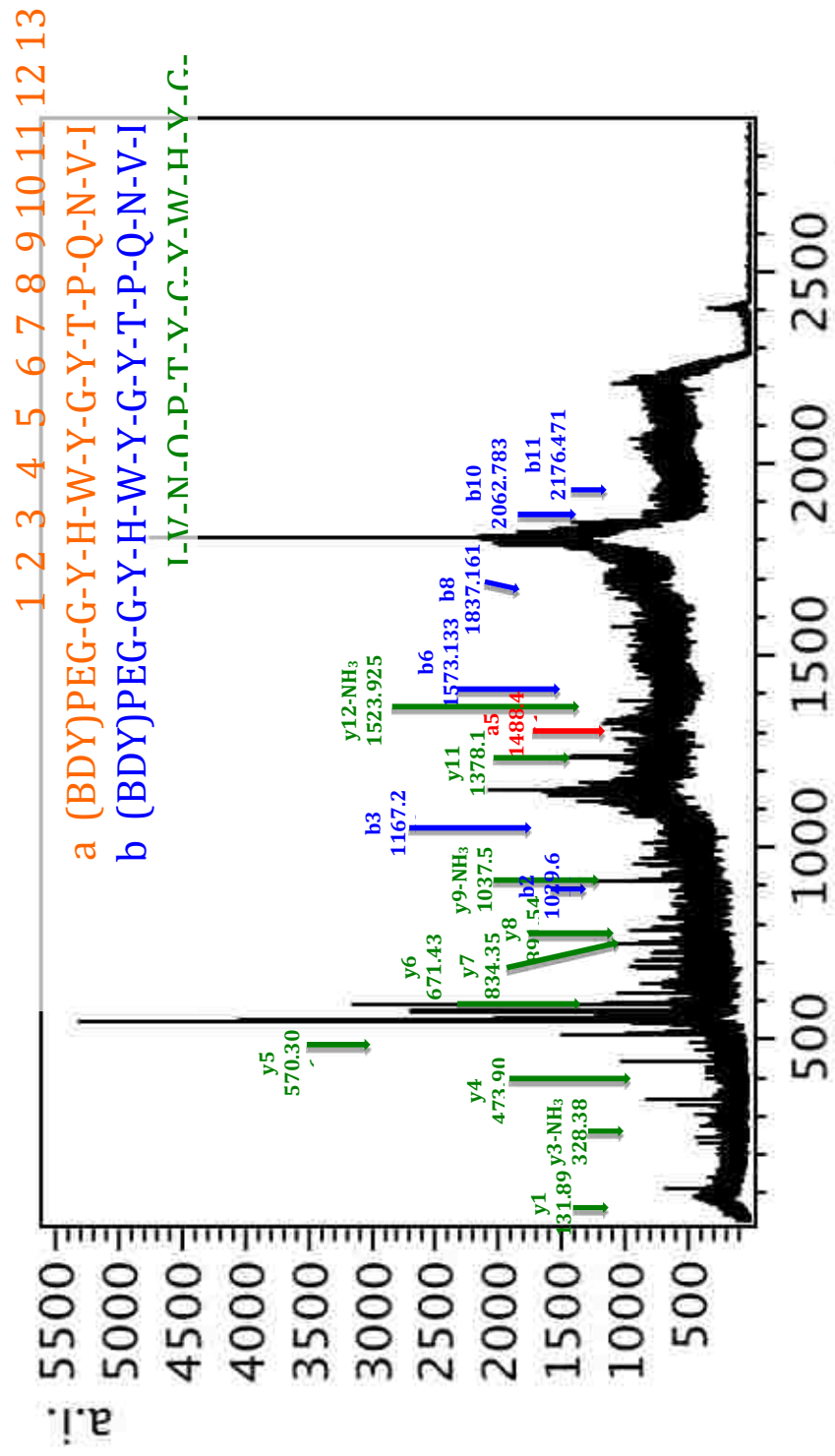


Figure C.6. MALDI-TOF MSMS of conjugate 4-9.

# Proton NMR of Compounds in Chapter 4

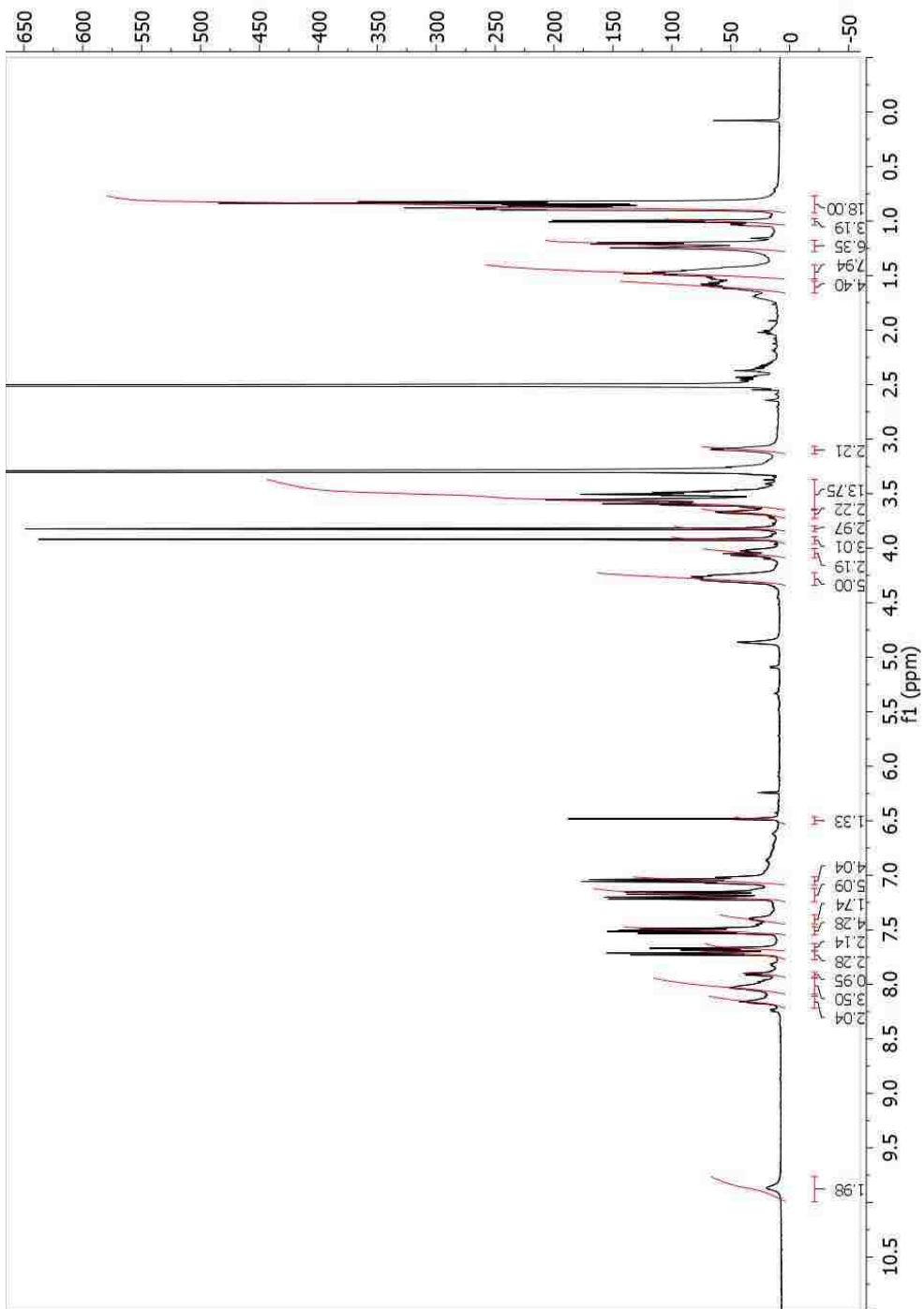
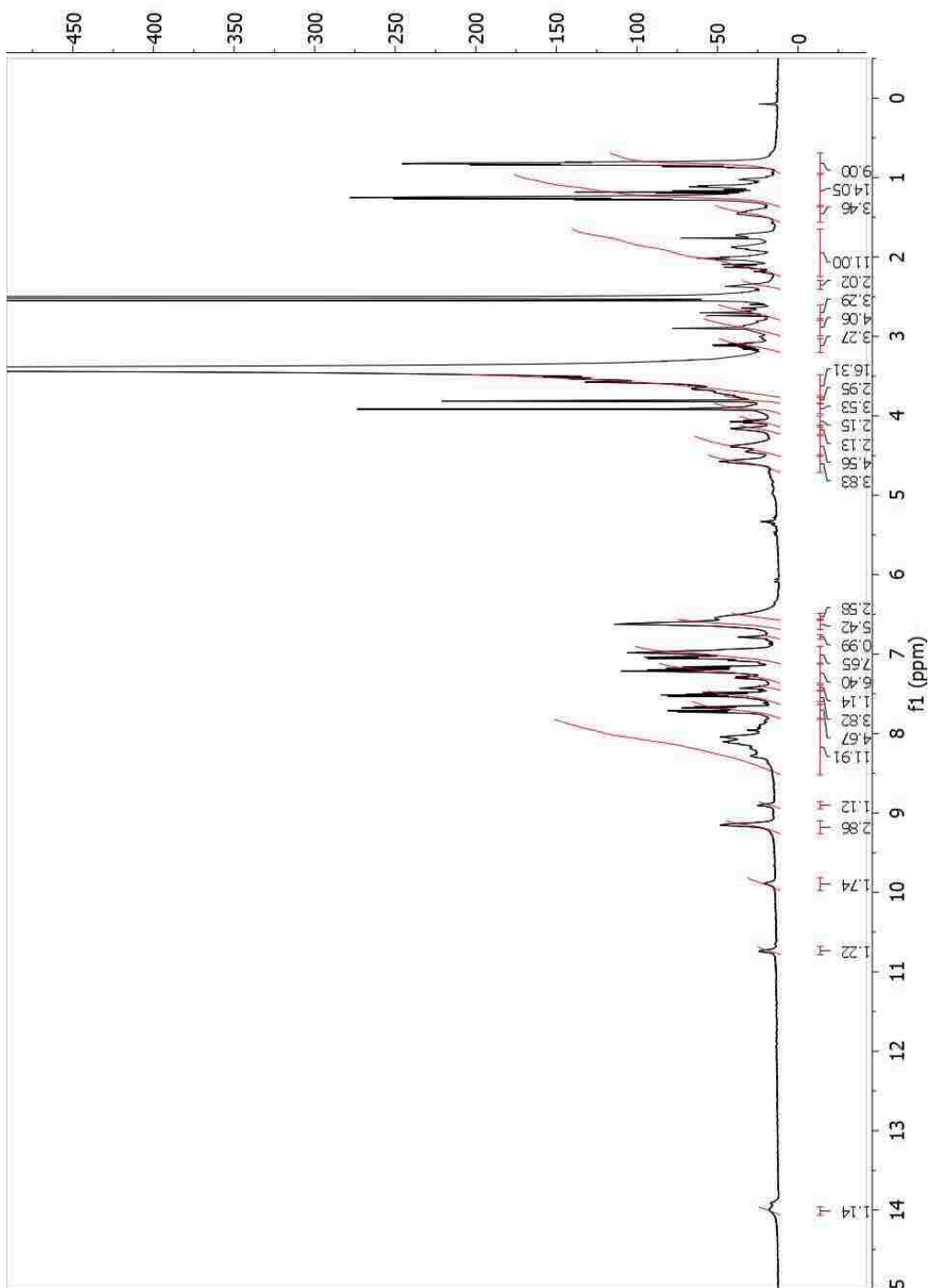


Figure C.7. Proton NMR of conjugate 4-8.



**Figure C.8.** Proton NMR of conjugate 4-9.



## HSQC NMR of Compounds in Chapter 4

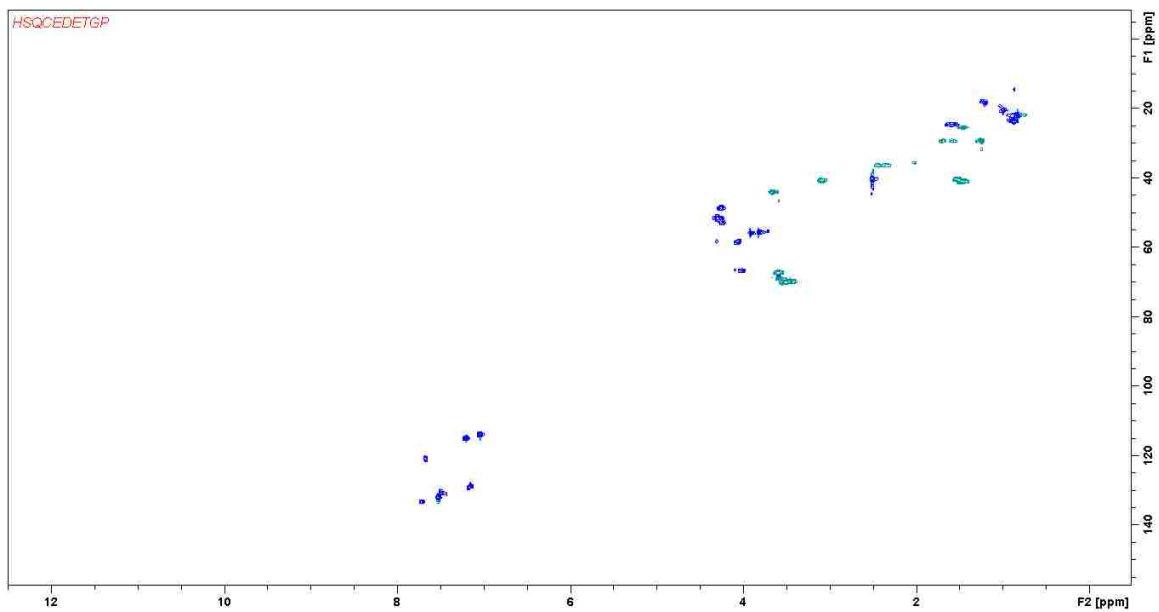


**Figure C.9.** HSQC NMR of Conjugate of 4-8.

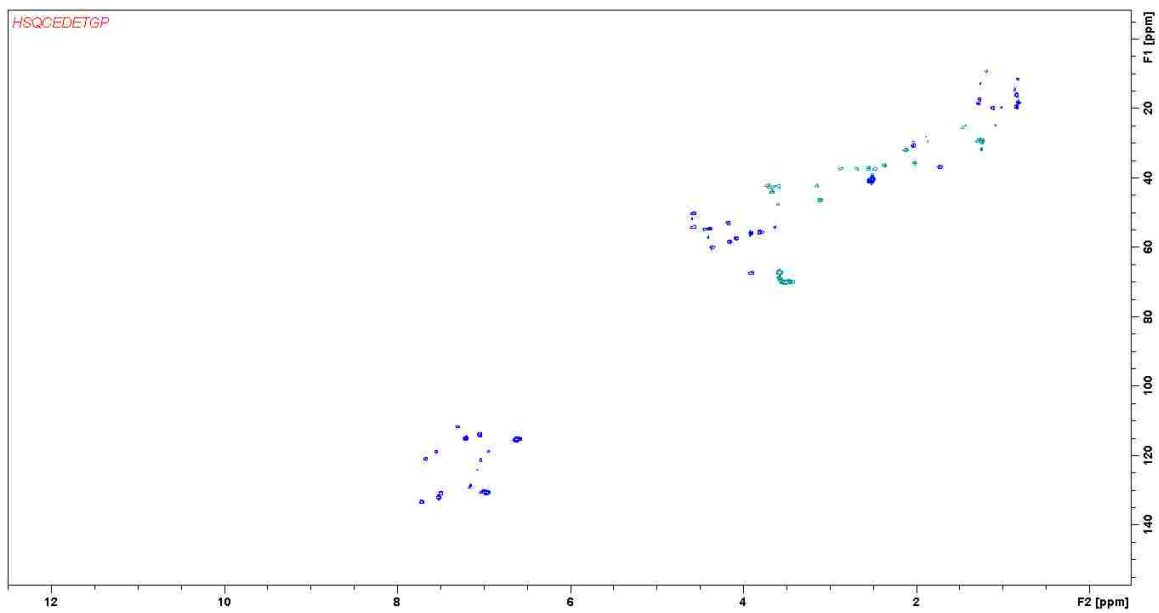


**Figure C.10.** HSQC NMR of Conjugate of 4-9.

## Boron NMR of Compounds in Chapter 4

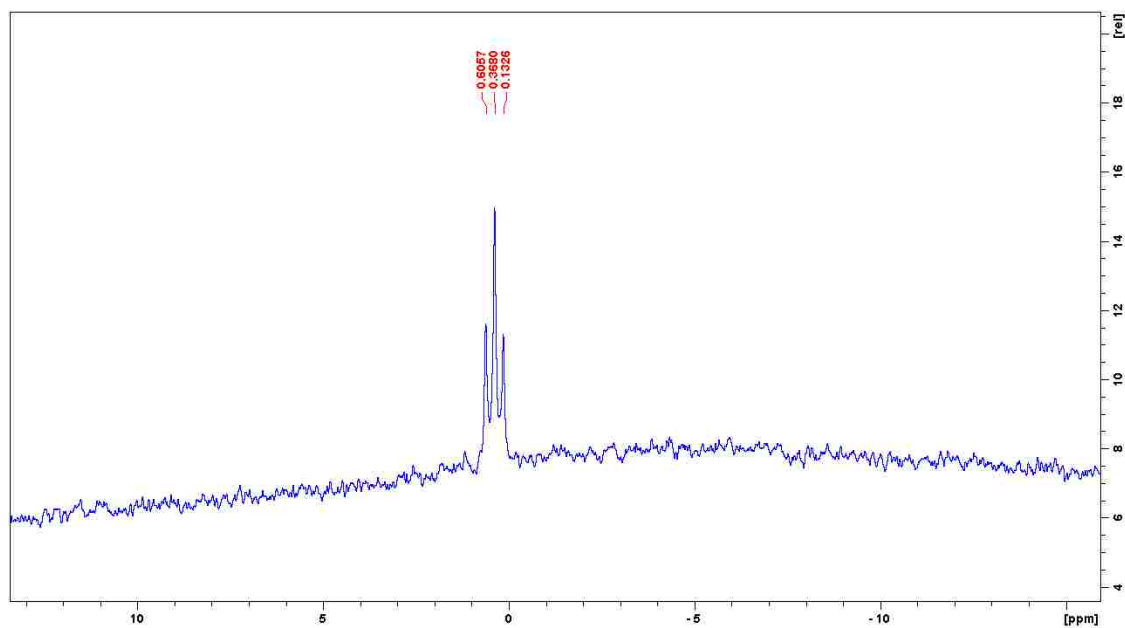


**Figure C.11.** Boron NMR of Conjugate of 4-8.

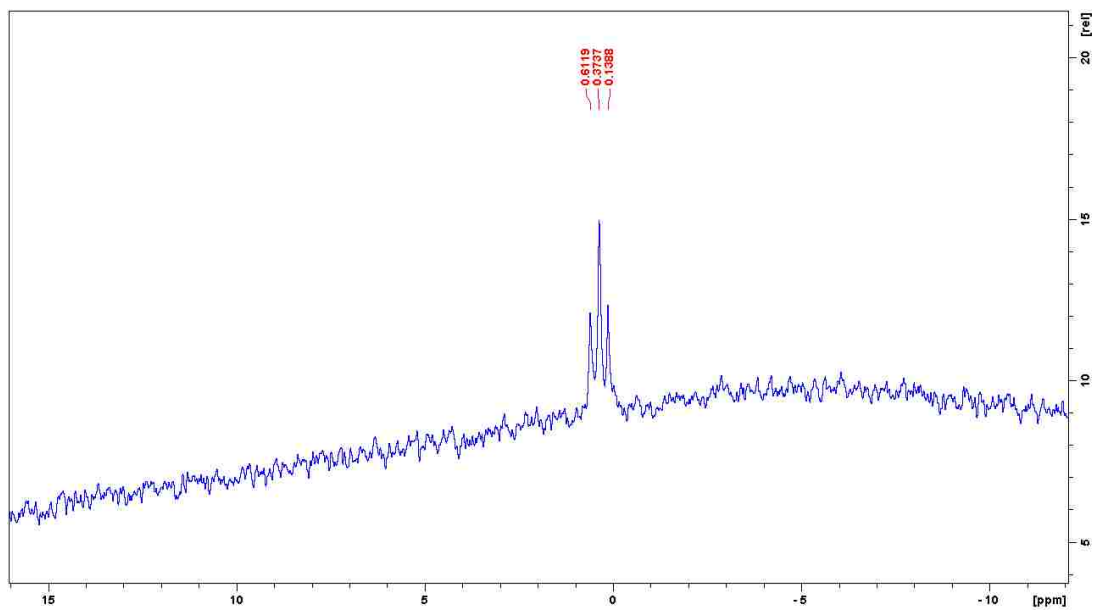


**Figure C.12.** Boron NMR of Conjugate of 4-9.

## APPENDIX D: Characterization of Chapter 5 Compounds

MALDI of Compounds in Chapter 5

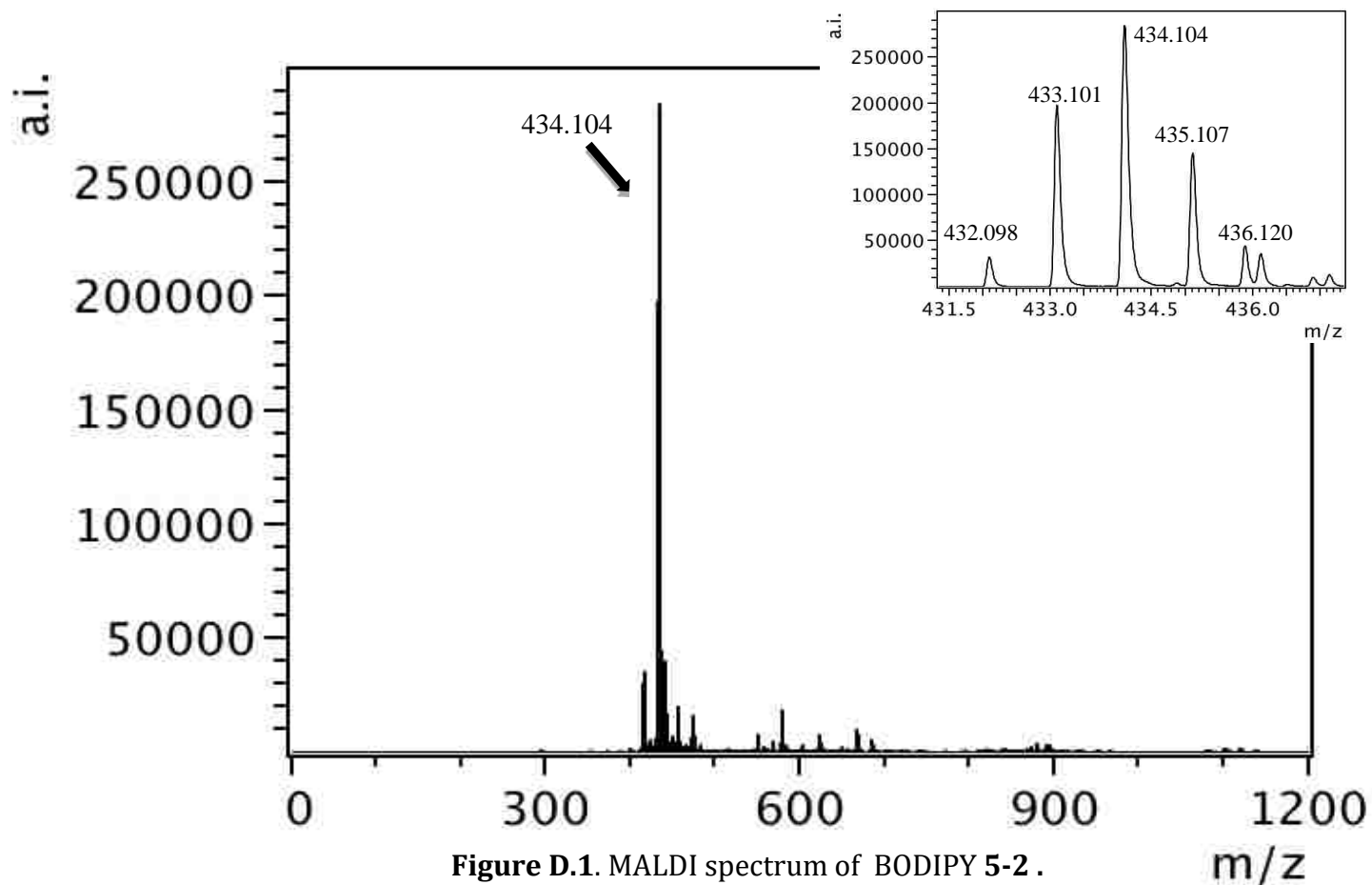
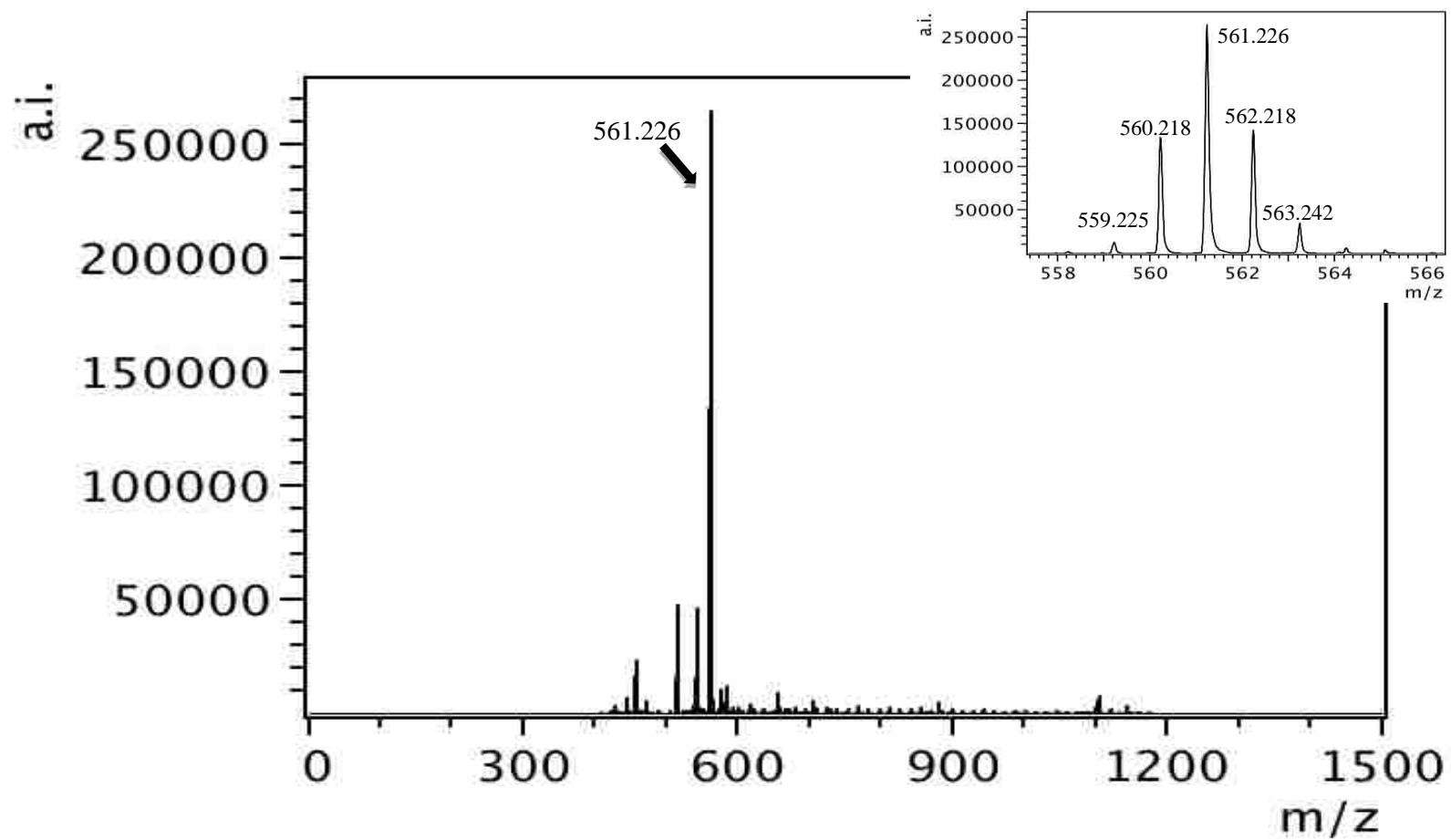


Figure D.1. MALDI spectrum of BODIPY 5-2 .



**Figure D.2.** MALDI spectrum of BODIPY 5-4.

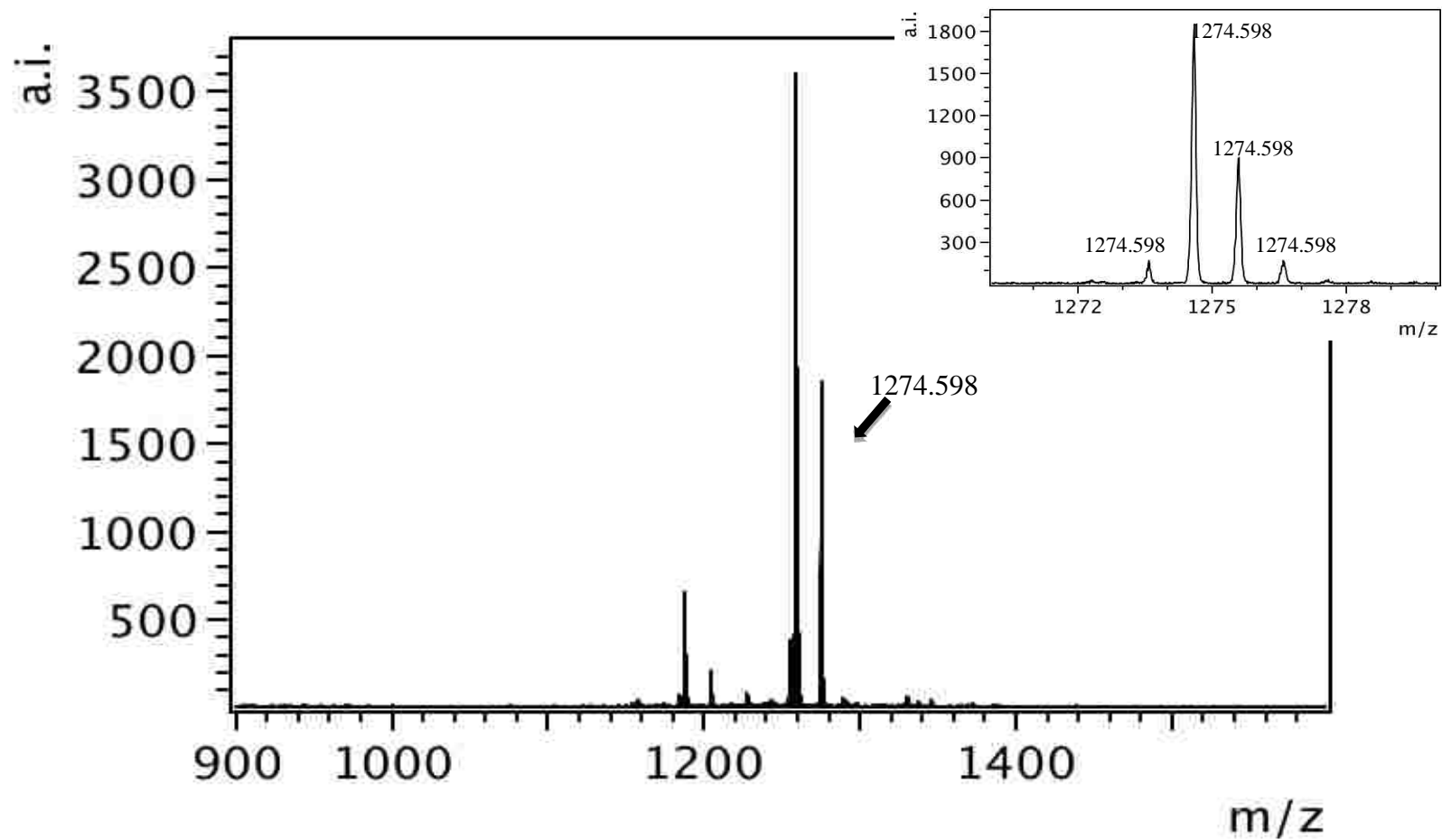


Figure D.3. MALDI spectrum of conjugate 5-6.

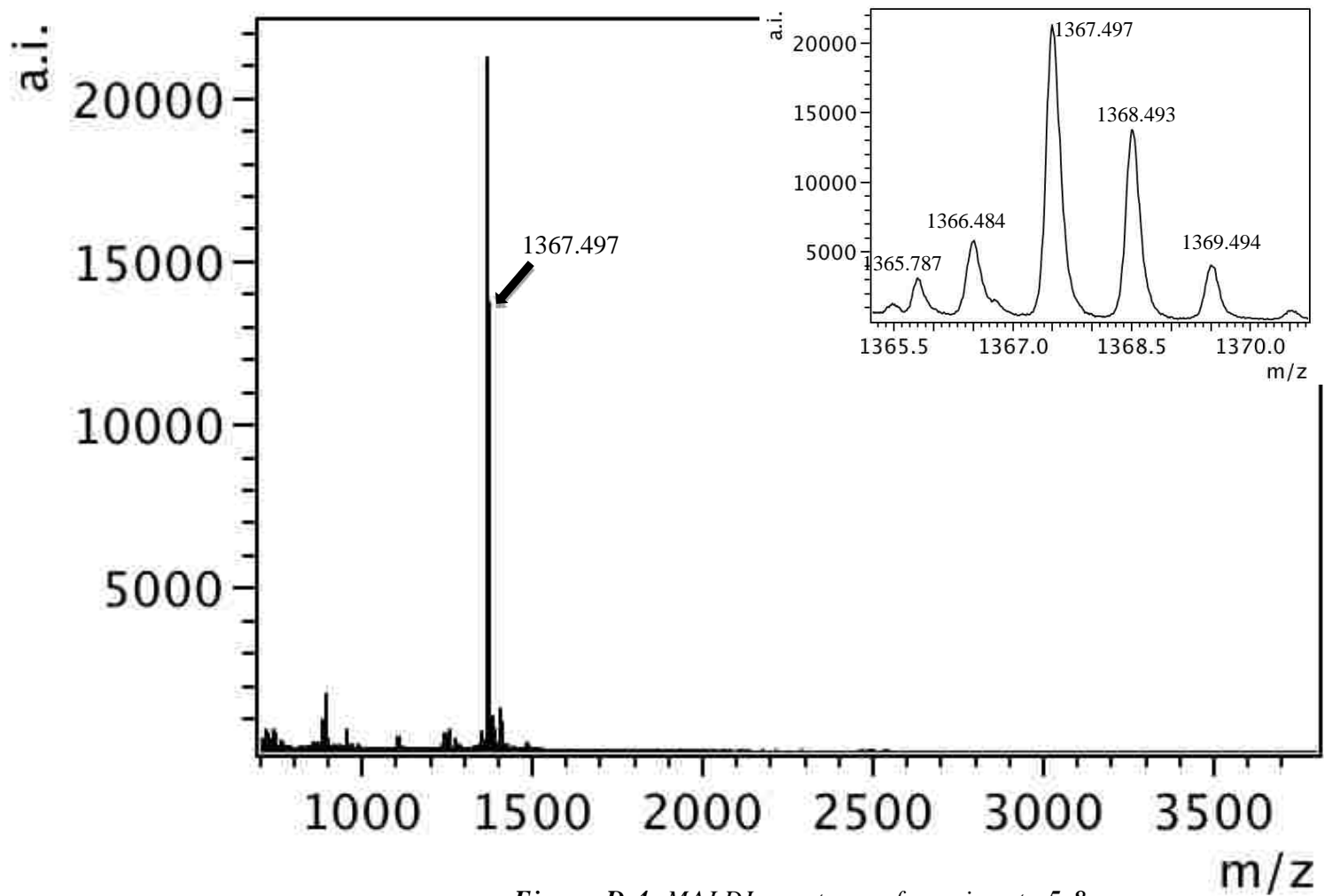
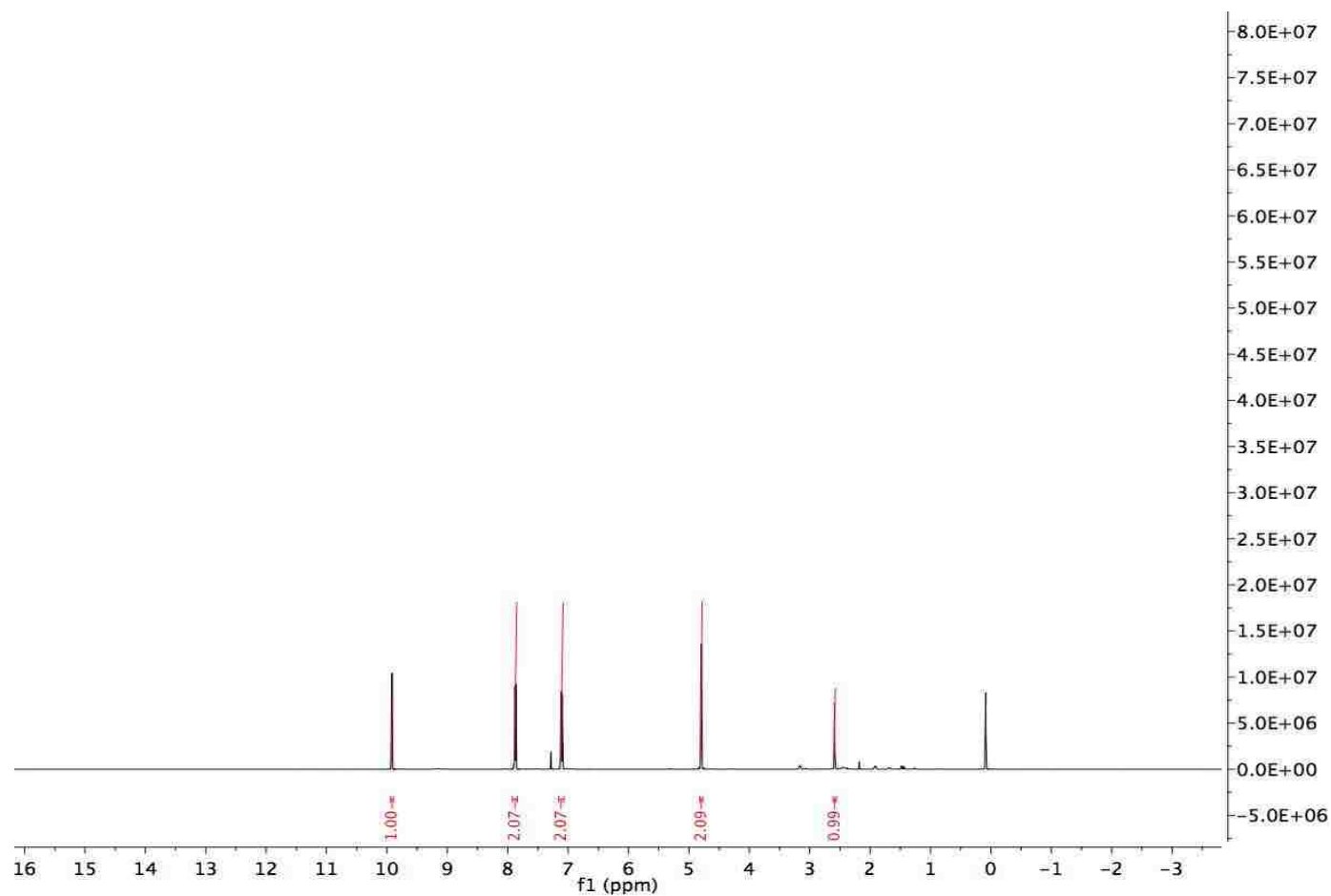
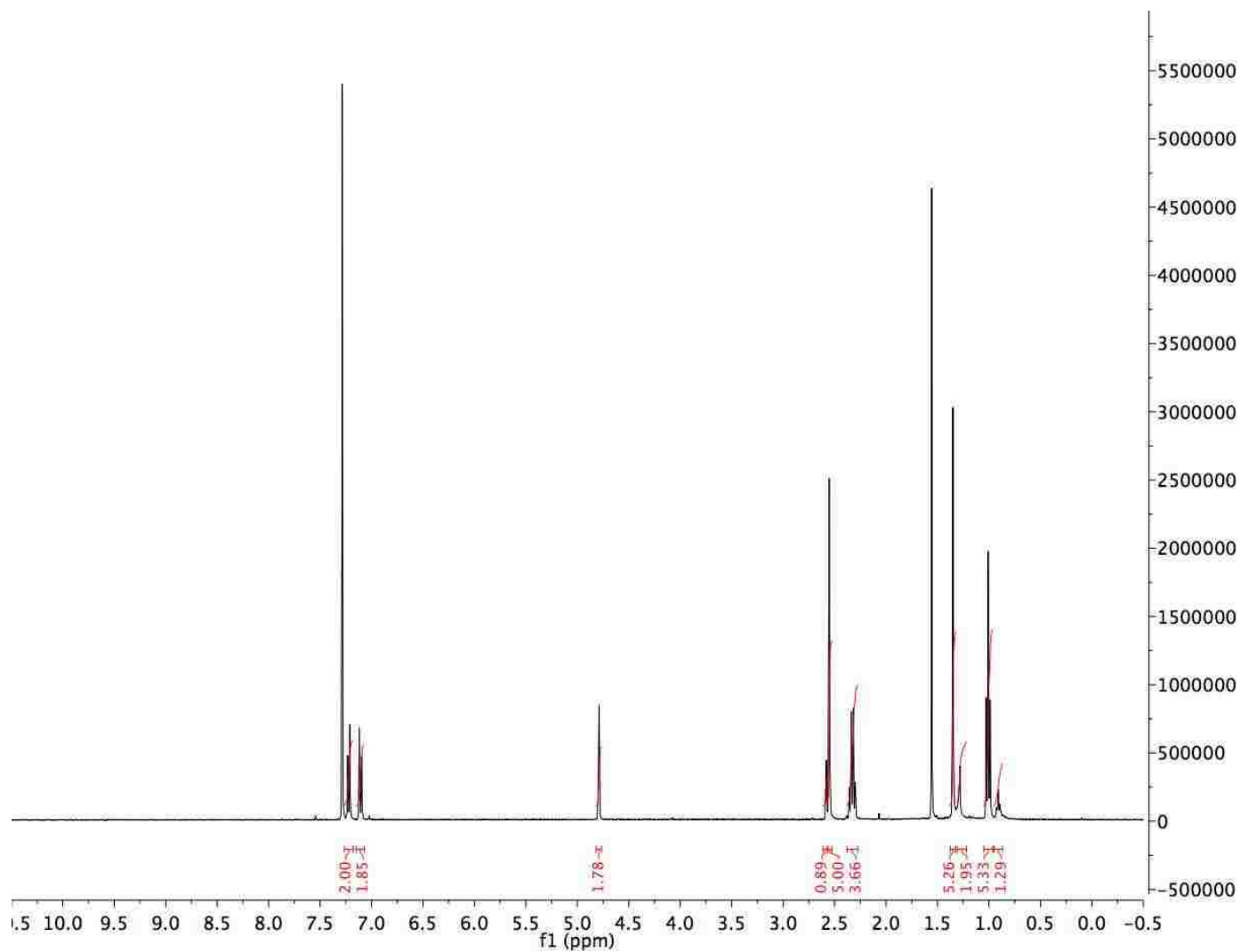


Figure D.4. MALDI spectrum of conjugate 5-8.

## Proton NMR of Compounds in Chapter 5



**Figure D.5.** NMR spectrum of compound 5-1.



**Figure D.6.** NMR spectrum of compound 5-2.



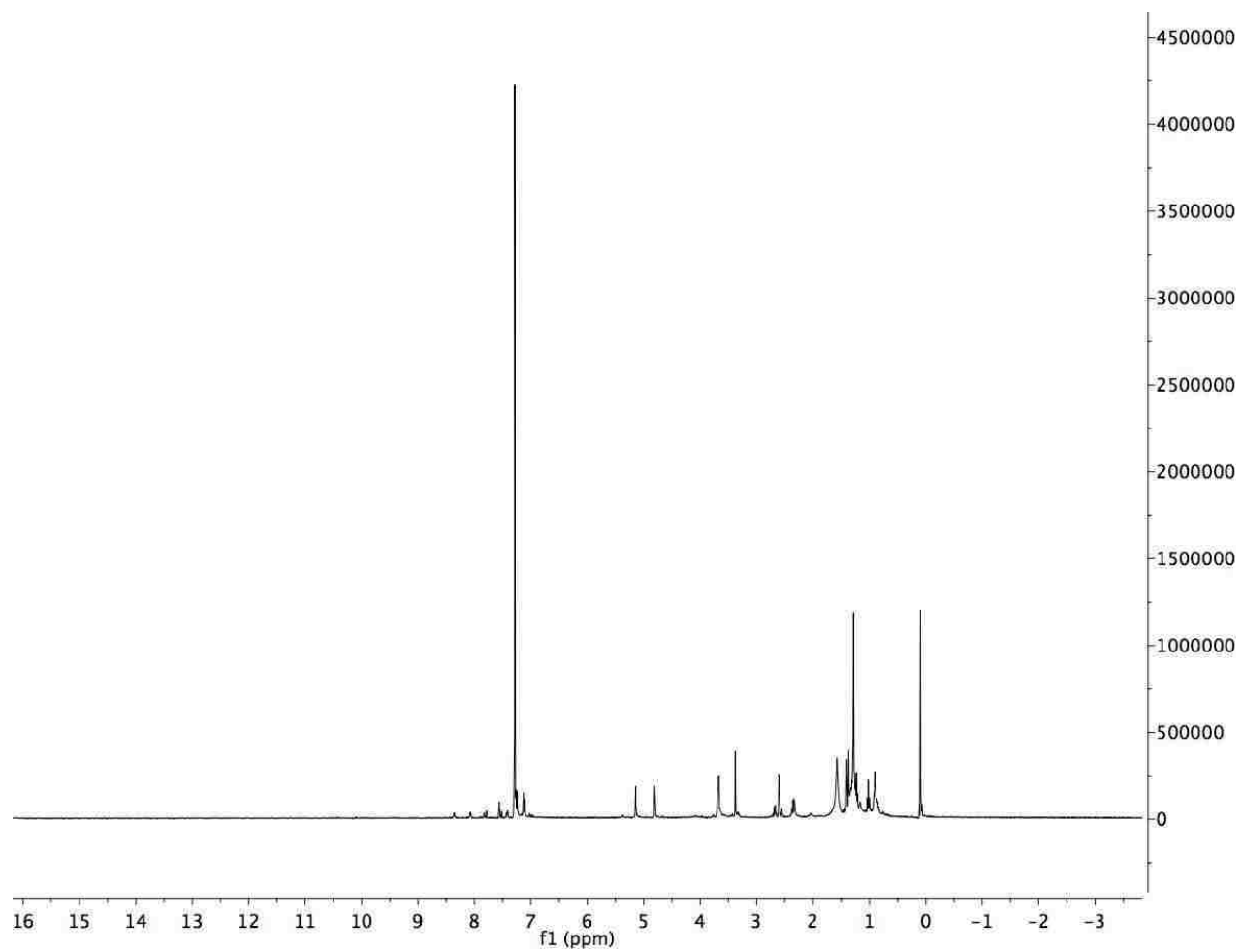


**Figure D.7.** NMR spectrum of compound 5-4.

## Boron NMR of Compounds in Chapter 5

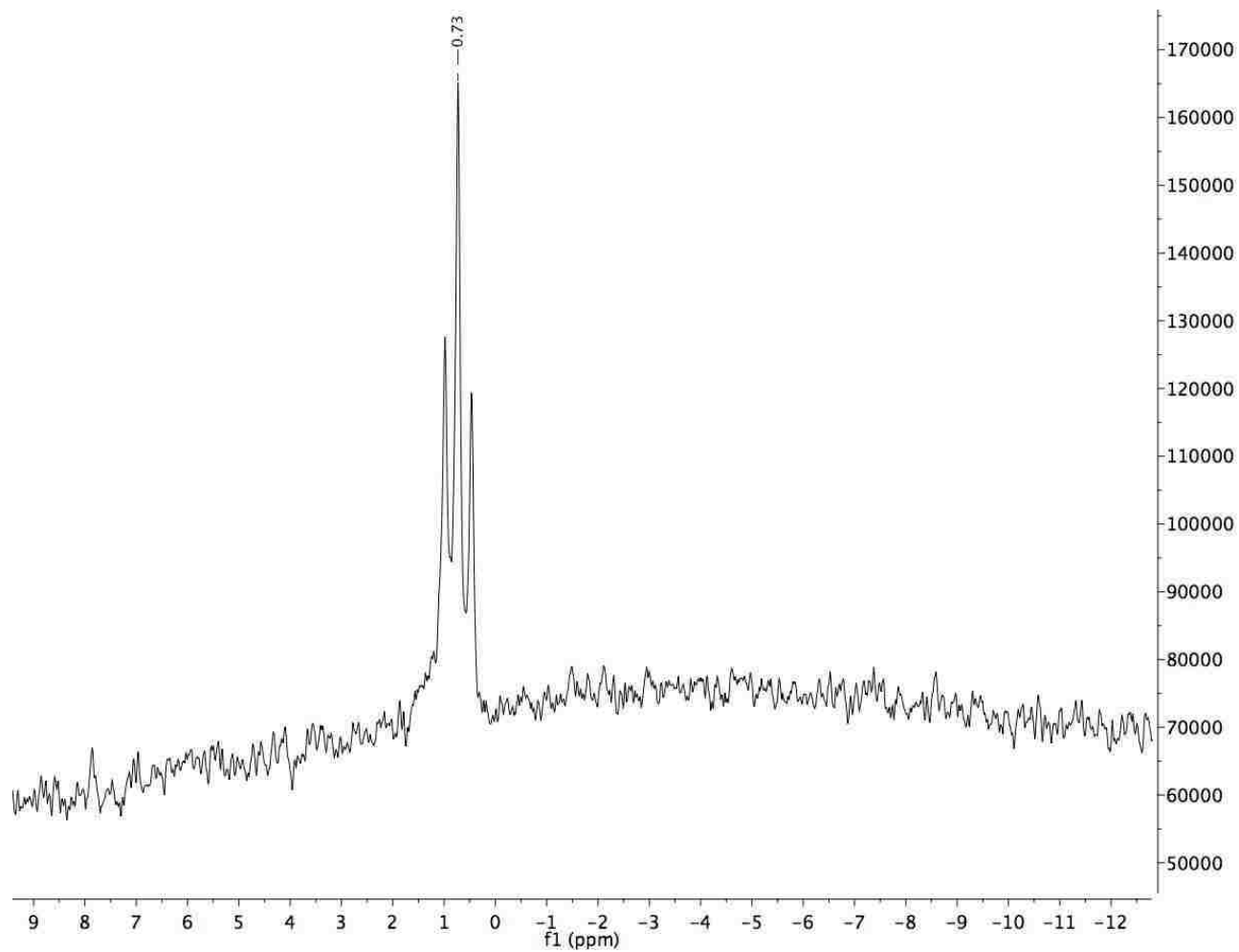


**Figure D.8.** Boron NMR spectrum of compound 5-2.

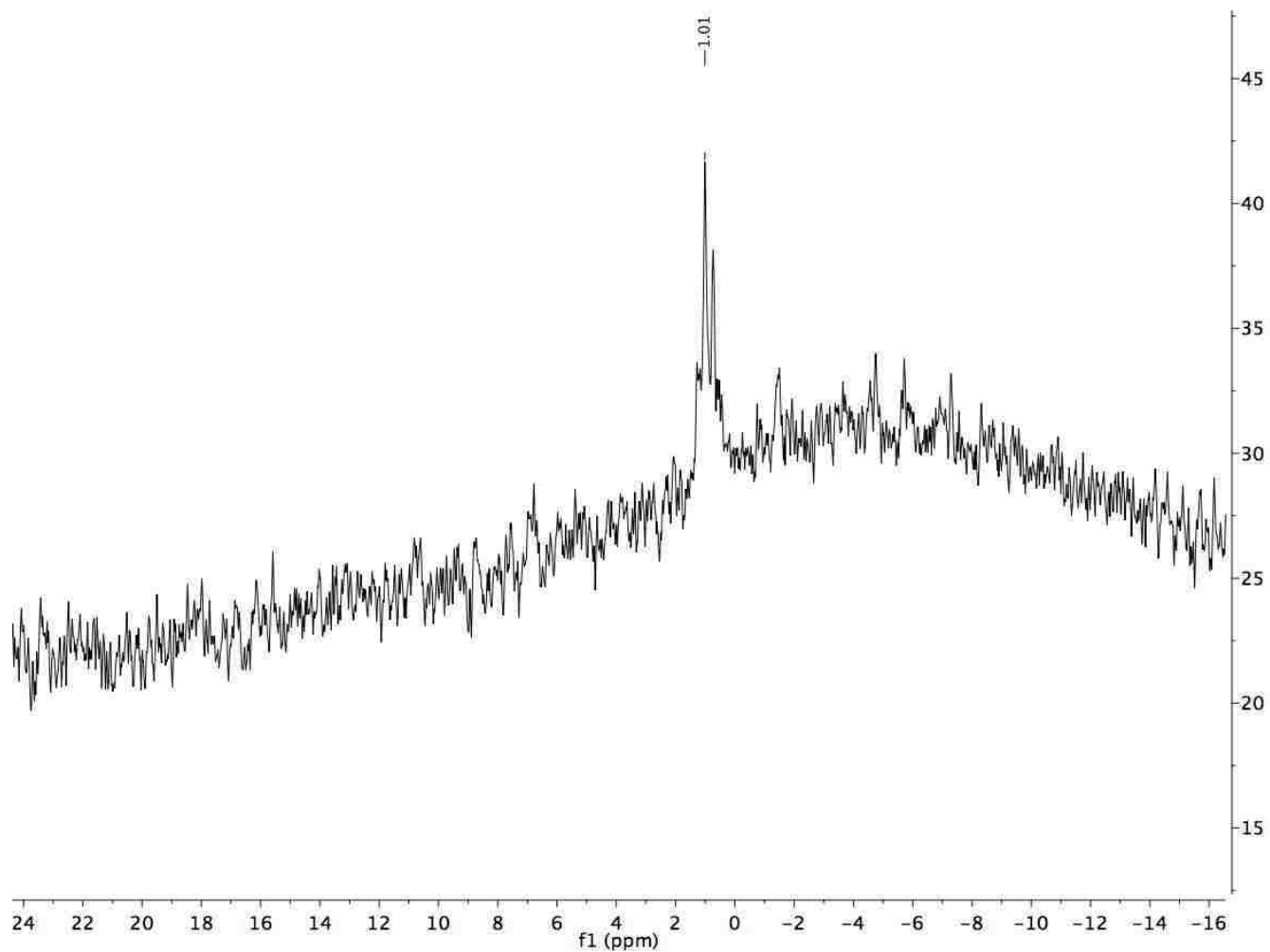


**Figure D.9.** Boron NMR spectrum of compound 5-4.

## APPENDIX E: Letters of Permission



The screenshot shows the RightsLink website interface. At the top left is the Copyright Clearance Center logo. To its right is the RightsLink logo. On the top right, there are navigation buttons for Home, Create Account, Help, and an email icon. Below the logos is the ACS Publications logo with the tagline "Most Trusted. Most Cited. Most Read." The main content area displays the following information:

**Title:** Synthesis of BODIPY-Peptide Conjugates for Fluorescence Labeling of EGFR Overexpressing Cells

**Author:** Ning Zhao, Tyrslai M. Williams, Zehua Zhou, et al

**Publication:** Bioconjugate Chemistry

**Publisher:** American Chemical Society

**Date:** May 1, 2017

Copyright © 2017, American Chemical Society

On the right side, there is a "LOGIN" button and a text box that reads: "If you're a copyright.com user, you can login to RightsLink using your copyright.com credentials. Already a RightsLink user or want to learn more?"

### PERMISSION/LICENSE IS GRANTED FOR YOUR ORDER AT NO CHARGE

This type of permission/license, instead of the standard Terms & Conditions, is sent to you because no fee is being charged for your order. Please note the following:

- Permission is granted for your request in both print and electronic formats, and translations.
- If figures and/or tables were requested, they may be adapted or used in part.
- Please print this page for your records and send a copy of it to your publisher/graduate school.
- Appropriate credit for the requested material should be given as follows: "Reprinted (adapted) with permission from (COMPLETE REFERENCE CITATION). Copyright (YEAR) American Chemical Society." Insert appropriate information in place of the capitalized words.
- One-time permission is granted only for the use specified in your request. No additional uses are granted (such as derivative works or other editions). For any other uses, please submit a new request.

BACK

CLOSE WINDOW

Copyright © 2017 Copyright Clearance Center, Inc. All Rights Reserved. [Privacy statement](#). [Terms and Conditions](#). Comments? We would like to hear from you. E-mail us at [customerservice@copyright.com](mailto:customerservice@copyright.com)

## VITA

Tyrslai Menyae Williams was born to Ranetta E. Williams in Baton Rouge, Louisiana where she completed her primary studies as salutatorian of her 2004 class. She completed her undergraduate degree from Southern University A&M College in May of 2011. Tyrslai first discovered an interest in public health and wanted to become a medical doctor until meeting Dr. Michelle Claville at Southern University, who introduced her to the endless possibilities of pursuing a doctoral program. In August of 2011, she enrolled in Louisiana State University to obtain her Doctor of Philosophy degree in organic chemistry under the direction of Dr. Graça H. Vicente. Tyrslai is currently a candidate for the Doctor of Philosophy in organic chemistry, which she will be awarded her degree at the August 2017 commencement at LSU, Baton Rouge.